FERMENTATION OF SYNTHESIS GAS TO ETHANOL

MEDIUM DESIGN, MASS TRANSFER AND

INTEGRATED MODEL

By

JOHN RANDALL PHILLIPS

Bachelor of Science in Chemical Engineering
University of Arkansas
Fayetteville, Arkansas
1981

Master of Science in Chemical Engineering
University of Arkansas
Fayetteville, Arkansas
1989

Submitted to the Faculty of the
Graduate College of the
Oklahoma State University
in partial fulfillment of
the requirements for
the Degree of
DOCTOR OF PHILOSOPHY
May, 2013

FERMENTATION OF SYNTHESIS GAS TO ETHANOL

MEDIUM DESIGN, MASS TRANSFER AND

INTEGRATED MODEL

Dissertation Approved:

Dr. Hasan K. Atiyeh

Dissertation Adviser

Dr. Raymond L. Huhnke

Dr. Mark R. Wilkins

Dr. Josh D. Ramsey

.

DEDICATION

This dissertation and the degree that it completes are testament to the work and support of many people that have guided me through my career. First my parents, Jack and Jo Phillips, encouraged me and all of my siblings to learn and discover. The family farm was my first laboratory.

Dr. Ron Elliott, as Biosystems and Agricultural Engineering Department Head, extended the opportunity to complete my graduate studies late in my career. The Oklahoma State administration, particularly Scott Fern, defended my right to study. And Dr. Dan Thomas added the resolve to cement that defense, and allowed me to continue my studies.

My committee, Dr. Josh Ramsey, Dr. Mark Wilkins, and particularly Dr. Ray Huhnke gave valued counsel and support. My advisor, Dr. Hasan Atiyeh provided the opportunities to research the syngas fermentation, the freedom to explore outside the boundaries, and the structure to complete the tasks. I have enjoyed these associations, and hope they continue for years to come.

My colleagues in the laboratory, Mamatha Devarapalli, Kan Liu, Karthic Ramachandriya and Jie Gao shared their insights and their challenges. I have learned much with them, and hope I have contributed to their progress. I have been assisted in the accomplishment of my studies by efforts of student researchers that advanced the laboratory work, including Nicole Remondet, Akshay Shedge, Viraj Patel and Brian Hercyk.

I am indebted and thankful for all your help and support. However, I am most thankful for the support, counsel, encouragement, sustenance, patience and love of my wife, Donna Phillips, to whom this work is dedicated.

JRP

Acknowledgements reflect the views of the author and are not endorsed by committee members or Oklahoma State University.

Name: JOHN RANDALL PHILLIPS

Date of Degree: May, 2013

Title of Study: FERMENTATION OF SYNTHESIS GAS TO ETHANOL

MEDIUM DESIGN, MASS TRANSFER AND INTEGRATED MODEL

Major Field: BIOSYSTEMS ENGINEERING

ABSTRACT: The U.S. Energy Information Administration projects ethanol as the most prominent biofuel through 2035. The need for biofuels is driven by increased national security, rural development, meeting transportation fuel requirements, improving the environment and sustainability. Currently, most ethanol is derived from corn grain or sugar crops, and diverting food and allocating arable land to supply energy demand is questionable land use policy and distorts our agricultural economy. Alternative feedstocks include lignocellulosic wastes and crops grown on marginal land tapped for the captured solar energy they contain. Conversion of lignocellulosic material and other wastes to synthesis gas, also called syngas, containing CO and H_2 makes this energy available for direct combustion, catalytic reforming to liquid hydrocarbons, or conversion to ethanol via fermentation by acetogenic autotrophs like *Clostridium ragsdalei*. Acetogenic bacteria convert syngas to ethanol in a series of elementary chemical reactions through the Wood-Ljungdahl pathway, in a simple process that proceeds at mild temperature and pressure. The fermentation exhibited more than 80% conversion of both CO and H_2, which is required for energy conservation in the ethanol fuel. Syngas fermentation has commercial potential that requires demonstrated productivity, stability and economy to be realized. The economy of the fermentation process depends on medium design that delivers highly functional nutrition to the bacteria at very low cost; the function and requirement for each component supplied is considered in the method applied for medium design. As CO and H_2 are only slightly soluble in aqueous medium the transfer of these gases is quantified and the effects assessed to define appropriate level of mass transfer and develop methods of control to achieve highest rates and conversions of CO and H_2. Further, methods of analysis are presented that reveal the conditions of reaction at the enzyme sites inside the cell where the fermentation reactions occur. The integrated model of the fermentation simultaneously considers the mass balance, mass transfer, thermodynamics and culture kinetics in a novel concept of fermentation that is amenable to computer analysis, and essential for fermentation process design and control.

TABLE OF CONTENTS

Chapter Page

Chapter Page

Chapter Page

LIST OF TABLES

Table Page

LIST OF FIGURES

Figure Page

Figure Page

Figure Page

Figure Page

CHAPTER I

INTRODUCTION

World energy demand is expected to grow from 549 exajoule (EJ=10^{18} J) in 2010 to 812 EJ in 2035 per the U.S. Energy Information Administration's Annual Energy Outlook for 2012 (EIA, 2012a). The U.S. demand for transportation fuels is projected to grow from 29.1 EJ in 2012 to 30.2 EJ in 2035 (221 to 229 billion gallons of petroleum), and the EIA projects that petroleum use will decline slightly. Consumption of liquid biofuel will increase from 1.25 EJ in 2010 (0.46 billion gallons of biodiesel and 13.5 billion gallons of ethanol), to 3.64 EJ projected in 2035 (3.0 billion gallons of biodiesel and 24.4 billion gallons of ethanol). The use of biofuels is expected to help lower the annual emission of CO_2 from 6 billion tonnes discharged to the atmosphere in 2005, 2 billion tonnes from transportation fuel. The accounting of biofuels by the EIA includes Biomass-to-Liquids (BTL), biodiesel and ethanol. BTL includes pyrolysis oil and Fischer-Tropsch liquids, and the share of BTL is expected to rise from 0 to 1.194 EJ in 2035 (9.04 billion gallons of petroleum). Biodiesel is primarily produced from soybean oil, but will include distillate derived from non-food grade corn oil, fats and greases, and produced by cyanobacteria and algae according to the EIA's Biofuels Issues and Trends for 2012 (EIA, 2012b) with biodiesel contributing 0.041 EJ in 2010 and 0.268 EJ in

2035. The major portion of biofuels produced in the U.S. as per the EIA projection is from ethanol with consumption of 1.207 EJ in 2010 (13.5 billion gallons of ethanol per year) that is almost exclusively supplied from corn, and rising to 2.180 EJ in 2035 with 1.54 EJ from corn (17.2 billion gallons of ethanol per year) and 0.64 EJ projected to derive from cellulosic feedstock (7.2 billion gallons of ethanol per year). The land area of the State of Oklahoma at 1.81×10^{11} m^2 (69,898 mi^2) (Census, 2000) with an average solar input of 5.4 GJ/m^2 (WEC, 2012) can supply the biomass required to supply the U.S. transportation demand for biofuel, captured from 978 EJ of incident sunlight (equivalent to 10,900 billion gallons of ethanol per year).

The Department of Energy characterizes potential processes for production of biofuels in either a biochemical or thermochemical platform (EERE, 2012). The biochemical platform converts lignocellulosic materials to a mix of hexoses (six carbon sugars derived from cellulose), pentoses (five carbon sugars derived from hemicellulose), and a remnant of lignin. The sugars are cleaned and conditioned for fermentation by yeast or bacteria, and the lignin is usually burned in a combined heat and power (CHP) process to recover significant energy from the lignin. The thermochemical platform encompasses gasification of the lignocellulosic materials with air, O_2 and steam to form syngas, and indirect heating or pyrolysis of the lignocellulosic material to produce oils and tars that resemble petroleum. Either process uses the cellulose, hemicelluloses and lignin fractions of the biomass, and will also be coupled to a CHP process to increase energy recovery. Syngas fermentation is a hybrid thermochemical/biochemical platform that takes advantage of the simplicity of the gasification process, and the specificity of the fermentation process to deliver ethanol and potentially other chemicals. The hybrid

process bypasses many of the complex pretreatment steps required to acquire sugars from biomass, provides the simple precursors CO and H_2 for fermentation, and uses the robustness and adaptability of the acetogenic bacteria to reduce the requirements for gas cleaning and adjustment by the water gas shift required for catalytic conversion of syngas.

Acetogenic bacteria convert CO, H_2 and CO_2 derived from biomass or waste materials into acetic acid (Drake et al., 2008). Synthesis of lipids, proteins and other complex cell components from the simple inorganic gas substrates (CO, H_2 and CO_2) is supported by this production of acetic acid. The capability of some acetogens to convert acetic acid to other compounds, particularly ethanol, is the basis for production of biofuels. The acetogenic pathway is possibly as old as life on the earth (Ferry and House, 2006), and has been optimized by evolution to ensure the survival of species that produce acetyl-CoA from small molecules in the environment. Acetyl-CoA is an intermediate metabolite that is further converted to synthesize cell mass and complex chemicals, and yield organic acids and alcohols, particularly acetic acid and ethanol. Knowledge of the acetogenic mechanisms will support successful process design for energy conservation in biofuels production

Biomass is converted to ethanol through a hybridization of the thermochemical platform of gasification and the biological platform of fermentation (Wilkins and Atiyeh, 2011). Energy rich biomass and waste materials are converted by gasification with limited oxygen to producer gas, a mixture of carbon monoxide (CO), hydrogen (H_2), carbon dioxide (CO_2), nitrogen (N_2) that is residual from oxidizing air, and other minor components such as ammonia (NH_3), hydrogen sulfide (H_2S) and tars (Ahmed et al.,

2006). When the oxidizing agent used in gasification is O_2, the product is called synthesis gas (syngas) and the concentrations of CO and H_2 will be enriched. After cooling and cleaning the syngas, it is converted to acetic acid, ethanol and other products by autotrophic bacteria. A key point of interest in any conversion process is preserving the energy content of the feedstock in the final liquid fuel. Energy is expended in each production step. The solid biomass is heated to a high temperature for the gasification step using the heating value of the solid resource. Energy recovered from the syngas as steam and energy lost to the environment are also deducted from the heating value of the syngas produced. Energy diverted to cell growth and lost as heat from the fermenter is deducted from the heating value of the ethanol product. Unconverted syngas and unrecovered acetic acid contain energy diverted from the ethanol product. The economy of the fermentation process will be enhanced through small improvements in efficiency that conserve energy and increase ethanol yield.

The bacteria used in syngas fermentation belong to a group of prokaryotic single cell organisms termed "acetogens". Acetogens are defined by use of the acetyl-CoA pathway for each of three purposes (Drake et al., 2008)

- Reductive synthesis of acetyl coenzyme A from CO_2
- Energy conservation (for growth)
- Assimilation of CO_2 into biomass

The cellular mechanisms of acetogenesis are present and used by bacteria, archaea, and eukaryotes alike. Acetogens inhabit a wide range of ecosystems and have diverse capacities for substrate utilization and product formation, dependent on the growth environment.

Conversion of syngas to fuel and chemicals by acetogenic bacteria is a technology on the verge of commercial success (EIA, 2012). The use of dedicated biomass energy crops, waste biomass, and municipal and industrial wastes as feedstocks for energy and chemical synthesis promotes reuse and recycling of materials consumed in our society. This can establish a true cycle of renewable, carbon neutral, energy and chemical production. The ultimate source of energy and carbon in this process is the photosynthetic capture of CO_2 by plants driven by solar energy.

The proposed production of ethanol from syngas is an energy process, and the retention of energy from the feedstock in the final product is important to commercial viability. Knowledge of the mechanisms of the fermentation, the effect of nutrients on fermentation kinetics, the mass and energy transfers, and the capabilities of the bacterial culture is required to design effective bioreactors and process control. The proposed research will explore medium design, gas to liquid mass transfer and an integrated model that are important for design and operation of commercial syngas fermentation processes.

The conversion of CO, H_2 and CO_2 by acetogenic bacteria to acetic acid and ethanol via the acetyl-CoA pathway is a process affected by the conditions inside and outside the cell as depicted in Figure 1.1. The conditions are characterized by parameters such as pH, temperature, and concentrations of nutrients, reactants like CO, H_2 and CO_2, and products like acetic acid and ethanol. Mass transfer affects the availability of CO, H_2 and CO_2 inside the cells. Nutrients provide components necessary to build cell material and activate enzymes and affect culture kinetics. Additionally, the cell kinetics are affected by other operating conditions such as pH, temperature and gas composition, affecting the ratio of products. Therefore, each intermediate reaction, *in*

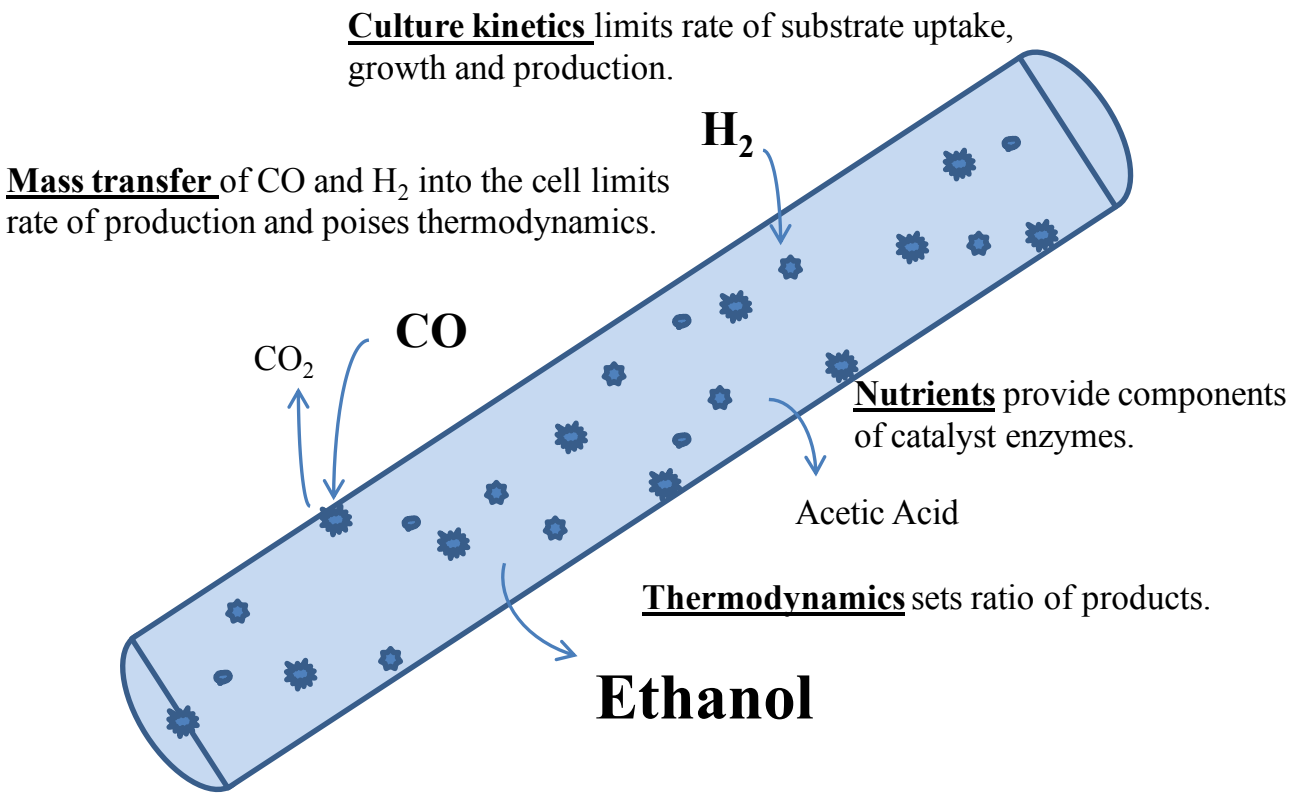

Figure 1.1 Major factors affecting syngas fermentation.

vivo, will depend on the concentration of its reactants and products. The concentrations of these intermediate metabolites define the individual reactions and connect the chain of reactions that determines the overall stoichiometry of production. The rate of each reaction in the acetyl-CoA pathway is determined by the concentrations of the metabolites involved and the kinetics of the enzymes constructed by the cell from the nutrients taken from the fermentation medium.

1.1 Medium Design

The acetogenic bacterial cell contains enzymes that support and perpetuate the fermentation reactions. Enzymes are constructed during cell growth from the syngas components and minerals, metals, vitamins and other nutrients supplied in the liquid medium. The bulk cell mass has an approximate composition which provides optimal culture activity. Excess and unnecessarily expensive nutrients included in the fermentation medium increase the cost of ethanol production and negatively affect process economics. When exploring cost reduction strategies, the function and requirement for each nutrient must be determined; this understanding will allow application of nutrient limitation for control of metabolic flux. Metabolic flux represents the internal distribution of carbon and energy through the pathways to the end products (Boghigian et al., 2010; Gheshlaghi et al., 2009). This distribution can be controlled to direct carbon and energy, as electrons, to production of a specific product, such as reduction of acetic acid to ethanol.

1.2 Mass Transfer

CO and H_2, the gases that carry energy to the process, are sparingly soluble in water and in the aqueous fermentation medium, and are consumed by active culture as

quickly as they are dissolved. These gases must be continuously replenished in the fermentation broth to maintain fast reaction rates. However, CO and H_2 are powerful reductants and can inhibit the activity of the cells when present near saturating concentrations. Appropriate supply of these reductant gases must be defined so that equipment and procedures can be designed to maintain activity in the fermenting culture. Increased mass transfer, alone, will not increase fermentation performance. A precise control of mass transfer of CO and H_2 to active cells will ensure their prolonged activity to make desired products.

Transfer of CO or H_2 from the gas into the liquid requires a concentration gradient across the stagnant liquid film at the gas/liquid interface. The rate of mass transfer will be the same as the rate of reaction, for both CO and H_2. A finite concentration of each gas will accumulate in the bulk liquid, and the resulting concentrations of CO, H_2 and CO_2 inside the cell determine the thermodynamic conditions of the fermentation and the product ratio. Syngas fermentation rate can be limited by either cell kinetics or mass transfer, but is optimal when these capabilities are balanced.

Syngas fermentation can be conducted in different types of reactors designed to promote mass transfer. The mass transfer capability of a trickle bed column reactor (TBR), a hollow fiber membrane reactor (HFR) and a continuously stirred tank reactor (CSTR) was determined and compared (Orgill et al., 2013). The study of mass transfer and fermentation in the CSTR is included in this workThe CSTR study included determination of overall mass transfer coeffient for transfer of O_2 into water ($k_{L,O2}a/V_L$) to establish capability of the CSTR to transfer CO H_2 and CO_2 in syngas fermentation.

1.3 Fermentation Model

The acetogenic fermentation transforms CO, H_2 and CO_2 to acetic acid by a series of elementary chemical reactions in the "Wood-Ljungdahl Pathway" or the "Acetyl CoA Pathway" (Ragsdale and Pierce, 2008). CO and CO_2 are converted to acetic acid and ethanol in sequenced enzymatic reactions using electrons derived from the reductant species, CO and H_2. The pathway reactions are defined in the literature, see Phillips et al. (1994) and Ragsdale (2008) and explained in more detail in Chapter 2 with the enzymes involved listed in Table 2.1. The defined reactions allow determination of directions and rates of mass flux, and thermodynamics. CO, H_2 and CO_2 are supplied from syngas by mass transfer into the bulk liquid, where cells consume the CO, H_2 and CO_2 in the defined series of reactions. Rates of these reactions are determined by the catalytic enzymes, and the end products are determined by the internal electrochemical potential of the cell. This potential is set by the balance of the rate of mass transfer and the rate of gas consumption by the cell. Many parameters can affect the fermentation results, and changing a single process parameter may cause multiple effects on the course of fermentation. Effective representation of fermentation *in silico* must simultaneously address the overall stoichiometry observed, mass transfer for CO, H_2 and CO_2, and reaction thermodynamics. Fermentation kinetics must be addressed at a gross fermentation scale using the specific (or per cell mass) rates for the culture tied to overall process parameters of pH, temperature, and substrate concentration in the cells; however, kinetic analysis should also include mass flux in the pathway circuits, and enzyme kinetics for specific reactions. Effective control algorithms must address mass transfer and culture kinetics in conversion of gas to the specified products. Application of

engineering analysis to the defined mass and energy flow makes syngas fermentation a unique laboratory for study of common fermentation mechanisms. The known mechanisms can be combined with data from the literature and experimentation to construct a computer model useful for analysis of syngas fermentation performance, design of process equipment, and formulation of process control.

1.4 Summary

Fermenter design, operating parameters and nutrients added in the medium can be used to establish control of the fermentation. The purpose of this research is to develop tools to aid commercialization of syngas fermentation. These tools are a method for production medium design, definition of mass transfer in a continuously stirred tank reactor (CSTR) and a model of syngas fermentation.

References

Ahmed, A., Cateni, B.G., Huhnke, R.L., Lewis, R.S. 2006. Effects of Biomass-Generated Producer Gas Constituents on Cell Growth, Product Distribution and Hydrogenase Activity of Clostridium Carboxidivorans P7(T). Biomass & Bioenergy, 30 (7), 665-672.

Bakker, A., Smith, J.M., Myers, K.J. 1994. How to Disperse Gases in Liquids. Chemical Engineering, 101 (12), 98-104.

Boghigian, B.A., Shi, H., Lee, K., Pfeifer, B.A. 2010. Utilizing Elementary Mode Analysis, Pathway Thermodynamics, and a Genetic Algorithm for Metabolic Flux Determination and Optimal Metabolic Network Design. Bmc Systems Biology, 4.

Census, U.S., 2000, http://www.census.gov/prod/cen2000/phc3-us-pt1.pdf#page=44, 11/6/2012

Drake, H.L., Gossner, A.S., Daniel, S.L. 2008. Old Acetogens, New Light. in: *Incredible Anaerobes: From Physiology to Genomics to Fuels*, (Eds.) J. Wiegel, R.J. Maier, M.W.W. Adams, Vol. 1125, pp. 100-128.

EERE, 2012, Biomass Multi-Year Program Plan, Washington, DC, http://www1.eere.energy.gov/biomass/pdfs/mypp_april_2012.pdf, 11/15/2012

EIA, 2012a, Annual Energy Outlook, Washington, D.C., http://www.eia.gov/forecasts/aeo/, 11/6/2012

EIA, 2012b, Biofuels Issues and Trends, Washington, D.C., http://www.eia.gov/biofuels/issuestrends/, 11/6/2012

Ferry, J.G., House, C.H. 2006. The Stepwise Evolution of Early Life Driven by Energy Conservation. Molecular Biology and Evolution, 23 (6), 1286-1292.

Gheshlaghi, R., Scharer, J.M., Moo-Young, M., Chou, C.P. 2009. Metabolic Pathways of Clostridia for Producing Butanol. Biotechnology Advances, 27 (6), 764-781.

Orgill, J.J., Atiyeh, H.K., Devarapalli, M., Phillips, J.R., Lewis, R.S., Huhnke, R.L. 2013. A Comparison of Mass Transfer Coefficients between Trickle-Bed, Hollow Fiber Membrane and Stirred Tank Reactors. Bioresource Technology, 133 (0), 340-346.

Phillips, J.R., Clausen, E.C., Gaddy, J.L. 1994. Synthesis Gas as Substrate for the Biological Production of Fuels and Chemicals. Applied Biochemistry and Biotechnology, 45-6, 145-157.

Ragsdale, S.W. 2008. Enzymology of the Wood-Ljungdahl Pathway of Acetogenesis. in: *Incredible Anaerobes: From Physiology to Genomics to Fuels*, (Eds.) J. Wiegel, R.J. Maier, M.W.W. Adams, Vol. 1125, pp. 129-136.

Ragsdale, S.W., Pierce, E. 2008. Acetogenesis and the Wood-Ljungdahl Pathway of CO_2 Fixation. Biochimica Et Biophysica Acta-Proteins and Proteomics, 1784 (12), 1873-1898.

WEC, 2012, World Energy Council, www.worldenergy.org, 11/6/2012.

Wilkins, M.R., Atiyeh, H.K. 2011. Microbial Production of Ethanol from Carbon Monoxide. Current Opinion in Biotechnology, 22 (3), 326-330.

CHAPTER II

LITERATURE REVIEW

2.1 Nomenclature

ABE – acetone butanol ethanol (fermentation)

Acetyl-CoA – acetyl coenzyme A

ACS – acetyl coenzyme A synthase (activity is associated with CODH enzyme)

ATP – adenosine triphosphate

CSTR – continuously stirred tank reactor

CoA or CoASH – coenzyme A

CODH – carbon monoxide dehydrogenase

F - Faraday constant (96.485 J/mV mol e^-)

FAD – flavin adenine dinucleotide oxidized

Fd_{Rd} – reduced ferredoxin (reduction requires with 2 e^-)

H_2ase – hydrogenase

$k_{L,i}a/V_L$ – volumetric mass transfer coefficient for gas i (i can represent O_2, CO, H_2 or CO_2)

k_L – liquid film mass transfer coefficient

a – area of the gas liquid interface

V_L – liquid volume into which gas is transferred

NADH – reduced nicotinamide adenine dinucleotide

NADPH – reduced nicotinamide adenine dinucleotide phosphate

R - gas constant (8.314 J/mol K)

T - temperature (K)

THF - tetrahydrofolate

Δp - protonmotive force (mV)

ΔpH - pH differential across the membrane

$\Delta \varphi$ - potential difference (mV) across the membrane

2.2 History of Autotrophic Acetogens

Acetogenesis was recognized in 1932 when production of acetic acid from H_2 and CO_2 by sewage sludge was reported (Fischer et al., 1932). Subsequently, Klass Wieringa (1936) isolated *Clostridium aceticum*, demonstrating synthesis of acetic acid from H_2/CO_2 with this pure culture. The type culture for acetogenesis, *Clostridium thermoaceticum*, reclassified and renamed as *Moorella thermoaceticum* (Collins et al., 1994), was isolated by Francis Fontaine (1942). Harland Wood and his student Lars Ljungdahl studied the acetyl-CoA pathway, providing definition of the incorporation of CO and of the tetrahydrofolate (THF) dependent reduction of CO_2 to a methyl group, in formation of acetyl-CoA. The acetyl-CoA pathway is also referred to as the Wood-Ljungdahl pathway of autotrophic growth. A detailed description of the history of discovery of acetogenesis is given in a review (Drake et al., 2008) and the enzymology is reviewed by Ragsdale (2008).

The production of alcohols from syngas was found for ethanol (Barik et al., 1988) and butanol (Worden et al., 1991). The process has been advanced near commercial

deployment by three companies, INEOS Bio (successor of Bioengineering Resources, Inc.), Coskata, Inc. and Lanza Tech (EIA, 2012). A fourth company, ZeaChem, produces acetic acid by syngas fermentation followed by catalytic production of ethanol.

2.3 Species and Habitat

Harold Drake (2008) cited 100 species of acetogens, from 22 genera in his review. These acetogens were of various morphologies (rods, cocci and spirochetes) with a wide range of temperature optima from 5 to 62^{o}C. These acetogens were isolated from habitats including soil, sewage sludge, feces, rumen fluid, sediments and industrial wastes. The pH conditions ranged from alkaline to acidic, and most habitats were not strictly anoxic. New species continue to be discovered, including moderately alkaliphilic acetogens that produce ethanol, for example *Alkalibaculum bacchi* represents yet another new genus and species (Allen et al., 2010; Liu et al., 2011).

The diversity and habitat of species of acetogens show the potential for additional species to be discovered. A range of fermentative capabilities may be expected from this diverse population, promising new products from syngas fermentation. Successful production using acetogens will likely use the conditions to which the strain has adapted through evolution. The natural environment would have a limited source of CO, if any; acetogens will have developed mechanisms that very effectively scavenge H_2 for reduction of CO_2 fixed in the autotrophic pathways. Nutrients essential to growth of functional cell mass are the object of competition between a consortium of bacteria and other organisms. Efficient mechanisms for nutrient uptake are required for the bacteria to thrive especially in the environment with very low nutrient concentrations. The mechanisms are optimized for energy conservation and growth of the acetogenic culture.

The optimized mechanisms represent an opportunity in fermentation processes to produce desired products when the mechanisms are defined.

2.4 Structure

Acetogens are found as rods, cocci and spirochetes, and can be either gram positive or gram negative (Drake et al., 2008). The typical ethanol producing acetogen is a rod shaped-gram positive motile bacterium that can form spores. *Clostridium carboxidivorans*, also known as strain P7, is described as

> "Gram-positive, motile rods (0.5 x 3 μm) occurring singly and in pairs. Cells rarely sporulate, but spores are subterminal to terminal with slight cell swelling. Obligate anaerobe with an optimum growth temperature of 38^{o}C and an optimum pH of 6.2. Grows autotrophically with H_2/CO_2 or CO and chemoorganotrophically …" (Liou et al., 2005)

The cell membrane is a phospholipid bilayer, embedded with proteins that mediate cell function (Cramer and Knaff, 1991) and enzymes of the acetyl-CoA pathway are closely associated with the cell membrane of acetogenic cells. There are 15 enzymes closely associated with the acetyl-CoA pathway (Ragsdale, 2008), see Table 2.1.

2.5 Pathway

The production of acetic acid and ethanol from syngas, CO, H_2 and CO_2, follows a sequenced set of elementary reactions as seen in Figure 2.1 (Phillips et al., 1994). Each reaction proceeds at an associated enzyme in a definite location within a cell, either free in the cytoplasm, tethered to the surface of the cell membrane or embedded in the membrane. Each cell acts independently, and the combined action of all cells sets the local conditions. Reactions inside cells are mediated by enzymes; each converts specific

reactants to specific products. The reactions inside the cell occur at local conditions of pH and chemical concentrations, which determine the activity of the enzymes and the form and availability of reactants. The simple inorganic chemical substrates CO, H_2 and CO_2, are transformed, step by step, to organic products such as acetic acid and ethanol. Some acetyl-CoA is diverted to form organic cell components, carbohydrates, proteins and lipids, however the majority of gas consumed provides energy for cell function, resulting in the formation of acetic acid and ethanol. The elementary reactions in the pathway sum to the overall stoichiometry of production as follows:

for production of acetic acid

$$4\,CO + 2\,H_2O \rightarrow CH_3COOH + 2\,CO_2 \quad (2.1)$$

$$4\,H_2 + 2\,CO_2 \rightarrow CH_3COOH + 2\,H_2O \quad (2.2)$$

and for production of ethanol

$$6\,CO + 3\,H_2O \rightarrow CH_3CH_2OH + 4\,CO_2 \quad (2.3)$$

$$6\,H_2 + 2\,CO_2 \rightarrow CH_3CH_2OH + 3\,H_2O \quad (2.4)$$

The overall stoichiometry is presented in a more general form in Appendix A. The details of the reactions in the acetyl-CoA pathway are discussed in the next section.

2.5.1 Production Reactions.

The acetyl-CoA (Wood-Ljungdahl) pathway has been defined over 70 years of research (Ragsdale, 2008) and is shown in Figure 2.1. Energy and carbon contained in syngas are used to produce acetyl-CoA. CO_2 is converted to a methyl cation in the tetrahydrofolate cycle, in a series of reactions that consume one ATP and 3 reducing equivalents (pairs of electrons and associated protons derived from CO or H_2). The methyl cation is transferred to acetyl-CoA synthase (ACS) via an enzyme that contains

cobalt (and is called the corrinoid/iron/sulfur protein, or CoFeSP). ACS combines the methyl cation with CO and Coenzyme A to form acetyl-CoA, which is either incorporated in cell components or released as acetic acid inside the cell. Conversion of acetyl-CoA to acetic acid via acetyl-phosphate replaces the ATP used in converting CO_2 to the methyl cation. Acetic acid can be released into the bulk liquid (by diffusion or facilitated diffusion) or reduced through acetaldehyde to ethanol consuming another 2 reducing equivalents. The enzymes acetaldehyde dehydrogenase and alcohol dehydrogenase that are required to reduce acetic acid to ethanol have been isolated from *Moorella thermoaceticum* (formerly *Clostridium thermoaceticum*) and *Clostridium formicoaceticum* (Fraisse and Simon, 1988; White et al., 1989). According to Fraisse (1988) and White (1989), and contrary to theory advanced from commercial acetone-butanol-ethanol (ABE) fermentation, acetic acid is converted directly to acetaldehyde and ATP is not consumed to form acetyl-CoA as precursor of acetaldehyde and ethanol. The aldehyde dehydrogenase and alcohol dehydrogenase were also found to be functional for reduction of other carboxylic acids to their respective alcohols, including reduction of butyric acid to butanol (White et al., 1989).

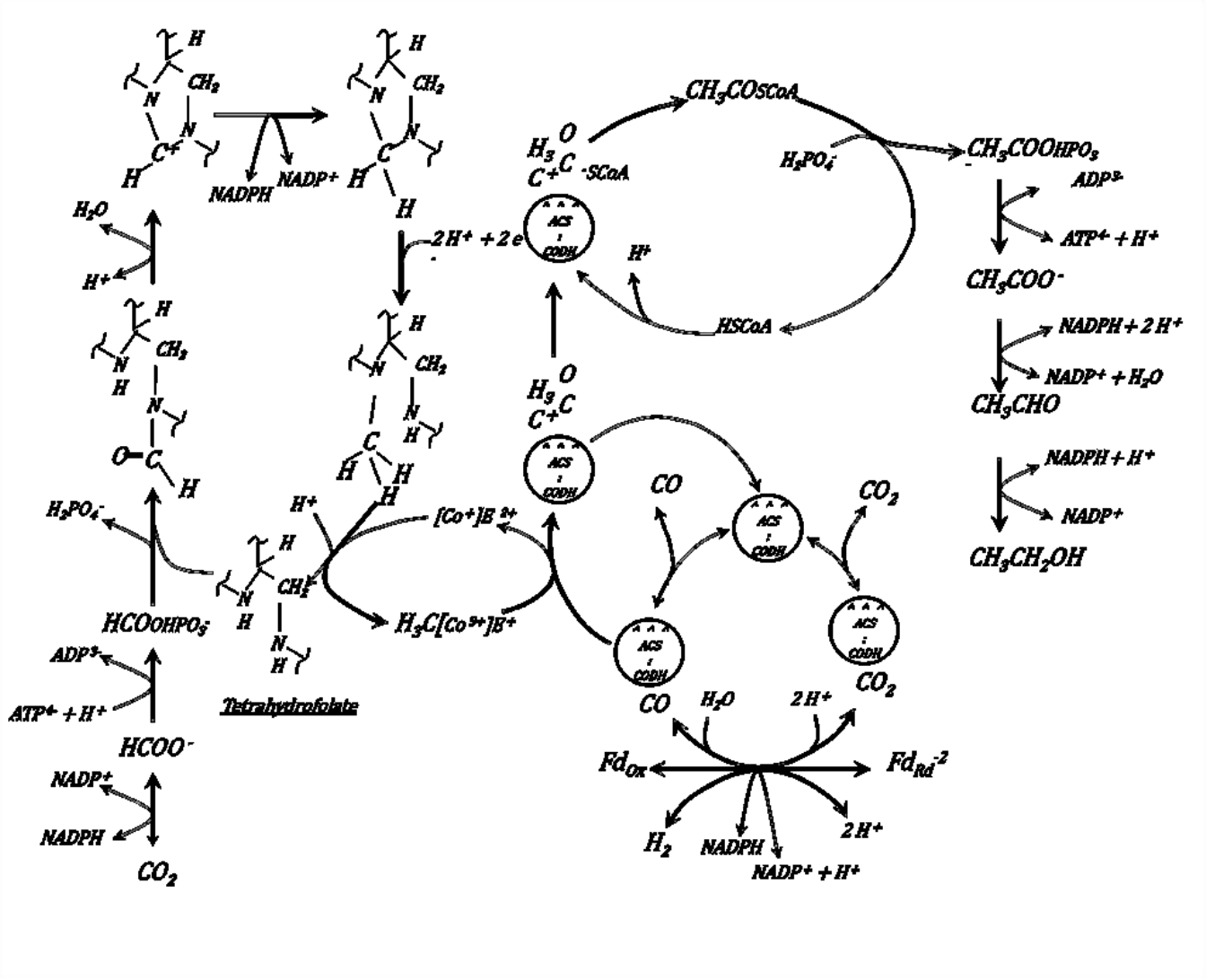

Figure 2.1 The Wood-Ljungdahl or Acetyl-CoA pathway (Phillips et al., 1994)

Carbon enters the pathway reactions as CO_2 or CO. CO_2 is required for formation of formate (Yamamoto et al., 1983), which is reduced on tetrahydrofolate to form the methyl group of acetyl-CoA. Key enzymes involved in the Wood-Ljungdahl pathway are listed in Table 2.1. The carbonyl of acetyl-CoA derives from CO bound to carbon monoxide dehydrogenase (CODH), transferred to the acetyl-CoA synthase (ACS) active site (Seravalli and Ragsdale, 2000) and condensed with the methyl group and coenzyme A to form acetyl-CoA (Figure 2.1).

Energy flow in the fermentation is effected by transfer of electrons (reducing equivalents). One pair of electrons ($2\ e^-$) is supplied for reaction in the cell by each CO oxidized on carbon monoxide dehydrogenase (CODH) or H_2 oxidized on hydrogenase (H_2ase); a pair of protons ($2\ H^+$) is released to the cytoplasm for each CO (Roberts et al., 1992) or H_2 (Ljungdhal, 1986) oxidized. The electrons are distributed to reaction sites within the cell by electron carriers like ferredoxin and NADH. Electrons from CODH and H_2ase are first transferred to the membrane associated clostridial ferredoxin (Shanmugasundaram and Wood, 1992), and then are transferred to other electron carriers like NADPH for use in pathway reactions and other cell function.

The protons released into the cytoplasm are consumed in the formation of acetyl-CoA, acetic acid and ethanol, maintaining the charge balance. One pair of protons is expelled from the cell for each acetyl-CoA formed. This pair of protons is carried across the membrane by an electron carrier containing flavin adenine dinucleotide (FAD), the electrons are transferred to another carrier and are used in the reduction of methylene-THF (tetrahydrofolate) to methyl-THF (Ljungdahl et al., 1980). The removal of the protons from the interior of the cell causes a differential of pH and electrochemical

potential across the membrane. Protons, as positively charged particles, are attracted to the more negatively charged interior of the cell and driven by the higher concentration of protons outside the cell (Ivey and Ljungdahl, 1986). This attractive force pulls protons through an ATP synthase and mechanically releases ATP from the enzyme. In Figure 2.1, one ATP is consumed in converting formate to formyl phosphate, and one ATP is recovered in conversion of acetyl phosphate to acetate. Product formation via the acetyl-CoA pathway yields no net ATP; in syngas fermentation, ATP is obtained only from the chemiosmotic mechanism of the ATP synthase (Ivey and Ljungdahl, 1986; Ragsdale, 1991).

Acetic acid is released from the acetate kinase enzyme to the cytoplasm (inside the cell) and is reduced to ethanol by carboxylic acid reductase (White et al., 1989), alcohol dehydrogenase and electron carriers like NADH that are not strongly associated with the membrane. Ethanol production is affected by the internal electrochemical potential of the cell, which is determined by the concentration of accumulated CO and H_2.

Table 2.1. Enzymes of the Wood Ljungdahl (Acetyl-CoA) Pathway

Enzyme	Reaction	Reference
Carbon monoxide dehydrogenase	$CO + 2\,H_2O \rightarrow CO_2 + 2\,\mathrm{H}^+ + 2\,\mathrm{e}^-$	(Roberts et al., 1992)
Hydrogenase	$H_2 \rightarrow 2\,\mathrm{H}^+ + 2\,\mathrm{e}^-$	(Ljungdhal, 1986)
Ferredoxin oxidoreductase	$Fd_{\mathrm{Rd}} \rightarrow Fd_{\mathrm{Ox}} + 2\,\mathrm{e}^-$	(Ragsdale et al., 1987)
Formate dehydrogenase	$CO_2 + \mathrm{NADPH} \rightarrow \mathrm{HCOO}^- + \mathrm{NADP}^+$	(Yamamoto et al., 1983)
Formate kinase	$\mathrm{HCOO}^- + \mathrm{ATP}^{4-} + \mathrm{H}^+ \rightarrow HCOOPO_3{}^- + \mathrm{ADP}^{3-}$	(Mejillano et al., 1989)
Formyl THF synthetase	$HCOOPO_3{}^- + \mathrm{THF} \rightarrow HCOTHF + HPO_4{}^{2-} + \mathrm{H}^+$	(Sun et al., 1969)
Methenyl THF cyclohydrolase	$HCOTHF + \mathrm{H}^+ \rightarrow HC^+THF + H_2O$	(Ljungdhal, 1986)
Methylene THF dehydrogenase	$HC^+THF + \mathrm{NADPH} \rightarrow H_2CTHF + NADP^+$	(Ljungdahl et al., 1980)
Methylene THF reductase	$H_2CTHF + 2H^+ + 2\mathrm{e}^- \rightarrow H_3CTHF$	(Park, 1991)
Methyl transferase	$H_3CTHF + H^+ + [\mathrm{Co}^+]\mathrm{E}^{2+} \rightarrow THF + H_3C[\mathrm{Co}^{3+}]\mathrm{E}^+$	(Ljungdhal, 1986)
Corrinoid-Iron-Sulfur Protein	$[\mathrm{Co}^+]\mathrm{E}^{2+}$	(Lu et al., 1990)
Acetyl-CoA Synthase	$H_3C[\mathrm{Co}^{3+}]\mathrm{E}^+ + CO + CoASH \rightarrow CH_3COSCoA + [\mathrm{Co}^+]\mathrm{E}^{2+} + H^+$	(Ragsdale, 2008)
Phosphotransacetylase	$CH_3COSCoA + HPO_4{}^{2-} + \mathrm{H}^+ \rightarrow CH_3COOHPO_3^- + \mathrm{CoASH}$	(Drake et al., 1981)
Acetate kinase	$CH_3COOHPO_3^- + \mathrm{ADP}^{3-} \rightarrow CH_3COO^- + ATP^{4-} + H^+$	(Drake et al., 1981)
Aldehyde dehydrogenase	$CH_3COO^- + \mathrm{NADPH} + 2H^+ \rightarrow CH_3CHO + NADP^+ + H_2O$	(White et al., 1989)
Alcohol dehydrogenase	$CH_3CHO + \mathrm{NADPH} + H^+ \rightarrow CH_3CH_2OH + NADP^+$	(Fraisse and Simon, 1988)

2.5.2 Key Oxidation/Reduction Reactions in the Acetyl-CoA Pathway.

Reactions that involve the transfer of electrons and protons are electrochemical reactions. Electrons are transferred from a reduced chemical as it is oxidized to a less reduced (or oxidized) chemical (Cramer and Knaff, 1991; Thauer et al., 1977). The reduced and oxidized forms of the electron donor, and the reduced and oxidized forms of the electron acceptor, are called a redox couple. The reaction releasing the oxidized form and a pair of electrons from the reduced form of the redox couple is called a "half cell reaction". Each half cell reaction (and redox couple) has a mid-point potential (expressed in mV) at which the concentrations of the reduced and oxidized forms are equal. CO_2/CO is a redox couple and the CO_2/CO half cell can be paired with the H_2 half cell. Mediated by ferredoxin in acetogens (Ragsdale et al., 1987), the combined half reactions comprise the "water gas shift" reaction, Equation 2.5. CO and H_2O can be converted to H_2 and CO_2 in this reversible reaction.

$$CO + H_2O \leftrightarrow CO_2 + H_2 \qquad 2.5$$

The elementary reactions of the pathway are balanced for charge and conserve elements when written correctly as in Figure 2.1. The chemical equations can be analyzed using the local conditions to establish thermodynamic relationships. Several important reactions of the pathway are characterized by paired electrochemical half-cell reactions. The electrons are supplied by the hydrogen (H^+/H_2) and CO_2/CO couples. Electrons are distributed to electron carriers such as ferredoxin (Fd_{Ox}/Fd_{Rd}) and nicotinamide adenine dinucleotide (NAD^+/NADH). In the terminal redox couple (CH_3COOH/CH_3CH_2OH) acetic acid is reduced to ethanol.

2.5.3 ATP and Cell Growth.

Autotrophic growth and production are dependent on transport of protons and electrons across the cell membrane to generate a protonmotive force that drives synthesis of ATP (Das and Ljungdahl, 1997). The protonmotive force consists of a pH differential plus a difference in electrochemical potential as shown in Equation 2.6 (Cramer and Knaff, 1991).

$$\Delta p = \Delta \varphi - \frac{2.3RT}{F}\Delta pH \qquad 2.6$$

Where Δp is the protonmotive force (mV) driving transfer of protons across the membrane, $\Delta \varphi$ is the potential difference (mV) across the membrane, ΔpH is the pH differential across the membrane, R is the gas constant (8.314 J/mol K), T is the temperature (K) and F is the Faraday constant (96.485 J/mV mol e^-).

The pH differential is formed by expulsion of protons outside of the cell in formation of the methyl group of acetyl-CoA. The potential difference is produced by oxidation inside the cell of the substrate gases, CO by CODH and H_2 by H_2ase, with reduction of electron carriers, including Fd, NAD, NADP and FAD. ATP for cell growth is produced when protons enter the cell through an ATP synthase, a protein cluster that spans the cell membrane and uses the mechanical energy of the protons to release ATP formed by combining ADP and phosphate bound to the ATP synthase enzyme.

2.6 Medium

Nutrient medium for bacterial growth is often designed for isolation of a pure species and growth of the isolated culture, further optimization is usually for the purpose of enhancing cell concentration (Saxena and Tanner, 2011). Low cost sources of nutrients, such as corn steep liquor and cotton seed extract, have been identified and

tested to reduce the cost of medium for production with some promising results with *C. ragsdalei* (Kundiyana et al., 2010; Maddipati et al., 2011). Growth rate can be increased dramatically by addition of nutrient rich components such as yeast extract and peptone; growth of *Clostridium ljungdahlii* was increased to as fast as a 3 hour doubling time for growth in peptone medium (Doyle, 1991). However, the initial fast growth was attributed to consumption of amino acids, and production of acetic acid or ethanol was detected in subsequent slower growth using some sugars or syngas. Growth of *C. ljungdahlii* in defined medium with less nutrients, having omitted the yeast extract, resulted in growth and increased production of ethanol (Phillips et al., 1993). The defined medium was the basis for methods of fermentation control in industrial application (Gaddy, 2007).

Medium used in commercial fermentation for fuel and bulk chemicals must have a minimal cost, yet support the required function and activity of the culture. Components purchased and added in the medium will have known function and quantity, and gross excess or nonfunctioning components will be eliminated. The medium formula used for growth of *C. ragsdalei*, also called *Clostridium* strain P11, was optimized for growth and maintenance in a microbiology laboratory (Saxena, 2008; Saxena and Tanner, 2011). The standard medium formulation (Saxena and Tanner, 2011) shown in Table 2.2, was entered in a spreadsheet. The cost of each component was tabulated using the research grade chemicals available in our laboratory as a basis, and a molar accounting was made of elemental nutrients supplied. In this accounting, yeast extract was the single chemically undefined component of the medium. The cost of this medium is $9.36 per

liter of medium, ten times the expected selling cost for ethanol (EIA, 2012). Lower cost nutrient medium is required to support commercial fermentation.

However, the designed medium must deliver cells that convert CO and H_2 at high rates, and remain active during the period of residence in the fermenter, 100 hours or more. The medium provides nitrogen (as ammonium) for production of proteins during cell growth. Sulfur is provided in reduced form (sulfide) to anchor metals that are the active sites of enzymes and as a component in proteins. Phosphate is used for energy transfer and metals (Ca, Mg, Fe, Ni, Zn, Mo, Se and W) are usually the active sites of enzymes. Vitamins required in cofactors, and not synthesized by the culture must be identified and included in the medium. The molar concentration of each element was scaled with a published composition of *Escherichia coli* (Bailey and Ollis, 1986) to calculate growth potential for each element in the *E. coli* analysis in Table 2.3. Elemental H, C and O are available in adequate supply from the syngas and the water in the medium. The estimated growth potential from the standard medium of Table 2.2 was 570 mg/L limited by Fe as shown in Table 2.3. Experiment with *C. ragsdalei* has demonstrated a maximum cell concentration of about 400 mg/L in the standard yeast extract medium (Maddipati et al., 2011).

Table 2.2 Composition and cost of standard yeast extract medium for *Clostridium ragsdalei* developed by Saxena (2008) and used as the base medium in the present study.

Component	Formula	Concentration	Cost[a]
		(mg/liter)	($/liter)
Yeast Extract	Undefined	1000	0.220
MES	$C_6H_{13}NO_4S.H_2O$	10000	8.600
Potassium Hydroxide	KOH	1165	0.137
Minerals			
Ammonium Chloride	NH_4Cl	3000	0.233
Calcium Chloride	$CaCl_2.2H_2O$	120	0.009
Magnesium Sulfate	$MgSO_4.7H_2O$	600	0.031
Potassium Chloride	KCl	300	0.020
Potassium Phosphate	KH_2PO_4	300	0.032
Trace Metals			
Cobalt Chloride	$CoCl_2.6H_2O$	2	0.0003
Ferrous Ammonium Sulfate	$FeH_{20}N_2O_{14}S_2$	8	0.0037
Manganese Sulfate	$MnSO_4.H_2O$	10	0.0014
Nickel Chloride	$NiCl_2.6H_2O$	2	0.0003
Nitrilotriacetic Acid	$C_6H_9NO_6$	20	0.0019
Sodium Molybdate	$Na_2MoO_4.2H_2O$	0.2	0.0001
Sodium Selenate	Na_2SeO_4	1	0.0014
Sodium Tungstate	$Na_2WO_4.2H_2O$	2	0.0009
Zinc Sulfate	$ZnSO_4.7H_2O$	10	0.0023
Vitamins			
Para-aminobenzoic Acid	$C_7H_7NO_2$	0.05	0.00002
Biotin	$C_{10}H_{16}N_2O_3S$	0.02	0.00157
Pantothenic Acid	$Ca(C_9H_{16}NO_5)_2$	0.05	0.00002
Folic Acid	$C_{19}H_{19}N_7O_6$	0.02	0.00005
MESNA	$C_2H_5NaO_3S_2$	0.10	0.00059
Nicotinic Acid	$C_6H_5NO_2$	0.05	0.00001
Pyridoxine	$C_8H_{11}NO_3.HCl$	0.10	0.00012
Riboflavin	$C_{17}H_{20}N_4O_6$	0.05	0.00003
Thiamine	$C_{12}H_{17}N_4OSCl.HCl$	0.05	0.00003
Thioctic Acid	$C_8H_{14}O_2S_2$	0.05.	0.00074
Cyanocobalamin	$C_{63}H_{88}CoN_{14}O_{14}P$	0.05	0.00217
Resazurin			
Resazurin	$C_{12}H_6NO_4Na$	1	0.010
Cysteine/Sulfide			
Cysteine	$C_3H_7NO_2S$	75	0.038
Sodium Sulfide	$Na_2S.9H_2O$	75	0.008
Total Cost per Liter			**$9.36**

[a]Cost was based on laboratory grade chemicals on 5/23/2011

Table 2.3 Summary of component elements and prediction of cell mass from standard yeast extract medium in Table 2.2.

Element	**% of Cell Dry Weight**[a]	**Predicted Cell Mass** (mg dry weight/L)
N	14.0	10,382
P	3.0	2,276
S	1.0	161,565
K	1.0	105,519
Na	1.0	1,493
Ca	0.5	6,544
Mg	0.5	11,836
Cl	0.5	442,366
Fe	0.2	570

[a] Based on elemental analysis of *E. coli* (Bailey and Ollis, 1986)

When cost of medium components and required concentration of the nutrients provided were compared, particular components targeted for elimination or reduction from the standard medium were MES, yeast extract, cysteine, potassium phosphate and magnesium sulfate. MES buffer costs $8.60 /L medium plus $0.14/L for KOH to charge the buffer. Cost of MES buffer was 93.5% of the medium cost. Ammonium chloride, a source of nutrient nitrogen, cost $0.23/L or 2.5% of the medium cost (Table 2.2), with predicted growth potential of 10,400 mg cells/L (Table 2.3). Yeast extract ($0.22/L), cysteine ($0.04/L), potassium phosphate ($0.03/L) and magnesium sulfate ($0.03/L) are also candidates for reduction.

The cell composition can be viewed as a functional stoichiometry of the cells, supplied by the nutrient medium. A nutrient limitation can be chosen to establish the rate limiting reaction in the pathway as a method to control metabolic flux in the fermentation and influence product specificity (Gaddy, 2007).

2.7 Mass Transfer

The low solubility of CO and H_2, the gases that provide the energy for syngas fermentation and the energy conserved in ethanol product, require that these gases be continually replenished in the fermentation broth to sustain production. The attainment of higher mass transfer represented in the volumetric mass transfer coefficients, $k_{L,CO}a/V_L$ and $k_{L,H2}a/V_L$ is of primary concern in most discussion of syngas fermentation (Munasinghe and Khanal, 2010). A model of syngas fermentation in the CSTR was developed to assess the potential for production of acetate (Vega et al., 1989), and mass transfer has been studied in various configurations of fermenters (Klasson et al., 1992b; Munasinghe and Khanal, 2010). Klasson (1992c), however, notes that the rate of mass transfer will not exceed the rate of reaction of the slightly soluble substrates, and that the applied mass transfer should balance the supply and consumption of CO and H_2.

2.8 Modeling of fermentation

Attempts to model syngas fermentation have correlated cell growth and productivity with the partial pressure of CO in the gas phase (Hurst and Lewis, 2010; Klasson et al., 1992a). The isolated focus on the CO concentration in the supply gas ignores both the presence of H_2 and CO_2 in the fermentation reactions, and the difference in concentration imposed by the transfer of each gas into the liquid phase. Growth of *C. ljingdahlii* on H_2/CO_2 (Phillips et al., 1994) shows H_2 to be a competent source of energy for growth and production in syngas fermentation. The requirement for CO_2 as carbon entering the methyl branch of the acetyl-CoA pathway in Figure 2.1 shows the importance of the CO_2 concentration in the production of acetyl-CoA and subsequent synthesis of acetic acid, ethanol and cell mass. Further, CO and H_2 are used together in

syngas fermentation (Phillips et al., 1993) and both provide electrons to the fermentation reactions. The supply of electrons from CO and H_2 are closely linked through ferredoxin, and the concentration of CO in the cell must be greatly reduced from the gas phase to achieve the inferred energetic equivalence with H_2. A single parameter model of syngas fermentation using CO partial pressure in the bulk gas is not adequate.

Production of acetic and butyric acids correlates with growth in the acetone butanol ethanol (ABE) fermentation and in fermentation of carbohydrates or syngas by acetogens. Solvent production in a stationary phase with little growth is attributed to loss of one ATP when butyryl-CoA is converted directly to butyraldehyde in butanol production (Worden et al., 1991) and when acetyl-CoA is converted directly to acetaldehyde in ethanol production (Rogers, 2006). These growth phenomena support a conceptual model of acidogenic growth and stationary alcohol production. Production via the acetyl-CoA pathway produces no ATP to support growth and avoids a net loss of ATP only if ethanol is derived from acetic acid as shown in Figure 2.1. Inspection of the Wood-Ljungdahl pathway extended to ethanol by Phillips (1994) suggests that the conceptual model of solvent production reported by Worden (Worden et al., 1991) and Rogers (2006) is not accurate in asserting direct reduction of the Coenzyme A derivative and loss of ATP.

Incorporation of the pathway to guide the mass balance will allow study of the mass flux through the cell's enzymes in production (Medema et al., 2012), and the inclusion of a thermodynamic analysis in the mass flux calculations can further enhance the utility of the mass flux analysis (Henry et al., 2007). The integration of the mass

balance, the mass transfer effects on concentration and the thermodynamic analysis allows a much clearer view of the conditions and mechanisms of the syngas fermentation.

References

Allen, T.D., Caldwell, M.E., Lawson, P.A., Huhnke, R.L., Tanner, R.S. 2010. Alkalibaculum Bacchi Gen. Nov., Sp. Nov., a Co-Oxidizing, Ethanol-Producing Acetogen Isolated from Livestock-Impacted Soil. International Journal of Systematic and Evolutionary Microbiology, 60, 2483-2489.

Bailey, J.E., Ollis, D.F. 1986. *Biochemical Engineering Fundamentals*. *2nd ed*. McGraw-Hill, New York,

Barik, S., Prieto, S., Harrison, S.B., Clausen, E.C., Gaddy, J.L. 1988. Biological Production of Alcohols from Coal through Indirect Liquefaction. Applied Biochemistry and Biotechnology, 18, 363-378.

Collins, M.D., Lawson, P.A., Willems, A., Cordoba, J.J., Fernandezgarayzabal, J., Garcia, P., Cai, J., Hippe, H., Farrow, J.A.E. 1994. The Phylogeny of the Genus Clostridium - Proposal of 5 New Genera and 11 New Species Combinations. International Journal of Systematic Bacteriology, 44 (4), 812-826.

Cramer, W.A., Knaff, D.B. 1991. Energy Transduction in Biological Membranes : A Textbook of Bioenergetics. Springer study ed. in: *Springer advanced texts in chemistry*, Springer-Verlag. New York, pp. xiv, 579 p.

Das, A., Ljungdahl, L.G. 1997. Composition and Primary Structure of the F1f0 Atp Synthase from the Obligately Anaerobic Bacterium Clostridium Thermoaceticum. Journal of Bacteriology, 179 (11), 3746-3755.

Doyle, M.L. 1991. Preferred Conditions for Growth and Product Formation by *Clostridium Ljungdahlii* Petc in Complex Media. University of Arkansas,

Drake, H.L., Gossner, A.S., Daniel, S.L. 2008. Old Acetogens, New Light. in: *Incredible Anaerobes: From Physiology to Genomics to Fuels*, (Eds.) J. Wiegel, R.J. Maier, M.W.W. Adams, Vol. 1125, pp. 100-128.

Drake, H.L., Hu, S.I., Wood, H.G. 1981. Purification of Five Components from Clostridium Thermoaceticum Which Catalyze Synthesis of Acetate from Pyruvate and Methyltetrahydrofolate. Properties of Phosphotransacetylase. Journal of Biological Chemistry, 256 (21), 11137-11144.

EIA, 2012, Biofuels Issues and Trends, Washington, D.C., http://www.eia.gov/biofuels/issuestrends/, 11/6/2012

Fischer, F., Lieske, R., Winzer, K. 1932. Biological Gas Reactions Ii Concerning the Formation of Acetic Acid in the Biological Conversion of Carbon Oxide and Carbonic Acid with Hydrogen to Methane. Biochemische Zeitschrift, 245, 2-12.

Fontaine, F.E. 1942. A New Type of Glucose Fermentation by *Clostridium Thermoaceticum* N. Sp. Journal of Bacteriology, 43, 700-715.

Fraisse, L., Simon, H. 1988. Observations on the Reduction of Non-Activated Carboxylates by Clostridium-Formicoaceticum with Carbon-Monoxide or Formate and the Influence of Various Viologens. Archives of Microbiology, 150 (4), 381-386.

Gaddy, J.L., D. K. Arora, C-W Ko, J. R. Phillips, R. Basu, C. V. Wikstrom and E. C. Clausen. 2007. Methods for Increasing the Production of Ethanol from Microbial Fermentation. 7285402.

Henry, C.S., Broadbelt, L.J., Hatzimanikatis, V. 2007. Thermodynamics-Based Metabolic Flux Analysis. Biophysical Journal, 92 (5), 1792-1805.

Hurst, K.M., Lewis, R.S. 2010. Carbon Monoxide Partial Pressure Effects on the Metabolic Process of Syngas Fermentation. Biochemical Engineering Journal, 48 (2), 159-165.

Ivey, D.M., Ljungdahl, L.G. 1986. Purification and Characterization of the F1-Atpase from Clostridium Thermoaceticum. J. Bacteriol., 165 (1), 252-257.

Klasson, K.T., Ackerson, C.M.D., Clausen, E.C., Gaddy, J.L. 1992a. Biological Conversion of Synthesis Gas into Fuels. International Journal of Hydrogen Energy, 17 (4), 281-288.

Klasson, K.T., Ackerson, M.D., Clausen, E.C., Gaddy, J.L. 1992b. Mass-Transport in Bioreactors for Coal Synthesis Gas Fermentation. Abstracts of Papers of the American Chemical Society, 204, 125-FUEL.

Kundiyana, D.K., Huhnke, R.L., Maddipati, P., Atiyeh, H.K., Wilkins, M.R. 2010. Feasibility of Incorporating Cotton Seed Extract in Clostridium Strain P11 Fermentation Medium During Synthesis Gas Fermentation. Bioresource Technology, 101 (24), 9673-9680.

Liou, J.S.-C., Balkwill, D.L., Drake, G.R., Tanner, R.S. 2005. Clostridium Carboxidivorans Sp. Nov., a Solvent-Producing Clostridium Isolated from an Agricultural Settling Lagoon, and Reclassification of the Acetogen Clostridium Scatologenes Strain Sl1 as Clostridium Drakei Sp. Nov. International Journal of Systematic and Evolutionary Microbiology, 55 (5), 2085-2091.

Liu, K., Atiyeh, H.K., Tanner, R.S., Wilkins, M.R., Huhnke, R.L. 2011. Fermentative Production of Ethanol from Syngas Using Novel Moderately Alkaliphilic Strains of Alkalibaculum Bacchi.

Ljungdahl, L.G., O'Brien, W.E., Moore, M.R., Liu, M.-T. 1980. [83] Methylenetetrahydrofolate Dehydrogenase from Clostridium Formicoaceticum and Methylenetetrahydrofolate Dehydrogenase, Methenyltetrahydrofolate

Cyclohydrolase (Combined) from Clostridium Thermoaceticum. in: *Methods in Enzymology*, (Ed.) L.D.W. Donald B. McCormick, Vol. Volume 66, Academic Press, pp. 599-609.

Ljungdhal, L.G. 1986. The Autotrophic Pathway of Acetate Synthesis in Acetogenic Bacteria. Annual Review of Microbiology, 40 (1), 415-450.

Lu, W.P., Harder, S.R., Ragsdale, S.W. 1990. Controlled Potential Enzymology of Methyl Transfer Reactions Involved in Acetyl-Coa Synthesis by Co Dehydrogenase and the Corrinoid/Iron-Sulfur Protein from Clostridium Thermoaceticum. Journal of Biological Chemistry, 265 (6), 3124-3133.

Maddipati, P., Atiyeh, H.K., Bellmer, D.D., Huhnke, R.L. 2011. Ethanol Production from Syngas by Clostridium Strain P11 Using Corn Steep Liquor as a Nutrient Replacement to Yeast Extract. Bioresource Technology, 102 (11), 6494-6501.

Medema, M.H., van Raaphorst, R., Takano, E., Breitling, R. 2012. Computational Tools for the Synthetic Design of Biochemical Pathways. Nature Reviews Microbiology, 10 (3), 191-202.

Mejillano, M.R., Jahansouz, H., Matsunaga, T.O., Kenyon, G.L., Himes, R.H. 1989. Formation and Utilization of Formyl Phosphate by N10-Formyltetrahydrofolate Synthetase: Evidence for Formyl Phosphate as an Intermediate in the Reaction. Biochemistry, 28 (12), 5136-5145.

Munasinghe, P.C., Khanal, S.K. 2010. Syngas Fermentation to Biofuel: Evaluation of Carbon Monoxide Mass Transfer Coefficient (K(L)a) in Different Reactor Configurations. Biotechnology Progress, 26 (6), 1616-1621.

Park, E.Y., J.E. Clark, D.V. DeVartanian and L.G. Ljungdahl. 1991. 5,10-Methylenetetrahydrofolate Reductases: Iron-Sulfur-Zinc Flavoproteins. in: *Chemistry and Biochemistry of Flavoenzymes*, (Ed.) F. Müller, Vol. 1, CRC Press. Boca Raton, pp. 389-400.

Phillips, J.R., Clausen, E.C., Gaddy, J.L. 1994. Synthesis Gas as Substrate for the Biological Production of Fuels and Chemicals. Applied Biochemistry and Biotechnology, 45-6, 145-157.

Phillips, J.R., Klasson, K.T., Clausen, E.C., Gaddy, J.L. 1993. Biological Production of Ethanol from Coal Synthesis Gas - Medium Development Studies. Applied Biochemistry and Biotechnology, 39, 559-571.

Ragsdale, S.W. 1991. Enzymology of the Acetyl-Coa Pathway of Co2 Fixation. Critical Reviews in Biochemistry and Molecular Biology, 26 (3-4), 261-300.

Ragsdale, S.W. 2008. Enzymology of the Wood-Ljungdahl Pathway of Acetogenesis. in: *Incredible Anaerobes: From Physiology to Genomics to Fuels*, (Eds.) J. Wiegel, R.J. Maier, M.W.W. Adams, Vol. 1125, pp. 129-136.

Ragsdale, S.W., Lindahl, P.A., Münck, E. 1987. Mössbauer, Epr, and Optical Studies of the Corrinoid/Iron-Sulfur Protein Involved in the Synthesis of Acetyl Coenzyme a by Clostridium Thermoaceticum. Journal of Biological Chemistry, 262 (29), 14289-14297.

Roberts, J.R., Lu, W.P., Ragsdale, S.W. 1992. Acetyl-Coenzyme a Synthesis from Methyltetrahydrofolate, Co, and Coenzyme a by Enzymes Purified from Clostridium Thermoaceticum: Attainment of in Vivo Rates and Identification of Rate-Limiting Steps. J. Bacteriol., 174 (14), 4667-4676.

Rogers, P., J-S Chen and M. J. Zidwick. 2006. Organic Acid and Solvent Production. in: *The Prokaryotes*, (Eds.) M. Dworkin, S. Falkow, E. Rosenberg, K.-H. Schleifer, E. Stackebrandt, Springer New York, pp. 511-755.

Saxena, J. 2008. Development of an Optimized and Cost-Effective Medium for Ethanol Production by *Clostridium* Strain P11. Dissertation. University of Oklahoma, 131.

Saxena, J., Tanner, R.S. 2011. Effect of Trace Metals on Ethanol Production from Synthesis Gas by the Ethanologenic Acetogen, Clostridium Ragsdalei. Journal of Industrial Microbiology & Biotechnology, 38 (4), 513-521.

Seravalli, J., Ragsdale, S.W. 2000. Channeling of Carbon Monoxide During Anaerobic Carbon Dioxide Fixation†. Biochemistry, 39 (6), 1274-1277.

Shanmugasundaram, T., Wood, H.G. 1992. Interaction of Ferredoxin with Carbon Monoxide Dehydrogenase from Clostridium Thermoaceticum. Journal of Biological Chemistry, 267 (2), 897-900.

Sun, A.Y., Ljungdahl, L., Wood, H.G. 1969. Total Synthesis of Acetate from Co2 Ii. Purification and Properties of Formyltetrahydrofolate Synthetase from Clostridium Thermoaceticum. J. Bacteriol., 98 (2), 842-844.

Thauer, R.K., Jungermann, K., Decker, K. 1977. Energy Conservation in Chemotrophic Anaerobic Bacteria. Microbiol. Mol. Biol. Rev., 41 (1), 100-180.

Vega, J.L., Antorrena, G.M., Clausen, E.C., Gaddy, J.L. 1989. Study of Gaseous Substrate Fermentations: Carbon Monoxide Conversion to Acetate. 2. Continuous Culture. Biotechnology and Bioengineering, 34 (6), 785-793.

White, H., Strobl, G., Feicht, R., Simon, H. 1989. Carboxylic Acid Reductase: A New Tungsten Enzyme Catalyses the Reduction of Non-Activated Carboxylic Acids to Aldehydes. European Journal of Biochemistry, 184 (1), 89-96.

Wieringa, K.T. 1936. Over Het Verwijnenvan Waterstofen Koolzuur Onder Anaerobe Voorwaarden. Antonie Leeuwenhoek, 3, 263-273.

Worden, R.M., Grethlein, A.J., Jain, M.K., Datta, R. 1991. Production of Butanol and Ethanol from Synthesis Gas Via Fermentation. Fuel, 70 (5), 615-619.

Yamamoto, I., Saiki, T., Liu, S.M., Ljungdahl, L.G. 1983. Purification and Properties of Nadp-Dependent Formate Dehydrogenase from Clostridium Thermoaceticum, a Tungsten-Selenium-Iron Protein. Journal of Biological Chemistry, 258 (3), 1826-1832.

CHAPTER III

OBJECTIVES

The proposed research will provide a working theory or conceptual model of the syngas fermentation as a basis for experimental design and planning in the ongoing research. The methods developed and the concepts of cellular mechanisms defined for the syngas fermentation are expected to be useful in research and process development in other fermentations for production of biofuels and chemicals. Mathematical description of the mechanisms of the conceptual model will provide a basis for process design in the commercial development and application of the syngas fermentation process.

3.1 Medium Design

The objective of the medium design study in Chapter 4 was to reduce the cost of production medium and show that *C. ragsdalei* can be used in economically viable syngas fermentation. This was done through successive revisions of medium composition to demonstrate the competency of the medium and identify functional requirements for specific components.

3.2 Mass Transfer

The objective of mass transfer studies in theis work is to understand and quantify the effect of mass transfer on the syngas fermentation. Mass transfer of CO, H_2 and CO_2

is defined in serum bottle fermentations in Chapter 5, including description of the rate limiting factors in batch syngas fermentation, effect of gas pressure and liquid volume on mass transfer and derivation of thermodynamic parameters from the fermentation data. The mass transfer capacity of the laboratory stirred tank fermenter (CSTR) was defined by O_2 transfer into water in Chapter 6, a correlation was developed for the volumetric mass transfer coefficient for O_2 transfer ($k_{L,O2}a/V_L$) and mass transfer into fermentation medium and water was compared. The mass transfer of CO, H_2 and CO_2 into syngas fermentation in the CSTR is presented in Chapter 7; control techniques and analysis methods were developed to establish the mass transfer required to maximize conversion of CO and H_2, maintain high activity of the culture, and attain reduction of acid species to alcohol.

3.3 Modeling

The objective of the modeling study in Chapter 8 was to develop a conceptual model for syngas fermentation that combines mass transfer and thermodynamic analysis to describe the conditions inside the cell using measured parameters during fermentation. The simulation of fermentation *in silico*, once validated, will allow fast and inexpensive testing of alternative control strategies, aid in the analysis of experimental data, and provide a basis for process design and control. Spreadsheet analysis of thermodynamic and mass transfer parameters for the fermentation data from serum bottle and CSTR fermentations predicted the intracellular gas concentrations and intracellular pH and ORP. The predictions of the model were used to guide CSTR operation presented in Chapter 7.

CHAPTER IV

METHOD FOR DESIGN OF PRODUCTION MEDIUM FOR FERMENTATION OF SYNTHESIS GAS TO ETHANOL BY ACETOGENIC BACTERIA

Note, this section was written for submission to *The Journal of Biological Engineering* and the format is dictated by the Journal's style.

4.1 Abstract

Biomass and waste materials can be converted to ethanol fuel by gasification and fermentation using acetogenic bacteria, such as *Clostridium ragsdalei*. Fuel ethanol is a high volume, low cost commodity, so capital and operating expenses must be very low to achieve profitable operation. The fermentation medium supplies minerals, metals and organic co-factors needed to build biomass and the functional enzyme platform that conducts the production reactions. Research directed toward commercial deployment of fermentation processes must consider cost and availability of medium components, and use economically viable medium. The cost and function of fermentation medium components compared to an approximate elemental composition of *E. coli* was used to assess potential of the medium for commercial use. This assessment was used to develop production medium for syngas fermentation to produce ethanol with *C. ragsdalei*. Cost of medium was reduced from $9.36/L to $0.25/L. Additional cost reduction can be achieved by eliminating components that are not required, using commercial components

purchased at bulk commodity prices, using H_2S and NH_3 from the syngas production in lieu of purchased sodium sulfide and ammonium chloride, and retaining the acetate buffer from ethanol distillation. These savings can reduce the medium cost below $0.01/L or $0.01 per gram of cells produced.

4.2 Keywords

Ethanol, syngas, biofuel, acetogen, *Clostridium*, fermentation, medium, cost, medium design

4.3 Background

Fossil carbon, particularly petroleum, has provided fuel and raw material to drive an economic and technological explosion over the last 150 years (EIA, 2012). World economies are based on fossil carbon technologies, and are entrenched in their use. Recent recognition of dwindling supply of these resources, and of the ecological damage wrought by release of CO_2 from the fossil carbon, has kindled interest in developing sustainable energy and chemical production from biomass that captures energy from the sun and CO_2 from the atmosphere. A key step in many processes to derive fuel and chemicals from biomass is fermentation, in which microbial organisms convert plant matter into useful products. One of these processes, synthesis gas fermentation, uses autotrophic acetogenic bacteria, typically of the genus *Clostridium*, to produce acetic acid and ethanol from carbon monoxide (CO) and hydrogen (H_2). CO and H_2 are formed in partial combustion or gasification of plant matter or waste materials (Kumar et al., 2009). The bacteria convert CO and H_2 to acetic acid and ethanol through a series of enzymatic

reactions in the Wood-Ljungdahl or Acetyl-CoA pathway (Phillips et al., 1994; Ragsdale, 2008). Each reaction in the pathway, as well as reactions that build cell materials, is promoted by an enzyme that typically contains metal ions, proteins and other organic cofactors that allow the reaction to proceed at reasonable rates under physiological conditions of temperature and pressure. Hydrogen, carbon and energy to build the carbohydrate structure of the cells can be completely derived from CO and H_2 in the synthesis gas, as reported for *Clostridium ljungdahlii* (Phillips et al., 1993) where sulfur was supplied as sulfide (S^{-2}) and the only required organic components were small amounts of the vitamins pantothenate, biotin and thiamine. The minerals, metals and organic cofactors that comprise the enzymes and biocatalyst cells are supplied in an aqueous medium solution.

Fuels and bulk chemicals are produced in high volumes for sale at low prices with small marginal profits. The low cost is essential, as use of these materials support commercial manufacturing and other economic and recreational activities. The cost of the aqueous medium is one of many operating costs associated with the fermentation process; others are capital cost of equipment, utility costs, labor costs and cost of feedstock. High cost of technically competent fermentation medium, alone, will cause the process to fail economically. The Biomass Program of the DOE (EERE, 2012) projects 2012 target feedstock cost of $0.195/L ($0.74/gal) ethanol for corn stover digestion to sugar and fermentation with plant operating costs of $0.372/L ($1.41/gal) to give a minimum selling price of $0.568/L ($2.15/gal). The cost allocated for saccharification and fermentation is $0.053/L ($0.20/gal) of ethanol. The cost of

fermentation medium can be only a fraction of this fermentation cost, less than $0.01/L of medium.

The base medium used with *Clostridium ragsdalei* was formulated for growth and isolation (Saxena, 2008; Saxena and Tanner, 2011), but was not optimized as an economic production medium. Previous studies at Oklahoma State University have used *C. ragsdalei*, also called Strain P11, in fermentation of syngas to produce ethanol (Kundiyana et al., 2010; Kundiyana et al., 2011; Maddipati et al., 2011). These studies substituted less expensive materials, such as corn steep liquor and cotton seed extract, for yeast extract in the fermentation medium and eliminated other medium components. Elimination of yeast extract in earlier studies with *C. ljungdahlii* (Phillips et al., 1993) increased ethanol production and left a chemically defined medium that was analyzed using a published elemental composition for *Escherichia coli* (Bailey and Ollis, 1986) to identify limiting and excess nutrients. Reformulation of the medium allowed increased growth and production of high concentrations of ethanol (20 to 48 g/L). Manipulation of the medium components provides a basis for commercial fermentation control (Gaddy, 2007).

Productivity, grams product per liter of fermenter per day (g/L d), is proportional to the concentration and activity of cells in fermentation. In the present study, the base medium for *C. ragsdalei* was reviewed using the *E. coli* model composition and systematically modified to identify the function and requirement for each component with the purpose to achieve higher cell concentrations and maintain activity in the synthesis gas fermentation. The cost of each component was also monitored to target expensive components for elimination and reduction. The overall goal of the work was

to design a medium appropriate in cost and function for commercial deployment of syngas fermentation using *C. ragsdalei* and extension of the method to other organisms and fermentations.

4.4 Methods

4.4.1 Microbial Catalyst and Culture Medium

Clostridium ragsdalei strain P11 was grown in 250 mL serum bottles (Wheaton, Millville, NJ), stoppered and crimp sealed containing 100 mL of fresh medium under 236 kPa (absolute) of syngas. The initial composition of syngas was 20 mole percent CO, 5% H_2, 15% CO_2 and 60% N_2 (20:5:15 CO:H_2:CO_2 syngas, Stillwater Steel Supply Company, OK, USA). Gas was replaced when the CO concentration in the headspace dropped below 5%, or the H_2 concentration dropped below 3%. A syngas source pressure of 236 kPa was used to replace the gas in the bottle headspace.

4.4.2 Medium Preparation

The standard yeast extract medium was used for maintenance of *C. ragsdalei* strain P11 as previously reported (Saxena, 2008). The medium contained yeast extract (Difco Laboratories, Detroit, MI), MES buffer (morpholino-ethane-sulfonic acid), minerals, trace metals, vitamins and resazurin as a redox indicator as shown in Table 4.1. All chemicals were purchased from Sigma-Aldrich (St. Louis, MO, USA) except yeast extract. The components of the standard yeast extract medium (base medium) and other media used in this study are shown in Table 4.2.

Medium components were dissolved in deionized water in a 1 L round bottom flask, the pH was adjusted to 6.0 to charge the MES buffer by addition of 2N KOH, and the medium just brought to a boil in a microwave to free dissolved gases, particularly O_2.

Table 4.1 Composition and cost of standard yeast extract medium developed by Saxena (2008) used as the base medium in the present study.

Component	Formula	Concentration	Cost[a]
		(mg/L)	($/L)
Yeast Extract	Undefined	1000	0.220
MES	$C_6H_{13}NO_4S.H_2O$	10000	8.600
Potassium Hydroxide	KOH	1165	0.137
Minerals			
Ammonium Chloride	NH_4Cl	3000	0.233
Calcium Chloride	$CaCl_2.2H_2O$	120	0.009
Magnesium Sulfate	$MgSO_4.7H_2O$	600	0.031
Potassium Chloride	KCl	300	0.020
Potassium Phosphate	KH_2PO_4	300	0.032
Trace Metals			
Cobalt Chloride	$CoCl_2.6H_2O$	2	0.0003
Ferrous Ammonium Sulfate	$FeH_{20}N_2O_{14}S_2$	8	0.0037
Manganese Sulfate	$MnSO_4.H_2O$	10	0.0014
Nickel Chloride	$NiCl_2.6H_2O$	2	0.0003
Nitrilotriacetic Acid	$C_6H_9NO_6$	20	0.0019
Sodium Molybdate	$Na_2MoO_4.2H_2O$	0.2	0.0001
Sodium Selenate	Na_2SeO_4	1	0.0014
Sodium Tungstate	$Na_2WO_4.2H_2O$	2	0.0009
Zinc Sulfate	$ZnSO_4.7H_2O$	10	0.0023
Vitamins			
Para-aminobenzoic Acid	$C_7H_7NO_2$	0.05	0.00002
Biotin	$C_{10}H_{16}N_2O_3S$	0.02	0.00157
Pantothenic Acid	$Ca(C_9H_{16}NO_5)_2$	0.05	0.00002
Folic Acid	$C_{19}H_{19}N_7O_6$	0.02	0.00005
MESNA	$C_2H_5NaO_3S_2$	0.10	0.00059
Nicotinic Acid	$C_6H_5NO_2$	0.05	0.00001
Pyridoxine	$C_8H_{11}NO_3.HCl$	0.10	0.00012
Riboflavin	$C_{17}H_{20}N_4O_6$	0.05	0.00003
Thiamine	$C_{12}H_{17}N_4OSCl.HCl$	0.05	0.00003
Thioctic Acid	$C_8H_{14}O_2S_2$	0.05.	0.00074
Cyanocobalamin	$C_{63}H_{88}CoN_{14}O_{14}P$	0.05	0.00217
Resazurin			
Resazurin	$C_{12}H_6NO_4Na$	1	0.010
Cysteine/Sulfide			
Cysteine	$C_3H_7NO_2S$	75	0.038
Sodium Sulfide	$Na_2S.9H_2O$	75	0.008
Total Cost per Liter			**$9.36**

[a]Cost was based on laboratory grade chemicals on 5/23/2011

Table 4.2 Composition of media used.

Medium	Base[a]	E3	E4	E5
Dry Components	**g/L**	**g/L**	**g/L**	**g/L**
Yeast Extract	1	1	0	0
MES Buffer	10	0	0	0
Stock Solutions	**mL/L**	**mL/L**	**mL/L**	**mL/L**
2 N KOH	10.38	0	0	0
Minerals	30	30	30	30[b]
Trace Metals	10	10	10	10
Vitamins	10	10	10	10
0.1% Resazurin	1	1	1	1
2.5% Cysteine/2.5% Sulfide	3	3	3	S^{2-} only
Total Cost ($/liter)	$9.36	$0.72	$0.50	$0.25

[a] Standard yeast extract medium developed by (Saxena, 2008)

[b] Detailed composition of Medium E5 including revised minerals are shown in Table 4.3.

The hot medium solution was purged with N_2 bubbled from a cannula into the liquid to remove residual O_2. A second N_2 purge was maintained in the headspace to ensure anoxic conditions as the medium cooled and was dispensed. Serum bottles were purged with N_2 to remove air. A No. 1 butyl rubber stopper (VWR Scientific, Radnor, PA, USA) was secured with a 30 mm aluminum crimp cap (Wheaton,Millville, NJ, USA). The bottles filled with the medium were autoclaved for 20 minutes at 121°C. The bottles were prepared for inoculation by replacing the N_2 in the headspace with 20:5:15 $CO:H_2:CO_2$ syngas to 134 kPa absolute, adding 0.3 mL of a solution containing 2.5% cysteine (w/v) and 2.5% sodium sulfide per 100 mL of medium, and shaken at 37°C until the bottles were warm and the pink color of the resazurin had disappeared.

4.4.3 Culture Inoculation

C. ragsdalei was initially grown in the standard yeast extract base medium. It was then transferred into revised medium with cumulative deletions and revisions to approach a minimized composition as shown in Table 4.2. Bottles were inoculated with 10 ml or 10% (v/v) of a culture that had been inoculated one week before. The inoculum

Table 4.3 Composition and cost of medium E5

Component	Formula	Concentration	Cost
		(mg/L)	($/L)
Yeast Extract	Undefined	0	0
MES	$C_6H_{13}NO_4S.H_2O$	0	0
Potassium Hydroxide	KOH	0	0
Sodium Bicarbonate	$NaHCO_3$	1750	0.099
Minerals			
Ammonium Chloride	NH_4Cl	1000	0.078
Calcium Chloride	$CaCl_2.2H_2O$	40	0.003
Magnesium Sulfate	$MgSO_4.7H_2O$	60	0.003
Potassium Chloride	KCl	0	0
Potassium Phosphate	KH_2PO_4	300	0.032
Trace Metals			
Cobalt Chloride	$CoCl_2.6H_2O$	2	0.0003
Ferrous Ammonium Sulfate	$FeH_{20}N_2O_{14}S_2$	8	0.0037
Manganese Sulfate	$MnSO_4.H_2O$	10	0.0014
Nickel Chloride	$NiCl_2.6H_2O$	2	0.0003
Nitrilotriacetic Acid	$C_6H_9NO_6$	20	0.0019
Sodium Molybdate	$Na_2MoO_4.2H_2O$	0.2	0.0001
Sodium Selenate	Na_2SeO_4	1	0.0014
Sodium Tungstate	$Na_2WO_4.2H_2O$	2	0.0009
Zinc Sulfate	$ZnSO_4.7H_2O$	10	0.0023
Vitamins			
Para-aminobenzoic Acid	$C_7H_7NO_2$	0.05	0.00002
Biotin	$C_{10}H_{16}N_2O_3S$	0.02	0.00157
Pantothenic Acid	$Ca(C_9H_{16}NO_5)_2$	0.05	0.00002
Folic Acid	$C_{19}H_{19}N_7O_6$	0.02	0.00005
MESNA	$C_2H_5NaO_3S_2$	0.10	0.00059
Nicotinic Acid	$C_6H_5NO_2$	0.05	0.00001
Pyridoxine	$C_8H_{11}NO_3.HCl$	0.10	0.00012
Riboflavin	$C_{17}H_{20}N_4O_6$	0.05	0.00003
Thiamine	$C_{12}H_{17}N_4OSCl.HCl$	0.05	0.00003
Thioctic Acid	$C_8H_{14}O_2S_2$	0.05.	0.00074
Cyanocobalamin	$C_{63}H_{88}CoN_{14}O_{14}P$	0.05	0.00217
Resazurin			
Resazurin	$C_{12}H_6NO_4Na$	1	0.010
Cysteine/Sulfide			
Cysteine	$C_3H_7NO_2S$	0	0
Sodium Sulfide	$Na_2S.9H_2O$	75	0.008
Total Cost per Liter			**$0.250**

typically exhibited cell growth and gas consumption, and was transferred into medium retaining the cumulative reductions, omissions and previous revisions in a progression from the standard medium. This procedure gave a progressive definition of the medium to minimize cost. The freshly inoculated bottles were filled to 236 kPa with 20:5:15 $CO:H_2:CO_2$ syngas, and placed upright on an orbital shaker (Innova 2100, New Brunswick Scientific, Enfield, CT, USA) at 150 rpm and 37^{o}C. Bottles were typically inoculated in triplicate.

Removal of the MES buffer, and the KOH that charged the buffer, allowed the pH to fall rapidly as acetic acid was produced in fermentation. Fermentation pH below 4.3 adversely affects the activity of *C. ragsdalei* with formation of floc from dispersed cells and slows gas uptake and production. This phenomenon was recognized and attributed to pH late in this series of fermentations. If the inoculum pH was low, the fresh fermentation would start with pH below 5.0 and would exhibit longer lag phase or fail. Culture activity can be sustained by sterile addition of 0.5 to 1% (v/v) of 7% $NaHCO_3$ solution as the fermentation pH approaches 4.5, and before transfer of inoculum. The purpose is to prevent pH from falling below 4.4 in operating fermentation and to maintain freshly inoculated fermentation near pH 5.0. The $NaHCO_3$ neutralizes a portion of the acetic acid produced and forms an acetate buffer with pK_a of 4.76, which stabilizes pH in the appropriate operating range between 4.5 and 5.0.

4.4.4 Sampling and Analysis

Each bottle was sampled on days 3, 4, 5, 6 and 7 following inoculation, and daily through a second week. Bottles were at times sampled more frequently, as seen for the base medium in Figure 4.1. Liquid samples were analyzed for pH and concentrations of

cells, ethanol and acetic acid. Cell concentration was determined as optical density (1.0 OD unit is approximately 0.4 g dry cell weight per liter) measured at 660 nm in a Cary 50 Bio UV-Vis spectrophotometer (Palo Alto, CA, USA). Liquid product concentrations were determined from a sample centrifuged (Fisher Scientific, Pittsburgh, PA, USA) for 10 min at 13,000 rpm to remove cells. Supernatant was mixed with an equal part of 0.085 M HCl to ensure all acetate was converted to the volatile free acetic acid form. The liquid sample was analyzed using a GC (Agilent Technologies, Wilmington, DE, USA) with a DB-FFAP capillary column (Agilent Technologies, Wilmington, DE, USA) and quantitation using a flame ionization detector (FID). Chromatograms were analyzed using the ChemStation data analysis software.

4.4.5 Data Management, Nutrient and Cost Accounting

Data was collected, plotted and derivative quantities calculated using Microsoft Excel. Composition of the medium was followed in a spreadsheet with concentrations of each component tabulated. The cost of the overall medium was calculated using prices for the chemical used in the laboratory. Prices were updated May 23, 2011 from the supplier's website. The molar concentrations of bio-available elements were tabulated for each medium composition, and the molar accounting for the base medium is shown as an example in Table 4.4. A published composition of the bacteria *E. coli* (Bailey and Ollis, 1986; Phillips et al., 1993) was used to estimate growth potential afforded by each element as in Table 4.5, using the element's mass percent from the *E. coli* analysis and the mass concentration of the element in the developed medium. The elemental growth potentials were used to assess the relative limitations imposed by the nutrients supplied.

Table 4.4. Elemental accounting for base medium.

Formula	Component	N	P	S	K	Na	Ca	Mg	Cl
	(mM)	(mM)	(mM)	(mM)	(mM)	(mM)	(mM)	(mM)	(mM)
$C_6H_{13}NO_4S.H_2O$	46.9	46.9		46.9					
KOH	20.8				20.8				
$NaHCO_3$	0					0			
NH_4Cl	56.1	56.1							56.1
$CaCl_2.2H_2O$	0.8						0.8		1.6
$MgSO_4.7H_2O$	2.4			2.4[a]				2.4	
KCl	4.0				4.0				4.0
KH_2PO_4	2.2		2.2		2.2				
$CoCl_2.6H_2O$	0.008								0.02
$FeH_{20}N_2O_{14}S_2$	0.020	0.041		0.08[a]					
$MnSO_4.H_2O$	0.059			0.06[a]					
$NiCl_2.6H_2O$	0.008								0.02
$C_6H_9NO_6$	0.105	0.105							
$Na_2MoO_4.2H_2O$	0.001					0.00			
Na_2SeO_4	0.005					0.01			
$Na_2WO_4.2H_2O$	0.006					0.01			
$ZnSO_4.7H_2O$	0.035			0.04[a]					
$C_7H_7NO_2$	0.000365	0.000							
$C_{10}H_{16}N_2O_3S$	0.000082	0.000	0.000						
$Ca(C_9H_{16}NO_5)_2$	0.000105	0.000					0.000		
$C_{19}H_{19}N_7O_6$	0.000045	0.000							
$C_2H_5NaO_3S_2$	0.000609					0.001			
$C_6H_5NO_2$	0.000406	0.000							
$C_8H_{11}NO_3.HCl$	0.000486	0.000							0.000
$C_{17}H_{20}N_4O_6$	0.000133	0.001							
$C_{12}H_{17}N_4OSCl.HCl$	0.000148	0.001							0.000
$C_8H_{14}O_2S_2$	0.000242			0.000					
$C_{63}H_{88}CoN_{14}O_{14}P$	0.000037	0.001	0.000						
$C_{12}H_6NO_4Na$	0.003981	0.004				0.004			
$C_3H_7NO_2S$	0.619	0.62		0.62					
$Na_2S.9H_2O$	0.312			0.31		0.62			
Element Total	(mM)	**103.8**	**2.2**	**47.8**[a]	**27.0**	**0.65**	**0.82**	**2.43**	**62.4**
Element Total	(mg/l)	1454	68	1531	1055	15	33	59	2212

[a] SO_4^{2-} is deemed not available to the acetogenic culture, and is not included in the total for calculation of growth potential.

Table 4.4 Continued. Elemental accounting for base medium.

Formula	Component	Fe	Co	Mn	Ni	Mo	Se	W	Zn
	(mM)	(mM)	(mM)	(mM)	(mM)	(mM)	(mM)	(mM)	(mM)
$C_6H_{13}NO_4S.H_2O$	46.9								
KOH	20.8								
$NaHCO_3$	0								
NH_4Cl	56.1								
$CaCl_2.2H_2O$	0.8								
$MgSO_4.7H_2O$	2.4								
KCl	4.0								
KH_2PO_4	2.2								
$CoCl_2.6H_2O$	0.008		0.008						
$FeH_{20}N_2O_{14}S_2$	0.020	0.020							
$MnSO_4.H_2O$	0.059			0.059					
$NiCl_2.6H_2O$	0.008				0.008				
$C_6H_9NO_6$	0.105								
$Na_2MoO_4.2H_2O$	0.001					0.001			
Na_2SeO_4	0.005						0.005		
$Na_2WO_4.2H_2O$	0.006							0.006	
$ZnSO_4.7H_2O$	0.035								0.035
$C_7H_7NO_2$	0.000365								
$C_{10}H_{16}N_2O_3S$	0.00008								
$Ca(C_9H_{16}NO_5)_2$	0.000105								
$C_{19}H_{19}N_7O_6$	0.000045								
$C_2H_5NaO_3S_2$	0.000609								
$C_6H_5NO_2$	0.000406								
$C_8H_{11}NO_3.HCl$	0.000486								
$C_{17}H_{20}N_4O_6$	0.000133								
$C_{12}H_{17}N_4OSCl.HCl$	0.000148								
$C_8H_{14}O_2S_2$	0.000242								
$C_{63}H_{88}CoN_{14}O_{14}P$	0.000037		0.000						
$C_{12}H_6NO_4Na$	0.003981								
$C_3H_7NO_2S$	0.619								
$Na_2S.9H_2O$	0.312								
Element Total	(mM)	**0.020**	**0.008**	**0.059**	**0.008**	**0.001**	**0.005**	**0.006**	**0.035**
Element Total	(mg/l)	1.14	0.498	3.25	0.494	0.079	0.418	1.12	2.27

Table 4.5. Summary of component elements and prediction of cell mass from standard yeast extract medium in Table 4.4.

Element	% of Cell Dry Weight[a]	Predicted Cell Mass mg dry weight/L
N	14.0	10,382
P	3.0	2,276
S	1.0	161,565
K	1.0	105,519
Na	1.0	1,493
Ca	0.5	6,544
Mg	0.5	11,836
Cl	0.5	442,366
Fe	0.2	570

[a] Based on elemental analysis of *E. coli* (Bailey and Ollis, 1986)

The spreadsheet was used to choose the order of revision of medium components and to track the progression of the medium design and reduction of cost.

4.5 Results

4.5.1 Base Medium

The course of a typical bottle fermentation using the base medium and a model producer gas (20% CO, 5% H_2, 15% CO_2 and 60% N_2, 20:5:15 CO:H_2:CO_2 syngas) is shown in Figure 4.1. Serum bottles were inoculated and first sampled after 50 h to accommodate a typical lag phase. Growth of *C. ragsdalei* starts and proceeds until some limiting condition is established; this is indicated by no further increase in cell mass concentration. Product formation accompanies gas consumption with initial production of acetic acid, which causes the pH to fall. Ethanol is produced only after the pH is below 5 (Figure 4.1). The base medium supported growth of *C. ragsdalei* to 0.60 OD_{660} (0.24 g/L) as seen in Figure 4.1, and was expected to support growth up to 0.57 g/L

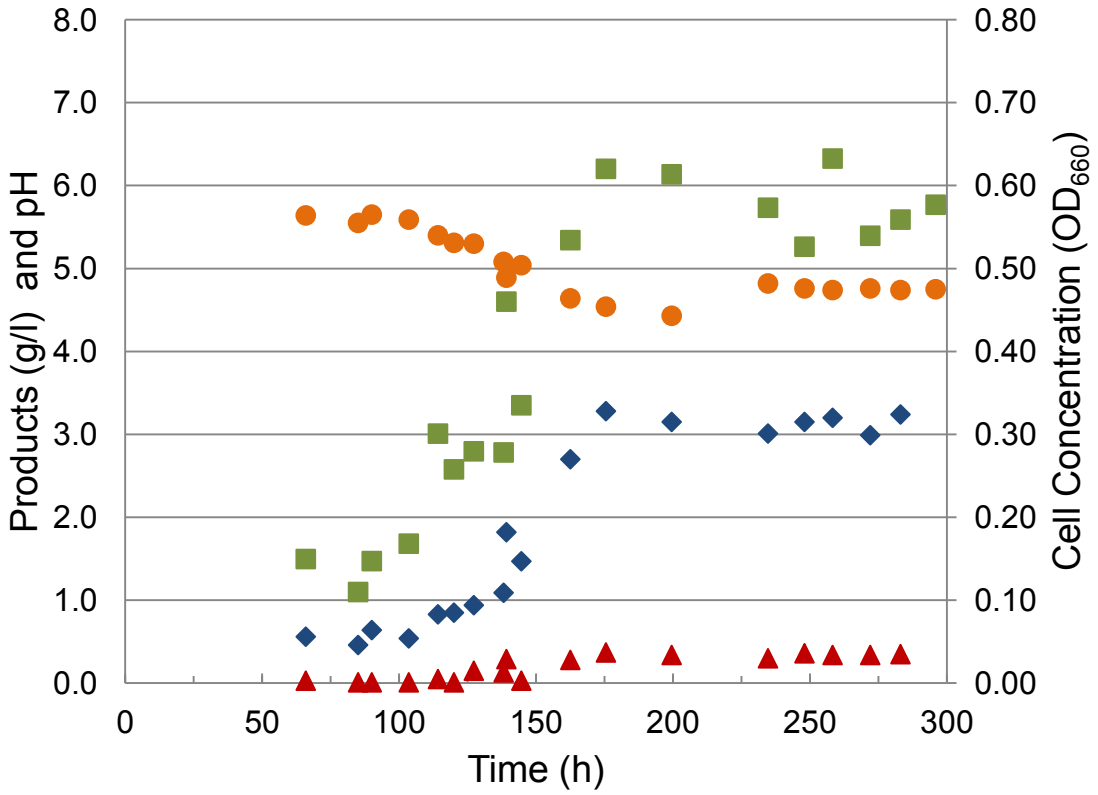

Figure 4.1 Course of fermentation for *C. ragsdalei* in microbial maintenance (base) medium. ● pH, ◆ Acetic acid, ▲ Ethanol, ■ Cells

based on the elemental analysis shown in Table 4.5. The predicted limiting elemental nutrient from Table 4.5 is Fe, which is a component of many enzymes and cofactors in acetogenic growth and production (Ragsdale, 2008).

The base medium is buffered using morpholinoethanesulfonic acid (MES) to maintain pH near the pK_a for MES of 6.1. The MES buffer capacity is proportional to the concentration of MES used, and potassium hydroxide (KOH) is used to charge the buffer to pH 6.0 by neutralizing a portion of the MES, which is added in the acid form. CO_2 from the initial charge of syngas is absorbed into the liquid, reacting to produce bicarbonate (HCO_3^-) and consuming the MES buffer as the pH drops to 5.8 prior to inoculation. The pH is lowered further to below 5.0 before *C. ragsdalei* begins to

produce the favored product ethanol. The cost of the MES and the KOH to charge the buffer is 93% of the total base medium cost (Table 4.1).

4.5.2 Medium E3

The omission of MES in the medium E3 (Table 4.2) is an obvious first step along the path to a low cost production medium. The course of fermentation using the medium without MES is shown in Figure 4.2. Growth and production are similar to that in the base medium, but initial pH is lower around 5.0 and pH drops quickly to near 4.0. The drop in pH limited cell growth and stopped cell function after 162 h. Medium E3 costs \$0.72/L, but cell growth in medium E3 without pH control did not exceed 0.46 OD_{660} (0.18 g/L), only 75% of growth seen in the base medium.

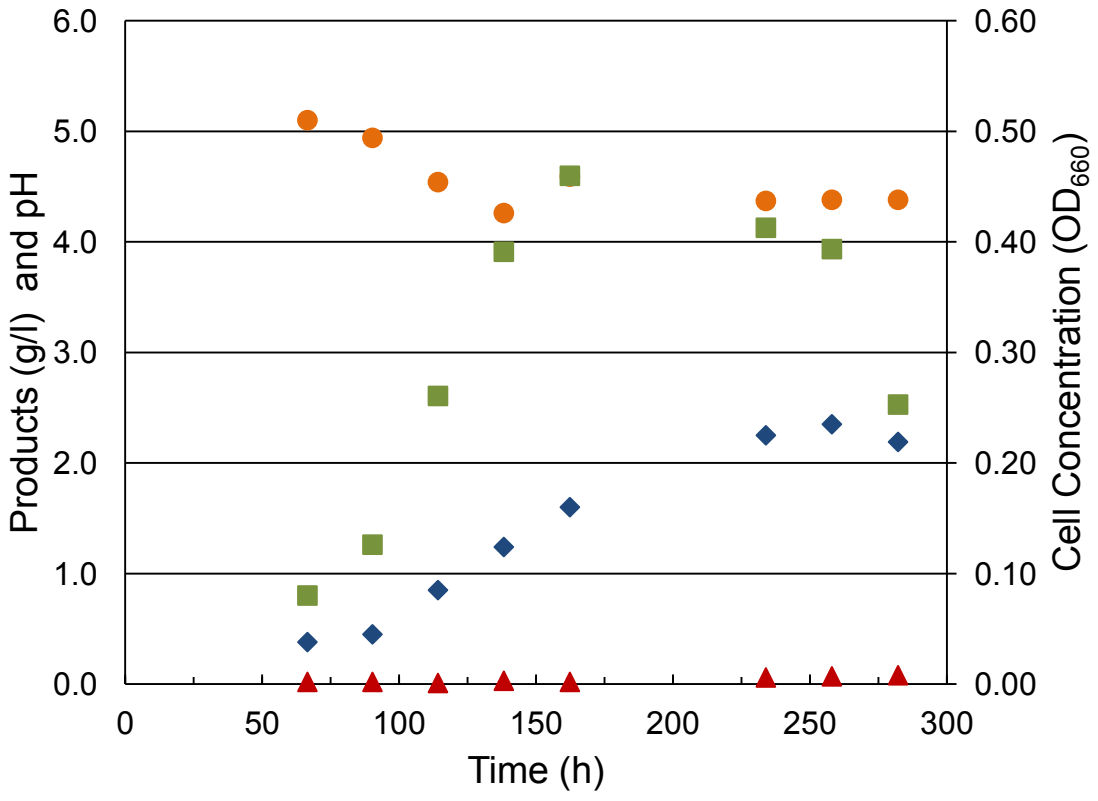

Figure 4.2 Course of fermentation for *C. ragsdalei* in medium without buffer, Medium E3 ● pH, ◆ Acetic acid, ▲ Ethanol, ■ Cells

Activity of *C. ragsdalei* is greatly reduced below pH 4.5, and formation of a buffer to stabilize the fermentation pH between 4.5 and 5.0 is needed. Acetic acid, with pK_a equal to 4.75, is produced from CO and H_2 in the syngas and forms the appropriate buffer when neutralized with an inexpensive mineral base such as sodium bicarbonate. Adjustment of pH in bottle fermentation using 0.5 to 1.0 ml of 7% (w/v) $NaHCO_3$ solution into 100 ml of fermentation broth, as needed to maintain pH above 4.5, became standard practice late in this study. The acetate buffer is a low cost replacement for MES, and is a byproduct of the fermentation. Figure 4.2 shows pH adjustment after 138 h (the pH symbol is coincident with the cell mass symbol at 162 h), but pH at 138 h is 4.26 and the effect of low pH is already inactivating the culture. The E3 medium with pH controlled above 4.5 supports growth and production of ethanol and acetic acid equivalent to the base medium (data not shown).

4.5.3 Medium E4

The composition of medium E4, which does not contain yeast extract is shown in Table 4.2. Yeast extract is an undefined growth promoter often used as a nutrient to support growth of microbial cultures, and represents 31% of the cost of the E3 medium. The approximate composition of yeast extract is available from Difco (Becton-Dickinson, 2006). Yeast extract provides minerals, metals, vitamins and carbohydrates, including proteins and free amino acids. Protein is up to 80% of the cell dry weight (Bailey and Ollis, 1986), and peptides and amino acids taken up by the cell can be incorporated directly into cell mass. Incorporation of amino acids should enhance growth rate and cell concentration, but requires little energy input that is provided by the syngas conversion to

ethanol and acetic acid. Energy from CO or H_2 is required for growth as OD_{660} did not increase on yeast extract alone in bottles inoculated without CO or H_2 (data not shown).

Syngas fermentation with *C. ragsdalei* in medium without both MES and yeast extract, medium E4 in Table 4.2, started quickly, but stopped early as pH dropped near 4.0 in the medium without buffer or pH control (Figure 4.3). Yeast extract at 1 g/L in the medium represented $0.22/L of medium or 31% of the cost of the E3 medium. This cost alone is prohibitive in production medium. Lastly, omission of yeast extract leaves the medium chemically defined and amenable to analysis of nutrient yields and kinetic contribution for individual nutrients.

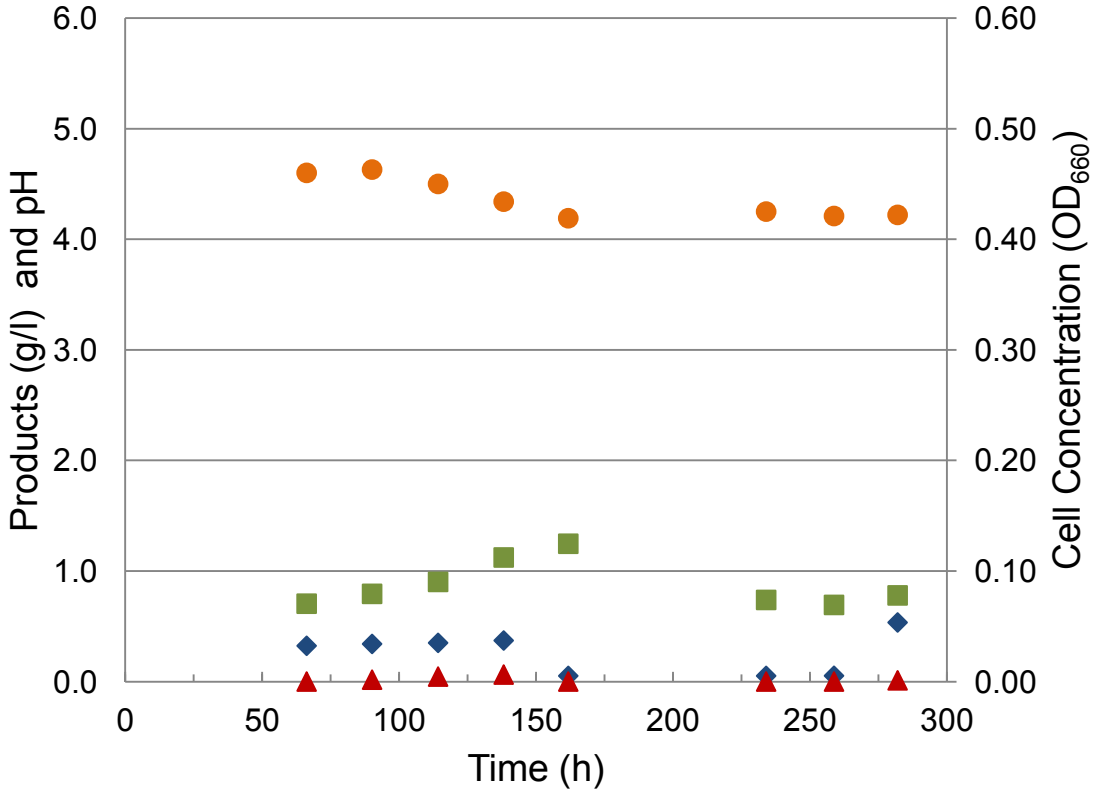

Figure 4.3 Course of fermentation for *C. ragsdalei* in medium with no buffer and no yeast extract (E4) medium ● pH, ◆ Acetic acid, ▲ Ethanol, ■ Cells

4.5.4 Medium E5

Inorganic nutrients present in the base medium at concentrations greater than 20 mM were added for convenience in a single mineral stock solution. These chemicals included NH_4^+, Ca^{2+}, Mg^{2+}, K^+ and PO_4^{3-}. The cost of the minerals solution added accounted for 36% of the E4 medium cost ($0.325/L), with 46% of the medium cost from NH_4Cl alone. The *E. coli* analysis (Table 4.5) showed these species to be imbalanced when compared to the expected growth limiting component, Fe^{2+}. Growth potential in the base medium for nitrogen (N) was 18 times that for Fe^{2+}; for K^+ 185 times, for Ca^{2+} 11 times and for Mg^{2+} 21 times the growth potential for Fe^{2+}. Growth potential expected for P was 4 times Fe^{2+} and from the reduced sulfur 5 times when sulfur from MES and sulfate was excluded. The mineral stock solution for medium E5 was revised to remove these excesses and balance the growth potential of the medium. This medium formulation, shown in Table 4.3, used the revised minerals solution and was used with the elimination of cysteine.

Sulfur added as sulfate (SO_4^{2-}) is not expected to be available to the acetogenic culture due to its high degree of oxidation. Growth potential of nutrient sulfur should be estimated from concentration of reduced sulfur, practically limited to the concentration of cysteine and sulfide. Cysteine is an amino acid that contains reduced sulfur, and is often added to anaerobic fermentation media as a reducing agent to scavenge O_2. However, cysteine and sulfide, the inorganic reduced form of sulfur, provide nutrient sulfur essential to formation of cell proteins and enzyme function. The active centers of many enzymes are metal ions that are coordinated by cysteine and sulfide bonds (Ragsdale, 1991). Cysteine costs 2.5 times per mole compared to sulfide, and sulfide as H_2S is a

typical contaminant in production of syngas and so may be available at no additional cost above the feedstock. When sulfate is not considered and all nutrient sulfur is taken from cysteine and sulfide, the base medium should support 5 times the growth capacity predicted for the base medium in Table 4.5 and omission of cysteine (67% of the reduced sulfur) should leave sufficient sulfur to support growth. Bottle fermentations using *C. ragsdalei* with only sulfide, reduced minerals, and no MES or yeast extract, medium E5 in Table 4.2, grew when the initial pH was higher than 5.0 (see Figure 4.4). This condition was reached when extra 2.5% sulfide solution was added inadvertently in preparation of one of triplicate bottles, and subsequently repeated. Sodium sulfide is a very strong base, but the start of growth with more sulfide was deemed to be from increased initial pH only when the impact of buffer formation and pH control was recognized.

Reliance on sulfide as the source of nutrient sulfur significantly reduces the cost of the medium, by \$0.04 per liter or 7.6% of the cost of E4 medium. *C. ragsdalei* can use sulfide as the sole source of nutrient sulfur. The resulting medium costs \$0.25/L, including \$0.10/L for $NaHCO_3$ to form an acetate buffer. Fermentation with *C. ragsdalei* in the E5 medium showed lower growth and the lag phase varied between E5 bottles with low growth limited by pH in the bottles, the course of fermentation is shown in Figure 4.4.

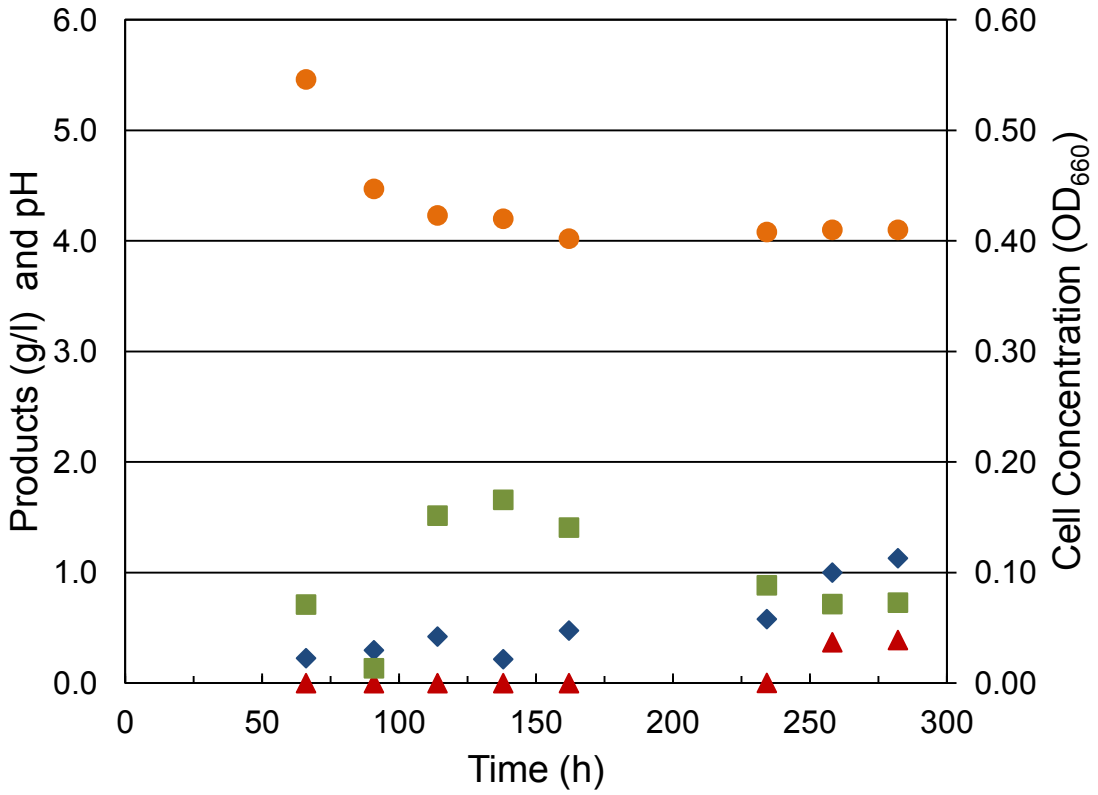

Figure 4.4 Course of fermentation for *C. ragsdalei* in revised (E5) medium ● pH, ◆ Acetic acid, ▲ Ethanol, ■ Cells.

4.6 Discussion

C. ragsdalei is proteolytic, growing quickly on yeast extract with low initial consumption of CO and H_2. *Clostridium* species are often proteolytic, and Doyle (Doyle, 1991) showed that *C. ljungdahlii* grows quickly on complex medium containing peptone with initial fast growth on amino acids, and a second (diauxic) growth phase on some sugars or syngas. In the present study, *C. ragsdalei* was incubated in yeast extract medium with neither CO nor H_2 in the headspace gas to test growth on the yeast extract (data not shown). Under a CO_2 atmosphere (without CO and H_2) small amounts of H_2 (0.15% of 180 mL gas and pressure increased by 9%, 9 kPa) and N_2 (10.0%) were produced, but under an N_2 atmosphere small amounts of H_2 (0.5% of 180 mL gas and

pressure decreased by 11%, 11 kPa) and CO_2 (1.7%) were produced. Little growth was noted on yeast extract in the bottles without CO or H_2. In the absence of yeast extract, *C. ragsdalei* will grow slowly on CO and H_2, and can exhibit a long lag phase before gas is consumed and growth begins.

The growth potential of the revised E5 medium from the *E. coli* model is 0.57 g_x/L matching the growth predicted in Table 4.5 for the base medium (versus 0.07 g_x/L observed for medium E5 due to low pH and 0.24 g_x/L observed for the base medium). Medium cost was reduced by 93% when the MES buffer was omitted from the E3 medium and cost drops from $9.36/L of the base to $0.25/L of the E5 medium, and from $16.42 to $0.44/$g_x$ growth potential. Further, 40% of the E5 medium cost is for bicarbonate to form the acetate buffer; in commercial fermentation the acetate will be retained in water recycled from ethanol recovery and the base cost will be negligible. Increased potential for growth per volume or increased cell concentration can be attained by increasing the concentration of all components in the medium. The present analysis uses costs for laboratory chemicals, and significant cost reduction will be realized through sourcing of industrial nutrients in bulk supply.

Vitamins are provided in yeast extract, but not all of the components of the vitamin solution will be required even in the minimized medium. For example, *C. ljungdahlii* requires only pantothenate, biotin and thiamine (Phillips et al., 1993). Cyanocobalamin, Vitamin B-12 contains cobalt like the corrinoid-iron-sulfur enzyme in acetogens (Lu et al., 1990), but the acetogens are competent to synthesize the enzyme using cobalt in the trace metals. Cost of cyanocobalamin represents 3.3% of the E5 medium cost. Hydrogen sulfide (H_2S) that is considered a poison to catalysts in other

syngas processing schemes could be obtained from the syngas production and used at no cost as the source of nutrient sulfur, which represents 12.5% of the E5 medium cost.

A summary of cost and performance of the medium through the revisions is presented in Figure 4.5. The cost was reduced dramatically, particularly by the substitution of acetate buffer for the MES buffer used in the maintenance medium, 93% cost reduction.

Removal of yeast extract left a defined growth medium, but slowed growth dramatically. Subsequent fermentations suggest a diauxic growth pattern with fast initial growth on yeast extract followed by slower, more productive growth using syngas (see

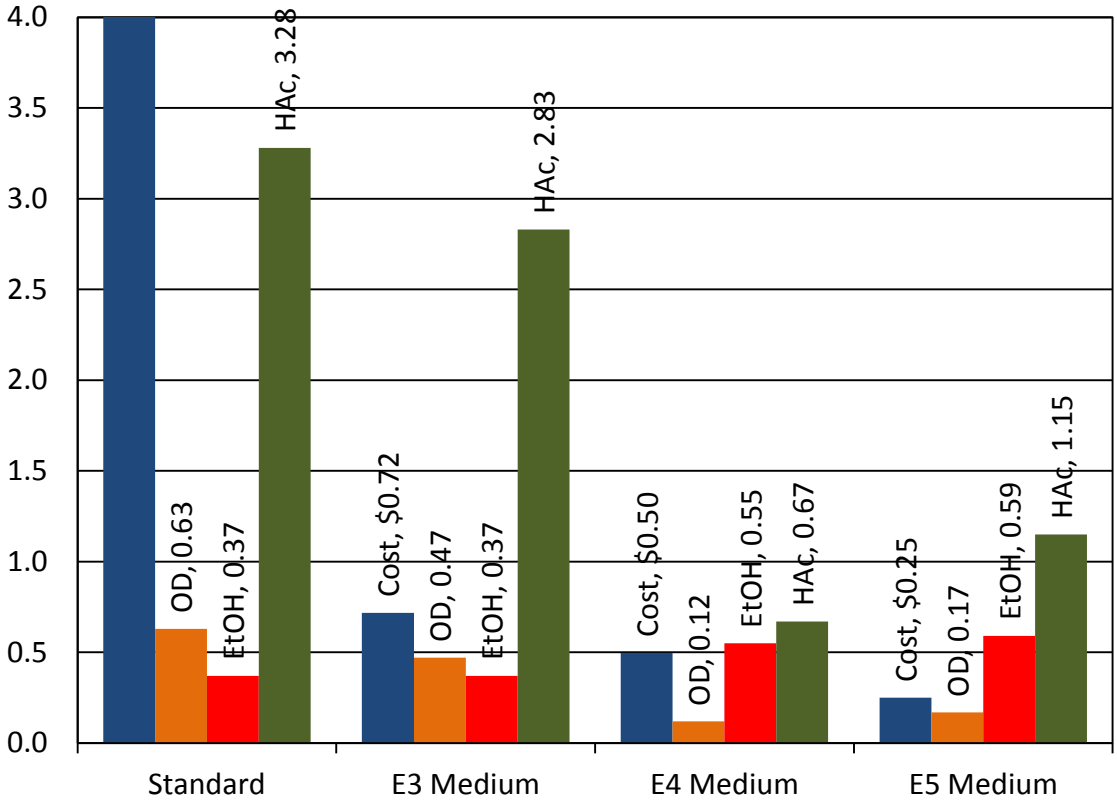

Figure 4.5 Summary of cost and performance through medium revisions. Cost ($/liter of medium), Cell concentration (OD_{660}), Ethanol (g/L), Acetic acid (g/L). (Note: Cost of standard medium is $9.36/L.)

Figure 5.10 and Figure B.1). Removal of yeast extract in medium E4 and E5 increased the concentration of ethanol produced by about 50%, although cell growth and acetic acid production were lower. These fermentations were particularly influenced by low pH and low initial cell concentration. The fast drop of pH in medium E5 (Figure 4.4) shows high activity of *C. ragsdalei* despite low growth when sulfide was the only source of reduced sulfur nutrient. The growth of *C. ragsdalei* when excess Na_2S solution raised the initial pH, revealed the detrimental effect of low initial pH in starting growth and of pH below 4.5.

The revised medium, without yeast extract, has been developed in subsequent studies for a Masters thesis (Gao, 2012).

4.7 Conclusions

The cost of production medium was reduced by more than 97%, from $9.36/L to $0.25/L. The estimated growth potential for syngas with all medium formulae used remained at 570 mg_x/L. The cost of production medium can be further reduced through refinement of medium design and commercial sourcing of components. Additional study is required to achieve optimum economics. The commercial process will retain the medium and cells as long as is economically useful, and economical supply of nutrients to maintain activity of the culture and productivity of the fermenter will be important to achieve a successful process.

References

Bailey, J.E., Ollis, D.F. 1986. *Biochemical Engineering Fundamentals*. *2nd ed*. McGraw-Hill, New York,

Becton-Dickinson. 2006. Bionutrients Tech Manual. 3rd ed. Sparks, MD, USA, pp. 28-29.

Doyle, M.L. 1991. Preferred Conditions for Growth and Product Formation by *Clostridium Ljungdahlii* Petc in Complex Media. University of Arkansas,

EERE, 2012, Biomass Multi-Year Program Plan, Washington, DC, http://www1.eere.energy.gov/biomass/pdfs/mypp_april_2012.pdf, 11/15/2012

EIA, 2012, Biofuels Issues and Trends, Washington, D.C., http://www.eia.gov/biofuels/issuestrends/, 11/6/2012

Gaddy, J.L., D. K. Arora, C-W Ko, J. R. Phillips, R. Basu, C. V. Wikstrom and E. C. Clausen. 2007. Methods for Increasing the Production of Ethanol from Microbial Fermentation. 7285402.

Gao, J. 2012. Development of Low Cost Medium for Ethanol Production from Syngas by *Clostridium Ragsdalei*. Oklahoma State University,

Kumar, A., Jones, D.D., Hanna, M.A. 2009. Thermochemical Biomass Gasification: A Review of the Current Status of the Technology. Energies, 2 (3), 556-581.

Kundiyana, D.K., Huhnke, R.L., Maddipati, P., Atiyeh, H.K., Wilkins, M.R. 2010. Feasibility of Incorporating Cotton Seed Extract in Clostridium Strain P11 Fermentation Medium During Synthesis Gas Fermentation. Bioresource Technology, 101 (24), 9673-9680.

Kundiyana, D.K., Wilkins, M.R., Maddipati, P., Huhnke, R.L. 2011. Effect of Temperature, Ph and Buffer Presence on Ethanol Production from Synthesis Gas by "Clostridium Ragsdalei". Bioresource Technology, 102 (10), 5794-5799.

Lu, W.P., Harder, S.R., Ragsdale, S.W. 1990. Controlled Potential Enzymology of Methyl Transfer Reactions Involved in Acetyl-Coa Synthesis by Co Dehydrogenase and the Corrinoid/Iron-Sulfur Protein from Clostridium Thermoaceticum. Journal of Biological Chemistry, 265 (6), 3124-3133.

Maddipati, P., Atiyeh, H.K., Bellmer, D.D., Huhnke, R.L. 2011. Ethanol Production from Syngas by Clostridium Strain P11 Using Corn Steep Liquor as a Nutrient Replacement to Yeast Extract. Bioresource Technology, 102 (11), 6494-6501.

Phillips, J.R., Clausen, E.C., Gaddy, J.L. 1994. Synthesis Gas as Substrate for the Biological Production of Fuels and Chemicals. Applied Biochemistry and Biotechnology, 45-6, 145-157.

Phillips, J.R., Klasson, K.T., Clausen, E.C., Gaddy, J.L. 1993. Biological Production of Ethanol from Coal Synthesis Gas - Medium Development Studies. Applied Biochemistry and Biotechnology, 39, 559-571.

Ragsdale, S.W. 1991. Enzymology of the Acetyl-Coa Pathway of Co2 Fixation. Critical Reviews in Biochemistry and Molecular Biology, 26 (3-4), 261-300.

Ragsdale, S.W. 2008. Enzymology of the Wood-Ljungdahl Pathway of Acetogenesis. in: *Incredible Anaerobes: From Physiology to Genomics to Fuels*, (Eds.) J. Wiegel, R.J. Maier, M.W.W. Adams, Vol. 1125, pp. 129-136.

Saxena, J. 2008. Development of an Optimized and Cost-Effective Medium for Ethanol Production by *Clostridium* Strain P11. Dissertation. University of Oklahoma, 131.

Saxena, J., Tanner, R.S. 2011. Effect of Trace Metals on Ethanol Production from Synthesis Gas by the Ethanologenic Acetogen, Clostridium Ragsdalei. Journal of Industrial Microbiology & Biotechnology, 38 (4), 513-521.

CHAPTER V

MASS TRANSFER IN SERUM BOTTLE FERMENTATIONS OF SYNGAS

5.1 Abstract

Mass transfer was defined for conversion of CO and H_2 to ethanol by *Clostridium ragsdalei*. Mass transfer capacity in bottles shaken upright at 150 rpm and 37°C was 7 h^{-1} as $k_{L,CO}a/V_L$ for CO transfer into 100 mL medium or 14 h^{-1} into 50 mL, and 13 h^{-1} as $k_{L,H2}a/V_L$ for H_2 transfer into 100 mL and 26 h^{-1} into 50 mL. Kinetic and thermodynamic parameters like the concentrations of CO and H_2 inside the cell defined as Henry's Law partial pressures, were obtained using the mass transfer analysis. Dissolved CO pressure ranged from 10^{-2} to 10^{-4} kPa, while dissolved H_2 ranged from saturation at up to 70 kPa to 1 kPa. Dissolved CO above 10^{-3} kPa inhibited H_2 uptake. Specific growth ranged from 0.15 to 0.01 h^{-1} as nutrients were depleted from the medium. Uptake of CO was initially over 0.05 mol CO/g cell h, but decreased to around 0.02 mol CO/g cell h as CO uptake became limited by mass transfer. Uptake of H_2 started low from CO inhibition, but matched CO at 0.02 mol H_2/g cell h in mass transfer limited fermentation. Batch fermentation of syngas by *C. ragsdalei* transitioned from kinetic limitation with high gas supply and low cell inventory, through mass transfer limitation with active growing cells, then back to kinetic limitation as nutrients to support growth were depleted. Syngas fermentation with *C. ragsdalei* in bottles produced up to 0.4 g/L of cells, 4 g/L of acetic

acid and 0.6 to 2.0 g/L of ethanol. Maximum conversions of 70 to 80% of CO and 70 to 90% of H_2 were attained.

5.2 Keywords

Mass transfer, inhibition, thermodynamics, syngas fermentation kinetics, acetogen

5.3 Nomenclature

dn_i/dt - molar rate of transfer of gas species *i* (CO, H_2, CO_2)

$D_{i,W}$ - diffusivity of gas *i* in water

$C_{i,L}$ - molar concentration of *i* in liquid (mol/L)

CODH – carbon monoxide dehydrogenase

H_i - Henry's Law constant for gas *i*

* - quantity derived from the Henry's law equilibrium

$k_{L,i}a/V_L$ – volumetric mass transfer coefficient for gas *i* (*i* can represent O_2, CO, H_2 or CO_2)

k_L – liquid film mass transfer coefficient

a – area of the gas liquid interface

V_L – liquid volume into which gas is transferred

p_i - partial pressure of *i*, p_i^* is partial pressure of dissolved *i*

q_i – specific uptake rate of gas *i*

V_G – volume of gas in bottle headspace (mL)

X – cell concentration (g_x/L)

μ – specific growth rate (g_x/g_x h or h^{-1})

5.4 Introduction

Conversion of biomass and waste materials to synthesis gas containing CO and H_2 as a precursor to production of fuels and chemicals offers a convenient method to simplify the production process, access all of the carbon and energy contained in the feedstock, and broaden the pool of potential energy feedstocks (Wilkins and Atiyeh, 2011). Biomass carbohydrate and noncarbohydrate fractions can be converted to syngas using gasification. The syngas can be converted by catalytic reforming to hydrocarbons using established technology (Griffin and Schultz, 2012), for example Fischer-Tropsch synthesis, but Fischer-Tropsch synthesis requires adjustment of the H_2:CO ratio and removal of contaminants such as H_2S that poison the catalyst. The catalytic processes are conducted at high temperature and pressure, increasing cost to construct and operate the process. Acetogenic bacteria can convert CO and H_2 to acetic acid, ethanol and other chemicals at mild conditions of atmospheric pressure and 37^{o}C (Gaddy, 2007; Wilkins and Atiyeh, 2011).

Stoppered serum bottles are frequently used as batch fermentation reactors in the laboratory. Serum bottles have been used to study the conversion of CO and H_2 to acetic acid and ethanol (Phillips et al., 1994) and in other anaerobic fermentations in which gas to liquid mass transfer is important. Typically, fermentation protocol will specify the agitation rate used as a matter of standard operating procedure, without specific understanding of the intensity of mass transfer applied. Little effort or thought is given to characterization of the serum bottle as a mass transfer device to conduct the fermentation. High pressure, 238 kPa absolute (20 psig) or more, has been used to ensure enough gas supply (Maddipati et al., 2011), and efforts have been made to correlate kinetics and

thermodynamics with the gas phase partial pressures applied (Hu et al., 2011). However, the partial pressure of CO, H_2, and CO_2 relevant to kinetics and thermodynamics of the fermentation are those inside the cell, where the enzymes catalyze reaction, and these partial pressures and the proportional dissolved gas concentrations are greatly affected by the mass transfer process. Microbial consumption of the dissolved gas creates a concentration difference, which is the potential for gas transfer into the liquid. Gas to liquid transport is typically represented by a model of liquid film controlled mass transfer (Bird et al., 2002), as in Equation 5.1.

$$-\frac{1}{V_L}\frac{dn_i}{dt} = \frac{k_{L,i}a}{V_L}\left(C_i^* - C_{i,L}\right) = \frac{k_{L,i}a}{V_L}\frac{\left(p_{i,G} - p_i^*\right)}{H_i} \qquad 5.1$$

The molar rate of transfer (dn_i/dt) of gas species i, such as CO or H_2, into a liquid volume V_L is proportional to the concentration difference. The concentration difference across a thin film of stagnant liquid between the gas/liquid interface and the turbulent bulk liquid can be given in terms of molar concentration $C_{i,L}$ or more conveniently for use with sparingly soluble gases, as the difference of gas partial pressures in equilibrium with the liquid concentration per Henry's Law, $C_{i,L} = p_i/H_i$, where H_i is the Henry's Law constant for gas i at process temperature. The liquid film presents the major resistance to gas transport to the cells. The quantity derived by the Henry's law equilibrium is here denoted by the asterisk (*), the concentration of the gas at the interface $C_i^* = p_{i,G}/H_i$ and the dissolved partial pressure $p_i^* = C_{i,L}\, H_i$, with $p_{i,G}$ being the partial pressure of i in the gas phase and $C_{i,L}$ being the bulk liquid concentration of i. The constant of proportionality is the volumetric mass transfer coefficient, ($k_{L,i}a/V_L$), which has units of reciprocal time as h^{-1}.

Mass transfer is studied in reactors, or fermenters, to define ($k_{L,i}a/V_L$) as a function of process parameters, such as agitation, flow, temperature or pressure (Munasinghe and Khanal, 2010; Vega et al., 1989). Agitation, temperature, interfacial area and volume are held nearly constant in serum bottle fermentation, and ($k_{L,i}a/V_L$) can be expected to be constant. However, the pressure and composition of the syngas in a serum bottle change dramatically with time over the course of fermentation and change the potential for gas transfer, which is the liquid film concentration difference. Much important information that characterizes the syngas fermentation, such as specific uptake rates for CO and H_2, and inhibition of cell function as affected by dissolved gas concentrations, can be derived from bottle fermentation if the mass transfer can be characterized.

Thermodynamics controls the direction and possible extent of the reactions in the production pathway, while kinetics describe the rates of reactions and the overall rates of CO and H_2 consumption, acetic acid and ethanol accumulation, and cell growth. The overall rates are expected to be proportional to cell mass (XV_L) in the fermenter, with the coefficient of proportionality being the specific growth rate (μ) for growth and the specific uptake rate (q_{CO} for CO and q_{H2} for H_2). Individual reaction rates are related to the concentrations of the reactants and products using a model, such as Michaelis-Mneten for enzyme mediated reactions (Shuler and Kargi, 2002). The specific growth and specific uptake rates are likewise correlated to the concentration of substrates, like CO and H_2 at the cell, in a kinetic model, such as the Monod equation (Shuler and Kargi, 2002). The concentrations of substrates and products that are important and available in syngas fermentation are the CO, H_2, acetic acid and ethanol dissolved in the bulk liquid. These concentrations are likewise thermodynamic quantities that we can measure or

derive. The dissolved CO and H_2 will be represented by the dissolved partial pressures, p_{CO}^* and p_{H2}^*, and these will be calculated from mass transfer analysis of the observed uptake.

The objective of the present study is to evaluate mass transfer in serum bottle fermentation, and determine the effect of pressure on the syngas fermentation, in particular the effect on mass transfer.

5.5 Materials and Methods

5.5.1 Microbial Catalyst and Culture Medium

All fermentations used *Clostridium ragsdalei* grown from stock culture provided by Dr. Ralph Tanner, University of Oklahoma. The culture was maintained at 37^{o}C and inoculation was typically 5% (v/v) from growing culture. *C. ragsdalei* was grown in 250 ml serum bottles (Wheaton, Millville, NJ), stoppered and crimp sealed containing 100 ml of fresh medium under 238 kPa (absolute) of syngas. The initial composition of syngas was 40 mole percent CO, 30% H_2 and 30% CO_2 (40:30:30 CO:H_2:CO_2 syngas) obtained from Stillwater Steel Supply Company (Stillwater, OK). The headspace was purged for 2 minutes before the bottle was filled to 238 kPa (20 psig).

5.5.2 Medium Preparation

The standard yeast extract medium for *C. ragsdalei* (Saxena, 2008) was used to prepare the inoculum. However, the production medium in the present study used less yeast extract, and used bicarbonate to form an acetate buffer instead of MES/KOH buffer. The production medium contained yeast extract (Difco Laboratories, Detroit, MI), sodium bicarbonate, minerals, trace metals, vitamins and resazurin as a redox indicator as shown in Table 5.. The medium components were dissolved in deionized water in a 1 liter round

bottom flask and the medium just brought to a boil in a microwave to free dissolved gases, particularly O_2. The hot medium solution was purged with N_2 bubbled from a cannula into the liquid to remove residual O_2. A second N_2 purge was maintained in the headspace to ensure anoxic conditions as the medium cooled and was dispensed. Serum bottles were purged with N_2 to remove air, before and after filling with medium. A No. 1 butyl rubber stopper (VWR Scientific, Radnor, PA) was secured with a 30 mm aluminum crimp cap (Wheaton, Millville, NJ). The bottles filled with 100 mL of medium, except when 50 mL of medium was used to increase the volume of gas supply relative to the medium volume in study of the effect of maintained pressure. All bottles were filled, purged and sealed, then autoclaved for 20 minutes at 121^{o}C. The bottles were prepared for inoculation by replacing the N_2 in the headspace with 40:30:30 $CO:H_2:CO_2$ syngas to 134 kPa, adding 0.2 mL/100 mL of a solution containing 4% cysteine (w/v) and 4% sodium sulfide, and shaken at 37^{o}C until the bottles were warm and the pink color of the resazurin disappeared. The freshly inoculated bottles were filled to the required initial pressure, 114, 134, 169 or 238 kPa, with 40:30:30 $CO:H_2:CO_2$ syngas, and placed upright on an orbital shaker (Innova 2100, New Brunswick Scientific, Enfield, CT) at 150 rpm and 37^{o}C.

Table 5.1 Composition of Fermentation Medium used in pressure studies.

Component	Formula	Concentration
		(mg/liter)
Yeast Extract	Undefined	500
Sodium Bicarbonate	$NaHCO_3$	1750
Minerals		
Ammonium Chloride	NH_4Cl	3000
Calcium Chloride	$CaCl_2.2H_2O$	120
Magnesium Sulfate	$MgSO_4.7H_2O$	600
Potassium Chloride	KCl	300
Potassium Phosphate	KH_2PO_4	300
Trace Metals		
Cobalt Chloride	$CoCl_2.6H_2O$	2
Ferrous Ammonium Sulfate	$FeH_{20}N_2O_{14}S_2$	8
Manganese Sulfate	$MnSO_4.H_2O$	10
Nickel Chloride	$NiCl_2.6H_2O$	2
Nitrilotriacetic Acid	$C_6H_9NO_6$	20
Sodium Molybdate	$Na_2MoO_4.2H_2O$	0.2
Sodium Selenate	Na_2SeO_4	1
Sodium Tungstate	$Na_2WO_4.2H_2O$	2
Zinc Sulfate	$ZnSO_4.7H_2O$	10
Vitamins		
Para-aminobenzoic Acid	$C_7H_7NO_2$	0.05
Biotin	$C_{10}H_{16}N_2O_3S$	0.02
Pantothenic Acid	$Ca(C_9H_{16}NO_5)_2$	0.05
Folic Acid	$C_{19}H_{19}N_7O_6$	0.02
MESNA	$C_2H_5NaO_3S_2$	0.10
Nicotinic Acid	$C_6H_5NO_2$	0.05
Pyridoxine	$C_8H_{11}NO_3.HCl$	0.10
Riboflavin	$C_{17}H_{20}N_4O_6$	0.05
Thiamine	$C_{12}H_{17}N_4OSCl.HCl$	0.05
Thioctic Acid	$C_8H_{14}O_2S_2$	0.05
Cyanocobalamin	$C_{63}H_{88}CoN_{14}O_{14}P$	0.05
Resazurin		
Resazurin	$C_{12}H_6NO_4Na$	1
Cysteine/Sulfide		
Cysteine	$C_3H_7NO_2S$	80
Sodium Sulfide	$Na_2S.9H_2O$	80

5.5.2.1 Effect of Pressure on Mass Transfer into 100 mL Medium

C. ragsdalei was inoculated from the same source bottle into eight identical serum bottles. The bottles were maintained two each at 114, 134, 169 and 238 kPa (2, 5, 10 and 20 psig) initial pressure. Each bottle contained 100 mL of fresh medium and 5 mL of inoculum, and was sampled 3 times per day. The gas in each bottle was replaced with fresh gas to the initial pressure charge at 24, 48 and 72 h after inoculation. The initial gas to liquid ratio was about 8, 10, 13 or 17 mmol per 100 mL medium.

5.5.2.2 Effect of Maintained Pressure on Mass Transfer into 50 mL Medium

C. ragsdalei was inoculated into eight identical serum bottles, the bottles were maintained two each at 114, 134, 169 and 238 kPa (2, 5, 10 and 20 psig) initial pressure. Each bottle contained 50 mL of fresh medium and 2.5 mL of inoculum, and was sampled twice per day to conserve culture volume. The supply of gas per mL of liquid (*G/L*) is 2.55 times the *G/L* for bottles with 100 mL initial liquid, about 10, 12, 15.5 and 22 mmol per 50 mL of medium.

5.5.3 Sampling and Analysis

A liquid sample was analyzed for pH and cell, ethanol, butanol, acetic acid and butyric acid concentrations. Cell concentration was determined as optical density measured at 660 nm in a Cary 50 Bio UV-Vis spectrophotometer (Palo Alto, CA, USA). Liquid product concentrations were determined from a sample centrifuged (Eppendorf, Hamburg, Germany) for 10 min at 13,000 rpm to remove cells. Supernatant was mixed with an equal part of 0.085 M HCl to ensure all acetate was converted to the volatile free acetic acid form. The liquid sample was analyzed using a GC (Agilent Technologies, Wilmington, DE) with a DB-FFAP capillary column (Agilent J&W) and quantitation

using a flame ionization detector (FID). Gas composition was determined using a GC (Agilent Technologies, Wilmington, DE, USA) with a capillary column with Carboxen 1010 PLOT stationary phase (Supelco, Bellefonte, PA, USA) and argon mobile phase. The GC ran isothermally at 80^{o}C with a thermal conductivity detector (TCD) for quantitation of the permanent gases H_2, N_2, CO and CO_2. Chromatograms for the liquid products and gases were analyzed using the ChemStation data analysis software.

5.5.4 Data Management

Data was collected, plotted and derivative quantities calculated using Microsoft Excel.

5.6 Results and Discussion

In early fermentations an unpredictable lag phase of about 50 h after inoculation was observed in serum bottles with *C. ragsdalei* starting with 238 kPa of rich syngas, containing 40:30:30 CO:H_2:CO_2 syngas (See Section 4.5). Fermentation would proceed rapidly when conversion began, so the lag was attributed to inhibition of cell function by the high supply of gas to the low cell concentration following inoculation. Fermentation was observed to consume CO and H_2 completely when allowed to proceed, with pressure in the bottle falling to as low as 65 kPa absolute (-5 psig) as seen in Figure 5.1. Following these observations, the effect of pressure on CO and H_2 uptake was examined in this study. Duplicate bottles at four pressures were used to obtain as much data with the same prepared medium and inoculum for direct comparison within the availability of analytical equipment. Individual data from each bottle is shown to better indicate the effects of pressure and reproducibility. As an example, the initial charge of bottle Pr2B5, seen in Figure 5.1, shows a loss of pressure on initial sampling to about 120 kPa; the

course of Pr2B5 through the remaining sampling of the initial charge (through 24 h) matches the course of bottles Pr2B1 and Pr2B2 initially at 114 kPa. After the intended pressure of 169 kPa was restored at 24 h, the course of bottle Pr2B5 matches that for bottle Pr2B6 at the same initial pressure.

5.6.1 Effect of Pressure on Mass Transfer

The change in the total pressure in the headspace due to gas consumption by *C. ragsdalei* bottle fermentations at varied initial pressures is shown in Figure 5.1. Duplicate bottles were prepared for each initial pressure, and fresh gas was replaced to the same initial pressure charge at 24, 48 and 72 hours after inoculation.

The total pressure in each bottle fell due to consumption of CO and H_2. The decrease in pressure in the fermentation bottles was slow over the first 24 h. The pressure decreased at a faster rate after 24 h as more cells were present (Figure 5.2). The rate of pressure decrease was very slow in both bottles charged to 238 kPa after 72 h; this is attributed to inhibition of *C. ragsdalei* at high CO partial pressure (p_{CO} = 95 kPa) after nutrients were depleted from the medium. Total pressure fell below 65 kPa in the bottles that started at 114 kPa. The initial charge of pressure was partially vented in the first sampling of bottle Pr2B5, giving the appearance of fast consumption compared to Pr2B6 at the same initial pressure.

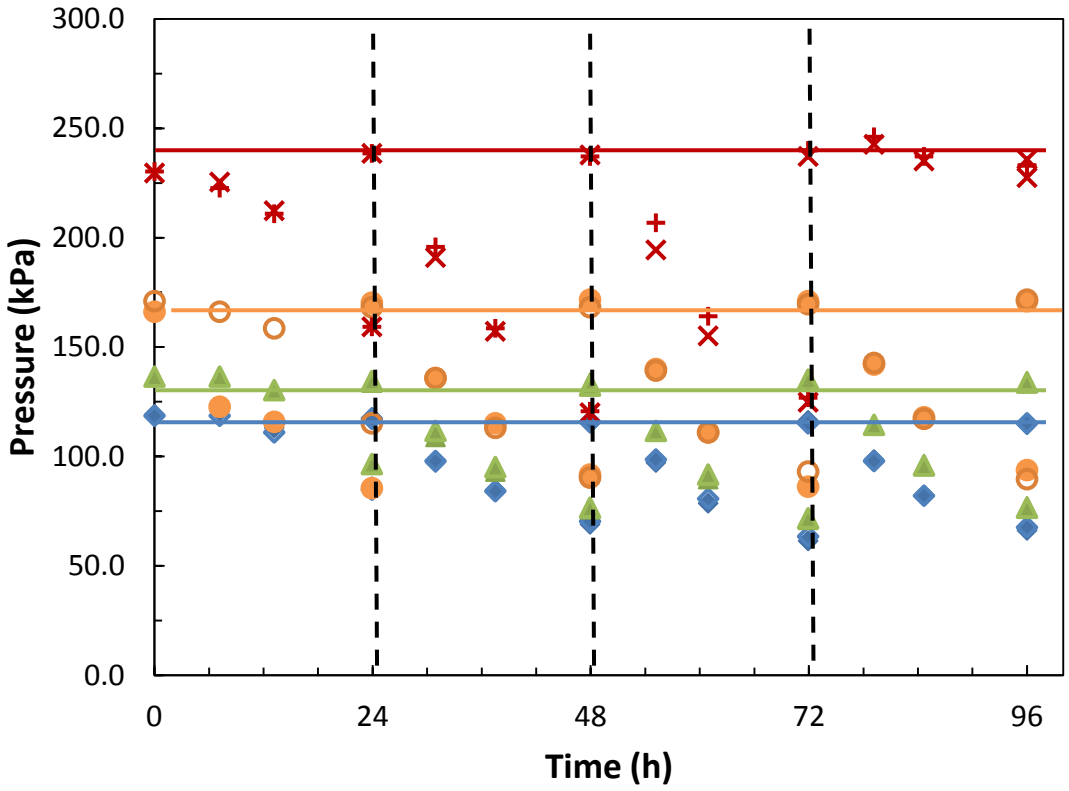

Figure 5.1 Pressure in bottles with 100 mL liquid through syngas fermentation at initial pressure indicated by the horizontal lines and fresh gas supply indicated by the vertical dashed lines. Bottles Pr2B1 (◆) and Pr2B2 (◇) have initial pressure of 114 kPa, Pr2B3 (▲) and Pr2B4 (△) 134 kPa, Pr2B5 (●) and Pr2B6 (○) 169 kPa, and Pr2B7 (×) and Pr2B8 (+) 238 kPa.

Growth of *C. ragsdalei* was similar for all bottles yielding an optical density at 660 nm (OD_{660}) of 0.6 to 0.7 in about 72 h of fermentation (Figure 5.2). Growth in all bottles appears exponential through the first 24 h; but slows after the gas is replenished at 24 h of fermentation. The bottles at 238 kPa approach maximum OD_{660} after gas was replaced in all bottles at 48 h, but all bottles achieve the same maximum OD_{660} near 0.70.

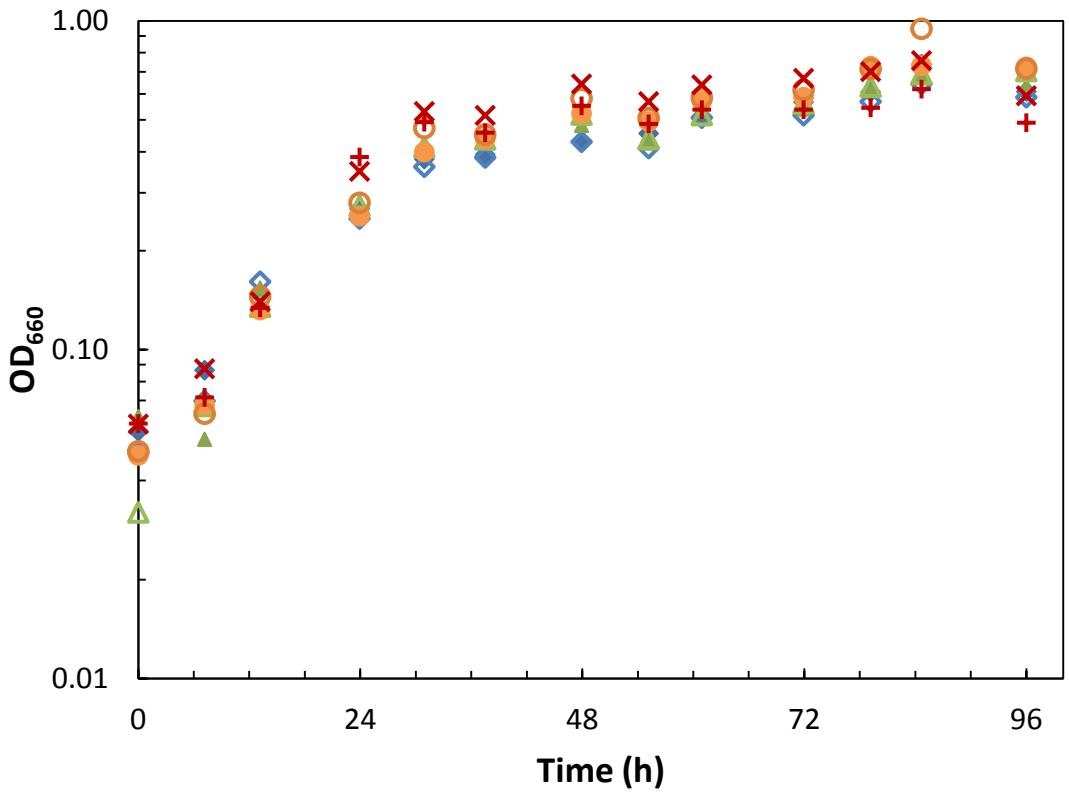

Figure 5.2 Cell growth in syngas fermentation bottles with 100 mL liquid at different initial gas pressures. Bottles Pr2B1 (◆) and Pr2B2 (◇) have initial pressure of 114 kPa, Pr2B3 (▲) and Pr2B4 (△) 134 kPa, Pr2B5 (●) and Pr2B6 (○) 169 kPa, and Pr2B7 (×) and Pr2B8 (+) 238 kPa.

The pH decreased through the course of fermentation with the higher pressure bottles maintaining a slightly lower pH (Figure 5.3). The pH was adjusted by addition of 1.0 ml of 7% $NaHCO_3$ solution to all bottles at 30 h. The pH in each bottle rose by 0.5 to 1.0 dependent on the acetic acid concentration. The pH of all bottles was raised again at 62 h by addition of 1.0 mL of 7% $NaHCO_3$ solution to each bottle, but the rise in pH was only about 0.4 since a stronger acetate buffer had been established. The $NaHCO_3$ neutralizes part of the acetic acid to form the acetate buffer that stabilizes pH in the fermentation medium. The lower pH at higher initial pressure was caused by higher production of acetic acid shown in Figure 5.4.

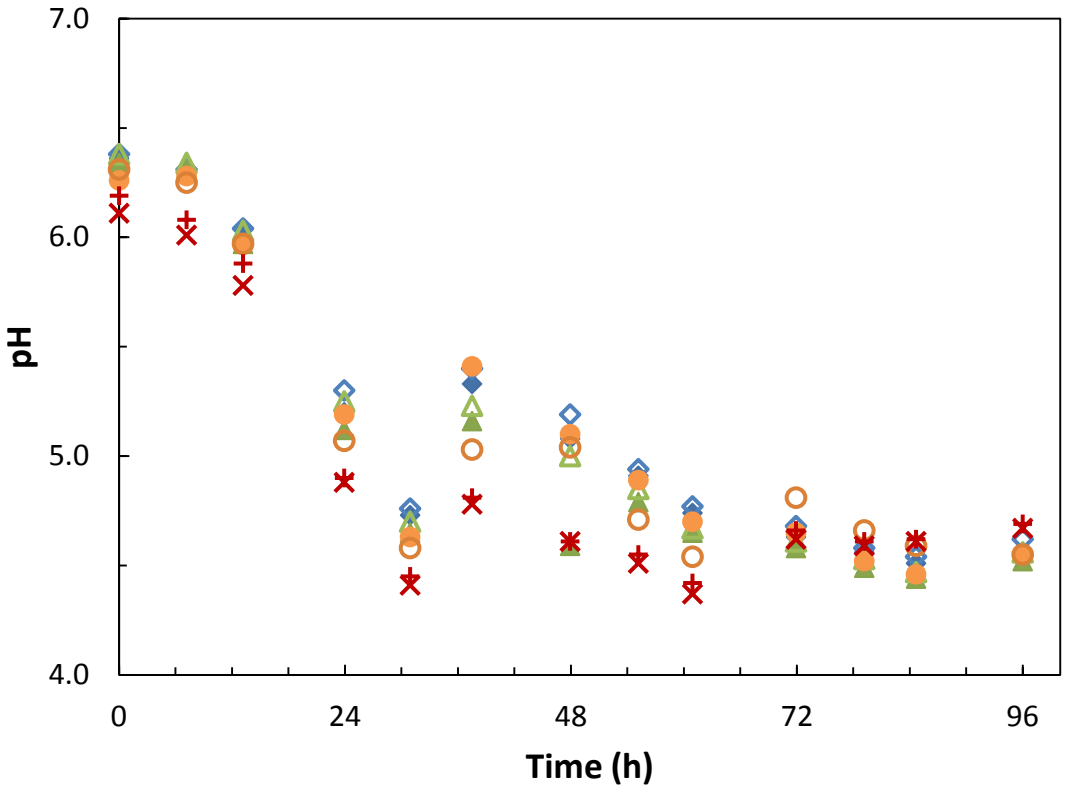

Figure 5.3 pH in syngas fermentation bottles with 100 mL liquid at different initial gas pressures. Bottles Pr2B1 (◆) and Pr2B2 (◇) have initial pressure of 114 kPa, Pr2B3 (▲) and Pr2B4 (△) 134 kPa, Pr2B5 (●) and Pr2B6 (○) 169 kPa, and Pr2B7 (×) and Pr2B8 (+) 238 kPa.

Acetic acid production is similar in all bottles for the first 24 h, after which, more acetic acid is produced in bottles with higher initial pressure. Higher acetic acid production and lower pH result from more gas available in bottles charged to 238 kPa versus bottles charged to 114 kPa, with slightly more than twice the CO and H_2 in the fresh gas.

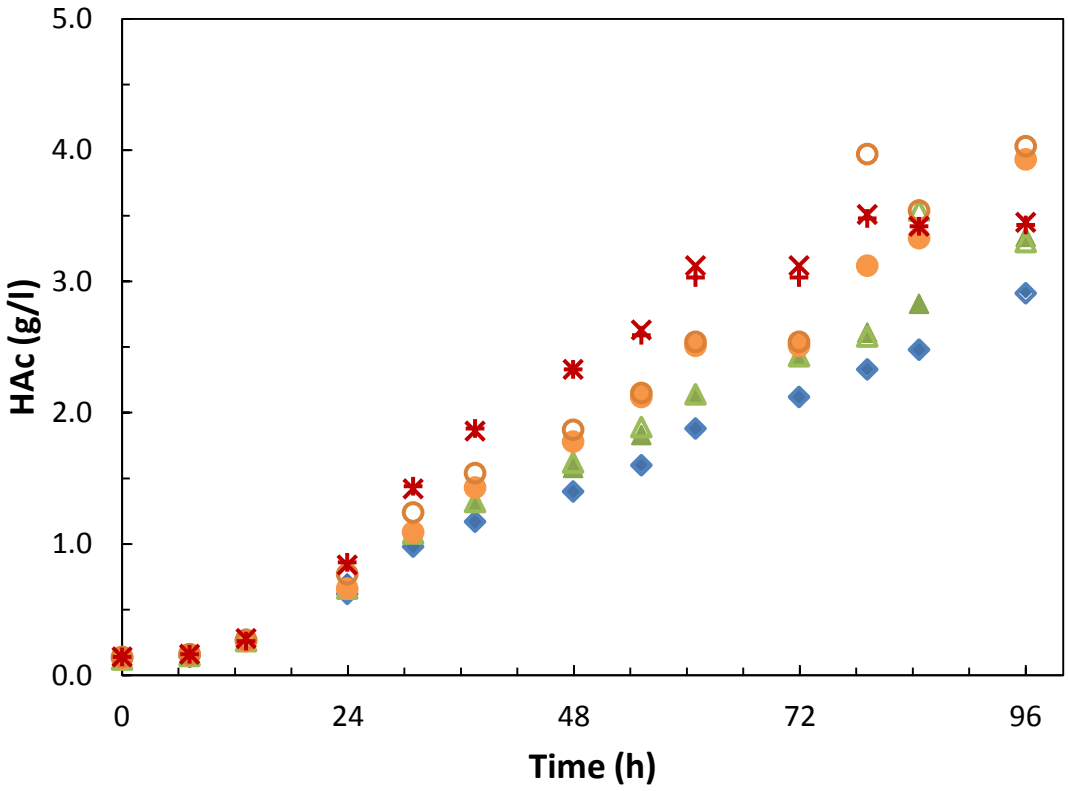

Figure 5.4 Acetic acid produced in syngas fermentation bottles with 100 mL liquid at different initial gas pressures. Bottles Pr2B1 (◆) and Pr2B2 (◇) have initial pressure of 114 kPa, Pr2B3 (▲) and Pr2B4 (△) 134 kPa, Pr2B5 (●) and Pr2B6 (○) 169 kPa, and Pr2B7 (×) and Pr2B8 (+) 238 kPa.

Low concentrations of ethanol, shown in Figure 5.5, were produced in all bottles after the gas was replaced at 24 h of fermentation, and the concentration of ethanol increased when gas was replenished at 48 h and again at 72 h. The ethanol concentration stabilized or even decreased as gas was depleted of CO and H_2. Fresh gas with high partial pressure of CO and H_2 increased the rate of transfer of CO and H_2 into the cells and accelerated the rate of ethanol production. The rate of CO and H_2 uptake was increased by the higher partial pressure (driving force for mass transfer), and the electrons from the higher CO and H_2 supply were used to reduce acetic acid to ethanol.

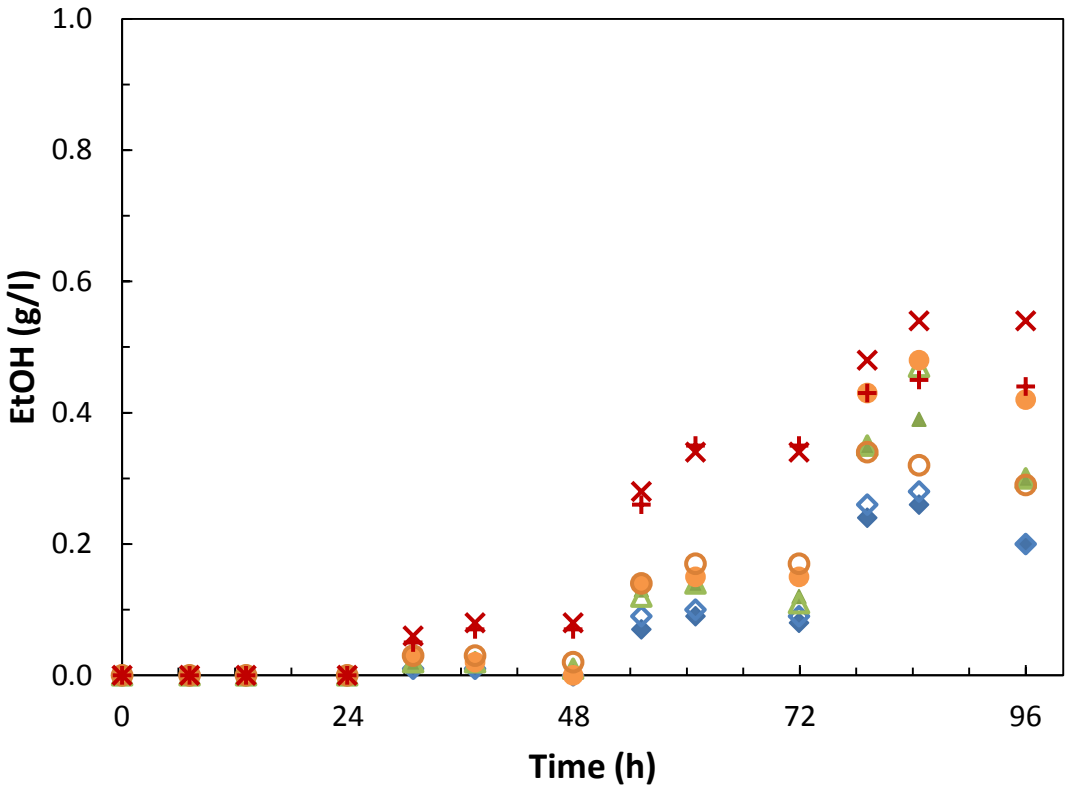

Figure 5.5 Ethanol produced in syngas fermentation bottles with 100 mL liquid at different initial gas pressures. Bottles Pr2B1 (◆) and Pr2B2 (◇) have initial pressure of 114 kPa, Pr2B3 (▲) and Pr2B4 (△) 134 kPa, Pr2B5 (●) and Pr2B6 (○) 169 kPa, and Pr2B7 (×) and Pr2B8 (+) 238 kPa.

As CO and H_2 were depleted from the remaining gas and the partial pressures fell, the rate of gas transfer and the rate of ethanol production slowed until ethanol production stopped and the remaining uptake of CO and H_2 was directed to production of acetic acid.

The fraction of CO and H_2 consumed in the fermentation for all bottles is shown in Figures 5.6 and 5.7. The apparent production of CO and H_2 at 0 and 8 h of fermentation is caused by absorption of CO_2 from the gas into the medium at pH 6.2. Bottle Pr2B5 at 169 kPa lost pressure to about 120 kPa on initial sampling, and apparent conversion is high compared to the other bottles. Figure 5.6 shows nearly identical % conversion without regard for initial syngas pressure between 24 and 96 h, this

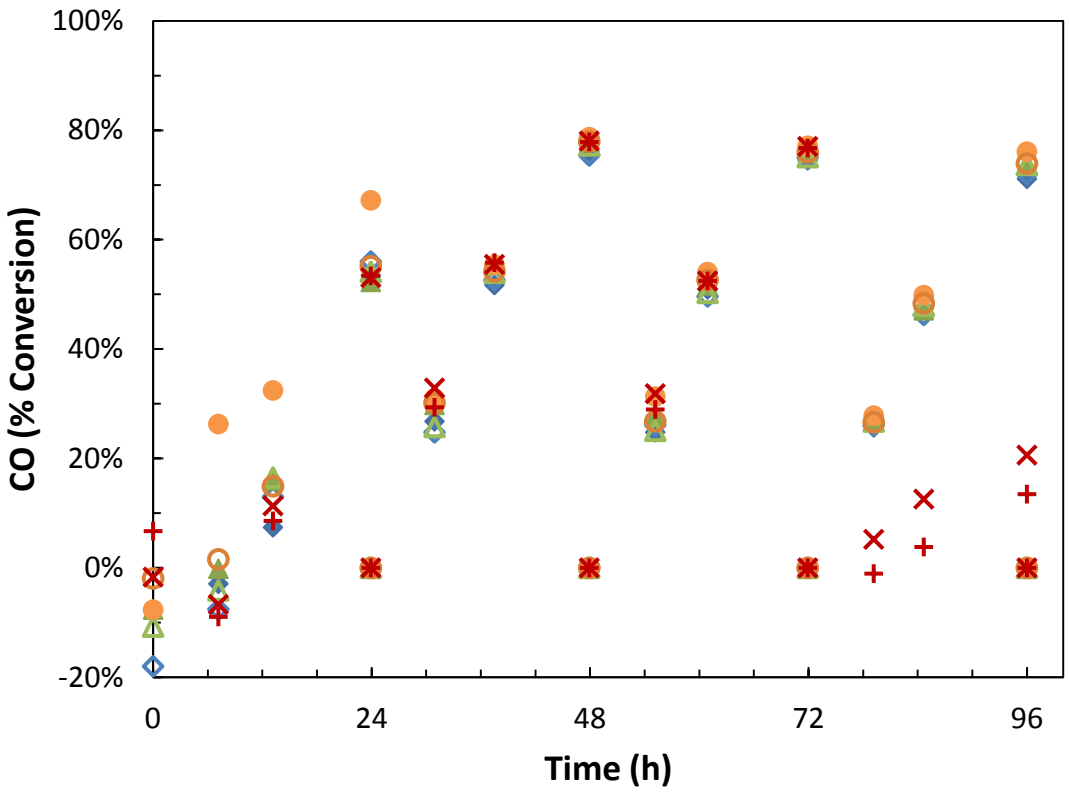

Figure 5.6 CO conversion in syngas fermentation bottles with 100 mL liquid at different initial gas pressures. Bottles Pr2B1 (◆) and Pr2B2 (◇) have initial pressure of 114 kPa, Pr2B3 (▲) and Pr2B4 (△) 134 kPa, Pr2B5 (●) and Pr2B6 (○) 169 kPa, and Pr2B7 (×) and Pr2B8 (+) 238 kPa.

indicates that the CO uptake is proportional to the partial pressure of CO during this period as expected for mass transfer limitation. The bottles at the highest initial pressure, 238 kPa, do not achieve the expected conversion after 72 h indicating a shift to a kinetic limitation.

The bottles at 238 kPa lagged in H_2 conversion after 20 h, especially when conversion of CO was less than 60%. High supply of CO establishes a preference for CO uptake, indicative of CO inhibition of the hydrogenase enzyme (Ragsdale and Ljungdahl, 1984). Notably the conversion of H_2 approached 90%, even as the CO conversion

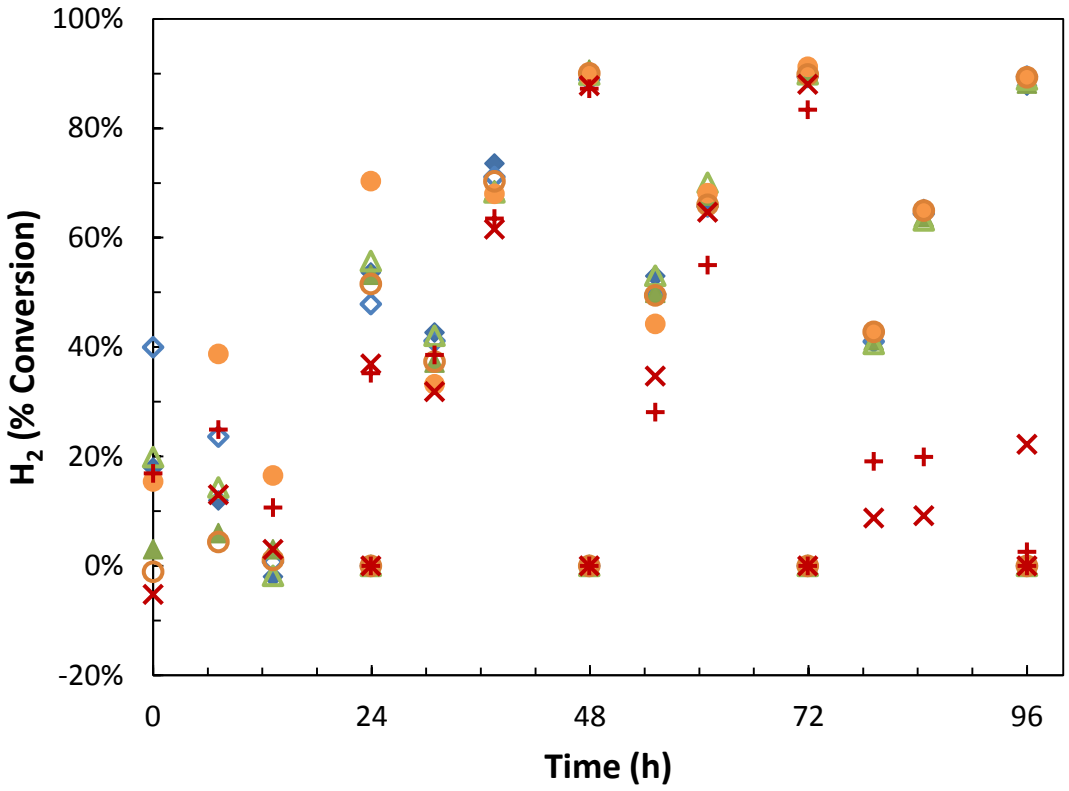

Figure 5.7 H_2 conversion in syngas fermentation bottles with 100 mL liquid at different initial gas pressures. Bottles Pr2B1 (◆) and Pr2B2 (◇) have initial pressure of 114 kPa, Pr2B3 (▲) and Pr2B4 (△) 134 kPa, Pr2B5 (●) and Pr2B6 (○) 169 kPa, and Pr2B7 (×) and Pr2B8 (+) 238 kPa.

remained below 80%, showing *C. ragsdalei* can uptake H_2 at nearly comparable rates to CO (Figure 5.11).

C. ragsdalei is able to simultaneously uptake CO and H_2 in all bottles between 20 and 80 h; the uptake is slow in the first 20 h and relative uptake is not well defined (Figures 5.6 and 5.7). Acetogens oxidize CO and H_2 to obtain electrons used in the production of acetyl Coenzyme A (Drake et al., 2008), acetic acid and ethanol in bacteria like *C. ragsdalei*. The electrons taken from CO and H_2 are passed through ferredoxin into the cell reactions. The directed flow of electrons from CO and H_2 to distribution indicates the water gas shift reaction that converts CO to H_2 and CO_2 is in equilibrium

(See Section 8.4.3 for detailed discussion). This is only true when the concentration of CO inside the cell is very low. In this case, the concentration of CO in the bulk liquid can be assumed to be zero for calculation of mass transfer, and the volumetric mass transfer coefficient for CO, $k_{L,CO}a/V_L$, can be calculated from the change of gas composition over time as in Equation 5.2 with $p_{CO}^* = 0$. Equation 5.1 is integrated for CO partial pressure changing over time to derive Equation 5.2.

$$\frac{k_{L,\mathrm{CO}}a}{V_L} = -\frac{V_G H_{CO}}{RTV_L(t_2 - t_1)} \ln \frac{(p_{CO,2} - p_{CO}^*)}{(p_{CO,1} - p_{CO}^*)} \qquad 5.2$$

The value of $k_{L,CO}a/V_L$, calculated assuming mass transfer limitation is the "apparent $k_{L,CO}a/V_L$", but will represent the actual capacity for mass transfer of CO when H_2 is also consumed and CO is mass transfer limited. The calculated apparent $k_{L,CO}a/V_L$ in fermentation bottles is shown in Figure 5.8. The calculated $k_{L,CO}a/V_L$ is low at the beginning of fermentation, but rises to about 6 to 8 h^{-1} for all bottles after 24 h. Slight decreases in the calculated $k_{L,CO}a/V_L$ follow each introduction of fresh gas (at 24 h, 48 h and 72 h). Since the surface area of the gas/liquid interface does not change, and agitation and volume of liquid are nearly constant, it is expected that $k_{L,CO}\,a/V_L$ will be nearly constant throughout the fermentation and the same for all bottles. The data in Figure 5.8 suggest that $k_{L,CO}a/V_L$ for 100 ml of aqueous medium in 250 ml Wheaton serum bottles shaken at 150 rpm is about 7 h^{-1}. The apparent $k_{L,CO}a/V_L$ for the bottles at high pressure, 238 kPa, falls to about 1 h^{-1} after gas is replaced at 72 h. Since $k_{L,CO}\,a/V_L$ is expected to remain unchanged, this observation suggests that a kinetic limit is established by the introduction of fresh syngas at 238 kPa. An inhibition of cell activity by CO, a powerful reductant, follows decreased energy demand as nutrients to support growth are depleted from the medium. The activity of *C. ragsdalei* in the intermediate

bottles (134 and 169 kPa) slowed after gas was replaced at 96 h (data not shown), but the bottles at 114 kPa continued to consume CO and H_2 beyond 100 h. The fermentation is seen to transition from a kinetic limitation imposed by low cell concentration, through mass transfer limitation that accompanies vigorous growth, to again establish kinetic limitation as growth slows from depletion of nutrients after 72 h for bottles at 238 kPa and after 96 h for bottles at 134 and 169 kPa.

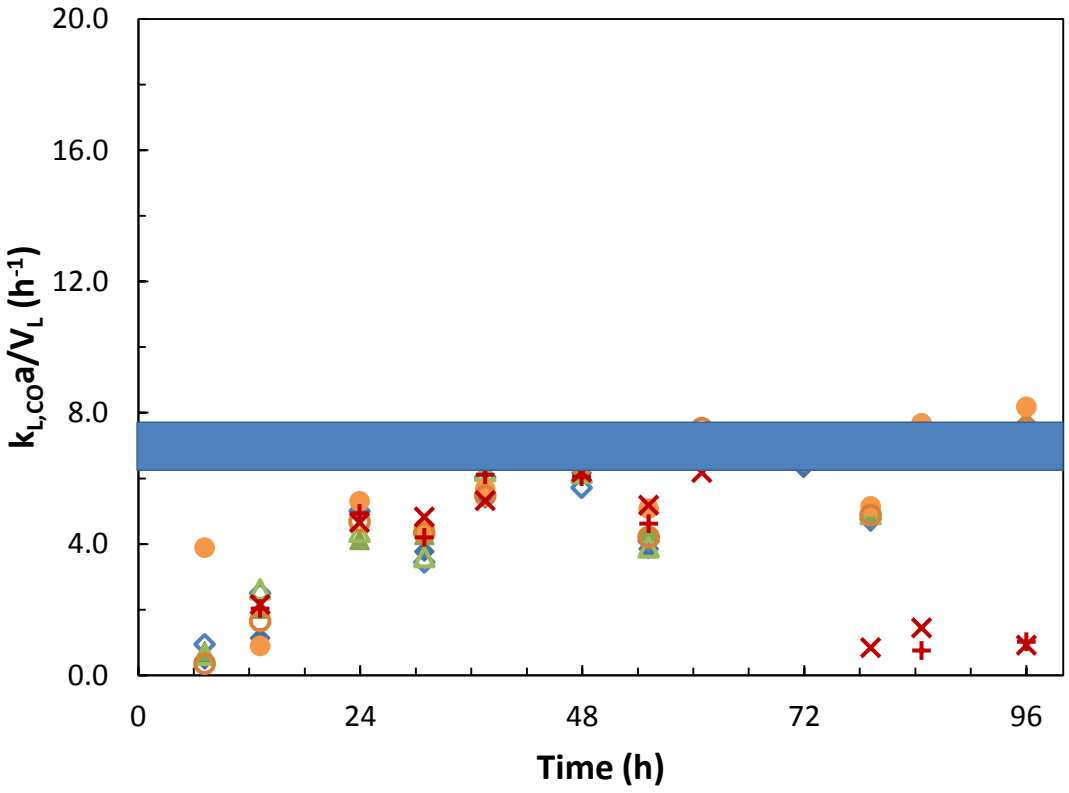

Figure 5.8 Apparent volumetric mass transfer coefficient for CO in syngas fermentation bottles with 100 mL liquid at different initial gas pressures. Bottles Pr2B1 (◆) and Pr2B2 (◇) have initial pressure of 114 kPa, Pr2B3 (▲) and Pr2B4 (△) 134 kPa, Pr2B5 (●) and Pr2B6 (○) 169 kPa, and Pr2B7 (×) and Pr2B8 (+) 238 kPa. The shaded area indicates the range of data deemed to be mass transfer limited.

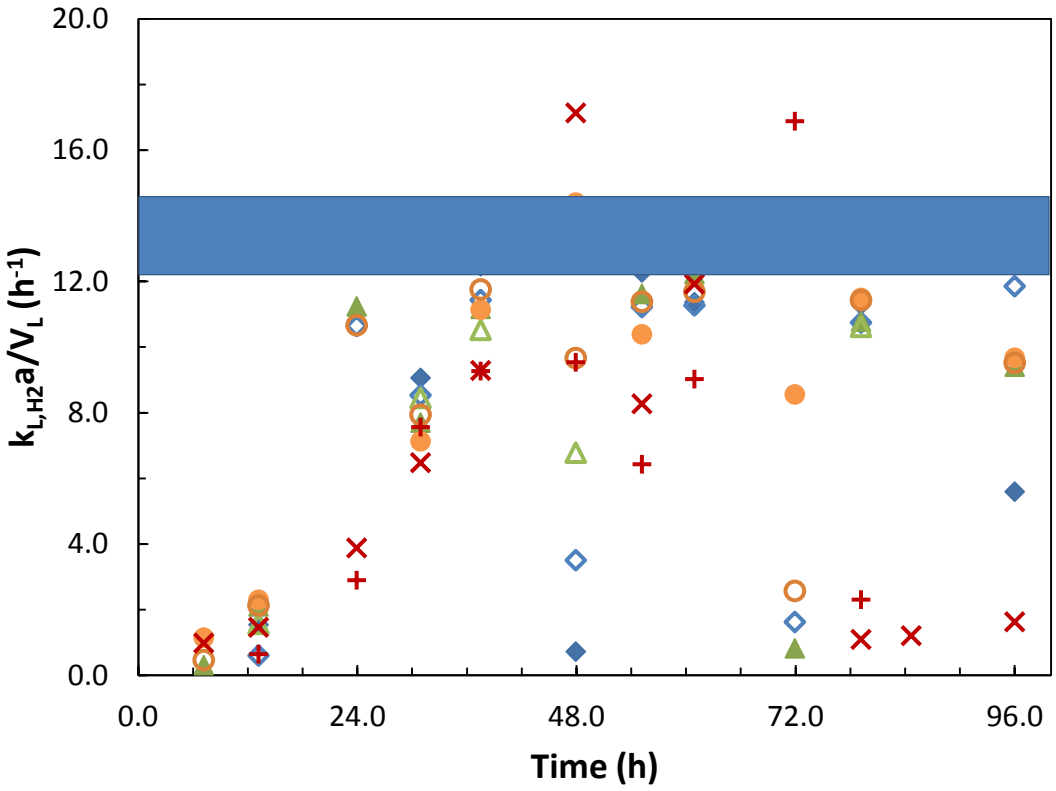

Figure 5.9 Apparent volumetric mass transfer coefficient for H_2 in syngas fermentation bottles with 100 mL liquid at different initial gas pressures. Bottles Pr2B1 (◆) and Pr2B2 (◇) have initial pressure of 114 kPa, Pr2B3 (▲) and Pr2B4 (△) 134 kPa, Pr2B5 (●) and Pr2B6 (○) 169 kPa, and Pr2B7 (×) and Pr2B8 (+) 238 kPa. The shaded area indicates the range of data deemed to be mass transfer limited.

The calculated apparent $k_{L,H2}a/V_L$ is shown in Figure 5.9. The $k_{L,H2}a/V_L$ is expected to be proportional to $k_{L,CO}a/V_L$ as shown in equation 5.3 (McCabe and Smith, 1976), where $D_{i,W}$ is the diffusivity of gas i in water.

$$\frac{k_{L,H2}a}{V_L} = \sqrt{\frac{D_{H2,W}}{D_{CO,W}}}\left(\frac{k_{L,CO}a}{V_L}\right) \qquad 5.3$$

The diffusivities of H_2, CO and CO_2 in water at 37°C are 6.24×10^{-5} cm^2/s, 2.50×10^{-5} cm^2/s and 2.69×10^{-5} cm^2/s respectively. The maximum observed value for $k_{L,CO}a/V_L$ of 7.5 h^{-1} between 48 and 96 h from Figure 5.8 scales using Equation 5.3 to 11.8 h^{-1} for

$k_{L,H2}a/V_L$, this expected value is slightly lower than the observed maximum values of about 13 h^{-1} seen in Figure 5.9. The uptake of H_2 is expected to be sensitive to CO concentration as CO is known to inhibit hydrogenase (Ragsdale and Ljungdahl, 1984) the enzyme that catalyzes oxidation of H_2. Hydrogenase of *Acetobacterium woodii* that is similar to the hydrogenase in acetogens was 50% inhibited by 7×10^{-9} M CO (equivalent to 8.5×10^{-4} kPa dissolved CO).

Characterization of mass transfer was the purpose of the overall study, and initial work was conducted in serum bottles. Experience with acetogens grown on CO and H_2 (Phillips et al., 1994) set the expectation that both CO and H_2 would be consumed by *C. ragsdalei* and that typically, initial consumption would be CO only, and that H_2 conversion would begin gradually and proceed until all CO and H_2 were consumed. This agrees with the observations of Hu et al. (2011) who concluded that CO is the preferred substrate. Established procedure was to inoculate acetogenic cultures into serum bottles containing syngas at 238 kPa (20 psig), and sample and replace the headspace with fresh gas daily (Maddipati et al., 2011). However, sampling a serum bottle once per day did not define the consumption of CO and H_2 with sufficient detail for mass transfer calculations. The studies described here used frequent sampling and allowed high conversion of the CO and H_2 to ensure a condition of mass transfer limitation that could be defined from the sampling data. The course of fermentation at initial charged pressures of 40:30:30 $CO:H_2:CO_2$ syngas showed initial fast CO uptake in Figure 5.6 and inhibited H_2 uptake in Figure 5.7; this was followed by a period of mass transfer limitation for both CO and H_2 where the uptake rate was proportional to the partial pressure of CO or H_2 in the gas, and late in fermentation accumulated CO again inhibited

uptake of H_2. This behavior affirms the conceptual model of syngas fermentation discussed in Section 5.3, in that high initial CO retarded cell activity and inhibited H_2 uptake, but allowed fast uptake of H_2 as CO became mass transfer limited.

5.6.2 Derivatives for Kinetic and Thermodynamic Parameters

Description of fermentation kinetics incorporates time differentials of measured parameters that describe the cell culture. The specific growth rate is the production of cell mass per unit of cell mass per time, g_x/g_x h or h^{-1}, and calculated as

$$\mu = \frac{1}{X}\frac{dX}{dt} \tag{5.4}$$

Where X is the cell mass concentration, in g/L. The specific uptake for CO (q_{CO}) or H_2 (q_{H2}) is the consumption of the gas per unit cell mass per time, mol/g_x h.

$$q_{CO} = \frac{1}{XV_L}\frac{dn_{CO}}{dt} \tag{5.5}$$

$$q_{H2} = \frac{1}{XV_L}\frac{dn_{H2}}{dt} \tag{5.6}$$

$$q_{CO+H2} = \frac{1}{XV_L}\frac{dn_{CO+H2}}{dt} \tag{5.7}$$

The differential quantities can be estimated at specific time using a curve fit of the cell concentration and curve fit of the gas inventory as discussed in Appendix B. The cell concentration and inventory of CO and H_2 are defined by a polynomial curve fit of the measured data. The analysis was applied for each of the eight bottles in the study with comparable results. The differential quantities derived from the curve fit analysis of carefully timed and taken fermentation data allow calculation of the specific growth, and specific uptake, and the contemporary dissolved concentrations of CO, H_2 and CO_2. This data can be correlated to study kinetics on the cellular level.

The rates of cell growth and consumption of CO, H_2 and the sum of CO and H_2 uptake are shown in Figures 5.10 and 5.11. Rates of growth and consumption rise through the first 24 h of the fermentation as the initial charge of syngas is consumed and cell growth begins. Cell growth rate shows a diauxic growth pattern, with fast growth up to 32 h of fermentation, slow growth from 36 h to 64 h, and a moderate growth rate from 72 to 84 h.

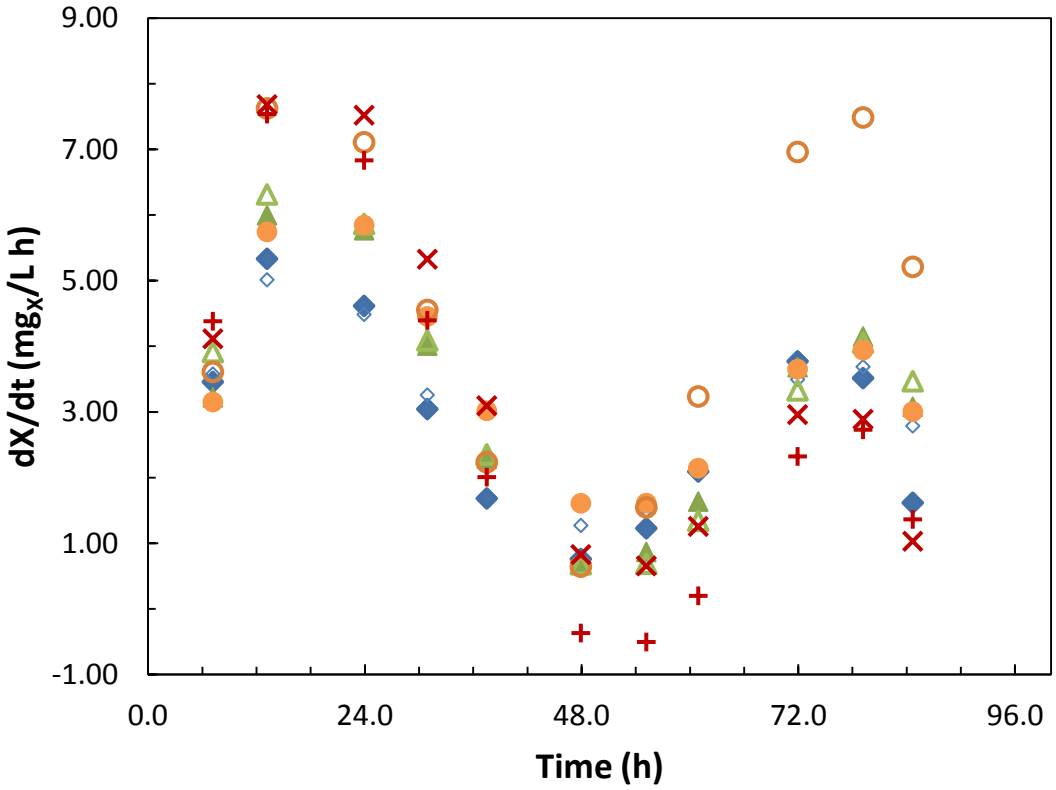

Figure 5.10 Growth rate of cell mass in syngas fermentation bottles with 100 mL liquid at different initial gas pressures. Bottles Pr2B1 (◆) and Pr2B2 (◇) have initial pressure of 114 kPa, Pr2B3 (▲) and Pr2B4 (△) 134 kPa, Pr2B5 (●) and Pr2B6 (○) 169 kPa, and Pr2B7 (×) and Pr2B8 (+) 238 kPa.

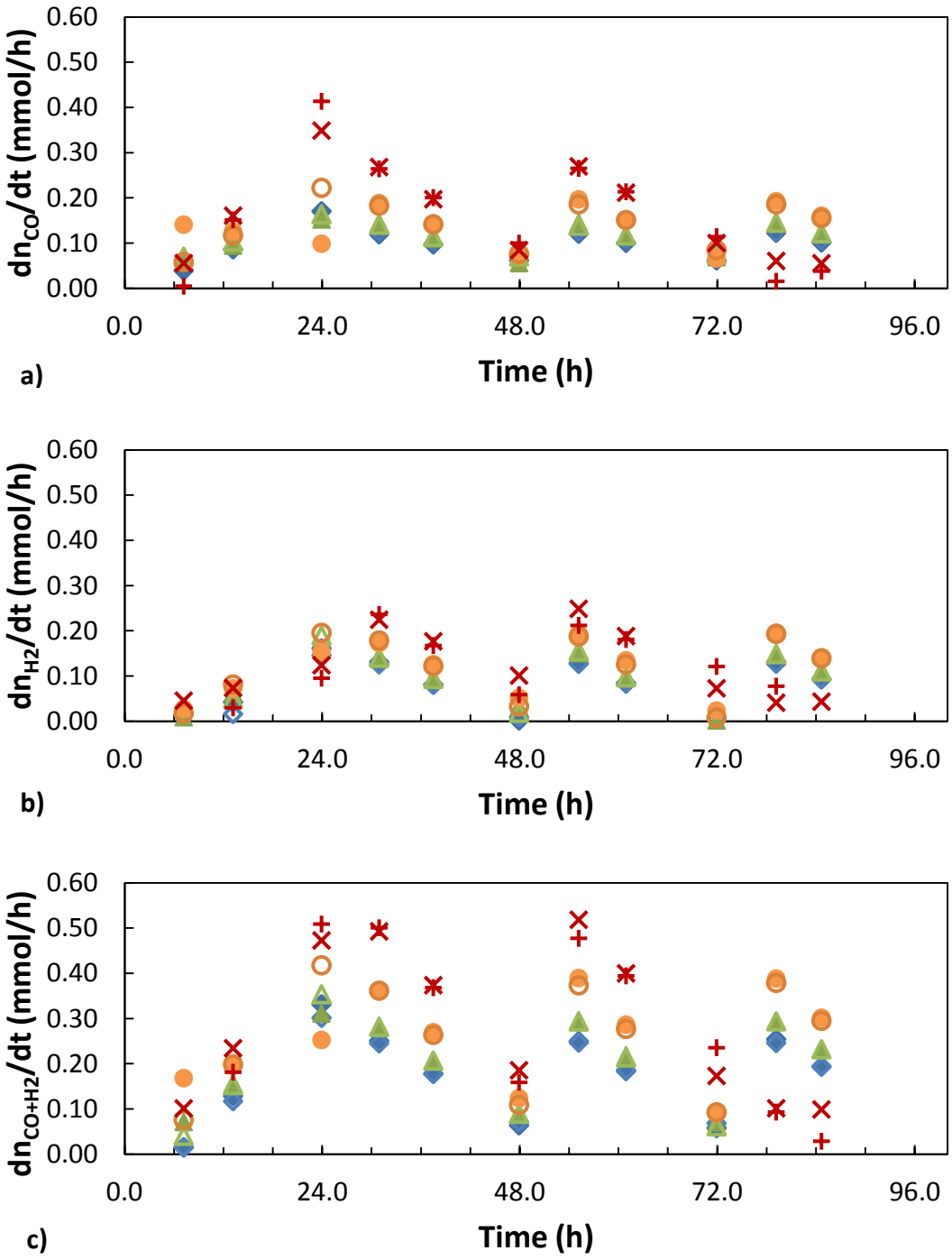

Figure 5.11 Molar rate of uptake for (a) CO, (b) H_2 and (c) $CO+H_2$ in syngas fermentation bottles with 100 mL liquid at different initial gas pressures. Bottles Pr2B1 (◆) and Pr2B2 (◇) have initial pressure of 114 kPa, Pr2B3 (▲) and Pr2B4 (△) 134 kPa, Pr2B5 (●) and Pr2B6 (○) 169 kPa, and Pr2B7 (×) and Pr2B8 (+) 238 kPa.

The fast initial growth might use the amino acids and proteins in yeast extract to synthesize cell materials, and the second moderate growth period might synthesize cell material from CO and H_2 taken from the syngas. About 85% of the cell mass in Figure 5.2 is formed in the first 48 h of fermentation in growth on yeast extract, but 50% of the acetic acid and 80% of the ethanol in Figures 5.4 and 5.5 is produced after 48 h during growth on syngas. Growth with yeast extract forms cell mass from preformed protein and amino acids, giving a high yield of cells from CO plus H_2 consumed. By contrast, protein must be synthesized from CO and H_2 when growth is on syngas, and more acetic acid and ethanol is accumulated with a lower yield of cell mass. This indicates that productivity, though proportional to cell concentration, is not linked to growth rate.

The increasing rate of uptake of CO and H_2 in the initial charge of syngas (up to 24 h) indicates a kinetic rate limit as the cell mass starts low and grows to a concentration that can process the CO and H_2 supplied, even as the mass transfer driving force is reduced by gas consumption (Figure 5.11c). The subsequent periods of declining consumption rate following replenishment of the syngas are consistent with mass transfer limitation for both CO and H_2 in that the transfer rate falls as the driving force is reduced.

Using Equation 5.1 to describe transfer of CO under mass transfer limitation from 24 h to 96 h of fermentation, and setting $p_{CO}^* = 0$, the mass transfer coefficient $k_{L,CO}a$ can be determined from a plot of dn_{CO}/dt versus p_{CO}, the partial pressure of CO in the gas phase (Figure 5.12). The slope of the line in Figure 5.12 is $k_{L,CO}a/H_{CO}$ and with H_{CO} = 121,560 L kPa/mol CO as the Henry's law constant for CO at 37°C (Hougen et al., 1954), $k_{L,CO}a$ is about 573 mL/h or $k_{L,CO}a/V_L$ is about 5.7 h^{-1} for transfer into V_L of 100 mL, slightly lower than 6 to 8 h^{-1} estimated from Figure 5.8. For the first sampling after the

syngas is replenished, dn_{CO}/dt does not fall on the line; this is consistent with lower estimated $k_{L,CO}a/V_L$ seen in Figure 5.8 at these points. The low $k_{L,CO}a/V_L$ seen in Figure 5.8 is associated with the procedure to replace gas, and may result from slow recovery from time off the shaker and low temperature (as low as 23°C) established as the gas is replaced. Calculation of $k_{L,CO}a/V_L$ using the integrated equation 5.2 and the instantaneous rates shown in Figure 5.11a, and $k_{L,CO}a/V_L$ derived from the graphical analysis of Figure 5.12 show good agreement supporting the assumptions made in the method development.

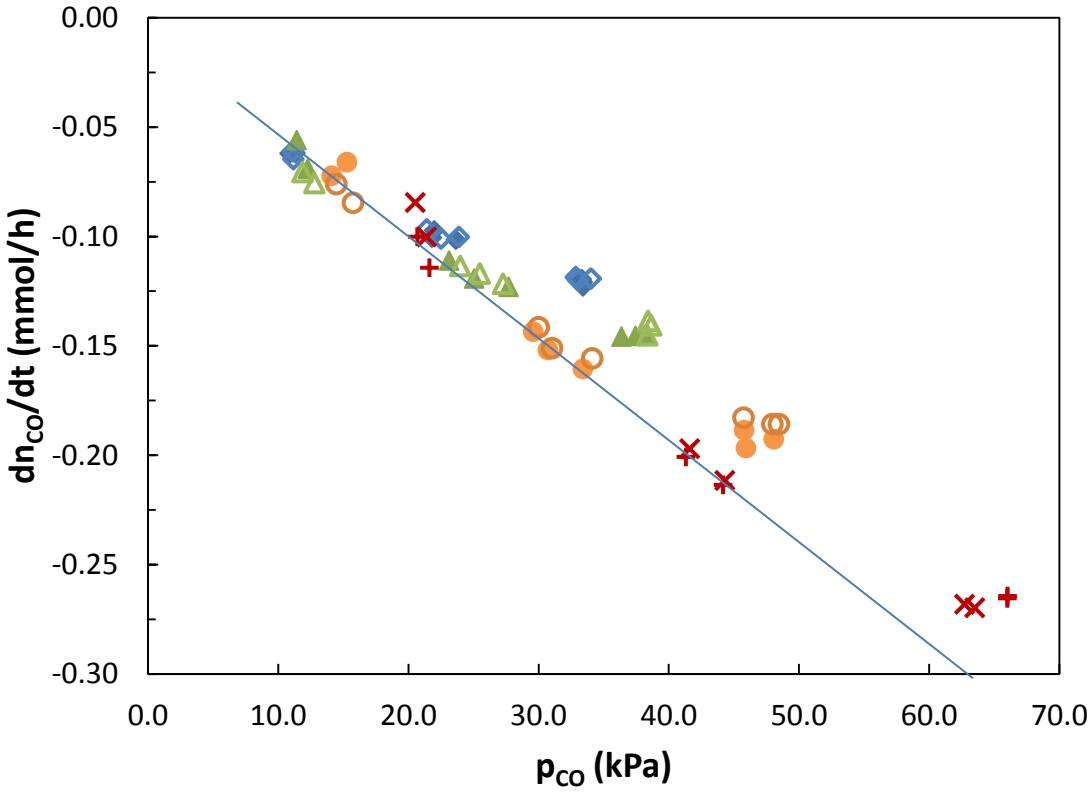

Figure 5.12 Molar rate for CO depletion (negative of uptake) versus partial pressure of CO in the gas headspace in syngas fermentation bottles with 100 mL liquid at different initial gas pressures. Bottles Pr2B1 (◆) and Pr2B2 (◇) have initial pressure of 114 kPa, Pr2B3 (▲) and Pr2B4 (△) 134 kPa, Pr2B5 (●) and Pr2B6 (○) 169 kPa, and Pr2B7 (×) and Pr2B8 (+) 238 kPa.

Equation 5.1 is also applied in Figure 5.13 to plot the rate of H_2 uptake against the partial pressure of H_2, $p_{H2,}$ for the mass transfer limited period from 24 h to 96 h. The slope of the line in Figure 5.13 is $k_{L,H2}a/H_{H2}$ and with H_{H2} = 140,260 L kPa/mol H_2 as the Henry's law constant for H_2 at 37°C (Hougen et al., 1954), $k_{L,H2}a$ is about 1350 ml/h or $k_{L,H2}a/V_L$ is about 13.5 h^{-1} into V_L = 100 mL, similar to the estimate from Figure 5.9. The rates of H_2 uptake when p_{H2} > 20 kPa fall well off the line and again indicate a kinetic limit to H_2 uptake, which is attributed to CO inhibition of the hydrogenase enzyme and indicates the dissolved CO concentration is more than 7×10^{-9} mol/L (Ragsdale and Ljungdahl, 1984).

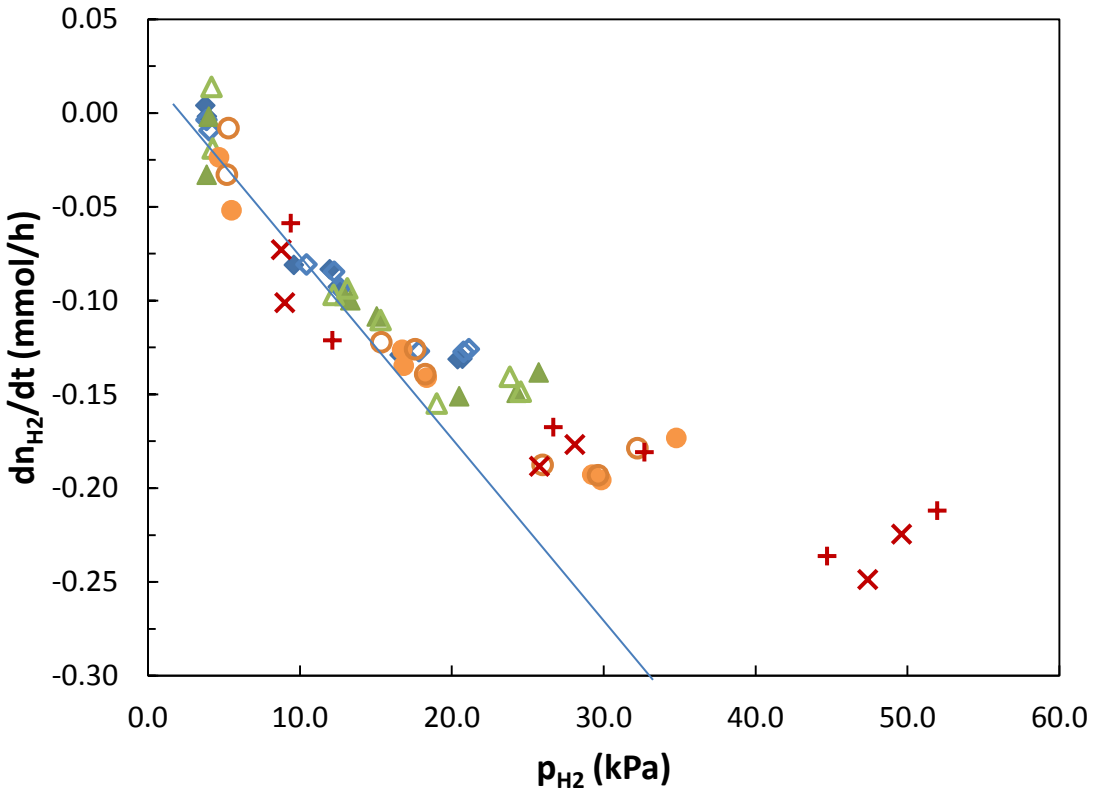

Figure 5.13 Molar rate for H_2 depletion (negative of uptake) versus partial pressure of H_2 in the gas headspace in syngas fermentation bottles with 100 mL liquid at different initial gas pressures. Bottles Pr2B1 (◆) and Pr2B2 (◇) have initial pressure of 114 kPa, Pr2B3 (▲) and Pr2B4 (△) 134 kPa, Pr2B5 (●) and Pr2B6 (○) 169 kPa, and Pr2B7 (×) and Pr2B8 (+) 238 kPa.

Specific growth rate (μ), grams of cells produced per hour per gram of cells (g_x/g_x h or h^{-1}), was calculated from the rate of cell growth in Figure 5.10 and the cell concentration derived from Figure 5.2. The specific growth rates in Figure 5.14 are high initially, with some uncertainty in measurement of the low cell concentrations, but correspond to cell doubling times of 3 to 6 h. The specific growth drops as the mass transfer limit is established, nutrients are depleted and pH drops, and probably do not represent the maximum possible growth rate in growth on syngas.

Specific uptake rate for CO (q_{CO}), moles of CO consumed per hour per gram of cells (mol CO/g_x h) shown in Figure 5.15, was calculated from the rate of CO uptake in

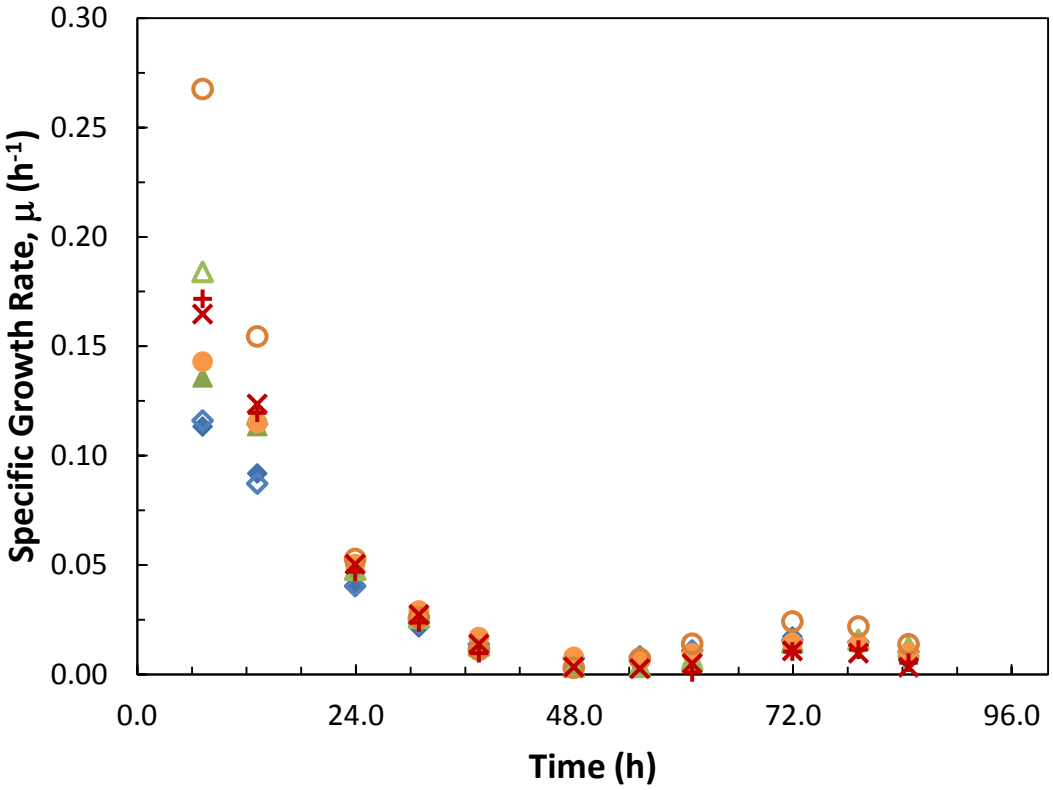

Figure 5.14 Specific growth rate of *C. ragsdalei* in syngas fermentation bottles with 100 mL liquid at different initial gas pressures. Bottles Pr2B1 (◆) and Pr2B2 (◇) have initial pressure of 114 kPa, Pr2B3 (▲) and Pr2B4 (△) 134 kPa, Pr2B5 (●) and Pr2B6 (○) 169 kPa, and Pr2B7 (×) and Pr2B8 (+) 238 kPa.

Figure 5.11a and the cell concentration derived from Figure 5.2. The specific uptake of CO is initially high as the concentration of CO in the bulk liquid is high (between 3.3×10^{-4} mol/L at fresh syngas saturation and 7×10^{-9} mol/L where H_2 inhibition is relieved (Ragsdale and Ljungdahl, 1984)). But specific uptake of CO slows as the concentration of CO in the bulk liquid and inside the cells drops as the mass transfer limitation for CO is established. Again the rates after 24 h of fermentation probably do not represent the maximum specific uptake rate possible for CO, as the rate is set by the mass transfer. The specific uptake for H_2 (q_{H2}) is shown in Figure 5.16 and is again

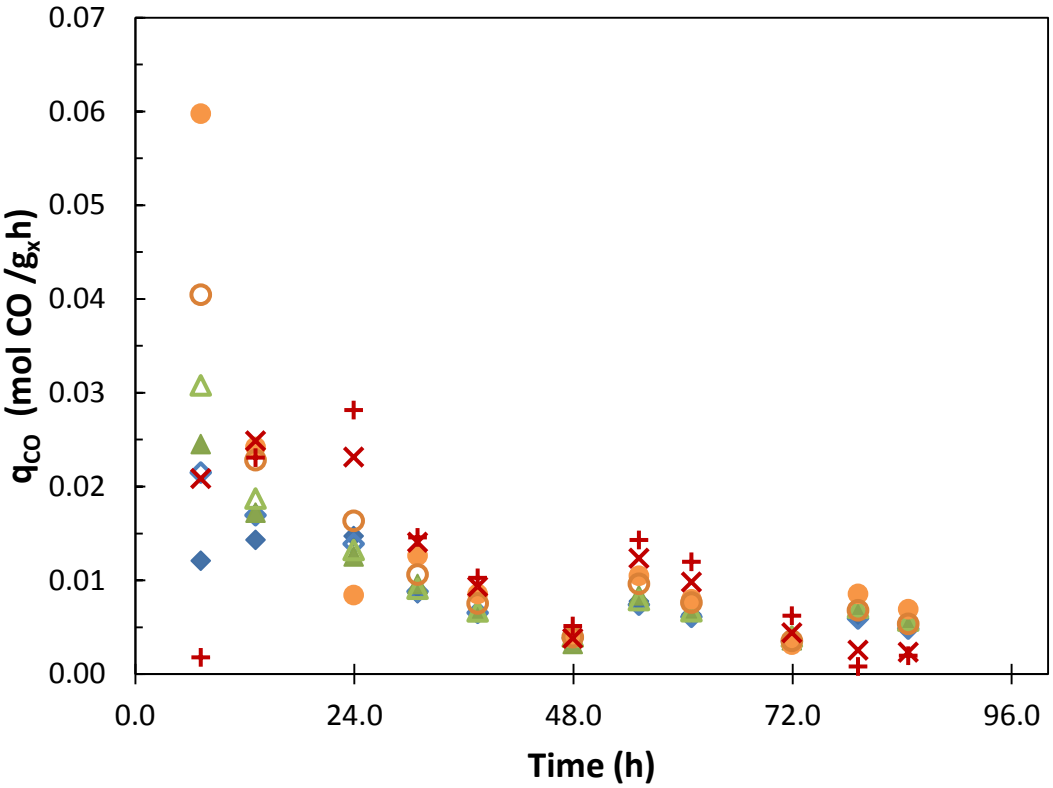

Figure 5.15 Specific uptake rate of CO for *C. ragsdalei* in syngas fermentation bottles with 100 mL liquid at different initial gas pressures. Bottles Pr2B1 (◆) and Pr2B2 (◇) have initial pressure of 114 kPa, Pr2B3 (▲) and Pr2B4 (△) 134 kPa, Pr2B5 (●) and Pr2B6 (○) 169 kPa, and Pr2B7 (×) and Pr2B8 (+) 238 kPa.

limited by the mass transfer from 24 h to 72 h. The specific uptake of H_2 is low before 24 h, and again for the bottles at 238 kPa after 72 h. The rate is suppressed by the high concentration of CO in these stages of fermentation. The high initial specific uptake rates seen for CO are not seen for H_2 since high concentrations of H_2 in the batch fermentation are always accompanied by high concentrations of CO and low concentrations of CO imply mass transfer limitation for H_2 as well. Again the rates after 24 h of fermentation probably do not represent the maximum specific uptake rate possible for H_2, as the rate is set by the mass transfer.

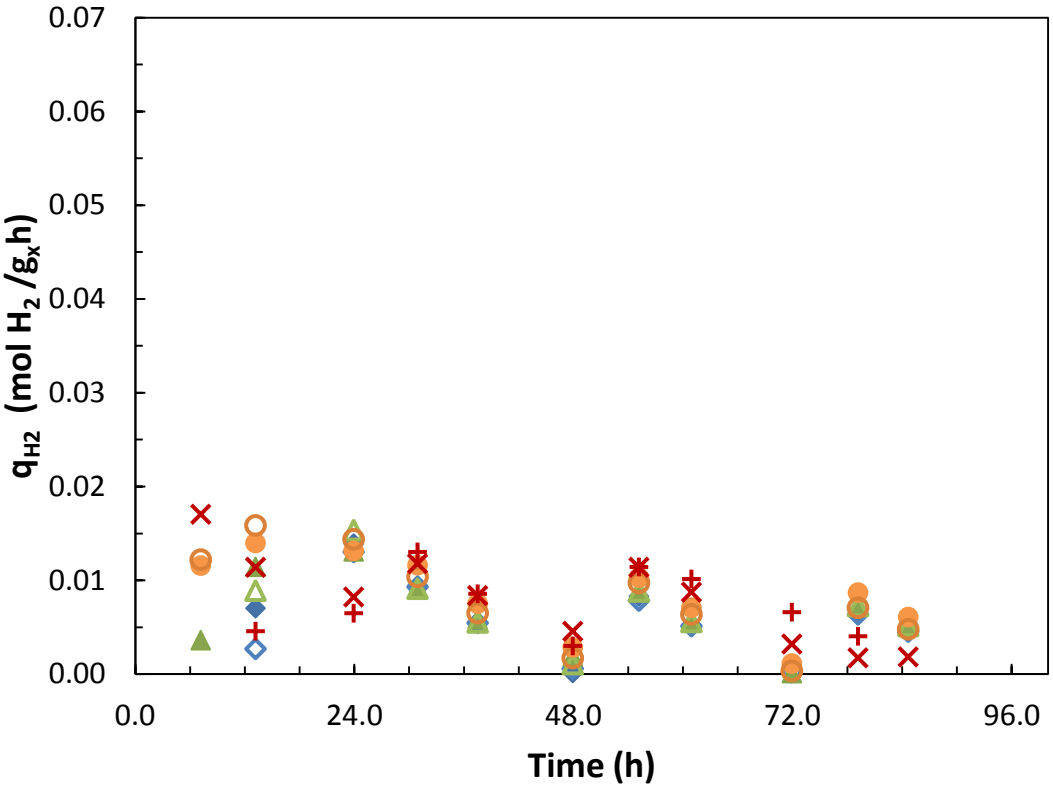

Figure 5.16 Specific uptake rate of H_2 for *C. ragsdalei* in syngas fermentation bottles with 100 mL liquid at different initial gas pressures. Bottles Pr2B1 (◆) and Pr2B2 (◇) have initial pressure of 114 kPa, Pr2B3 (▲) and Pr2B4 (△) 134 kPa, Pr2B5 (●) and Pr2B6 (○) 169 kPa, and Pr2B7 (×) and Pr2B8 (+) 238 kPa.

The molar uptake rate of H_2 from the curve fit of experimental data was used with $k_{L,CO}\,a/V_L$ and the measured H_2 partial pressures in Equation 5.3 to estimate the dissolved pressure of H_2 (Figure 5.17 for Bottle Pr2B6). The partial pressures of CO, H_2 and CO_2 in the gas are shown for comparison. Dissolved CO_2 is assumed to be in equilibrium with CO_2 in the gas, as the rate of transfer is low and CO_2 is more soluble than CO and H_2. The dissolved pressures of H_2 and CO_2 and the assumption of thermodynamic equilibrium of the water gas shift reaction (See Section 8.4.3) were used to estimate the partial pressure of dissolved CO, which is also shown in Figure 5.17, and is 4 orders of magnitude lower than the partial pressure of CO in the gas.

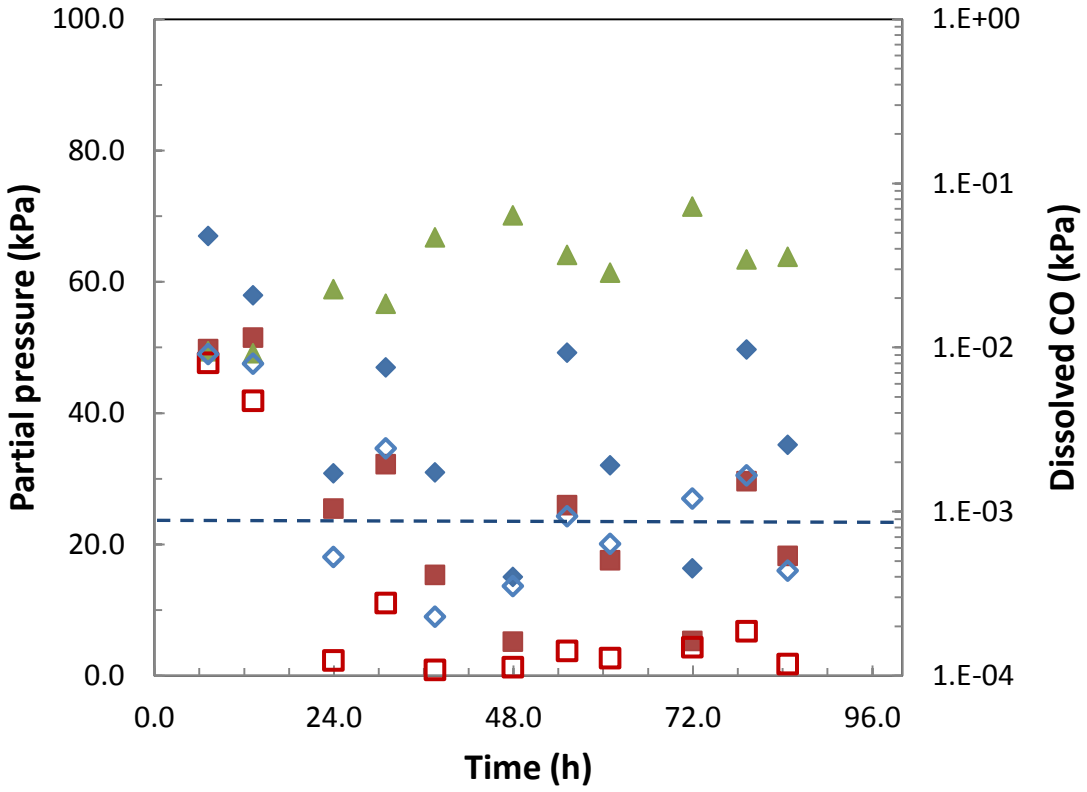

Figure 5.17 Partial pressures of CO, H_2 and CO_2 in bottle Pr2B6 with 100 mL liquid syngas fermentation. CO (◆), H_2 (■), CO_2 (▲), dissolved H_2 (□) left axis and dissolved CO (◇) right axis. CO concentration as dissolved CO for 50% inhibition of hydrogenase of *A. woodii* is indicated by the dashed line (Ragsdale and Ljungdahl, 1984).

The partial pressure of dissolved CO inside the cell is plotted for all bottles in Figure 5.18 and is more than 10^4 times lower than the partial pressure of CO in the gas headspace. The low concentration of dissolved CO inside the cell supports the initial assumption of transfer to zero used in estimation of $k_{L,CO}a/V_L$. The dissolved CO is shown relative to the value of 8.5×10^{-4} kPa (7×10^{-9} mol/L CO) reported by (Ragsdale and Ljungdahl, 1984) to inhibit the hydrogenase of *A. woodii* by 50%, which is shown by the dashed line. The bottles initially charged to 114 or 134 kPa are generally at or below the 50% inhibition after 20 h, while the bottles initially at 169 kPa fall below the reported inhibition as the gas is

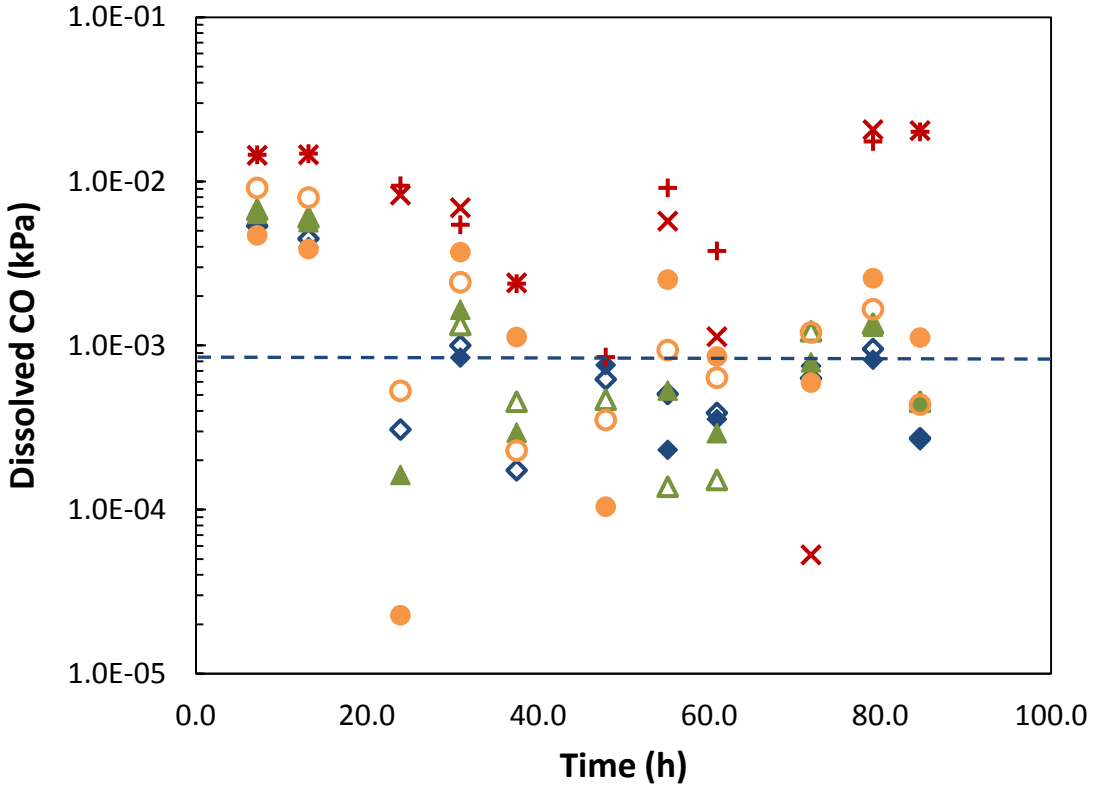

Figure 5.18 Partial pressure of dissolved CO in syngas fermentation bottles with 100 mL liquid at different initial gas pressures. Bottles Pr2B1 (◆) and Pr2B2 (◇) have initial pressure of 114 kPa, Pr2B3 (▲) and Pr2B4 (△) 134 kPa, Pr2B5 (●) and Pr2B6 (○) 169 kPa, and Pr2B7 (×) and Pr2B8 (+) 238 kPa. CO concentration for 50% inhibition of hydrogenase of *A. woodii* is indicated by the dashed line (Ragsdale and Ljungdahl, 1984)

depleted. The bottles initially at 234 kPa are generally well above the level of 50% inhibition, but fall below the line before gas is replaced at 48 h and 72 h. This agrees with the inhibition of H_2 uptake seen in the bottles (Figures 5.7 and 5.13).

The partial pressures of dissolved CO and H_2 calculated in this analysis represent the conditions inside the cells that drive the reactions of the production pathway. The dissolved pressures, p_{CO}^* and p_{H2}^*, are important kinetic and thermodynamic parameters, and are the appropriate concentrations for use in calculations and models of thermodynamics and enzymology of the fermentation.

The sampling data in the study, with bottles containing 100 ml of medium that were sampled frequently, was of sufficient quality to derive time derivatives of cell concentration, and CO and H_2 inventory in each bottle. Frequent careful sampling provided data suitable for estimation of kinetic and thermodynamic parameters from serum bottle fermentation. The derivative quantities allow calculation of the kinetic parameters, specific uptake and specific growth, and of thermodynamic quantities, like the dissolved concentrations of CO, H_2 and CO_2 at discrete points in time. These derived parameters can be correlated with the observed fermentation parameters to improve our model of syngas fermentation.

This work developed techniques that derive mass transfer, kinetic and thermodynamic parameters from batch syngas fermentation in serum bottles; application of the techniques in study of syngas fermentation remains to be done.

5.6.3 Effect of Maintained Pressure on Mass Transfer into 50 mL Medium

Sections 5.6.1 and 5.6.2 show an experiment with extensive sampling and depletion of each charged volume of gas to obtain well defined data curves to quantify

mass transfer into 100 mL liquid in the bottle fermentation. The curves generated for consumption of CO and H_2, as well as the production of cell mass, CO_2, acetic acid and ethanol were suited to derivation of instantaneous rates at any time and the calculation of the dissolved gas concentrations as partial pressures. However, the rates were dominated by the mass transfer limits that were a primary objective of the experimental protocol. A modified experimental protocol was used to better isolate the effect of syngas pressure on the fermentation. The same initial pressures of fresh syngas were used with transfer into half the volume of liquid medium (50 mL). The supply of gas per ml of liquid (*G/L*) is 2.55 times the *G/L* for bottles with 100 ml initial liquid, and the gas supply was further increased as the headspace was replaced after each sample to maintain constant gas supply, after growth was established in all bottles. Less frequent samples were taken (every 12 h) and curve fit equations used in Section 5.6.2 could not be obtained. Consumption rates for CO and H_2 were obtained from the cumulative uptake, but these rates represent an average over the period from gas replenishment and sampling. The uptake rates, specific uptake, and dissolved CO pressure derived with these rates are similar to those obtained in Section 5.6.2, but do not represent conditions at a particular time and will not be shown here.

The total pressure at sampling and after gas replacement in all bottles is shown in Figure 5.19; the vertical dashed lines indicate when gas was replenished. The initial gas charge is consumed under a kinetic limitation that manifests as a lag phase (slow growth and consumption) over the first 37 h of fermentation. This is similar, but more pronounced, to the kinetic limitation seen in bottles with 100 ml liquid, Figure 5.1. After sampling at 37 h, the gas in each bottle was replaced after each sample with fresh gas to

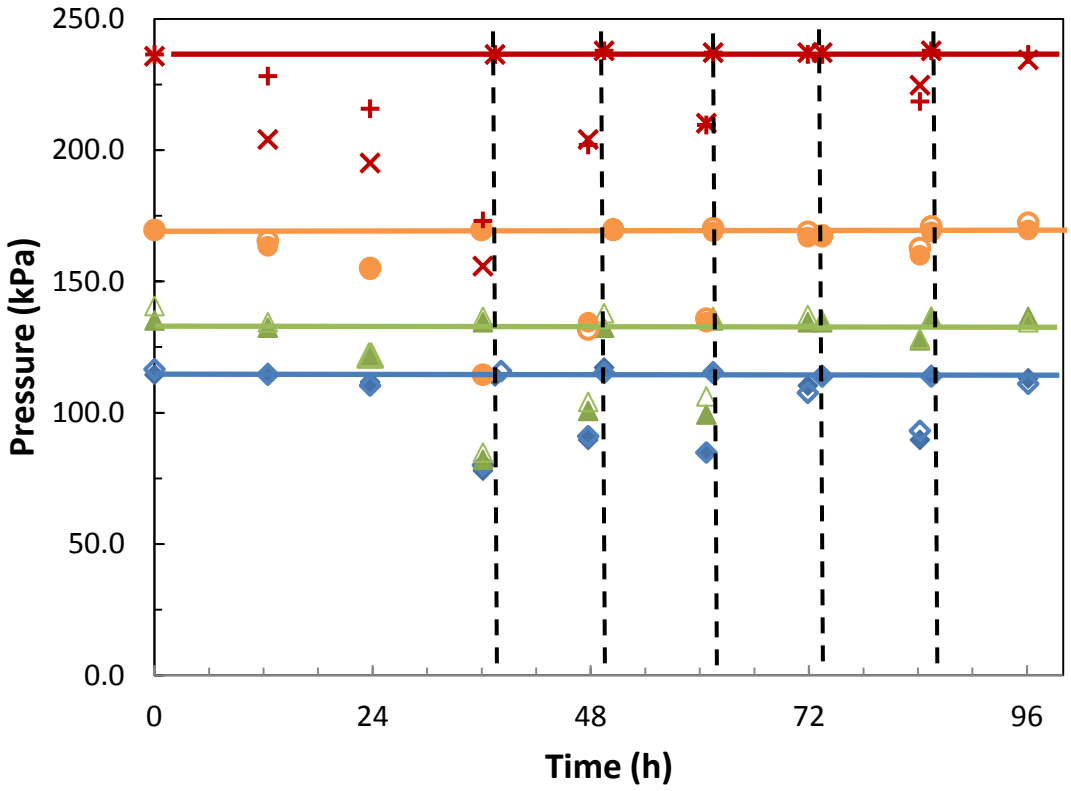

Figure 5.19 Pressure through syngas fermentation in bottles with 50 mL medium with initial pressure indicated by the horizontal lines and fresh gas supply indicated by the vertical dashed lines. Bottles Pr3B1 (◆) and Pr3B2 (◇) have initial pressure of 114 kPa, Pr3B3 (▲) and Pr3B4 (△) 134 kPa, Pr3B5 (●) and Pr3B6 (○) 169 kPa, and Pr3B7 (×) and Pr3B8 (+) 238 kPa.

maintain the pressure near the initial pressure charge, at 38, 50, 62, 74 and 86 h of fermentation.

The fermentation into 50 mL of medium yielded slightly higher cell concentration than in 100 mL, Figure 5.2. Growth in 50 mL medium was similar in all bottles through 61 h of fermentation as seen in Figure 5.20. The sustained supply of CO and H_2 maintained steady production of cell mass and higher yield of cells from the nutrient medium. Cell mass increased faster in bottles maintained at higher pressure as uptake, particularly of CO, was faster. But the maximum cell concentration was the same at all pressures.

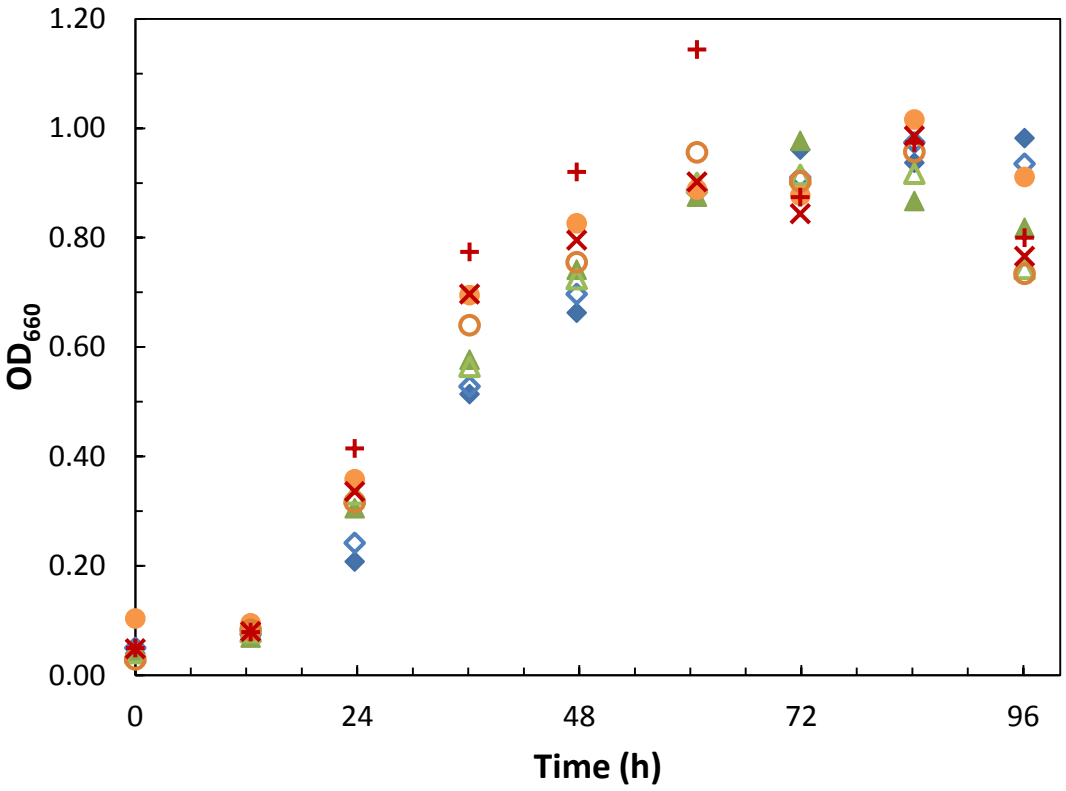

Figure 5.20 Cell concentration in syngas fermentation bottles with 50 mL medium maintained at different gas pressures. Bottles Pr3B1 (◆) and Pr3B2 (◇) were maintained at 114 kPa, Pr3B3 (▲) and Pr3B4 (△) 134 kPa, Pr3B5 (●) and Pr3B6 (○) 169 kPa, and Pr3B7 (×) and Pr3B8 (+) 238 kPa.

The pH of the fermentation broth in Figure 5.21 drops from 6.3 to around 5.0 in 24 h, and then below 4.5 at 37 h. The pH was adjusted higher with addition of 0.5 mL 7% $NaHCO_3$ to all bottles at 37 h and again at 60 h. Ethanol production begins as the pH falls below 5.0 and increases after 37 h. Fermentation pH is an important thermodynamic parameter, and ethanol production is favored at lower pH.

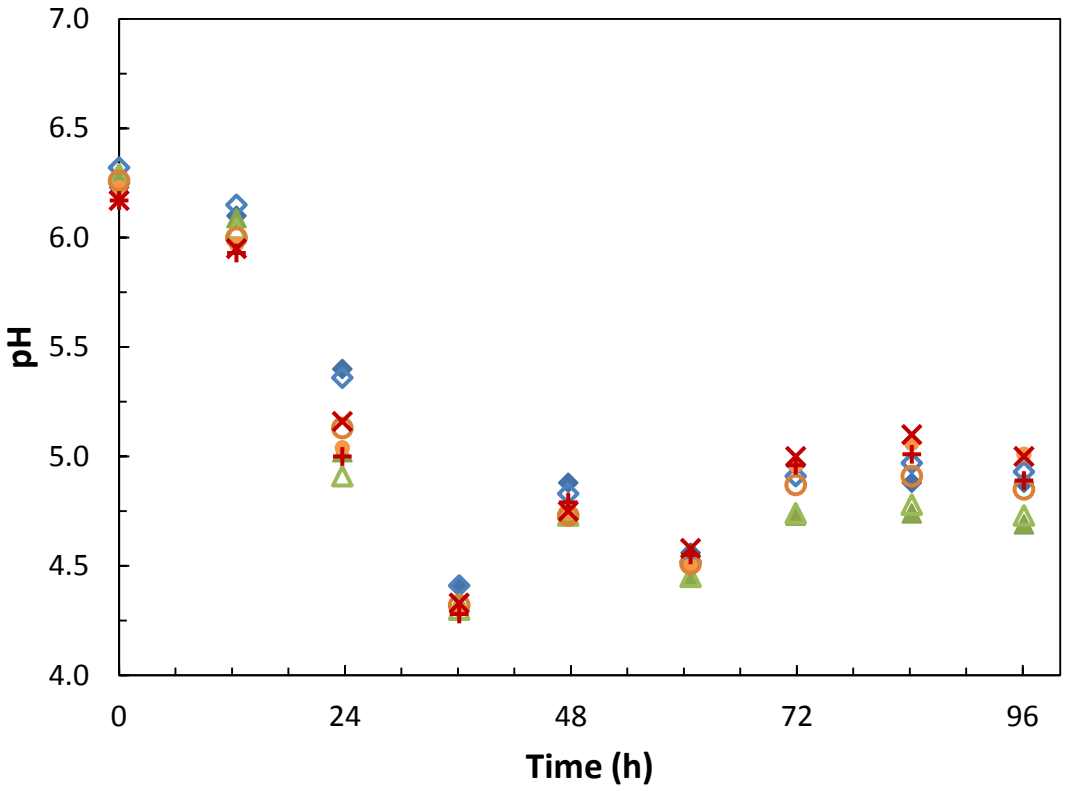

Figure 5.21 pH in syngas fermentation bottles with 50 mL medium maintained at different gas pressures. Bottles Pr3B1 (◆) and Pr3B2 (◇) were maintained at 114 kPa, Pr3B3 (▲) and Pr3B4 (△) 134 kPa, Pr3B5 (●) and Pr3B6 (○) 169 kPa, and Pr3B7 (×) and Pr3B8 (+) 238 kPa.

Figure 5.22 shows acetic acid concentration near 4 g/l is attained at 50 h in all bottles and concentration then increases in bottles with lower pressure and decreases in bottles maintained at higher pressure. Ethanol in Figure 5.23 accumulates after 24 h of fermentation and ethanol production at 96 h is best at the highest and lowest maintained pressures (238 and 114 kPa). Total productivity, acetic acid plus ethanol, is highest at 96 h for the bottles maintained at the lowest pressure, 114 kPa.

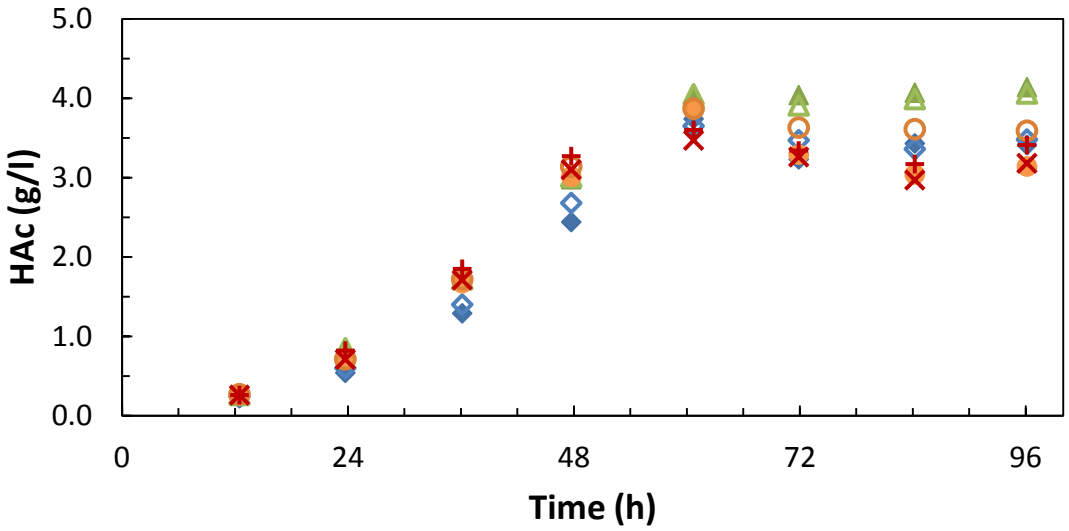

Figure 5.22 Acetic acid production in syngas fermentation bottles with 50 mL medium maintained at different gas pressures. Bottles Pr3B1 (◆) and Pr3B2 (◇) were maintained at 114 kPa, Pr3B3 (▲) and Pr3B4 (△) 134 kPa, Pr3B5 (●) and Pr3B6 (○) 169 kPa, and Pr3B7 (×) and Pr3B8 (+) 238 kPa.

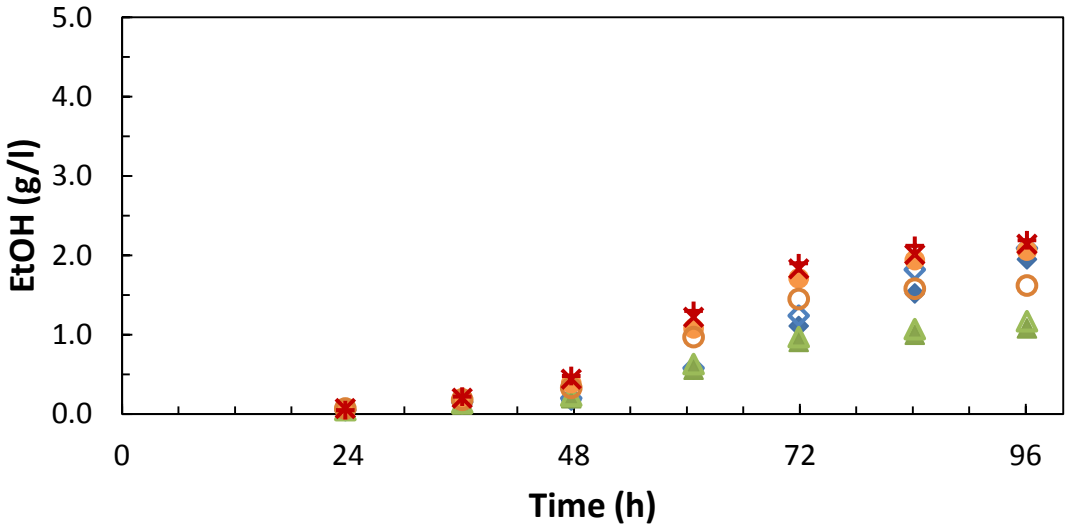

Figure 5.23 Ethanol production in syngas fermentation in serum bottles with 50 mL medium maintained at different gas pressures. Bottles Pr3B1 (◆) and Pr3B2 (◇) were maintained at 114 kPa, Pr3B3 (▲) and Pr3B4 (△) 134 kPa, Pr3B5 (●) and Pr3B6 (○) 169 kPa, and Pr3B7 (×) and Pr3B8 (+) 238 kPa.

The cumulative uptake of CO, H_2 and CO+H_2 in all bottles is presented in Figure 5.24. CO uptake is favored in bottles with higher pressure, Figure 5.24a, as higher concentration of CO at the oxidizing enzyme, carbon monoxide dehydrogenase or CODH, increases the rate of reaction. But uptake of H_2 in Figure 5.24b is not increased by high pressure, since higher concentration of CO slows the rate of reaction of H_2 on hydrogenase. Both CO and H_2 are competent as reductant in the pathway reactions, and the combined uptake of CO plus H_2 is seen in Figure 5.24c. While highest uptake was achieved at the highest pressure, the advantage is only about 15% and is achieved with lower conversion of CO and especially of H_2, which reduces the conservation of energy from the feed gas to the liquid product.

The conversion of CO is shown for all bottles in Figure 5.25 and conversion of H_2 is shown in Figure 5.26. The percent conversion of CO is similar in all bottles from 37 to 72 h of fermentation, indicating that again CO mass transfer is limited and dependent on the partial pressure of CO in the gas. However, the percent conversion of H_2 is higher at all times in the bottles at 114 and 134 kPa, and lowest at the highest pressure, 238 kPa. This indicates that although mass transfer is limiting for CO, the concentration of CO is high enough to inhibit hydrogenase and impose a kinetic limitation for H_2 uptake.

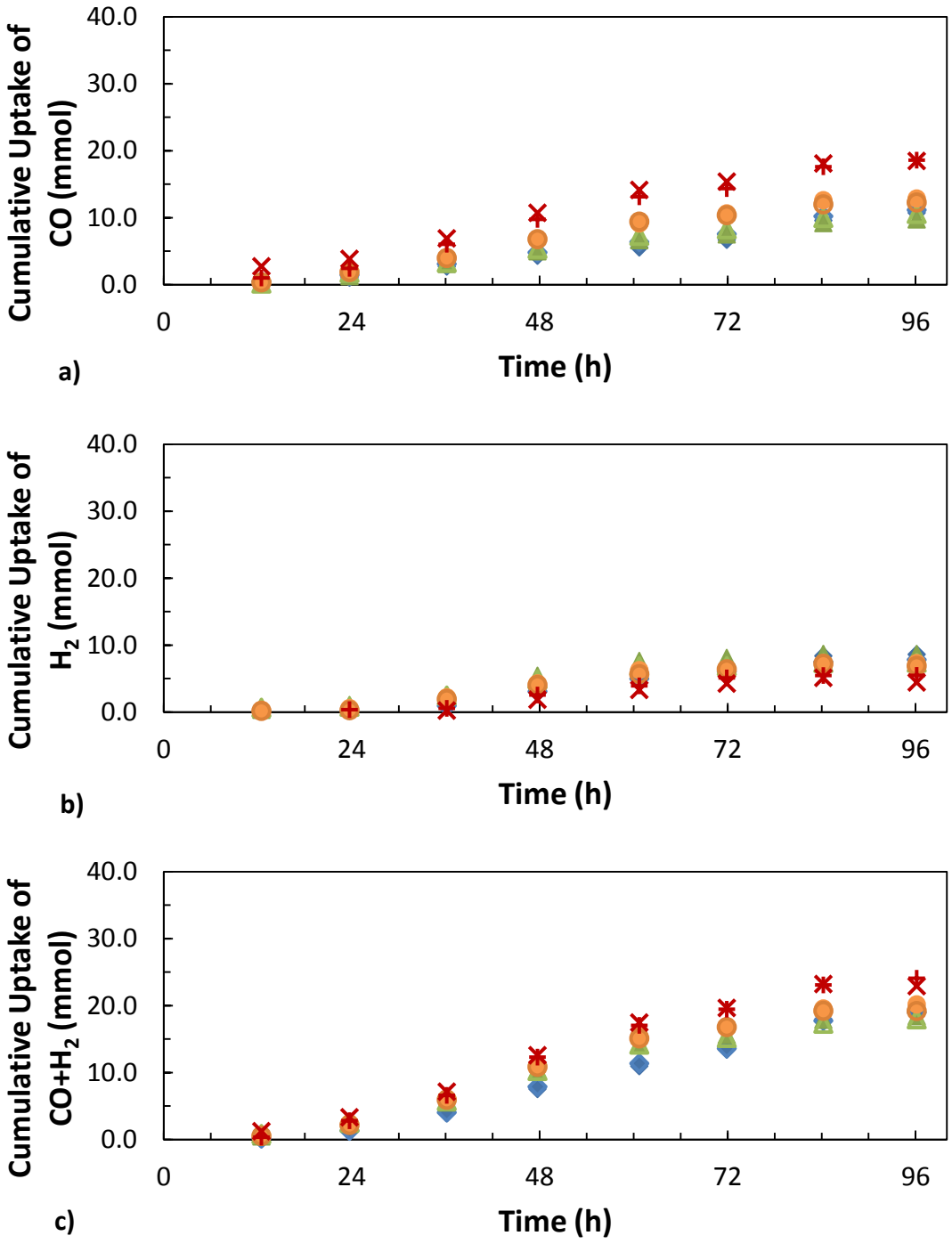

Figure 5.24 Cumulative uptake of (a) CO, (b) H_2 and (c) CO+H_2 in syngas fermentation bottles with 50 mL medium maintained at different gas pressures. Bottles Pr3B1 (◆) and Pr3B2 (◇) were maintained at 114 kPa, Pr3B3 (▲) and Pr3B4 (△) 134 kPa, Pr3B5 (●) and Pr3B6 (○) 169 kPa, and Pr3B7 (×) and Pr3B8 (+) 238 kPa.

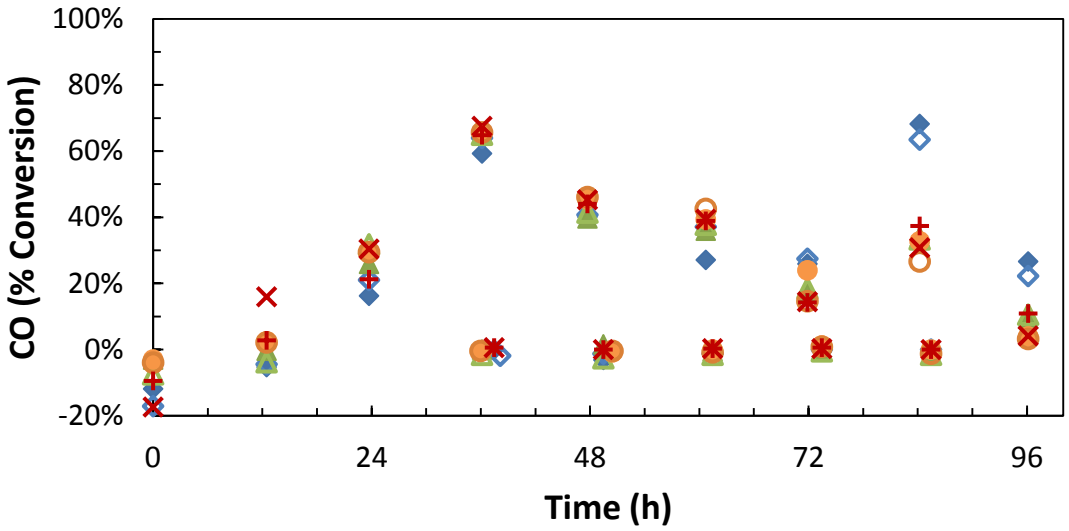

Figure 5.25 CO conversions in syngas fermentation bottles with 50 mL medium maintained at different gas pressures. Bottles Pr3B1 (◆) and Pr3B2 (◇) were maintained at 114 kPa, Pr3B3 (▲) and Pr3B4 (△) 134 kPa, Pr3B5 (●) and Pr3B6 (○) 169 kPa, and Pr3B7 (×) and Pr3B8 (+) 238 kPa.

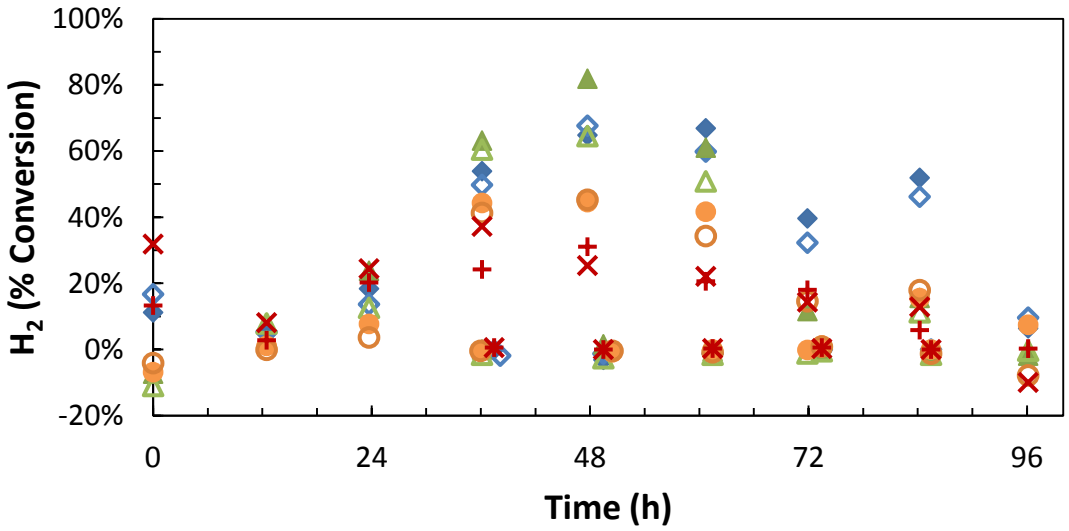

Figure 5.26 H_2 conversions in syngas fermentation bottles with 50 mL medium maintained at different gas pressures. Bottles Pr3B1 (◆) and Pr3B2 (◇) were maintained at 114 kPa, Pr3B3 (▲) and Pr3B4 (△) 134 kPa, Pr3B5 (●) and Pr3B6 (○) 169 kPa, and Pr3B7 (×) and Pr3B8 (+) 238 kPa.

The volumetric mass transfer coefficient for CO, $k_{L,CO}\,a/V_L$ is shown in Figure 5.27. The maximum apparent $k_{L,CO}a/V_L$ is attained with similar values in all bottles at 36 h and 48 h, and is about 14 h^{-1}. This is two times the $k_{L,CO}a/V_L$ of 7 h^{-1} shown in Figure 5.8, and is expected as all aspects of mass transfer are similar, except that V_L, the liquid volume into which gas is transferred, is reduced by half. Apparent $k_{L,CO}a/V_L$ rises to the maximum as cell concentration approaches its maximum and the cells are still very active. This fermentation experiment with only 50 mL liquid volume and pressure maintained near the initial charge was typically kinetically limited with mass transfer limitation for CO only between 36 h and 84 h.

The apparent volumetric mass transfer coefficient for H_2, $k_{L,H2}\,a/V_L$, is shown versus time in Figure 5.28. Apparent $k_{L,H2}a/V_L$ reaches the maximum of 22 h^{-1} (estimated using $k_{L,CO}\,a/V_L$ of 14 h^{-1} from Figure 5.27 in equation 5.3) only in the lower pressure

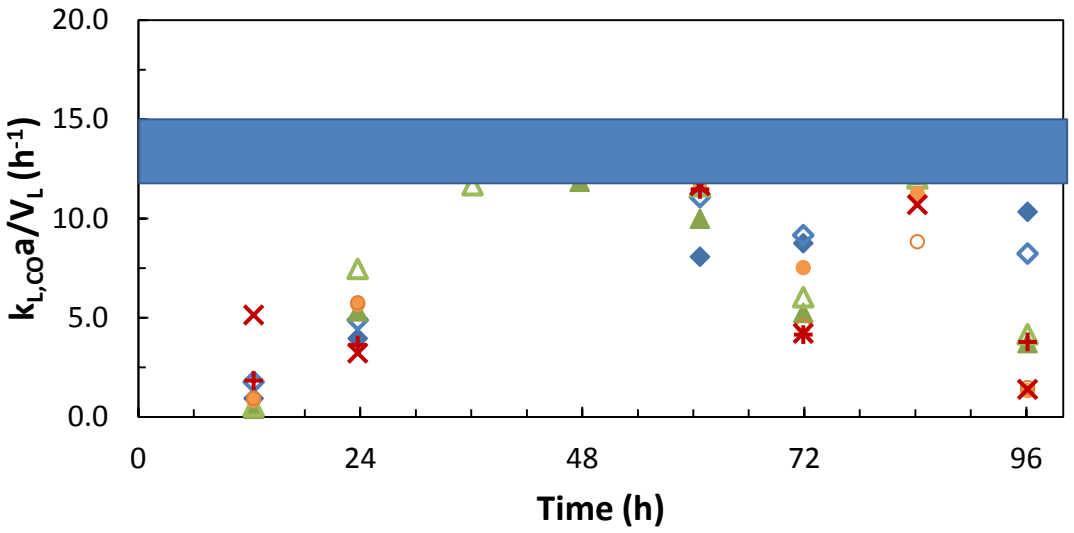

Figure 5.27 Apparent volumetric mass transfer coefficient for CO in the course of syngas fermentation bottles with 50 mL medium maintained at different gas pressures. Bottles Pr3B1 (◆) and Pr3B2 (◇) were maintained at 114 kPa, Pr3B3 (▲) and Pr3B4 (△) 134 kPa, Pr3B5 (●) and Pr3B6 (○) 169 kPa, and Pr3B7 (×) and Pr3B8 (+) 238 kPa. The shaded area indicates the range of data deemed to be mass transfer limited.

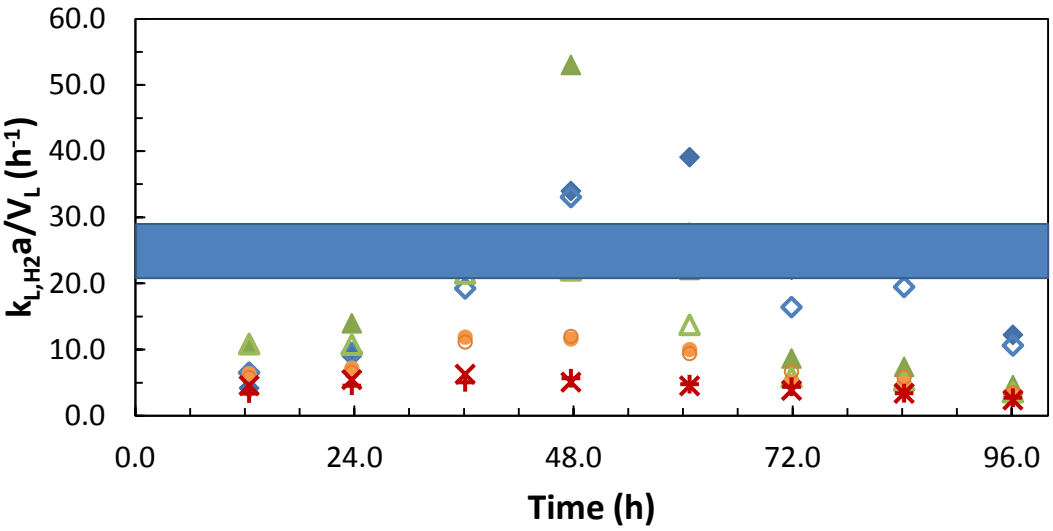

Figure 5.28 Apparent volumetric mass transfer coefficient for H_2 in the course of syngas fermentation bottles with 50 mL medium maintained at different gas pressures. Bottles Pr3B1 (◆) and Pr3B2 (◇) were maintained at 114 kPa, Pr3B3 (▲) and Pr3B4 (△) 134 kPa, Pr3B5 (●) and Pr3B6 (○) 169 kPa, and Pr3B7 (×) and Pr3B8 (+) 238 kPa. The shaded area indicates the range of data deemed to be mass transfer limited.

bottles at 114 and 134 kPa, the CO inhibition of H_2 uptake is not fully relieved at any time in the fermentations with 238 or 169 kPa gas supply. The apparent $k_{L,H2}a/V_L$ of 53 h^{-1} at 48 h was due to very low quantitation of H_2 relative to CO and CO_2 in the raw data, and was considered to be an outlier. High values of $k_{L,H2}a/V_L$ of 33 h^{-1} and 38 h^{-1} observed in bottles Pr3B1 and Pr3B2 at 48 h and 61 h are plausible, but again low quantitation for H_2 in the raw data raise doubt of the validity of the data. Otherwise, the observed maximum value, between 21 and 28 h^{-1} in 50 mL medium is again about twice the $k_{L,H2}a/V_L$ of 13 h^{-1} into 100 mL of liquid observed in Figure 5.9.

The estimated dissolved partial pressure of CO is shown for all bottles in Figure 5.29. The estimated p_{CO}^* is not correct, as the analysis for calculation of p_{CO}^* assumes that hydrogenase is active. The actual value of p_{CO}^* is probably much higher than

indicated at 12 and 24 h, and again after 72 h, since H_2 uptake is very low. The values from 36 to 60 h may be high, since H_2 is consumed at these times, but the hydrogenase is at least partially inhibited. The estimated p_{CO}^* is seen to be arithmetically near 0 (much less than p_{CO} > 40 kPa in the gas) for purposes of defining mass transfer limitation, but higher than 8.5×10^{-4} kPa or 7×10^{-9} mol/L CO reported to inhibit hydrogenase by 50% (Ragsdale and Ljungdahl, 1984).

C. ragsdalei maintained under a range of syngas pressure near the fresh composition shifted substrate consumption from predominately CO at 238 kPa

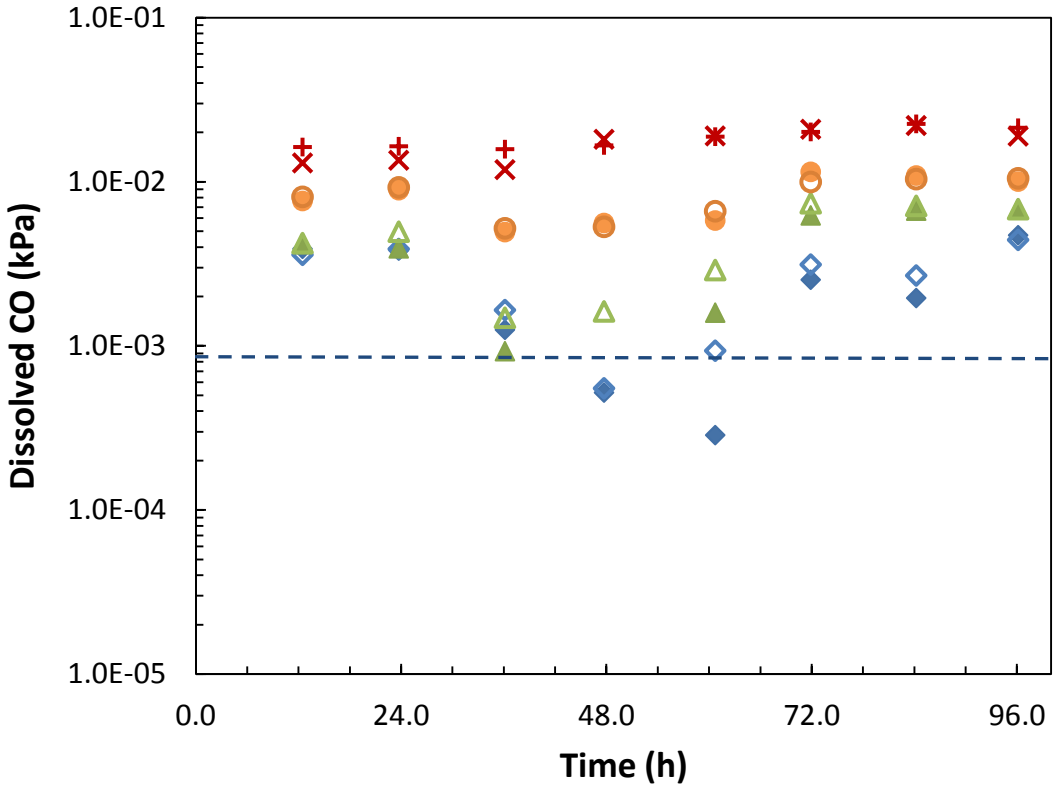

Figure 5.29 Partial pressure of dissolved CO in syngas fermentation bottles with 50 mL medium maintained at different gas pressures. Bottles Pr3B1 (◆) and Pr3B2 (◇) have initial pressure of 114 kPa, Pr3B3 (▲) and Pr3B4 (△) 134 kPa, Pr3B5 (●) and Pr3B6 (○) 169 kPa, and Pr3B7 (×) and Pr3B8 (+) 238 kPa. CO concentration for 50% inhibition of hydrogenase of *A. woodii* is indicated by the dashed line (Ragsdale and Ljungdahl, 1984)

maintained pressure, to a balanced uptake of CO and H_2 at 114 kPa maintained. The products of syngas fermentation, cell mass, acetic acid and ethanol were only slightly affected by the change in pressure. Inhibition of H_2 uptake was apparent in all bottles, and was relieved only in the lower pressure bottles as cell growth increased energy demand and kinetic capacity. The assumption of constant $k_{L,CO}a$ in the serum bottles was supported, with the observed $k_{L,CO}a/V_L$ and $k_{L,H2}a/V_L$ in Figures 5.27 and 5.28 doubling for 50 mL of medium compared to the previous experiments with 100 mL of medium in the bottles, Figures 5.8 and 5.9.

5.7 Conclusions

Fermentation of CO and H_2 from synthesis gas was studied in serum bottles with particular effort to define the gas to liquid mass transfer. CO was assumed to be mass transfer limited, and mass transfer capacity was described as the volumetric mass transfer coefficient, $k_{L,CO}a/V_L$, which was found to be 7 h^{-1} with 100 mL liquid volume and 14 h^{-1} with 50 mL liquid volume, in 250 mL serum bottles shaken upright at 150 rpm. This suggests a constant value of $k_{L,CO}a$ of 700 mL/h for these conditions. The value of $k_{L,H2}a/V_L$ indicating the capacity for mass transfer of H_2 is calculated to be 13 h^{-1} into 100 mL liquid volume, or $k_{L,H2}a$ of 1300 mL/h at the same conditions. The dissolved CO concentration , as equilibrium partial pressure, was shown to be 10,000 times lower than the gas phase partial pressure, supporting the initial assumption of transfer to zero concentration for mass transfer limited CO. The dissolved CO concentration around p_{CO}^* of 8.5×10^{-4} kPa slowed the uptake of H_2 by inhibition of hydrogenase. H_2 uptake rate increased when p_{CO}^* was decreased below this value by mass transfer limitation.

References

Bird, R.B., Stewart, W.E., Lightfoot, E.N. 2002. Transport Phenomena. 2nd ed, J. Wiley. New York, pp. xii, 895 p.

Drake, H.L., Gossner, A.S., Daniel, S.L. 2008. Old Acetogens, New Light. in: *Incredible Anaerobes: From Physiology to Genomics to Fuels*, (Eds.) J. Wiegel, R.J. Maier, M.W.W. Adams, Vol. 1125, pp. 100-128.

Gaddy, J.L., D. K. Arora, C-W Ko, J. R. Phillips, R. Basu, C. V. Wikstrom and E. C. Clausen. 2007. Methods for Increasing the Production of Ethanol from Microbial Fermentation. 7285402.

Griffin, D.W., Schultz, M.A. 2012. Fuel and Chemical Products from Biomass Syngas: A Comparison of Gas Fermentation to Thermochemical Conversion Routes. Environmental Progress & Sustainable Energy, n/a-n/a.

Hougen, O.A., Watson, K.M., Ragatz, R.A. 1954. *Chemical Process Principles*. *2d ed*. Wiley, New York,, pp.v.

Hu, P., Bowen, S.H., Lewis, R.S. 2011. A Thermodynamic Analysis of Electron Production During Syngas Fermentation. Bioresource Technology, 102 (17), 8071-8076.

Maddipati, P., Atiyeh, H.K., Bellmer, D.D., Huhnke, R.L. 2011. Ethanol Production from Syngas by Clostridium Strain P11 Using Corn Steep Liquor as a Nutrient Replacement to Yeast Extract. Bioresource Technology, 102 (11), 6494-6501.

McCabe, W.L., Smith, J.C. 1976. *Unit Operations of Chemical Engineering*. *3rd ed*. McGraw-Hill, New York, NY,

Munasinghe, P.C., Khanal, S.K. 2010. Syngas Fermentation to Biofuel: Evaluation of Carbon Monoxide Mass Transfer Coefficient (K(L)a) in Different Reactor Configurations. Biotechnology Progress, 26 (6), 1616-1621.

Phillips, J.R., Clausen, E.C., Gaddy, J.L. 1994. Synthesis Gas as Substrate for the Biological Production of Fuels and Chemicals. Applied Biochemistry and Biotechnology, 45-6, 145-157.

Ragsdale, S.W., Ljungdahl, L.G. 1984. Hydrogenase from Acetobacterium-Woodii. Archives of Microbiology, 139 (4), 361-365.

Saxena, J. 2008. Development of an Optimized and Cost-Effective Medium for Ethanol Production by *Clostridium* Strain P11. Dissertation. University of Oklahoma, 131.

Shuler, M.L., Kargi, F. 2002. *Bioprocess Engineering Basic Concepts*. *2nd ed*. Prentice Hall PTR, Upper Saddle River, NJ, USA, pp.553.

Vega, J.L., Antorrena, G.M., Clausen, E.C., Gaddy, J.L. 1989. Study of Gaseous Substrate Fermentations: Carbon Monoxide Conversion to Acetate. 2. Continuous Culture. Biotechnology and Bioengineering, 34 (6), 785-793.

Wilkins, M.R., Atiyeh, H.K. 2011. Microbial Production of Ethanol from Carbon Monoxide. Current Opinion in Biotechnology, 22 (3), 326-330.

CHAPTER VI

OXYGEN MASS TRANSFER IN A CONTINUOUSLY STIRRED TANK REACTOR

6.1 Abstract

The continuously stirred tank reactor (CSTR) is commonly used to promote mass transfer in fermentations that consume gas phase substrates. The overall mass transfer coefficient of O_2 in the liquid, $k_{L,O2}a/V_L$, is modeled assuming the gas is in plug flow from inlet to outlet of the CSTR. The logarithmic mean of the differences between the inlet and effluent O_2 concentrations with the bulk liquid O_2 concentration defines $k_{L,O2}a/V_L$. $k_{L,O2}a/V_L$, is correlated with the gas flow and agitator speed. The use of a sparger for the inlet gas increases $k_{L,O2}a/V_L$ and contributes up to 80% of $k_{L,O2}a/V_L$ at low agitation. Transfer of O_2 from air into water exhibited $k_{L,O2}a/V_L$ of 5 h^{-1} at 100 sccm and 150 rpm up to 115 h^{-1} for 400 sccm and 900 rpm. Mass transfer into fermentation medium exhibited $k_{L,O2}a/V_L$ up to 100% higher than transfer into water, with $k_{L,O2}a/V_L$ of 140 h^{-1} observed for aeration of medium at 400 sccm gas flow and 900 rpm in a 3.0 L CSTR. This study establishes the plug flow model of gas contact in the CSTR, and verifies the form of the correlation describing the dependence of $k_{L,O2}a/V_L$ on gas flow and agitation speed.

6.2 Keywords

CSTR, mass transfer, aeration, plug flow model, fermentation medium

6.3 Nomenclature

$C_{i,L}$ – molar concentration of *i* in liquid (mol/L)

C_S – saturated concentration of gas *i* in liquid (mol/L)

CSTR – continuously stirred tank reactor

dn_i/dt – molar rate of transfer of gas species *i* (CO, H_2, CO_2)

D – impeller diameter in CSTR (mm)

$D_{i,W}$ – diffusivity of gas *i* in water

D_o – orifice diameter (mm)

D_P – bubble diameter (mm)

f – fraction of gas saturation (C_L/C_S)

g – acceleration of gravity (9.8 m/s^2)

g_c – force constant

G – gas flow (sccm)

G/L – gas to liquid loading

H_i – Henry's Law constant for gas *i*

* – quantity derived from the Henry's law equilibrium

$k_{L,i}a/V_L$ – volumetric mass transfer coefficient for gas *i* (*i* can represent O_2, CO, H_2 or CO_2)

k_L – liquid film mass transfer coefficient

a – area of the gas liquid interface

V_L – liquid volume into which gas is transferred

L – liquid height in CSTR (mm)

N – agitation speed (rpm)

N_A – Aeration Number (dimensionless)

N_{Fr} – Froude Number (dimensionless)

N_P – Power Number (dimensionless)

N_Q – Flow Number (dimensionless)

p_i – partial pressure of i, p_i^* is partial pressure of dissolved i

P – power input (W)

Q – impeller flow (m^3/min)

t – time (s, min, h)

T – tank diameter of CSTR (mm)

V_s – superficial velocity of gas in CSTR (m/s)

y_G – molar fraction of gas i in gas phase

α – exponent of gas flow in correlation

β – exponent of power input in correlation

γ – proportionality constant for correlation

ρ – fluid density, gas or liquid (g/L)

σ – surface tension of liquid

6.4 Introduction

The continuously stirred tank reactor (CSTR) is commonly used in fermentation processes. A specific application of the CSTR as a fermenter is in the supply of a sparingly soluble gas, such as oxygen (O_2) to maintain growth in aerobic cultures (Garcia-Ochoa and Gomez, 2009). The conversion of synthesis gas components CO, H_2 and CO_2 to produce acetic acid and ethanol by bacteria, especially *Clostridium* species, requires transfer of these sparingly soluble gas species from the gas phase into solution in the aqueous medium that the bacteria inhabit (Bredwell et al., 1999). This mass transfer must occur at a rate sufficient to replace the gas species as they are consumed by the culture. The transfer of CO and H_2 maintain a low concentration of these species in the liquid that supports culture activity and poises the thermodynamic position of the production reactions. The CSTR is the most common fermenter used in study of synthesis gas fermentation (Hu et al., 2010; Kundiyana et al., 2010; Maddipati et al., 2011; Phillips et al., 1993). Charpentier (1981) reviewed gas liquid mass transfer presenting the development of film theory and the modifications assuming surface renewal at the gas liquid interface. The form of the mass transfer model is in either case

$$\frac{1}{V_L}\frac{dn_i}{dt} = \frac{k_{L,i}a}{V_L}\left(C_i^* - C_{L,i}\right) \tag{6.1}$$

Where gas i is transferred from bulk gas with surface area a into the liquid volume V_L at the molar rate dn_i/dt. The transfer is driven by a concentration difference where the concentration of i is C_i^* at the gas/liquid interface and $C_{L,i}$ in the bulk liquid. Pure film theory assumes diffusion through a stagnant liquid film and k_L, the liquid film mass transfer coefficient, is proportional to the diffusivity of i in water $D_{i,w}$, while the surface renewal theories predict proportionality to $D_{i,w}^{1/2}$. Experimental data generally fits the

surface renewal model (Charpentier, 1981). Charpentier (1981) discusses the application of several contactor designs, including the bubble columns, packed trickle beds and CSTR (as mechanically agitated tanks). The CSTR retains a high liquid volume with easily varied intensity of mixing at variable gas flows, and is useful over a range of gas to liquid loading (G/L) and required $k_{L,i}a/V_L$. Charpentier (1981) asserts that for the CSTR, "Their principal disadvantage is that both the liquid and gas phase are almost completely backmixed." He describes the gas holdup and the specific interfacial area (a/V_L) as dependent on gas flow at low agitation speed (N) and largely dependent on N above a critical speed, with a transition range where both G and N are effective in increasing $k_{L,i}a/V_L$. Above the critical agitator speed a/V_L is linear with increasing N. Further, Charpentier includes contributions of power input from both the sparger and the mechanical agitator in gas dispersion for mass transfer, asserting that sparger power is more important at low agitation speed. Generally the bubble diameter is dependent on the orifice diameter (D_o), surface tension of the liquid (σ), and density (ρ) difference of the gas and liquid as, $D_p = (6D_o\sigma g_c/g(\rho_L-\rho_G))^{1/3}$. However, at high gas flow, gas exits the orifice in a jet that breaks up into a swarm of larger bubbles. The dimensionless Flow Number ($N_Q=Q/ND^3$) is constant at $0.93T/D$ where Q is impeller flow,D is the impeller diameter and T is the tank diameter. The Power Number ($N_P=P/\rho N^3D^5$) is also constant. Flow is proportional to N and to D^3 and input power is proportional to $N^3$and to D^5; this is in agreement with the affinity laws for mixers.

In a recent review Garcia-Ochoa and Gomez(2009) discussed O_2 transfer in fermentation and the determination of k_La/V_L for use in Equation 6.1. The correlations generally fit the form

$$\frac{k_{L,i}a}{V_L} = \gamma V_S^{\alpha}(P/V_L)^{\beta} \qquad 6.2$$

Where γ is a constant of proportionality, V_s is the superficial gas velocity or volumetric gas flow, (P/V_L) is the power input to the liquid volume, and α and β are constant exponents. In the correlations reviewed, α ranges from 0.3 to 0.8 for water, and β ranges from 0.4 to 1.1. N^3 can be substituted for (P/V_L), and when N is used α ranged from 0.9 to 2.7. Garcia-Ochoa and Gomez (2009) presented empirical correlations of k_La/V_L from dimensionless numbers related to mass transfer; these correlations generally simplify to the form of Equation 6.2 for set fermenter geometry. Garcia-Ochoa (2009) constructed a mass transfer model that fits data from the literature within +/-15%. Further, k_La/V_L was found to increase with ionic concentration from smaller bubble size and decreased coalescence compared to water. k_La/V_L decreased with increased viscosity and upon addition of surfactants or antifoam, and increased with increased temperature and upon addition of hydrocarbons (alkanes). Methods for determination of k_La/V_L for the air/water system are discussed including the method employed in the present study.

Mass transfer capacity was compared in a CTSR, a trickle bed and a bubble column used for methane production from syngas using a mixed culture of methanogens (Klasson et al., 1992a). k_La/V_L was 2.1 h^{-1} in the bubble column, 55.1 h^{-1} in the trickle bed and in the CSTR 26.1 h^{-1} at 300 rpm and 101.1 h^{-1} at 450 rpm. Klasson (1992) follows Charpentier (1981) and assumed, "perfect mixing in both the gas and liquid phases." The value of the mass transfer coefficient for CO was calculated as in Equation 6.1 with the liquid concentration assumed to be 0 for mass transfer limitation and assuming the concentration at the interface was in equilibrium by Henry's Law with the effluent gas partial pressure of CO ($C_i^* = p_{CO}/H_{CO}$). This is an example of the mixed

flow assumption for mass transfer. The values reported for $k_{L,CO}a/V_L$ were repeated (Bredwell et al., 1999) without qualification of the mixed flow assumption.

A practical primer for engineering design of gas dispersion in a CSTR is presented in (Bakker et al., 1994), including a discussion of impeller design and CSTR geometry, illustration of the flow pattern from a radial flow turbine and gas flooding of the impeller when agitator speed is insufficient to disperse the gas flow applied. Bakker (1994) suggests guidelines for fermenter geometry and design equations that predict flooding, full engagement of the gas by the impeller, and correlate k_La/V_L using the geometric ratios and dimensionless numbers. CSTR mass transfer is expected to follow Equation 6.2, with suggested values for α of 0.6, β of 0.6 and γ of 0.015 s^{-1} (54 h^{-1}) for the air/water system.

The purpose of this study is to provide a basis for CSTR design at the commercial scale. The mass transfer in a laboratory scale fermenter was characterized for O_2 transfer from air into water. CSTR scale up typically assumes similar geometry (Bakker et al., 1994), and the type and placement of impellers, baffles and the gas sparger will be important to increase the utility of the results. A typical commercial CSTR will have a liquid height to tank diameter ratio of more than 2; but this was not feasible in the laboratory fermenter. However, defined geometry of the laboratory CSTR that follows the recommendations of Bakker et al. (1994) as closely as possible was used in the present study to best simulate commercial geometry for scale up.

Mass transfer is often cited as a major impediment to the commercial success of the synthesis gas fermentation process (Bredwell et al., 1999; Klasson et al., 1992b). The objective of the present study is to define mass transfer in the laboratory CSTR as a basis

for comparative study of mass transfer in the CSTR, trickle bed and hollow fiber contactors for syngas fermentation. The present study will determine if the mixed flow or plug flow model applies for gas contact, and develop a correlation based in published models of $k_{L,O2}a/V_L$ in the CSTR with an air/water system.

6.5 Models for Estimation of Mass Transfer Coefficient

The controlling liquid film mass transfer is represented by Equation 6.3 that defines the volumetric mass transfer coefficient, $k_{L,O2}a/V_L$ for O_2 transfer to and from water.

$$\frac{1}{V_L}\frac{dn}{dt} = \frac{k_L a}{V_L}(C_i - C_L) = \frac{k_L a}{V_L}\frac{(p_i - p_L)}{H} \qquad 6.3$$

Where,

V_L is the volume (m^3) of liquid into which O_2 is transferred, and in which the concentration is monitored

n is moles of O_2 dissolved in the liquid

k_L is the liquid film mass transfer coefficient (m/h), assumed to be controlling

a is the area of the gas/liquid interface (m^2)

C_i is the concentration of O_2 at the gas/liquid interface (mol/m^3)

C_L is the concentration of O_2 in the bulk liquid (mol/m^3)

p_i is the partial pressure of O_2 at the gas/liquid interface (kPa)

p_L is the partial pressure of O_2 in the bulk liquid (kPa)

H is the Henry's Law constant for O_2 (kPa m^3/mol)

6.5.1 $k_{L,O2}a/V_L$ from Graphical Solution

Graphical determination of the volumetric mass transfer coefficient ($k_{L,O2}a/V_L$) for transfer of O_2 into water is described as the dynamic method of Garcia-Ochoa and Gomez (2009) and used to characterize $k_{L,O2}a/V_L$ in Orgill et al. (2013). The derivation is presented here to document the assumptions and clarify the equation development. If n is viewed as the moles of O_2 dissolved in the liquid volume V_L, then

$$\frac{1}{V_L}\frac{dn}{dt} = \frac{d(n/V_L)}{dt} = \frac{dC_L}{dt} = \frac{k_L a}{V_L}(C_i - C_L) \tag{6.4}$$

describes the changing concentration of O_2 in the liquid. Substituting

$$x = (C_i - C_L) \tag{6.5}$$

And for constant C_i

$$dx = -dC_L \tag{6.6}$$

Then, substituting Equations 6.4 and 6.5 in Equation 6.6 and integrating from time t_1 to time t_2

$$\frac{dx}{dt} = \frac{-k_L a}{V_L}x \tag{6.7}$$

$$\int_{x_1}^{x_2}\frac{dx}{x} = \frac{-k_L a}{V_L}\int_{t_1}^{t_2} dt \tag{6.8}$$

$$ln\left(\frac{x_2}{x_1}\right) = \frac{-k_L a}{V_L}(t_2 - t_1) \tag{6.9}$$

$$ln\left(\frac{(C_i - C_L)_2}{(C_i - C_L)_1}\right) = \frac{-k_L a}{V_L}(t_2 - t_1) \tag{6.10}$$

Two different boundary conditions are used in aeration experiments with air and stripping of O_2 with N_2. Equation 6.11 for saturating with air

$$C_i = \frac{p_i}{H} = C_s \tag{6.11}$$

and Equation 6.12 for stripping with nitrogen.

$$C_i = 0 \tag{6.12}$$

Where C_S is the saturated concentration of O_2 from air (21% O_2) at operating temperature and pressure. The operating equation for saturation of liquid with air is then

$$ln\left(\frac{C_S - C_L}{C_S - 0}\right) = ln\left(1 - \frac{C_L}{C_S}\right) = ln(1 - f_{O2}) = \frac{-k_L a}{V_L} t \tag{6.13}$$

Where $C_L = 0$ at $t = 0$, and $C_L = C_L$ at t. The term (C_L/C_S) is the fraction of saturation of O_2 in the bulk liquid (f_{O2}). The operating equation for stripping of O_2 with nitrogen is

$$ln\left(\frac{0 - C_L}{0 - C_S}\right) = ln\left(\frac{C_L}{C_S}\right) = ln(f_{O2}) = \frac{-k_L a}{V_L} t \tag{6.14}$$

Since $C_i = 0$ at all t, and $C_L = C_S$ at $t = 0$. The volumetric mass transfer coefficient can be determined from a plot of (f_{O2}) versus t for stripping with N_2, and from a plot of (1-f_{O2}) versus t for saturating with air. The slope of the linear portions of these plots will be $-k_{L,O2}a/V_L$.

6.5.2 $k_{L,O2}a/V_L$ from Discrete Interval Data

Alternatively, $k_{L,O2}a/V_L$ can be calculated for discrete time intervals in the data by modifying Equation 6.10 as in Equation 6.15. The boundary conditions become $f_i = 1$ for aeration, and $f_i = 0$ for stripping.

$$ln\left(\frac{(C_i - C_L)_2}{(C_i - C_L)_1}\frac{C_S}{C_S}\right) = ln\left(\frac{(f_i - f_L)_2}{(f_i - f_L)_1}\right) = \frac{-k_L a}{V_L}(t_2 - t_1) \tag{6.15}$$

6.5.3 $k_{L,O2}a/V_L$ from O_2 Mass Balance and df_L/dt

A more rigorous analysis of aeration and stripping recognizes the change of O_2 concentration in the air or N_2 stream as O_2 is transferred to and from the water. The

concentration of O_2 at the interface (C_i) changes with time, and restating Equation 6.4 and dividing by the concentration from air saturation, C_S.

$$\frac{1}{V_L}\frac{dn}{dt} = \frac{d(n/V_L)}{dt} = \frac{dC_L}{dt} = \frac{k_L a}{V_L}(C_i - C_L) \quad 6.16$$

$$\frac{1}{C_S}\frac{dC_L}{dt} = \frac{k_L a}{V_L}\frac{(C_i - C_L)}{C_S} \quad 6.17$$

The mass balance can be restated in terms of f.

$$\frac{df_L}{dt} = \frac{k_L a}{V_L}(f_i - f_L) \quad 6.18$$

The fraction of O_2 saturation in the bulk liquid (f_L) is observed directly from the ORP probe, and the fraction saturation at the gas/liquid interface is proportional to the mole fraction of O_2 in the gas (y_G) by Henry's Law.

$$f_i = \frac{y_G P/H}{0.21 P/H} = \frac{y_G}{0.21} \quad 6.19$$

The inlet O_2 mole fraction (y_i) is 0.21 for aeration or 0 for N_2 stripping, and the mole fraction of O_2 in the gas leaving the water (y_o) can be estimated from the mass balance noting that O_2 leaving the water goes into the gas and O_2 entering the water comes from the gas. $k_{L,O2}a/V_L$ can then be calculated from the observed rate of change of f_L taken from a curve fit of the measured data. Equation 6.20 shows the calculation, which incorporates the logarithmic mean of the concentration difference to account for the change of driving force as each gas bubble transits the liquid volume.

$$\frac{df_L}{dt} = \frac{k_L a}{V_L}\left(\frac{\left(y_{G,i}/_{0.21} - f_L\right) - \left(y_{G,o}/_{0.21} - f_L\right)}{\ln\frac{\left(y_{G,i}/_{0.21} - f_L\right)}{\left(y_{G,o}/_{0.21} - f_L\right)}}\right) \quad 6.20$$

6.5.4 Plug Flow Model of Gas Mass Transfer

The analysis of sections 6.5.1 and 6.5.2 assume that the gas phase remains at the inlet concentration of O_2, either $y_{O2} = 0.21$ for air or $y_{O2} = 0$ for N_2. This is true for perfectly mixed gas when little or no O_2 is transferred. The assumption of perfectly mixed gas with conversion (Charpentier, 1981; Klasson et al., 1992a) assumes a constant composition of the gas at the effluent O_2 concentration. This is the mixed flow model of gas mass transfer, and $k_{L,O2}a/V_L$ is defined as in Equation 6.21.

$$\frac{1}{V_L}\frac{dn}{dt} = \left(\frac{k_L a}{V_L}\right)_{Mixed}\left(C_{i,o} - C_L\right) \quad 6.21$$

Where $C_{i,o}$ is the concentration of O_2 in Henry's law equilibrium with the effluent gas. In this perfectly mixed case, O_2 is absorbed from gas entrained from the headspace and a submerged sparger is neither needed nor effective.

Typical CSTR design has gas entry through a submerged sparger, with a tall vessel baffled to retain gas in the liquid and minimize entrainment of spent gas. Air ($y_{O2,i} = 0.21$) enters, is broken into small bubbles, which are retained in the liquid circulation with transfer of O_2 into the water until a diminished bubble with depleted O_2

($y_{O2,o}$ << 0.21) exits the liquid into the headspace. The driving force for O_2 transfer is the partial pressure of O_2 in the bubble and its associated concentration at the liquid interface

$$\frac{y_{O2}P}{H_{O2}} - C_L = (C_i - C_L) \tag{6.22}$$

The fraction of O_2 in the gas bubble decreases during its residence in the liquid and as the concentration difference is diminished, the rate of mass transfer falls. The mass transfer driving force is represented by the logarithmic mean of the concentration difference for inlet air and the concentration difference for effluent gas, in analogy with the LMTD used in heat exchanger design. The gas is said to be in plug flow (not back mixed), and $k_{L,O2}a/V_L$ is defined as in Equation 6.23.

$$\frac{1}{V_L}\frac{dn}{dt} = \left(\frac{k_L a}{V_L}\right)_{Plug} \frac{(C_{i,i} - C_L) - (C_{i,o} - C_L)}{\ln \dfrac{(C_{i,i} - C_L)}{(C_{i,o} - C_L)}} \tag{6.23}$$

This is the plug flow model of mass transfer that applies in the CSTR.

6.6 Materials and Methods

6.6.1 CSTR Experimental Set Up

Experiments were conducted in a BioFlo 110 laboratory fermenter system (New Brunswick, Enfield, CT) with a 3.0 L glass vessel. . The vessel was heated by an external heating blanket to maintain temperature at 37°C. Gas, either air or N_2 from cylinders, was introduced in the bottom of the vessel, under the agitator impellers, through a stainless steel fritted sparger. Two Rushton impellers designed for radial flow to promote gas dispersion were used in all experiments. Gas flow was controlled by thermal conductivity mass flow controllers (Porter, Hatfield, PA). The gas pressure was monitored between the mass flow controller and the sparger, and in the effluent tubing before a rotameter, check valve and discharge to atmosphere. A chilled water condenser

removed water from the effluent gas, drying the gas and returning the condensed water to the CSTR. Effluent gas flow was monitored with the rotameter. The pressures and rotameter flow indication correlated to the flow set on the mass flow controller.

Performance of the CSTR is dependent on the geometry of the assembled components. Bakker et al. (1994) suggest preferred CSTR geometry, and define a correlation of CSTR performance for O_2 transfer into/from water. Two Rushton gas dispersion impellers each with 6 flat blades mounted vertically around a central horizontal disc were used to circulate the liquid and break the gas into small bubbles. The 51 mm impellers were installed in a 124 mm diameter tank or D/T equals 0.41, where Bakker et al. (1994) recommends $0.3 < D/T < 0.5$. The 3.0 L fermenter was configured according to the suggestions of Bakker et al. (1994), locating the bottom Rushton impeller one impeller diameter (51 mm) above the dished bottom of the CSTR vessel, and the second impeller 51 mm above the first. Liquid volume in the CSTR was chosen to be 80% of the vessel volume, or 2.5 L, which resulted in a liquid height to tank diameter ratio (L/T) of 1.69. L/T of 2.0 would be preferred, but this could not be achieved in the BioFlo 110. The resting liquid level was about 90 mm above the top impeller. Bakker et al. (1994) suggests adding a third impeller when the L/T is greater than 1.70; but experiments using a third impeller, either Rushton or marine, resulted in high entrainment of gas from the headspace when vortices formed from highly turbulent flow at the liquid surface.

A baffle ring was used to direct the radial flow vertically at the vessel wall and minimize vortex formation. The four baffles were 13 mm wide and 140 mm long. The

top of the baffles was placed at the 2.0 L level of the vessel, so that the baffles spanned the zone of radial flow from the Rushton impellers.

6.6.2 CSTR Mass Transfer Model

Bakker et al. (1994) give a correlation of mass transfer for O_2 into water. The correlation estimates the volumetric mass transfer coefficient ($k_{L,O2}a/V_L$) and the gas holdup (α) from the agitation speed, the superficial gas velocity, and the geometric ratios of the configured CSTR. The correlation uses dimensionless numbers derived from the CSTR parameters, such as the Aeration Number (N_A)

$$N_A = \frac{G}{ND^3} \tag{6.24}$$

the Froude Number (N_{Fr})

$$N_{Fr} = \frac{N^2 D}{g} \tag{6.25}$$

and the Power Number (N_P)

$$N_P = \frac{P}{\rho N^3 D^5} \tag{6.26}$$

Where gas flow G is in volumetric units (m^3/s), agitator speed N (s^{-1}), impeller diameter D (m), acceleration of gravity (g = 9.8 m/s^2), power input P (W), liquid density (ρ = 1000 kg/m^3). The numbers are dimensionless and all units must be consistent. N_P is assumed constant at 5.5 for a flat bladed turbine in turbulent regime. The correlation predicts P, α and $k_{L,O2}a/V_L$ as a function of N and G. The onset of gas flooding is indicated by

$$N_A > N_{A,FL} = 30 N_{Fr} \left(\frac{D}{T}\right)^{3.5} \tag{6.27}$$

Where the Aeration number N_A predicts flooding at $N_{A,FL}$, T is the CSTR tank diameter (m) . The gas is considered "completely dispersed" or engaged by the impeller when

$$N_A > N_{A,CD} = 30(N_{Fr})^{0.5}\left(\frac{D}{T}\right)^{0.5} \quad 6.28$$

The Bakker correlation, coded in a spreadsheet, modeled expected performance of the CSTR for O_2 transfer into deionized water.

6.6.3 Mass transfer for aeration of deionized water

The volumetric mass transfer coefficient for transfer of O_2 ($k_{L,O2}a/V_L$) from air into deionized water was determined by monitoring the fraction of O_2 saturation (f_{O2}) in the bulk liquid as air was sparged through 2.5 L of water at various agitation speeds and various air flows. Agitation speeds were 150, 400, 650 or 900 rpm, maintained by the BioFlo 110 controller (New Brunswick, Enfield, CT). Air flows were 60, 100, 200 and 400 sccm, maintained by the mass flow controller on the feed gas. Reactor pressures were between 3.5 and 7.0 kPa gauge dependent on flow, with typical atmospheric pressure about 100.0 kPa. The fraction O_2 saturation was measured by a dissolved oxygen probe (Ingold, Mettler-Toledo, Columbus, OH), transmitted from the New Brunswick BioFlo 110 controller, and recorded at the minimum sampling time of 0.2 minutes in the associated BioCommand software. Agitator speed, pH and temperature were also recorded when the gas supply was switched from air to N_2, or from N_2 to air, over the course of each experiment (12 min intervals at 100 sccm gas flow to 6 min intervals at 400 sccm gas flow). Agitator output (as an indicator of power input to maintain speed), inlet and outlet pressure, and effluent flow were manually recorded for the course of each experiment.

The volumetric mass transfer coefficient was determined from a plot versus time of $\ln(1-f_{O2})$ for aeration

$$ln(1 - f_{O2}) = \frac{-k_L a}{V_L} t \quad (6.29)$$

and of ln(f_{O2}) for stripping.

$$ln(f_{O2}) = \frac{-k_L a}{V_L} t \quad (6.30)$$

The derivation of this dependency is given in section 6.5.1, and assumes that the O_2 concentration in the saturating air or stripping N_2 does not change appreciably. The slope of the linear plot is -$k_{L,O2}a/V_L$ for O_2 at the conditions of agitator speed and gas flow in the particular CSTR configuration. The slope of the aeration plot as f_{O2} increased from 0.2 to 0.8 was used to determine $k_{L,O2}a/V_L$.

6.6.4 Mass Transfer for Aeration in Fermentation Medium

Growth of microbial culture will require growth medium containing minerals, trace metals, vitamins and other nutrients that promote growth of the bacteria rather than the deionized water used in the initial mass transfer studies. Accordingly, the mass transfer studies were replicated in the proposed microbial growth medium that will be used in subsequent studies. The medium composition is given in Table 6.1. Medium was prepared in the CSTR with all components, except cysteine and sulfide. Cysteine and sulfide are used as sulfur source and reducing agents to react with O_2 in the medium; omission of cysteine and sulfide allows use of f_{O2} to measure O_2 mass transfer rate. The CSTR filled with medium was sterilized in an autoclave at 121^{o}C for 20 min and cooled to ambient temperature before use in the experiments.

Table 6.1 Composition of fermentation medium used in aeration studies in the CSTR.

Component	Formula	Concentration
		(mg/liter)
Yeast Extract	Undefined	500
MES Buffer	$C_6H_{13}NO_4S$	10000
Potassium Hydroxide	KOH	1264
Minerals		
Ammonium Chloride	NH_4Cl	2500
Calcium Chloride	$CaCl_2.2H_2O$	100
Magnesium Sulfate	$MgSO_4.7H_2O$	500
Potassium Chloride	KCl	250
Potassium Phosphate	KH_2PO_4	250
Trace Metals		
Cobalt Chloride	$CoCl_2.6H_2O$	2
Ferrous Ammonium Sulfate	$FeH_{20}N_2O_{14}S_2$	8
Manganese Sulfate	$MnSO_4.H_2O$	10
Nickel Chloride	$NiCl_2.6H_2O$	2
Nitrilotriacetic Acid	$C_6H_9NO_6$	20
Sodium Molybdate	$Na_2MoO_4.2H_2O$	0.2
Sodium Selenate	Na_2SeO_4	1
Sodium Tungstate	$Na_2WO_4.2H_2O$	2
Zinc Sulfate	$ZnSO_4.7H_2O$	10
Vitamins		
Para-aminobenzoic Acid	$C_7H_7NO_2$	0.05
Biotin	$C_{10}H_{16}N_2O_3S$	0.02
Pantothenic Acid	$Ca(C_9H_{16}NO_5)_2$	0.05
Folic Acid	$C_{19}H_{19}N_7O_6$	0.02
MESNA	$C_2H_5NaO_3S_2$	0.10
Nicotinic Acid	$C_6H_5NO_2$	0.05
Pyridoxine	$C_8H_{11}NO_3.HCl$	0.10
Riboflavin	$C_{17}H_{20}N_4O_6$	0.05
Thiamine	$C_{12}H_{17}N_4OSCl.HCl$	0.05
Thioctic Acid	$C_8H_{14}O_2S_2$	0.05
Cyanocobalamin	$C_{63}H_{88}CoN_{14}O_{14}P$	0.05
Resazurin		
Resazurin	$C_{12}H_6NO_4Na$	1
Cysteine/Sulfide		
Cysteine	$C_3H_7NO_2S$	0
Sodium Sulfide	$Na_2S.9H_2O$	0

6.6.5 Experimental Procedure for Mass Transfer Analysis in the CSTR

The CSTR was started with heating to 37°C, and saturation with O_2 at 650 rpm and 100 sccm air flow for about 1 h. Each data acquisition run began with a short record of the fully aerated liquid, followed by stripping of the O_2 with N_2, saturation with air, and subsequent stripping and saturation to complete the data set. Stripping and aeration were initiated by switching ball valves in the supply tubing to the mass flow controller. Headspace volume was about 421 ml in the CSTR, and flow of air or N_2 was maintained for more than 3 retention times of gas in the headspace to ensure that the headspace O_2 content changed more than 95% from that of the previous gas before starting the next phase; from 20.9 % to 1.0% O_2 in stripping, and from 0.0% to 19.9% in aeration. Each stripping or aerating procedure was maintained for 12 min at 100 sccm gas flow, 9 min for 200 sccm flow and 6 min for 400 sccm flow. A typical data set started with stripping of aerated liquid with 100 sccm flow and 400 rpm agitation. Stripping would be followed by saturation at the same flow and agitation, and agitation would be increased to 650 rpm for stripping and aeration, then to 900 rpm. The gas flow was then increased to 200 sccm and the agitation reset to 400 rpm to repeat the procedures at 400, 650 and 900 rpm agitation. The gas flow would then be increased to 400 sccm and the procedures repeated to complete the data set.

Each data set was saved in a spreadsheet file and analyzed to determine $k_{L,O2}a/V_L$ for each stripping and aerating procedure. The data was accumulated and replicate runs averaged to determine a mean and standard deviation.

6.7 Results and Discussion

6.7.1 Mass transfer for aeration of deionized water

The volumetric mass transfer coefficient, $k_{L,O2}a/V_L$ for O_2 transfer into 2.5 L of deionized water in the 3.0 L CSTR at various agitation speeds and gas flow rates is shown in Figure 6.1. The data is presented as the average of at least triplicate samples of each point, with error bars representing +/- one standard deviation of the replicates. Data was taken for saturation with O_2 from air (aeration) and stripping of O_2 into N_2, which are expected to have the same $k_{L,O2}a/V_L$. Data for aeration and stripping were similar and only the data for aeration will be presented. Solid lines represent the prediction of the Bakker correlation coded in a spreadsheet. The value of $k_{L,O2}a/V_L$ predicted by the correlation is lower than $k_{L,O2}a/V_L$ observed in the experiment. $k_{L,O2}a/V_L$ in the CSTR follows the Bakker correlation in the effect of agitation speed and gas flow, with the curve shifted up, effected by the finely divided gas bubbles produced by the sparger. Equation 6.31 as suggested by Bakker et al. (1994) for $k_{L,O2}a/V_L$ roughly predicts the trend of the experimental data and uses the form of Equation 6.2 with $\gamma \approx 1.5\times10^{-5}$, and (P/V_L) replaced with N^3.

$$\frac{k_{L,O2}a}{V_L} \propto G^{0.6}N^{1.8} \qquad 6.31$$

The superficial gas velocity, $V_S = 4G/\pi T^2$ can be used instead of G. The errors in prediction of $k_{L,O2}a/V_L$ from the correlation were highest at the highest gas flow of 400 sccm, from 18 to 36% less than $k_{L,O2}a/V_L$ from the experiment. Higher agitation improved the agreement between the correlation predictions and experimental data. The predicted $k_{L,O2}a/V_L$ from the correlation was more than 70% less than that from the

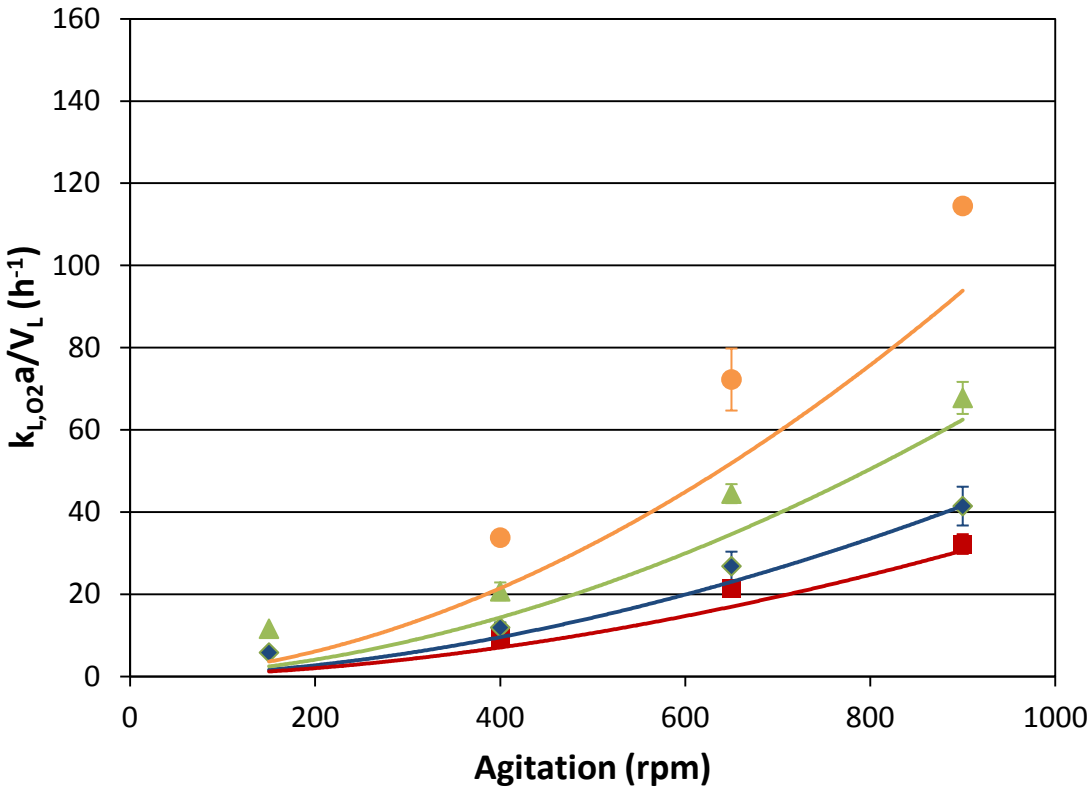

Figure 6.1 Volumetric mass transfer coefficient $k_{L,O2}a/V_L$ for aeration of 2.5 L DI water in the 3.0 L CSTR. Feed gas flow; 60 sccm (■), 100 sccm (◆), 200 sccm (▲) and 400 sccm (●). The predictions of the Bakker model are indicated by the solid lines for 60, 100, 200 and 400 sccm gas flow.

experiment at 150 rpm, 20 to 36% less at 400 rpm, 14 to 28% less at 650 rpm and 0 to 18% less at 900 rpm.

A generalized fit of the data based on the Bakker et al. (1994) correlation was derived by adding a contribution to $k_{L,O2}a/V_L$ for the bubbles generated by the sparger power input. The contribution from the sparger was found as the difference between the experimental value of $k_{L,O2}a/V_L$ and the value found from the correlation at the lowest agitation (150 or 400 rpm) for each gas flow case. Each contribution at 60, 100, 200 and 400 sccm was the average of four data points. The sparger contribution increased with gas flow as shown in Figure 6.2. Lacking a theoretical basis to model the contribution of

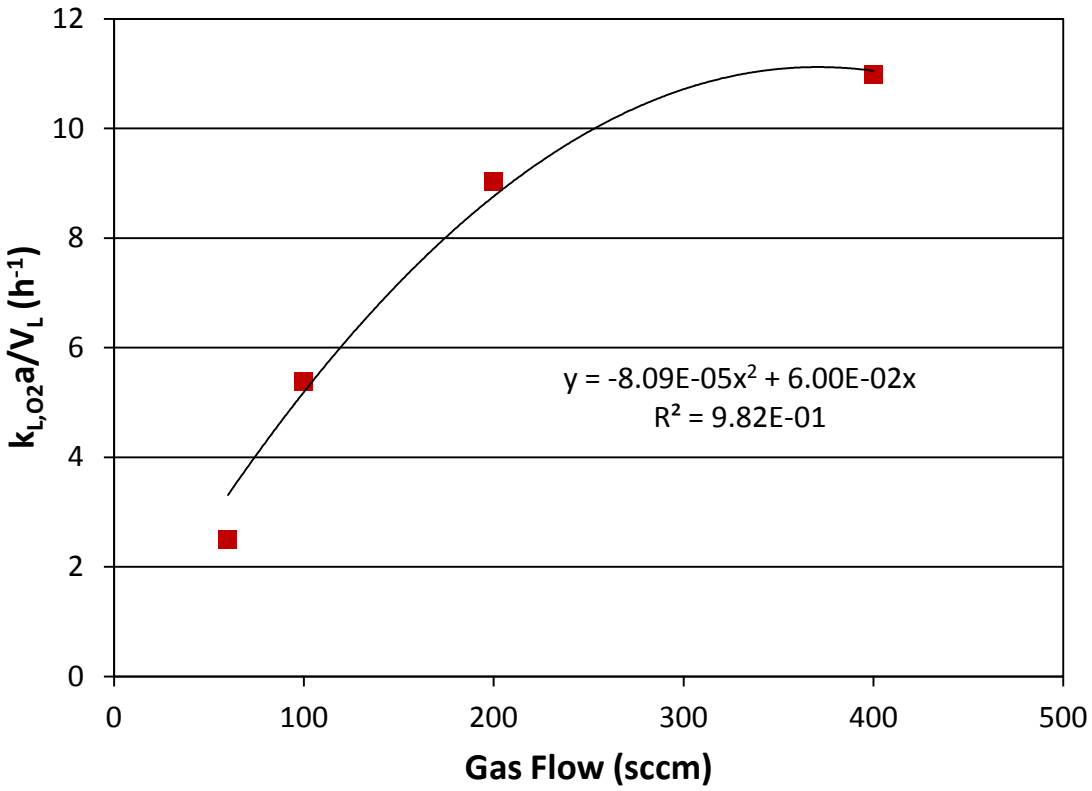

Figure 6.2 Contribution to $k_{L,O2}a/V_L$ from gas flow through the sparger, with a polynomial curve fit equation.

the sparger, a smooth curve was obtained from the data with a polynomial fit. The equation from Figure 6.2 is best used between 60 and 400 sccm gas flow, but can be used for flow to 0 sccm. The predicted $k_{L,O2}a/V_L$ is applicable only to transfer of O_2 into deionized water through a similar sparger in a similar 3.0 L CSTR, but the concept and the technique should apply to any sparged mass transfer contactor. The generalized fit correlation for $k_{L,O2}a/V_L$ adds the sparger contribution to the result from the Bakker et al. (1994) correlation. The prediction of the generalized fit correlation is compared to the experimental data in Figure 6.3. Each data point from Figure 6.1 is calculated with the generalized fit correlation and the predictions are indicated by the dashed lines. The predicted $k_{L,O2}a/V_L$ values with the modified Bakker et al. (1994) correlation are within

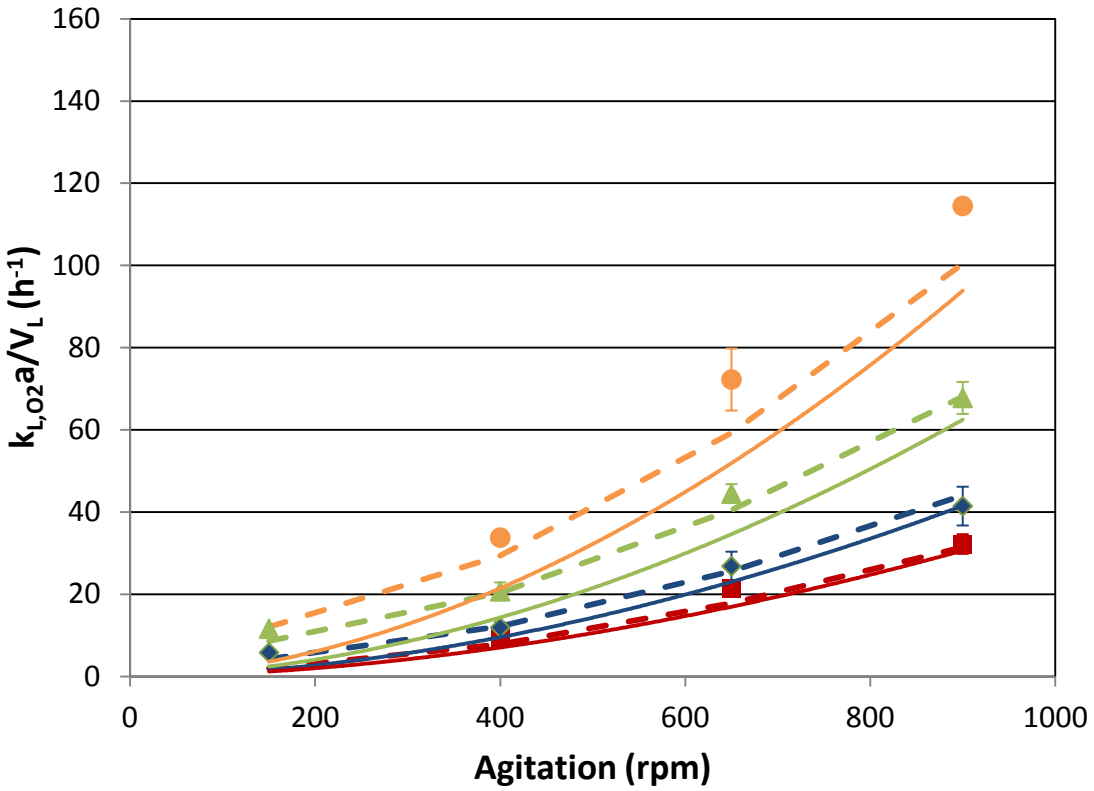

Figure 6.3 Volumetric mass transfer coefficient $k_{L,O2}a/V_L$ from generalized fit correlation compared to experiment. Feed gas flow; 60 sccm (■), 100 sccm (◆), 200 sccm (▲) and 400 sccm (●) and the generalized fit correlation is indicated by the dashed lines. The predictions of the Bakker model are indicated by the solid lines for 60, 100, 200 and 400 sccm gas flow.

±10% for 400 to 900 rpm and 200 or 400 sccm. The prediction of the low values for $k_{L,O2}a/V_L$ with 150 rpm agitation or 60 sccm gas flow are up to 17% below the experimental values and the predicted values of $k_{L,O2}a/V_L$ at 400 sccm are 12 to 18% less than the experimental values.

6.7.2 Mass Transfer for Aeration in Fermentation Medium

The $k_{L,O2}a/V_L$ was determined for at least triplicate runs with varied agitation speed and gas flow in the standard fermentation medium instead of deionized water. The bubbles produced from the sparger were visibly smaller, with an estimated diameter of 1

to 2 mm in medium versus 2 to 3 mm in deionized water. The smaller bubbles were entrained more effectively by the liquid flow in the stirred medium. Apparent $k_{L,O2}a/V_L$ was higher in medium than in DI water as seen in Figure 6.4. For gas flow of 100 sccm, mass transfer improved to 207% of transfer into deionized water at 400 rpm, 155% at 650 rpm and 106% at 900 rpm agitation. $k_{L,O2}a/V_L$ with 200 sccm air flow (Figure 6.5) increased to 217% of transfer into deionized water at 400 rpm, 165% at 650 rpm and 127% at 900 rpm. $k_{L,O2}a/V_L$ with 400 sccm air flow (Figure 6.6) increased to 218% of transfer into deionized water at 400 rpm, 164% at 650 rpm and 118% at 900 rpm. The

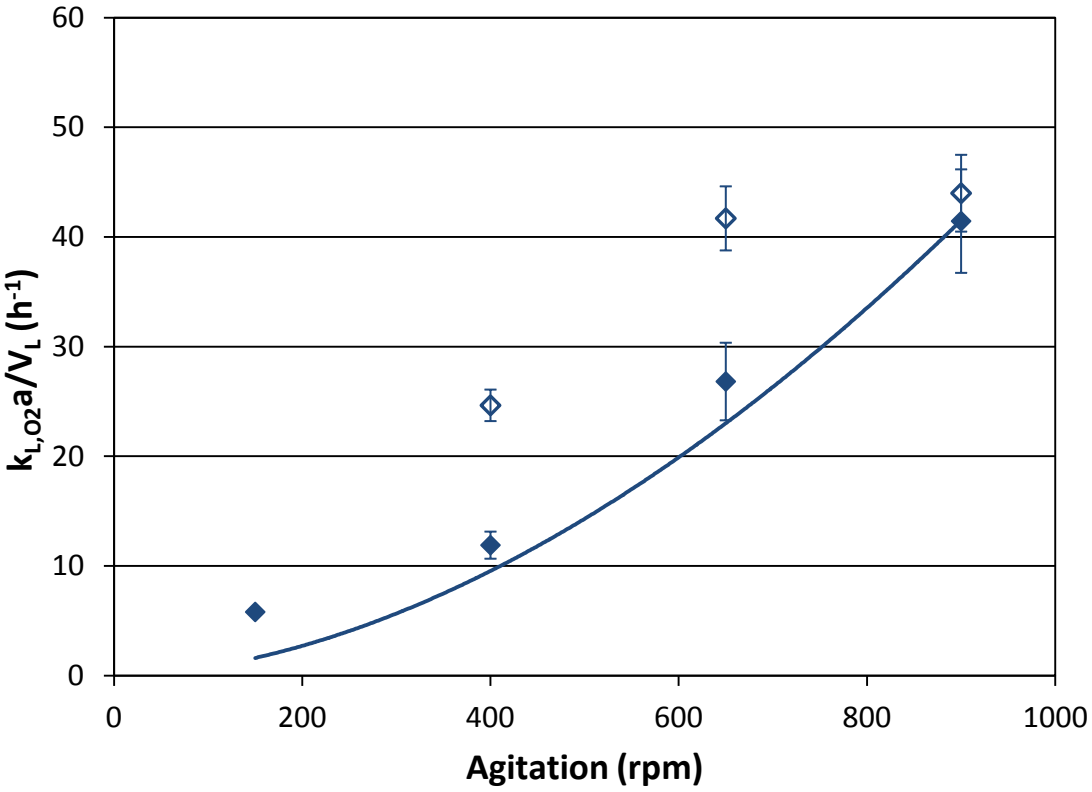

Figure 6.4 Volumetric mass transfer coefficient $k_{L,O2}a/V_L$ for aeration of 2.5 L fermentation medium at 100 sccm air flow in the 3.0 L CSTR. DI water (◆), medium (◇). The prediction of the Bakker model for water is indicated by the solid line for 100sccm gas flow.

increase in $k_{L,O2}a/V_L$ when O_2 was transferred into medium was diminished at high agitation speed (650 and 900 rpm) and especially at the lowest air flow (100 sccm). The cause was suspected to be entrainment of gas, N_2 with very low O_2 that remained in the vessel head space. The mass transfer in medium was enhanced by the chemical additions to the water, including ions from salts and hydrocarbon compounds from the yeast extract. These chemical additions lowered the surface tension and increased $k_{L,O2}a/V_L$ as expected (Garcia-Ochoa and Gomez, 2009).

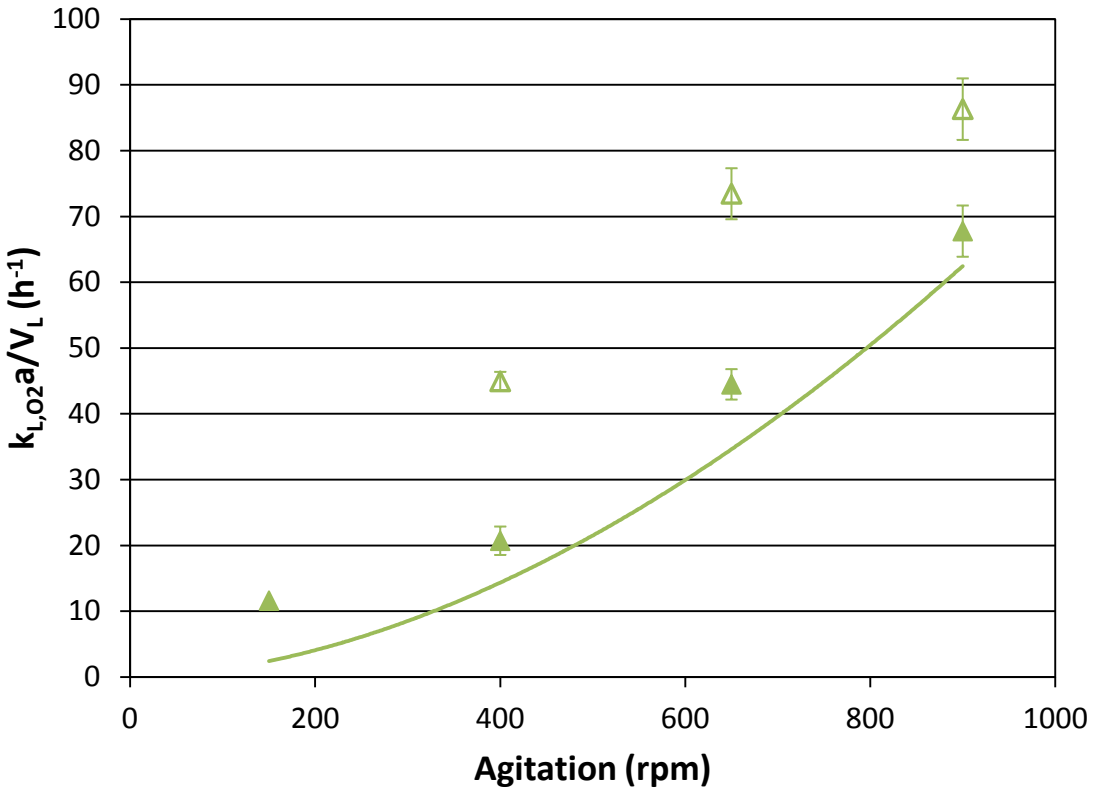

Figure 6.5 Volumetric mass transfer coefficient $k_{L,O2}a/V_L$ for aeration of 2.5 L fermentation medium at 200 sccm air flow in the 3.0 L CSTR. DI water (▲), medium (△). The prediction of the Bakker model for water is indicated by the solid line for 200 sccm gas flow.

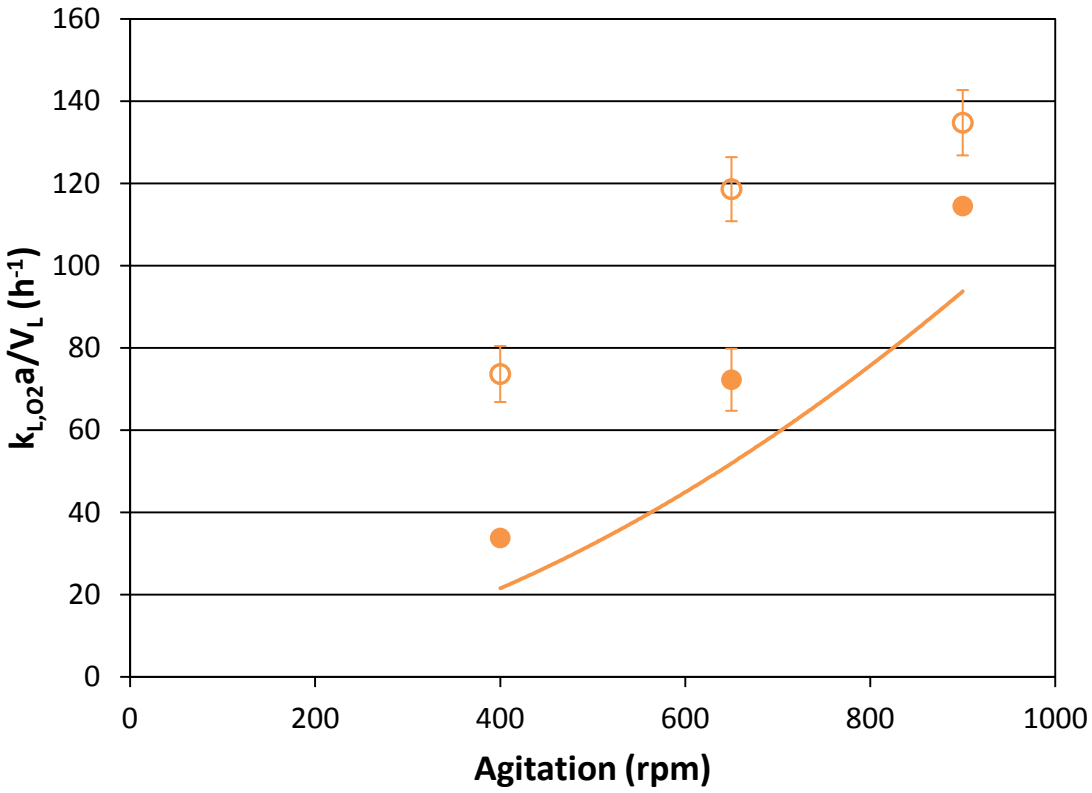

Figure 6.6 Volumetric mass transfer coefficient $k_{L,O2}a/V_L$ for aeration of 2.5 L fermentation medium at 400 sccm air flow in the 3.0 L CSTR. DI water (●), medium (○). The prediction of the Bakker model for water is indicated by the solid line for 400 sccm gas flow.

6.7.3 Evaluation of Method Error

The observed values of $k_{L,O2}a/V_L$ at high agitation were lower than expected, which suggests that gas from the headspace was entrained in the highly agitated liquid and reduced the apparent mass transfer. Lagging concentration of O_2 in the headspace gas when entrained by vortex formation would oppose the mass transfer process (aeration or stripping) and depress the apparent $k_{L,O2}a/V_L$ observed in the experiment. This effect would be pronounced at high agitation speed where vortex formation is prominent, and exaggerated in medium compared to deionized water and at low gas flow where the head space gas retention time is long. This hypothesis was tested by comparing the change of

headspace concentration with the change of concentration in the bulk liquid. The concentrations of O_2 in the headspace ($f_H = y_o/0.21$) and in the spent gas leaving the liquid ($f_s = y_s/0.21$) were calculated and plotted over time with measured f_{O2} in the water. This comparison at 100 sccm, 200 sccm and 400 sccm is shown in Figure 6.7. The O_2 in the liquid, f_{O2}, rises faster than the headspace concentration (liquid leads) only for low gas flow of 100 sccm and high agitation at 650 or 900 rpm. Otherwise, the O_2 concentration in the headspace rises faster (liquid lags) in every case. The differences in concentration are small at any time and though entrained gas from the headspace would tend to enhance observed $k_{L,O2}a/V_L$, the effect of entrained gas will be negligible. The high rates of O_2 transfer despite the small concentration differences between the headspace and the bulk liquid, the driving force being at times positive and at other times negative for transfer of O_2 into the liquid from the headspace, are not supported in the mixed flow model of mass transfer, but are consistent with gas in plug flow.

The derivation of the graphical determination of $k_{L,O2}a/V_L$ from aeration assumes that the transfer of O_2 is from air with a constant molar concentration of 21% O_2 (see section 6.5.1 and Garcia-Ochoa and Gomez (2009)). The concentration of O_2 in the spent gas leaving the liquid ($f_s = y_s/0.21$) differs from air ($f_s = 1$), by 10% for high gas flow of 400 sccm with low agitation of 400 rpm, to 40% for low gas flow of 100 sccm with high agitation of 900 rpm. The low O_2 content in the gas leaving the liquid implies that the driving force for mass transfer is lower than the driving force assumed to be from fresh air, and the calculated $k_{L,O2}a/V_L$ reported above is low. This deviation is most significant at low gas flow and high agitation speed.

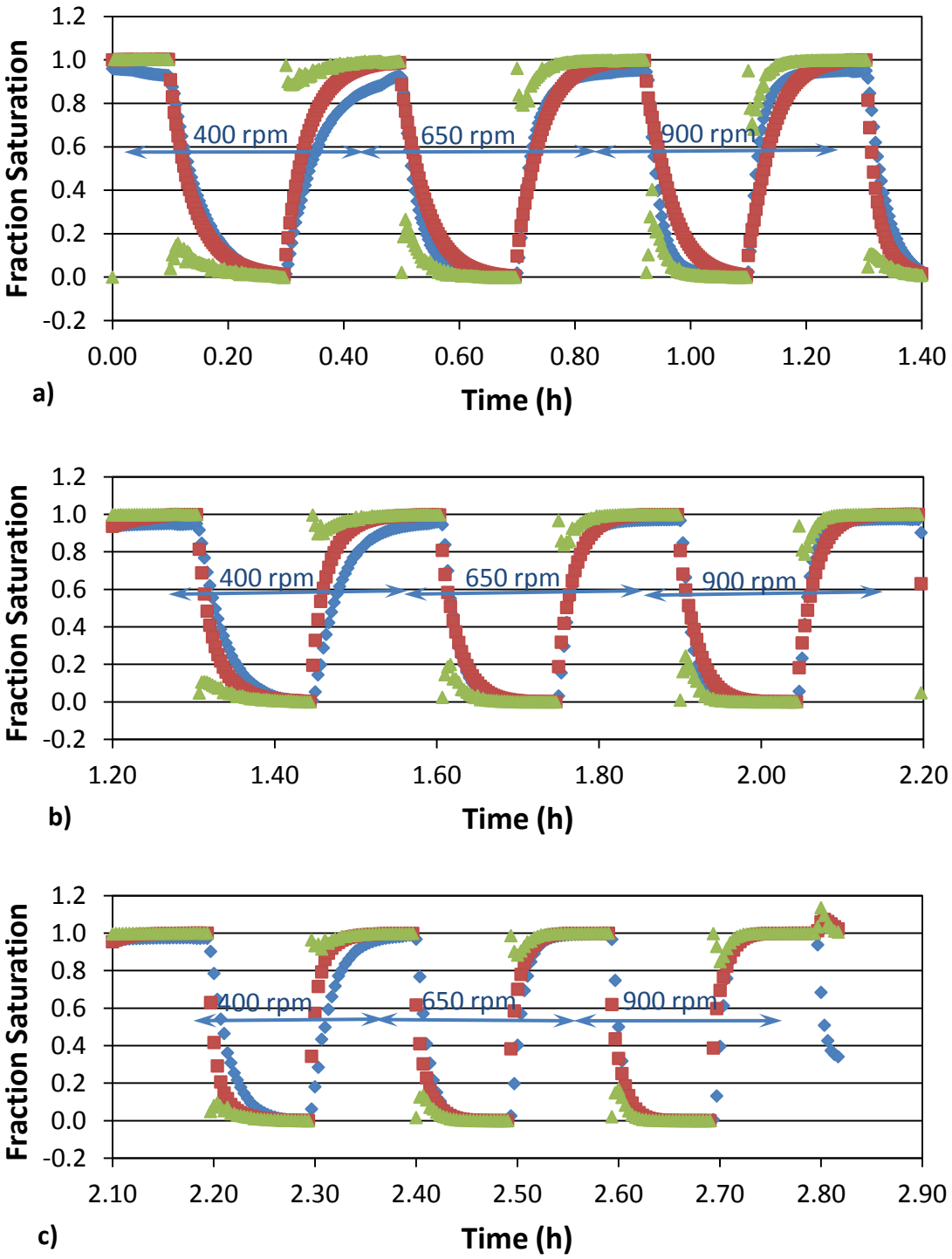

Figure 6.7 O_2 fraction of (21% O_2) air saturation in the bulk liquid, headspace and in the gas leaving the liquid volume for a) 100, b) 200 and c) 400 sccm air flow into fermentation medium in the 3.0 L CSTR. Successive aeration and stripping at 400, 650 and 900 rpm are shown at each flow. O_2 fraction of air saturation in: Bulk liquid (◆), Headspace (■), Spent gas (▲).

Transfer of O_2 from air at high rates into the liquid volume illustrates that the majority of O_2 is transferred from the flow of fresh gas, and that transfer from the spent gas in the headspace is negligible. The assumption of a perfectly mixed gas phase (Garcia-Ochoa and Gomez, 2009; Klasson et al., 1992a) and a mixed flow model using the concentration difference from the headspace gas to the bulk liquid to characterize mass transfer is clearly not appropriate for the CSTR data. The observed mass transfer is dependent on the average concentration of O_2 in a gas bubble as it circulates in the liquid. The concentration difference characteristic of mass transfer is best represented by the logarithmic mean of the concentration differences between the bulk liquid and the inlet gas, and the bulk liquid and the gas leaving the liquid, as for gas in plug flow through the liquid.

A change in the gas flow seen on the effluent rotameter indicated significant change of molar flow from absorption of O_2 from air into water in aeration and desorption of O_2 from the water into N_2 in stripping. This change was sharp, consistent, and lagged the switch from N_2 to air, or air to N_2 in proportion to the retention time of gas in the inlet tubing. The observed flow change was up to -2% of the total gas flow when aeration was initiated, and +2% when stripping was initiated. The change of effluent flow estimated from the rotameter calibration was up to 8 sccm at 400 sccm inlet flow and 900 rpm. This change in flow is from transferred O_2, occurred sharply and declined to the steady state flow as equilibrium was approached. The importance of this transfer is revealed in Figure 6.7 in the O_2 concentrations calculated for the spent gas leaving the liquid. These values were calculated from a mass balance on O_2 passing through the

liquid, since the rate of accumulation of O_2 in the liquid is also the rate of depletion of O_2 from the gas, the O_2 content of the spent gas can be estimated.

The change in O_2 content from 100 sccm of gas (Figure 6.7(a)) is about 18% at 400 rpm, 25% at 650 rpm and up to 40% (about 8.4 sccm O_2 from 100 sccm) at 900 rpm. The mass transfer analysis assumes that the gas phase changes only negligibly in transit through the liquid. The measured concentration change of up to 40% is not negligible and the concentration difference that drives mass transfer in Equation 6.23 is reduced by up to 22% at low gas flow and high agitation. The value of $k_{L,O2}a/V_L$ derived from the graphical analysis of section 6.5.1 and presented in Figures 6.1 through 6.6 is lower than the actual $k_{L,O2}a/V_L$.

The rate of change of O_2 saturation was derived from a polynomial curve fit of f_{O2} from selected experimental data and used to calculate $k_{L,O2}a/V_L$ (see section 6.5.3 and example in Figure 6.8). Values for $k_{L,O2}a/V_L$ derived from this curve fit are shown for 100 sccm gas flow at 400, 650 and 900 rpm in aeration and stripping in Figure 6.9, along with the values from the graphical solution and the average of the values for the corresponding discrete time intervals (t_1 to t_2) using equation 6.32 (see section 6.5.2). The analysis is repeated for 400 sccm gas flow in Figure 6.10.

$$ln\left(\frac{(1-f_L)_2}{(1-f_L)_1}\right) = \frac{-k_L a}{V_L}(t_2 - t_1) \qquad 6.32$$

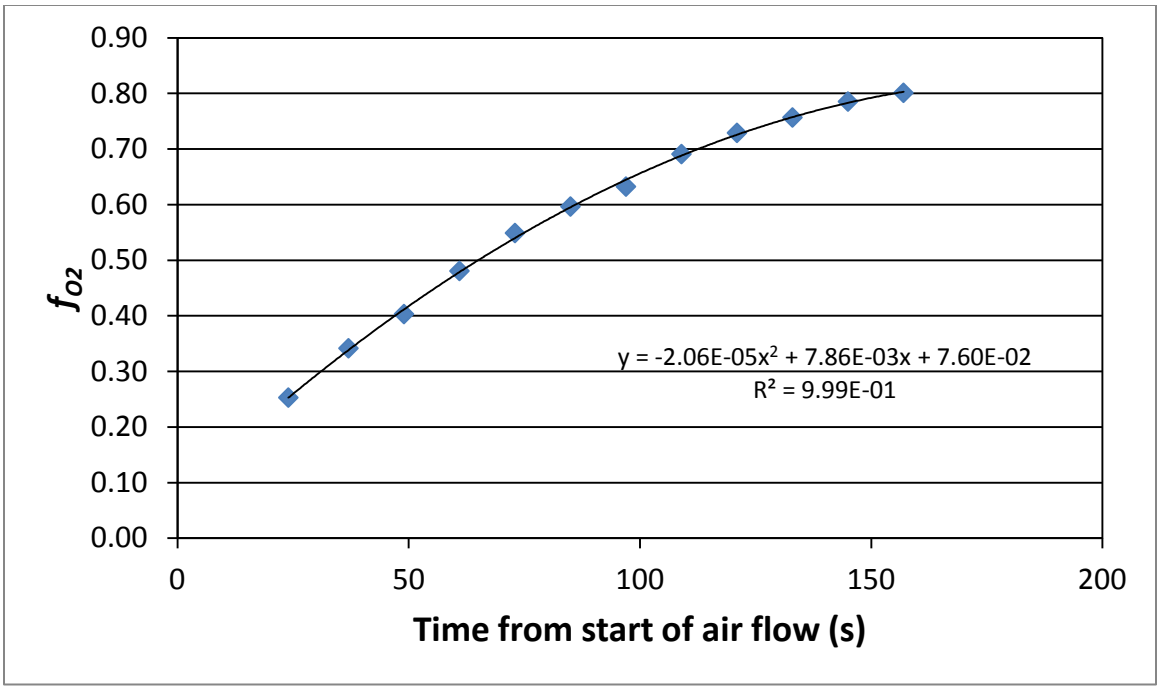

Figure 6.8 Curve fit of O_2 fraction for transfer from air into water for 100 sccm air flow and 900 rpm in the 3.0 L CSTR.

The response time of the ORP electrode is a limiting factor in the direct measurement of O_2 transfer, however the minimum value of $1/k_{L,O2}a/V_L$ is 32 s in our data and this is near the recommended minimum of 50 s (Garcia-Ochoa and Gomez, 2009) to ensure adequate response of the electrode. The minimum sampling delay for the BioCommand data acquisition system is 0.2 minutes. The sampling period for saturation of the liquid volume (20% to 80% saturation) was less than one minute at high agitation speeds (650 or 900 rpm) and high gas flow (400 sccm).

In Figure 6.9 $k_{L,O2}a/V_L$ with the corrected concentration difference is similar to $k_{L,O2}a/V_L$ from the previous analysis at 400 rpm, but at 49.5 h^{-1} is 20% higher at 900 rpm. The value for $k_{L,O2}a/V_L$ of 123 h^{-1} shown in Figure 6.10 for O_2 transfer into water represents a 7% increase over the value of 115 h^{-1} from Figure 6.1. These higher values of $k_{L,O2}a/V_L$ will match the expected trend predicted by the analysis of Bakker et al.

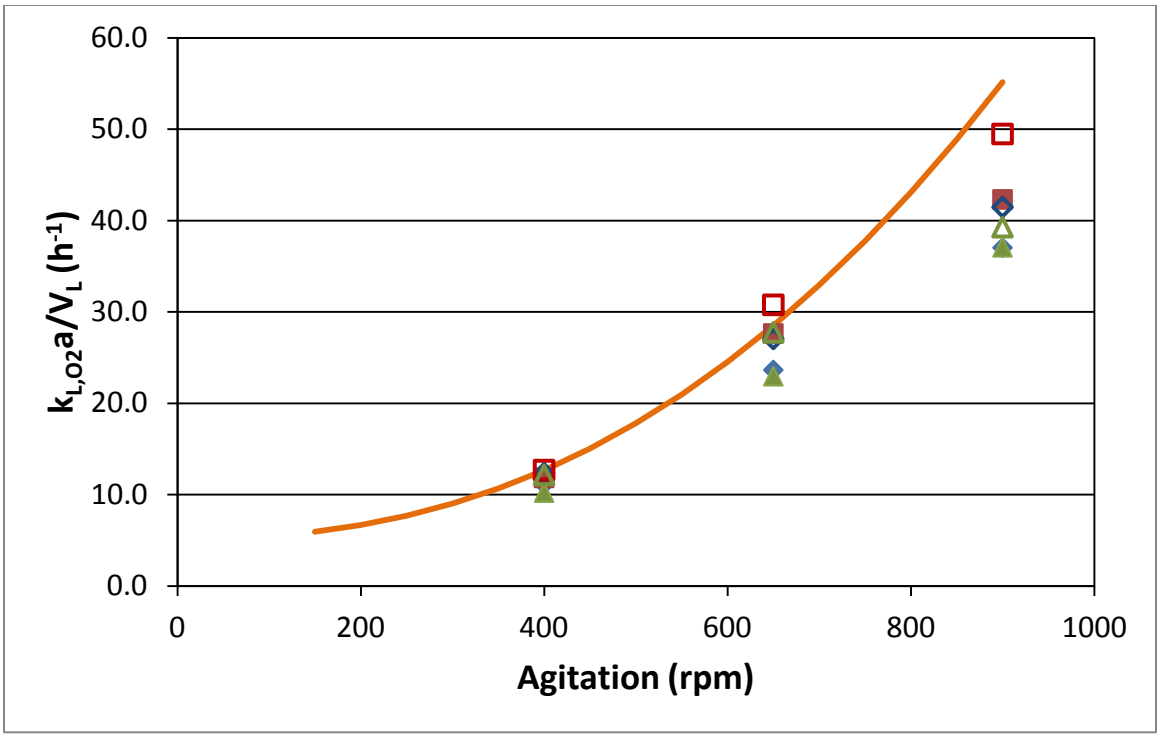

Figure 6.9 Volumetric mass transfer coefficient for O_2, $k_{L,O2}a/V_L$, for 100 sccm air flow in the 3.0 L CSTR. Estimation using: graphical method (◆), curve fit of f_{O2} (■), equation over discrete sampling interval (▲), model of Equation 6.33 (—). Closed symbols represent aeration, and the open symbols represent stripping of O_2 into N_2.

(1994) and Equation 6.2. The value of γ in Equation 6.2 must be higher than predicted by the correlation of Bakker et al. (1994) and the sparger contribution must be included to fit the experimental data.

The volumetric mass transfer coefficient $k_{L,O2}a/V_L$ depends on the agitation speed and the volumetric gas flow as well as the CSTR geometry and liquid properties. $k_{L,O2}a/V_L$ is also dependent on the gas flow through the chosen sparger. This effect appears additive to the mass transfer from agitation and gas flow. $k_{L,O2}a/V_L$ in the 3.0 L CSTR is represented by Equation 6.33.

$$\frac{k_{L,O2}a}{V_L} = 3.83 \times 10^{-7} G^{0.6} N^{2.34} + (0.06G - 8.09 \times 10^{-5} G^2) \qquad 6.33$$

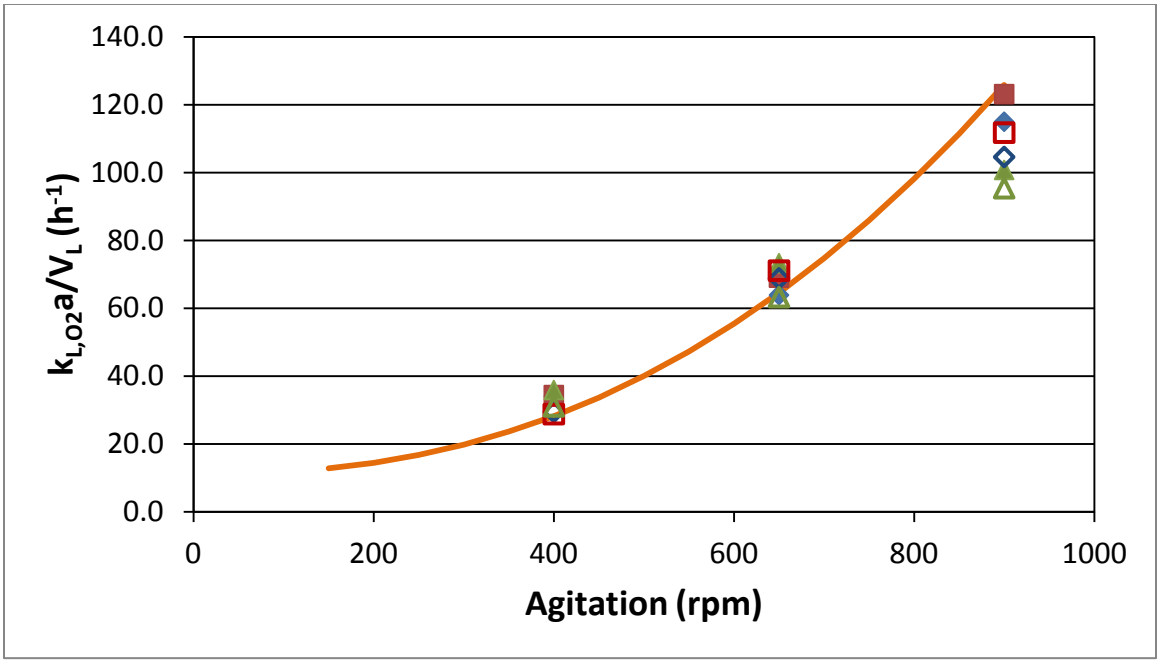

Figure 6.10 Volumetric mass transfer coefficient for O_2, $k_{L,O2}a/V_L$, for 400 sccm air flow in the 3.0 L CSTR. Estimation using: graphical method (◆), curve fit of f_{O2} (■), equation over discrete sampling interval (▲), model of Equation 6.33 (—). Closed symbols represent aeration, and the open symbols represent stripping of O_2 into N_2.

For $k_{L,O2}a/V_L$ in h^{-1}, N in rpm, and G in sccm. The term in parentheses represents the sparger contribution to $k_{L,O2}a/V_L$ as a function of gas flow. The fit of the model is shown in Figures 6.9 and 6.10 as the solid line, and is ±10% from the curve fit analysis of $k_{L,O2}a/V_L$.

6.8 Conclusions

The plug flow volumetric mass transfer coefficient for O_2 transfer into water, $k_{L,O2}a/V_L$, is a function of gas flow (G) and agitator speed (N). An additive contribution to $k_{L,O2}a/V_L$ was identified for gas flow through the sparger.

The concentration difference across the liquid film at the gas/liquid interface is diminished by fast transfer of O_2 as air transits the liquid, and gas entrained from the headspace has little effect on mass transfer. The concentration difference that drives

transfer of O_2 from plug flow gas is the logarithmic mean of the difference of the bulk liquid concentration of O_2, from the Henry's Law concentrations from O_2 partial pressure in the incoming air and in the residual gas exiting the liquid. The log mean concentration difference defines $k_{L,O2}a/V_L$ for plug flow gas in the CSTR. The specification of the mass transfer model is essential to interpretation of reported $k_{L,O2}a/V_L$.

Mass transfer of O_2 into fermentation medium increased the apparent $k_{L,O2}a/V_L$ by more than 100% at low agitator speed of 400 rpm, $k_{L,O2}a/V_L$ increased by 60% at 650 rpm and 6% to 28% at 900 rpm. The observed effect of medium versus water may have been reduced at high agitation speed by the limitations of the measuring equipment or by depletion of the driving force when O_2 was transferred at high rates. The addition of nutrient compounds in the water reduces the surface tension visibly decreasing the size of bubbles formed.

Apparent $k_{L,O2}a/V_L$ for plug flow gas as high as 140 h^{-1} into fermentation medium was demonstrated in the 3.0 liter CSTR at 400 sccm gas flow and 900 rpm agitator speed. This likely represents a minimum attainable value, diminished by the fast change of O_2 concentration in the feed gas as it transits the liquid volume.

References

Bakker, A., Smith, J.M., Myers, K.J. 1994. How to Disperse Gases in Liquids. Chemical Engineering, 101 (12), 98-104.

Bredwell, M.D., Srivastava, P., Worden, R.M. 1999. Reactor Design Issues for Synthesis-Gas Fermentations. Biotechnology Progress, 15 (5), 834-844.

Charpentier, J.-C. 1981. Mass-Transfer Rates in Gas-Liquid Absorbers and Reactors. in: *Advances in Chemical Engineering*, (Eds.) G.R.C.J.W.H. Thomas B. Drew, V. Theodore, Vol. Volume 11, Academic Press, pp. 1-133.

Garcia-Ochoa, F., Gomez, E. 2009. Bioreactor Scale-up and Oxygen Transfer Rate in Microbial Processes: An Overview. Biotechnology Advances, 27 (2), 153-176.

Hu, P., Jacobsen, L.T., Horton, J.G., Lewis, R.S. 2010. Sulfide Assessment in Bioreactors with Gas Replacement. Biochemical Engineering Journal, 49 (3), 429-434.

Klasson, K.T., Ackerson, M.D., Clausen, E.C., Gaddy, J.L. 1992a. Bioconversion of Synthesis Gas into Liquid or Gaseous Fuels. Enzyme and Microbial Technology, 14 (8), 602-608.

Klasson, K.T., Ackerson, M.D., Clausen, E.C., Gaddy, J.L. 1992b. Mass-Transport in Bioreactors for Coal Synthesis Gas Fermentation. Abstracts of Papers of the American Chemical Society, 204, 125-FUEL.

Kundiyana, D.K., Huhnke, R.L., Wilkins, M.R. 2010. Syngas Fermentation in a 100-L Pilot Scale Fermentor: Design and Process Considerations. Journal of Bioscience and Bioengineering, 109 (5), 492-498.

Maddipati, P., Atiyeh, H.K., Bellmer, D.D., Huhnke, R.L. 2011. Ethanol Production from Syngas by Clostridium Strain P11 Using Corn Steep Liquor as a Nutrient Replacement to Yeast Extract. Bioresource Technology, 102 (11), 6494-6501.

Orgill, J.J., Atiyeh, H.K., Devarapalli, M., Phillips, J.R., Lewis, R.S., Huhnke, R.L. 2013. A Comparison of Mass Transfer Coefficients between Trickle-Bed, Hollow Fiber Membrane and Stirred Tank Reactors. Bioresource Technology, 133 (0), 340-346.

Phillips, J.R., Klasson, K.T., Clausen, E.C., Gaddy, J.L. 1993. Biological Production of Ethanol from Coal Synthesis Gas - Medium Development Studies. Applied Biochemistry and Biotechnology, 39, 559-571.

CHAPTER VII

MASS TRANSFER FOR SYNGAS FERMENTATION IN A CONTINUOUSLY STIRRED TANK REACTOR

7.1 Abstract

Mass transfer of CO and H_2 into syngas fermentation medium with *Clostridium ragsdalei* was determined in a continuously stirred tank reactor (CSTR). Mass transfer was represented by $k_{L,CO}a/V_L$ determined for mass transfer limited CO uptake. The mass transfer limit for CO was indicated by concurrent H_2 uptake, assuming equilibrium of the water gas shift inside the cells. CO inhibited H_2 uptake at dissolved CO partial pressure of 10^{-3} kPa, which supports the assumption of CO mass transfer limitation when H_2 is also consumed. Concurrent conversions of over 95% for each of CO and H_2 were achieved, and concurrent conversion gave the highest uptake rate of CO + H_2. The value of $k_{L,CO}a/V_L$ increased with agitation speed, gas flow and cell concentration. Mass transfer into active fermentation enhanced $k_{L,CO}a/V_L$ by a factor of 12 compared to a correlation for mass transfer for CO into water derived in the same CSTR. Surface renewal theory of liquid film mass transfer predicts $k_{L,H2}a/V_L$ for H_2 will be proportional

to $k_{L,CO}a/V_L$ by the square root of the ratio of their diffusivities; this proportionality was found when CO was mass transfer limited. For 600 rpm agitation, 0.015 vvm gas flow and 320 mg/L cell concentration, $k_{L,CO}a/V_L$ was 87 h^{-1} for plug flow gas in the CSTR.

7.2 Keywords

Syngas fermentation, mass transfer, CO, CSTR,

7.3 Nomenclature

$C_{i,L}$ - molar concentration of *i* in liquid (mol/L)

Cnv_i - molar conversion of *i*

CSTR – continuously stirred tank reactor

D – impeller diameter in CSTR (mm)

$D_{i,W}$ - diffusivity of gas *i* in water

dn_i/dt - molar rate of transfer of gas species *i* (CO, H_2, CO_2)

E – enhancement factor for mass transfer (dimensionless)

G – gas flow (sccm)

H_i - Henry's Law constant for gas *i* (kPa L/mol)

* - quantity derived from the Henry's law equilibrium

$k_{L,i}a/V_L$ – volumetric mass transfer coefficient for gas *i* (*i* can represent O_2, CO, H_2 or CO_2)

k_L – liquid film mass transfer coefficient

a – area of the gas liquid interface

V_L – liquid volume into which gas is transferred

L – liquid height in CSTR (mm)

N – agitation speed (rpm)

ORP – oxidation reduction potential versus the standard hydrogen electrode (mV SHE)

p_i – partial pressure of gas i (kPa),

p_i^* - partial pressure of dissolved gas by Henry's Law

P_T – pressure, total (kPa)

q_i – specific uptake rate of gas i (mol/g_x h)

t – time (s, min, h)

t_d – doubling time for cell growth (h)

T – tank diameter of CSTR (mm)

vvm – volume of gas per volume of liquid per minute

y_i – molar fraction of gas i in gas phase

ΔG_r – Gibbs free energy change of reaction (kJ/mol)

μ – specific growth rate (g_x/g_x h or h^{-1})

7.4 Introduction

The continuously stirred tank reactor (CSTR) is commonly used in fermentation processes. The conversion of synthesis gas components CO, H_2 and CO_2 to produce acetic acid and ethanol by bacteria, especially *Clostridium* species, requires transfer of these sparingly soluble gas species from the gas phase into solution in the aqueous medium that the bacteria inhabit. This mass transfer must occur at a rate sufficient to replace the gas species as they are consumed by the culture. The transfer of CO and H_2 maintains a low concentration of these species in the liquid that supports culture activity

and poises the thermodynamic position of the production reactions. The CSTR is the most common fermenter used in study of synthesis gas fermentation (Hu et al., 2010; Kundiyana et al., 2010; Phillips et al., 1993).

Mass transfer is often cited as a major impediment to the commercial success of the synthesis gas fermentation process (Klasson et al., 1992c). For sustained syngas fermentation the rate of CO and H_2 transfer into the liquid should match the kinetic capacity of the cell culture to convert each species (Klasson et al., 1992a). Mass transfer capacity greater than the kinetic capacity of the culture will cause dissolved CO and H_2 to accumulate, and inhibition by these powerful reductant species can result. In particular, CO is known to inhibit hydrogenase, the enzyme that catalyzes the uptake of H_2 (Hurst, 2005; Lazarus et al., 2009; Menon and Ragsdale, 1996; Terrill et al., 2012; Wilkins and Atiyeh, 2011). Uptake of H_2 is essential for conservation of the energy in syngas in the ethanol produced. Excess mass transfer of CO and H_2 must be avoided to maintain high rates of production and maintain efficiency of power applied.

The purpose of this study is to provide a basis for CSTR design in commercial scale fermentation of synthesis gas. This part of the study will examine the transfer of CO and H_2 into fermentation broth to supply fermentation by *Clostridium ragsdalei*.

7.5 Modeling

7.5.1 Sparingly soluble gas substrates

CO and H_2 are sparingly soluble in water and their solubility depends on the partial pressure of the individual species according to Henry's Law. For CO, as an example

$$C_{CO} = y_{CO}\, P_T / H_{CO} \qquad 7.1$$

Where C_{CO} is the liquid phase concentration of CO (mol/L), y_{CO} is the gas phase mol fraction of CO, P_T is the total pressure (kPa), and H_{CO} is the Henry's Law constant for CO (kPa L/mol). The Henry's Law constants for CO, H_2, CO_2 and O_2 at 37°C are given in Table 7.1. Saturated concentration of either CO or H_2 in water under 100 kPa of pure gas will be less than 10^{-3} mol/L. CO and H_2 must be continuously replenished in the liquid medium to support active fermentation. The lowest concentrations of CO and H_2 are inside the cell where the enzymes that catalyze oxidation reside. CO_2, in contrast, is produced in fermentation that consumes CO. CO_2 is transferred from inside the cell through the liquid phase to the gas phase. The concentration of CO_2 will be highest inside the cell.

Table 7.1 Henry's Law constants and diffusivities for gases in water at 37°C [a]

	H (kPa L/mol)	D_W (m^2/s)
CO	121561	2.50×10^{-9}
H_2	140262	6.24×10^{-9}
CO_2	4240	2.69×10^{-9}
O_2	101300	3.25×10^{-9}

[a] After (Hougen et al., 1954)

7.5.2 Liquid film controlling mass transfer

The rate of mass transfer of substrate gas from the bulk gas through the gas-liquid interface and the bulk liquid into the cell as shown in Figure 7.1 can be described by film theory (Bird et al., 2002). Diffusion of gas components within the bulk gas is very fast relative to the consumption rate and the concentration of CO, H_2 and CO_2 is uniform

throughout the bubble. The concentration of each species in the liquid at the interface is at equilibrium with the bulk gas partial pressure as predicted by Henry's Law, Equation 7.1. A stagnant film of liquid surrounds the bubble and dissolved gas must transfer through this film by diffusion to the bulk liquid. Diffusion is driven by concentration difference and is dependent on the gas diffusivity through water and the thickness of the film. The liquid outside of the film is assumed to be mobile and turbulent (Charpentier, 1981), and gas in the bulk liquid is dispersed by bulk flow at rates far exceeding diffusion, the bulk liquid is assumed to be well mixed and homogeneous. CO, H_2 and CO_2 are transferred into the cell by a diffusion process through the cell membrane, which is 6 to 9 nm thick. *C. ragsdalei* cells are typically 0.5 μm diameter by 3 μm, and even at low cell density (0.02 g cells/L) there are more than 10^{10} cells/L of bulk liquid. The

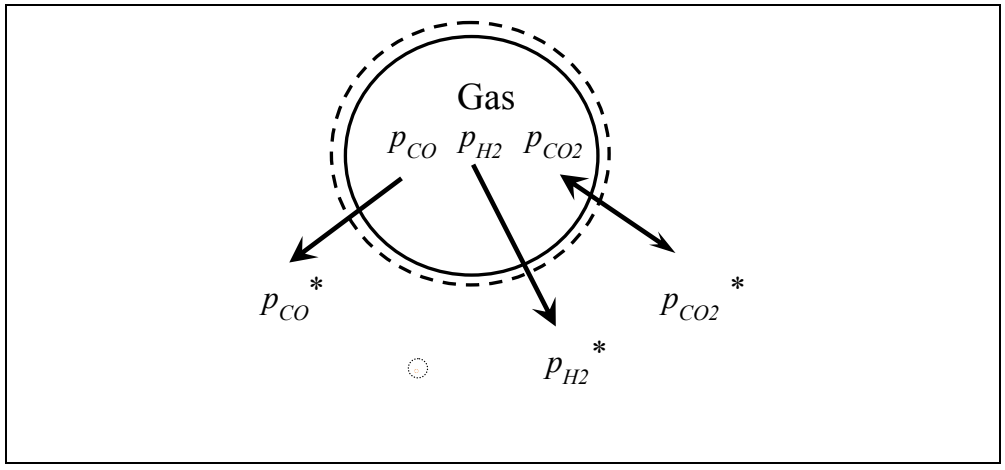

Figure 7.1 Gas to liquid mass transfer in CSTR. Partial pressure in the gas phase, p_{CO}, p_{H2}, p_{CO2} and in the bulk liquid phase p_{CO}^*, p_{H2}^*, p_{CO2}^*. Bubble boundary is indicated by the solid line and the liquid film by the dashed line, a single cell is indicated inside the small circle, scale of the bubble is 1 mm diameter, size of the cell is 0.5 μm diameter by 3 μm length, There are more than 10^{10} cells per liter of fermentation broth.

surface area of the cell mass will exceed the area of the gas-liquid interface by 2 to 3 orders of magnitude in a typical fermentation. The film of stagnant liquid at the gas-liquid interface is the major resistance to transfer of CO, H_2 and CO_2 into the cells. The molar rate of gas transfer is proportional to the difference in concentration from the surface of the liquid to the bulk liquid.

The partial pressure of each component in the gas phase is the product of its mole fraction and the total pressure, for CO

$$p_{CO} = y_{CO} P_T \tag{7.2}$$

Gas mass transfer is governed by

$$-\frac{1}{V_L}\frac{dn_{CO}}{dt} = \left(\frac{k_{L,\mathrm{CO}}a}{V_L}\right)\left(C_{CO}^{*} - C_{CO,L}\right) = \frac{\left(\frac{k_{L,\mathrm{CO}}a}{V_L}\right)}{H_{CO}}\left(p_{CO} - p_{CO}^{*}\right) \tag{7.3}$$

Where $C_{CO,L}$ is the concentration of CO (mol/L) in the bulk liquid, C_{CO}^{*} is concentration of CO (mol/L) in equilibrium by Henry's Law with the bulk gas, p_{CO}^{*} is the CO partial pressure (kPa) in equilibrium by Henry's Law with the concentration of CO dissolved in the bulk liquid, H_{CO} is the Henry's Law constant for CO (kPa L /mol) and V_L is the volume (L) of liquid into which gas is transferred. The molar rate of transfer is $-dn_{CO}/dt$ (mol CO/h) where the negative sign denotes consumption from n_{CO} moles of bulk gas.

The constant of proportionality in Equation 7.3 ($k_{L,CO}a/V_L$) is the overall liquid film mass transfer coefficient for CO with units of reciprocal time (h^{-1}). The area of the gas/liquid interface is a. The term $k_{L,CO}$ is the liquid film mass transfer coefficient for CO (L/m^2 h). $k_{L,CO}$ includes effects of turbulence in the liquid, hydrodynamic conditions like

viscosity that affect film thickness, and the effect of diffusivity in the aqueous phase. The film mass transfer coefficient k_L is different for each gas species.

7.5.3 Water gas shift reaction is in equilibrium

CO and H_2 are consumed simultaneously in typical syngas fermentation. Electrons from oxidized CO and H_2 pass to ferredoxin before distribution to other electron carriers and reactions inside the cell (Hu et al., 1984; Ragsdale, 2004; Ragsdale and Ljungdahl, 1984). The electrons are energetically equivalent, and the transfer is directed from CO and H_2 to ferredoxin. The water gas shift has been reported using a graphite flake to transfer electrons between carbon monoxide dehydrogenase (CODH) and hydrogenase (H_2ase) (Lazarus et al., 2009), and is similarly conducted in acetogenic bacteria with ferredoxin replacing the graphite. Electrons are transferred from ferredoxin to other electron carriers and used in the production reactions of the Wood-Ljungdahl pathway or for cell growth and function. The water gas shift reaction in Equation 7.4 relates concentrations of CO, H_2 and CO_2 inside the cell mediated by ferredoxin.

$$CO + H_2O \leftrightarrow CO_2 + H_2 \tag{7.4}$$

Since both CO and H_2 are consumed and the water gas shift proceeds neither from CO to H_2, nor from H_2 to CO, the water gas shift is assumed to be at thermodynamic equilibrium. The Gibbs free energy change for the water gas shift reaction is equal to zero ($\Delta G_r = 0$) at equilibrium (Nicholls and Ferguson, 2002). The concentration of CO inside the cell must be very low ($p_{CO}^* < p_{H2}^*/10{,}000$) to be in equilibrium with H_2; where p_{CO}^* and p_{H2}^* represent the partial pressure of each gas inside the cell, which is the same as in the bulk liquid as in Figure 7.1. The CO partial pressure is reduced from more than 10 kPa in the gas bubble to less than 10^{-3} kPa inside the cell; at the same time the partial

pressure of H_2 is reduced from more than 10 kPa in the gas to about 1 kPa in the cell. The change in CO partial pressure is effected by the concentration difference required to transfer CO into the cell.

7.5.4 CO assumed mass transfer limited

The capacity of the fermenter to transfer gas into the liquid is characterized by the volumetric mass transfer coefficient for transfer of CO ($k_{L,CO}a/V_L$). CO transfers from the gas bubble through a stagnant liquid film that controls the rate of mass transfer, then through the well mixed bulk liquid and the cell membrane into the cell. The very low concentration of CO inside the cell can be neglected in calculation of mass transfer through the controlling liquid film and p_{CO}^* can be assumed to be 0, so that Equation 7.3 becomes

$$-\frac{1}{V_L}\frac{dn_{CO}}{dt} = \frac{\left(\frac{k_{L,\mathrm{CO}}a}{V_L}\right)}{H_{CO}}\left(p_{CO} - p_{CO}^*\right) = \frac{\left(\frac{k_{L,\mathrm{CO}}a}{V_L}\right)}{H_{CO}}\,p_{CO} \qquad 7.5$$

$k_{L,CO}a/V_L$ (h^{-1}) can be calculated from dn_{CO}/dt, the rate of CO uptake (mol/h), and p_{CO}, the partial pressure of CO in the gas phase (kPa).

7.5.5 Syngas is in plug flow regime for mass transfer

The transfer of CO into zero concentration under mass transfer was used by Klasson (1992b), but under the assumption of a well mixed gas phase the rate of mass transfer was considered proportional to the partial pressure of CO in the effluent gas for calculation of $k_{L,CO}a/V_L$. The study of O_2 transfer from air into liquid reported in Chapter 6 showed that O_2 was depleted from the inlet gas as it passed through the liquid, and that backmixing of spent gas from the headspace did not influence mass transfer. Transfer of

CO and H_2 into the fermentation medium is expected to show a similar change in concentration of CO and H_2 in transit of the liquid.

In a CSTR, fresh gas enters as a bubble and is suspended in the liquid as CO and H_2 are removed by mass transfer to the cells. The bubble, depleted of CO and H_2, leaves the liquid into the headspace of the fermenter. The difference of CO concentration between the bubble surface and the bulk liquid falls as CO is consumed from the gas bubble. Overall in the CSTR, the effective concentration difference is best represented with a plug flow model, and calculated as the logarithmic mean of the concentration difference between the inlet and the bulk liquid, and the concentration difference between the effluent and the bulk liquid as shown in Equation 7.6.

$$-\frac{1}{V_L}\frac{dn_{CO}}{dt} = \frac{\left(\frac{k_{L,\mathrm{CO}}a}{V_L}\right)}{H_{CO}} \frac{\left(p_{CO,i} - p^*_{CO}\right) - \left(p_{CO,o} - p^*_{CO}\right)}{ln\frac{\left(p_{CO,i} - p^*_{CO}\right)}{\left(p_{CO,o} - p^*_{CO}\right)}} \qquad 7.6$$

Similar equations can be written to describe mass transfer for H_2 and CO_2.

In the present study, the calculation of $k_{L,CO}a/V_L$ in the CSTR assumes plug flow of the syngas in transit of the liquid volume, and assuming $p_{CO}^* = 0$, represents the partial pressure of CO in the gas, p_{CO} in Equation 7.5, as the logarithmic mean of the CO partial pressure in the inlet and outlet gas.

$$-\frac{1}{V_L}\frac{dn_{CO}}{dt} = \frac{\left(\frac{k_{L,\mathrm{CO}}a}{V_L}\right)}{H_{CO}} \frac{\left(p_{CO,i} - p_{CO,o}\right)}{ln\left(\frac{p_{CO,i}}{p_{CO,o}}\right)} \qquad 7.7$$

7.5.6 Species mass transfer is independent

Mass transfer of CO is independent of mass transfer of H_2 and CO_2, with the rate of CO transfer dependent on the diffusivity of CO and concentration difference for CO alone. Mass transfer of H_2 and CO_2 are also independent of each other and of CO. However, for mass transfer into fermentation medium, mass transfer is limited to the few mmole of gas that will saturate the liquid volume. Mass transfer is sustained only in the presence of reaction, and the rate of reaction will match the rate of mass transfer for each gas species, CO, H_2 and CO_2. The reaction of these gas species is not independent, being related through the stoichiometry, enzymology and thermodynamics. In particular, accumulation of CO to about 7×10^{-9} mol/L in the cell will inhibit the hydrogenase enzyme about 50% (Ragsdale and Ljungdahl, 1984) and slow or stop H_2 uptake. Optimum mass transfer will provide high rate of CO transfer into a fermentation condition that allows uninhibited uptake of H_2 at rates that can be as high as those for CO (Phillips et al., 1994). Mass transfer balanced with kinetic capacity can provide high conversions of the energy content of syngas, in CO and H_2, into ethanol at rates that deliver high productivity.

7.5.7 Mass transfer coefficients from surface renewal theory

The volumetric mass transfer coefficients for H_2 ($k_{L,H2}a/V_L$) and CO_2 ($k_{L,CO2}a/V_L$) differ from $k_{L,CO}a/V_L$, but are proportional. The area of the gas/liquid interface and the liquid volume are the same for all gases, as is the intensity of turbulence in the liquid. The coefficients for these gases will differ due to their diffusivity in the fermentation broth ($D_{i,W}$) through the liquid film, and the measured $k_{L,CO}a/V_L$ from Equation 7.7 is

adjusted to predict values of $k_{L,H2}a/V_L$ and $k_{L,CO2}a/V_L$ based on the surface renewal theory for film transfer (McCabe and Smith, 1976).

$$\frac{k_{L,CO}a}{V_L} = \sqrt{\frac{D_{CO,W}}{D_{H2,W}}}\left(\frac{k_{L,H2}a}{V_L}\right) = \sqrt{\frac{D_{CO,W}}{D_{CO2,W}}}\left(\frac{k_{L,CO2}a}{V_L}\right) \quad 7.8$$

$k_{L,H2}a/V_L$ and $k_{L,CO2}a/V_L$ are determined from Equation 7.8, and represent the actual capacity of the fermenter to transfer H_2 and CO_2. This capacity can remain unused, in which case H_2 or CO_2 will accumulate in the bulk liquid and in the cell up to saturation of the dissolved gas. The fermentation broth was assumed to be like water, which is 98% of the medium.

7.6 Materials and Methods

7.6.1 Microbial Catalyst

C. ragsdalei grown from stock culture provided by Dr. Ralph Tanner, University of Oklahoma was used. The culture was maintained at 37^{o}C and inoculation was typically 5% (v/v) from growing culture. *C. ragsdalei* was grown in 250 ml serum bottles (Wheaton, Millville, NJ, USA), stoppered and crimp sealed containing 100 ml of fresh medium under 238 kPa (absolute) of syngas. Inoculum for the CSTR was the third passage of *C. ragsdalei* from stock culture.

7.6.2 Medium Preparation

The standard yeast extract medium was optimized for maintenance of *C. ragsdalei* (Saxena, 2008) and was used in serum bottles for growth of inoculum and in the CSTR. Medium contained yeast extract (Difco Laboratories, Detroit, MI, USA),

morpholinoethanesulfonic acid (MES) buffer and KOH to charge the buffer to pH 6.0, minerals, trace metals, vitamins and resazurin as a redox indicator as shown in Table 7.2. Medium for growth in serum bottles was prepared by dissolving the components in deionized water in a boiling flask, and heating to just boiling (about 4 minutes for 600 mL medium). The hot medium in the flask was purged with N_2 as it cooled with a cannula submerged to bubble through the medium and strip residual O_2, and a second cannula in the headspace to assist in exclusion of air. A foam rubber plug was loosely inserted in the flask mouth to restrict flow during purging. As the medium cooled serum bottles were purged with N_2 for 2.5 min each with a cannula inserted to the bottom of the bottle and a No. 1 butyl rubber stopper (VWR Scientific, Radnor, PA, USA) placed loosely over the bottle mouth. Medium was dispensed by pipette into the purged bottles and the purge was continued for 2.5 min before the bottles were closed with the stopper and crimp sealed. Medium was autoclaved for 20 min at 121^{o}C, cooled and stored in a dark space at room temperature before use. A solution (0.5 mL/100 mL) of 4% cysteine (w/v) and 4% sodium sulfide ($Na_2S.9H_2O$) was added, and the headspace gas replaced by purging for 2 min with syngas before inoculation. Syngas was supplied through a syringe needle (22G1.5, Becton Dickinson, Franklin Lakes, NJ, USA) and vented through a second needle. Bottles with cysteine and sulfide for reduction and purged with syngas were placed on a shaker at 37^{o}C until warm and colorless before inoculation.

Table 7.2 Composition of Fermentation Medium used in CSTR studies

Component	Formula	Concentration
		(mg/liter)
Yeast Extract	Undefined	500
MES Buffer	$C_6H_{13}NO_4S$	10000
Potassium Hydroxide	KOH	1264
Minerals		
Ammonium Chloride	NH_4Cl	2500
Calcium Chloride	$CaCl_2.2H_2O$	100
Magnesium Sulfate	$MgSO_4.7H_2O$	500
Potassium Chloride	KCl	250
Potassium Phosphate	KH_2PO_4	250
Trace Metals		
Cobalt Chloride	$CoCl_2.6H_2O$	2
Ferrous Ammonium Sulfate	$FeH_{20}N_2O_{14}S_2$	8
Manganese Sulfate	$MnSO_4.H_2O$	10
Nickel Chloride	$NiCl_2.6H_2O$	2
Nitrilotriacetic Acid	$C_6H_9NO_6$	20
Sodium Molybdate	$Na_2MoO_4.2H_2O$	0.2
Sodium Selenate	Na_2SeO_4	1
Sodium Tungstate	$Na_2WO_4.2H_2O$	2
Zinc Sulfate	$ZnSO_4.7H_2O$	10
Vitamins		
Para-aminobenzoic Acid	$C_7H_7NO_2$	0.05
Biotin	$C_{10}H_{16}N_2O_3S$	0.02
Pantothenic Acid	$Ca(C_9H_{16}NO_5)_2$	0.05
Folic Acid	$C_{19}H_{19}N_7O_6$	0.02
MESNA	$C_2H_5NaO_3S_2$	0.10
Nicotinic Acid	$C_6H_5NO_2$	0.05
Pyridoxine	$C_8H_{11}NO_3.HCl$	0.10
Riboflavin	$C_{17}H_{20}N_4O_6$	0.05
Thiamine	$C_{12}H_{17}N_4OSCl.HCl$	0.05
Thioctic Acid	$C_8H_{14}O_2S_2$	0.05
Cyanocobalamin	$C_{63}H_{88}CoN_{14}O_{14}P$	0.05
Resazurin		
Resazurin	$C_{12}H_6NO_4Na$	1
Cysteine/Sulfide		
Cysteine	$C_3H_7NO_2S$	200
Sodium Sulfide	$Na_2S.9H_2O$	200

For the CSTR, the medium components were dissolved in deionized water in a 1 L flask and diluted to 2500 mL in the CSTR vessel. The CSTR vessel was assembled with all ports sealed, except the vent condenser was open to atmosphere and covered with paper and aluminum foil. The medium and CSTR assembly were autoclaved for 20 min at 121^{o}C. The hot vessel containing the medium solution was taken from the autoclave, set in place and sparged with N_2 to remove residual O_2 as it cooled to 37^{o}C. N_2 was fed to the CSTR through a sterile filter using a mass flow controller. Then 7.5 mL of a solution containing 4% cysteine (w/v) and 4% sodium sulfide was added to the cooled medium and kept at 37^{o}C under N_2 purge at 150 rpm agitation until the pink color of the resazurin disappeared, more than 30 min, before inoculation. Inoculation of the CSTR used 5% v/v of growing *C. ragsdalei* from the third passage from stock in serum bottles.

7.6.3 CSTR Experimental Set Up

CSTR scale up typically assumes similar geometry (Bakker et al., 1994), and the type and placement of impellers, baffles and gas sparger used in experiment are important to ensure utility of the results. A typical commercial CSTR will have a liquid height to tank diameter ratio (*L/T*) of more than 2. This was not feasible in the laboratory fermenter used in this experiment. However, defined geometry of the laboratory CSTR that followed the recommendations of Bakker et al. (1994) as closely as possible was used in these studies to best simulate commercial geometry for scale up. The impeller spacing was one impeller diameter (*D*) above the bottom and *D* between the two Rushton impellers *L/T* used was 1.69, and *D/T* was 0.41.

Experiments were conducted in a 3.0 L BioFlo 110 laboratory fermenter system (New Brunswick, Enfield, CT, USA). The vessel was heated by an external heating

blanket to maintain temperature at 37°C. A model syngas contained 38.5% CO, 28.5 % H_2, 28.5% CO_2 and 5% N_2 (38:28.5:28.5:5 CO:H_2:CO_2:N_2 syngas mix, Stillwater Steel and Supply Company, Stillwater, OK, USA) was introduced in the bottom of the vessel, under the agitator impellers, through a stainless steel fritted sparger. Gas flow was controlled from the cylinders by thermal conductivity mass flow controllers (Porter, Hatfield, PA, USA). The mass flow controllers each had a maximum flow of 200 sccm (except only 100 sccm for H_2) and total flow was typically less than 20 sccm, with a maximum of 80 sccm. Two Rushton impellers designed for radial flow to promote gas dispersion were used in all experiments. A chilled water condenser removed water from the effluent gas returning the condensed water to the CSTR, and the effluent gas then bubbled through chilled water to collect ethanol stripped from the fermentation. The effluent gas pressure was indicated on a pressure gauge in the tubing from the bubbler before a rotameter, check valve and discharge to a fume hood.

Performance of the CSTR is dependent on the geometry of the assembled components. Bakker et al. (1994) suggest preferred CSTR geometry, and define a correlation of CSTR performance for O_2 transfer into and from water. Two Rushton gas dispersion impellers each with 6 flat blades mounted vertically around a central horizontal disc were used to circulate the liquid and break the gas into small bubbles. The 51 mm impellers were installed in a 124 mm diameter tank so the ratio of the impeller diameter to the tank diameter (D/T) equals 0.41, where Bakker et al. (1994) recommend $0.3 < D/T < 0.5$. The 3.0 L fermenter was configured according to the suggestions of Bakker et al. (1994), locating the bottom Rushton impeller one impeller diameter (51 mm) above the dished bottom of the CSTR vessel, and the second impeller

51 mm above the first. Liquid volume in the CSTR was chosen to be 80% of the vessel volume, or 2.5 L, which resulted in a liquid height to tank diameter ratio (*L/T*) of 1.69. The resting liquid level was about 90 mm above the top impeller. A baffle ring was used to direct the radial flow vertically at the vessel wall and minimize vortex formation. The four baffles were 13 mm wide and 140 mm long. The top of the baffles was placed at the 2.0 L level of the vessel, so that the baffles spanned the zone of radial flow from the Rushton impellers.

The BioFlo 110 fermenter system delivers agitator speeds adjustable from 0 to 1200 rpm. Agitator speed typically was started at 150 rpm, with low gas engagement, and increased or decreased to maintain conversion as explained below. A maximum of 900 rpm was used in the present study.

The BioFlo 110 system connected to an autoclavable pH probe (Mettler-Toledo, Woburn, MA, USA) monitors pH and can add base and acid to maintain pH at a selected set point, or within a range. The pH in the present CSTR study was maintained at or above 4.60 by addition of autoclave sterilized 7% sodium bicarbonate ($NaHCO_3$) solution controlled by the BioFlo 110 system. The oxidation-reduction potential (ORP) was monitored separately using an autoclavable ORP probe (Mettler-Toledo, Woburn, MA, USA).

7.6.4 Sampling and Analysis

Up to 9 gas samples and 6 liquid samples were withdrawn from the CSTR in each of the first 4 days, and then with decreasing frequency of sampling for the next 10 days. A liquid sample was analyzed for pH and cell, ethanol, butanol, acetic acid and butyric acid concentrations. Cell concentration was determined as optical density measured at

660 nm in a UV-2100 spectrophotometer (Cole Parmer, Vernon Hills, IL, USA). Liquid product concentrations were determined from a sample centrifuged (Fisher Scientific, Pittsburgh, PA, USA) for 10 minutes at 13,000 rpm to remove cells. Supernatant was mixed with an equal part of 0.085 M HCl to ensure all acetate was converted to the volatile free acetic acid form. The liquid sample was analyzed using a GC (Agilent Technologies, Wilmington, DE, USA) with a DB-FFAP capillary column (Agilent J&W, Wilmington, DE, USA) and quantitation using a flame ionization detector (FID). Gas composition was determined using a GC (Agilent Technologies, Wilmington, DE, USA) with a capillary column with Carboxen 1010 PLOT stationary phase (Supelco, Bellefonte, PA, USA) and argon mobile phase. The GC ran isothermally at 80^{o}C with a thermal conductivity detector (TCD) for quantitation of the permanent gases H_2, N_2, CO and CO_2. Chromatograms for the liquid products and gases were analyzed using the ChemStation data analysis software.

7.6.5 Data Management

Data was collected, plotted and derivative quantities calculated using Microsoft Excel.

7.7 Results and Discussion

7.7.1 Summary of syngas fermentations in the CSTR

Seven batch fermentations with continuous gas flow were run in the 3.0 L CSTR to assess mass transfer into fermentation medium inoculated with active *C. ragsdalei*. The first fermentation, named in Table 7.3 as SGIE1, was conducted with gas mixed through the mass flow controllers (about 42 mole % CO, 11% H_2, 42% CO_2 and 5% N_2) at a total flow of 75 sccm to achieve a target of 0.030 vvm (volume of gas flow per

volume of liquid per minute). Agitation was controlled between 150 and 400 rpm, achieved a total uptake of 1,042 mmol of CO plus H_2, and produced 0.27 g/L of cells, 0.1 g/L ethanol and 6.0 g/L of acetic acid after 125 h (Table 7.3). However, there was essentially no uptake of H_2 due to CO inhibition of hydrogenase, and the conversion of CO did not exceed 36% at any time. The medium used in these studies has a limited growth potential and did not support enough cell mass to process the gas supplied at this flow. This run demonstrated $k_{L,CO}a/V_L$ of 52 h^{-1} at 400 rpm and 75 sccm gas flow, but was very inefficient in conservation of the energy from CO and H_2 in the feed gas (Table 7.3).

Table 7.3 Summary of syngas fermentations in the CSTR.

Experiment	**SGIE1**	**SGIE2**	**SGIE3**	**SGIE4**	**SGIE5**	**SGIE6**	**SGIE7**
Gas flow (sccm)	75	38.2	17.5	17.7	17.7	17.7	17.7
vvm	0.030	0.015	0.008	0.008	0.008	0.008	0.008
Max. Agitation (rpm)	400	600	280	650	900	700	400
Cumulative Uptake (mmol)	1042	1573	1600	1900	1680	1700	1000
Cell Conc (mg/L)	270	320	328	304	350	310	270
Ethanol (g/L)	0.1	0.13	0.09	0.13	0.19	0.24	1.05
Acetic acid (g/L)	6.0	6.6	7.0	7.0	6.6	6.7	5.0
Max CO conversion	36%	86%	68%	92%	95%	95%	71%
Max H_2 Conversion	0%	82%	75%	94%	96%	95%	77%
Max $k_{L,CO}a/V_L$ (h^{-1})	52	87	22.5	46.3	63.8	73.6	23.0
at G (sccm)[a]	75	38.2	17.5	17.7	19.4	20.3	17.7
at N (rpm)[a]	400	600	280	650	900	700	300

[a] Gas flow and agitation speed for maximum $k_{L,CO}a/V_L$

The second fermentation (SGIE2) used a constant flow of N_2 of 10 sccm in the mixed feed gas to define the inlet and effluent gas flows and aid in the material balance calculation. The feed rate of the substrate gases CO, H_2 and CO_2 were controlled to supply only the amount that could be converted by *C. ragsdalei* in the CSTR. The total gas flow was up to 38.2 sccm (0.015 vvm) with 10 sccm of N_2 constant flow. Agitation was maintained at 600 rpm, cumulative uptake of 1573 mmol of CO plus H_2 was achieved over 330 h of fermentation (Table 7.3). Cell concentration reached 0.32 g/L, with 0.13 g/L of ethanol and 6.6 g/L of acetic acid produced. Energy conservation was improved with CO conversion of up to 86% and H_2 conversion up to 82% achieved. Most of the gas (86%) was consumed in the first 100 h, and $k_{L,CO}a/V_L$ of 87 h^{-1} was achieved at 600 rpm and 38.2 sccm.

A syngas mix of 40:30:30 $CO:H_2:CO_2$ was used in the bottle studies, and was planned to be used for the CSTR studies. N_2 was added to this gas mix as an inert tie component to aid in the calculation of the material balance. Subsequent fermentations were conducted with a 38:28.5:28.5:5 $CO:H_2:CO_2:N_2$ syngas mix from a single cylinder with 38.0 mole % CO, 28.5% H_2, 28.5% CO_2 and 5% N_2. Since N_2 is not expected to be consumed or produced in the fermentation, the inlet flow of N_2 should equal the effluent flow of N_2, and the effluent flow and conversion of the other components can be scaled from the GC gas analysis and the known inlet flow rate as in Equations 7.9 and 7.10.

$$G_o = G_i\left(\frac{y_{N2,i}}{y_{N2,o}}\right) \tag{7.9}$$

$$Cnv_{CO} = 1 - \left(\frac{y_{CO,o}}{y_{CO,i}}\right)\left(\frac{y_{N2,i}}{y_{N2,o}}\right) \tag{7.10}$$

Where the effluent gas flow is G_o and the inlet gas flow G_i in mol/h, y_{CO} and y_{N2} are the mole fraction of CO and N_2 (inlet and effluent as for G), and Cnv_{CO} is the conversion of CO. Conversion of H_2 (Cnv_{H2}) and CO_2 (Cnv_{CO2}) are defined as for CO in Equation 7.10. Conversion of CO_2 will typically be negative, and this indicates production of CO_2 as would be expected from the reaction stoichiometry for CO (Equation 7.11) and H_2/CO_2 (Equation 7.12).

$$6\,CO + 3\,H_2O \rightarrow CH_3CH_2OH + 4\,CO_2 \qquad 7.11$$

$$6\,H_2 + 2\,CO_2 \rightarrow CH_3CH_2OH + 3\,H_2O \qquad 7.12$$

Fermentations SGIE3, SGIE4, SGIE5 and SGIE6 used the 38:28.5:28.5:5 $CO:H_2:CO_2:N_2$ syngas mix and an initial feed rate of 17.7 sccm, which is about 0.008 vvm. Agitation was started at 150 rpm until first CO, and then H_2 conversion was established. Agitation was increased, in some experiments more aggressively, to increase conversion at the constant gas flow. The performance of these fermentation runs is reported in Table 7.3. Again, most of the gas was consumed in the first 100 h. These fermentations used a strain of *C. ragsdalei* recently obtained from Dr. Tanner, the strain grew well, but produced low amounts of ethanol. The recent strain of *C. ragsdalei* may have adapted to environmental pressure in culture maintenance and selected for a more efficient use of yeast extract in production of cell mass. The higher initial growth on yeast extract consumed available reductant (electrons from CO and H_2) and heightened acetic acid production. An earlier established strain of *C. ragsdalei* known to produce ethanol was used in run SGIE7.

7.7.2 Syngas fermentation in the CSTR SGIE7

The seventh fermentation (SGIE7) used the strain of *C. ragsdalei* that produced more ethanol and the gas mix at 17.7 sccm (0.008 vvm). Cumulative uptake seen in Figure 7.2 reached only 1000 mmol of CO plus H_2 over 330 h of fermentation. Cell concentration, shown in Figure 7.3, reached 0.27 g/L with 1.05 g/L of ethanol and 5.0 g/L of acetic acid produced. Agitation was held at 150 rpm through 43 h of fermentation then increased to 200, 250, 300 and 400 rpm; H_2 conversion fell sharply at 400 rpm and the agitation was reduced to 150 rpm for the remainder of the run (Figure 7.4).

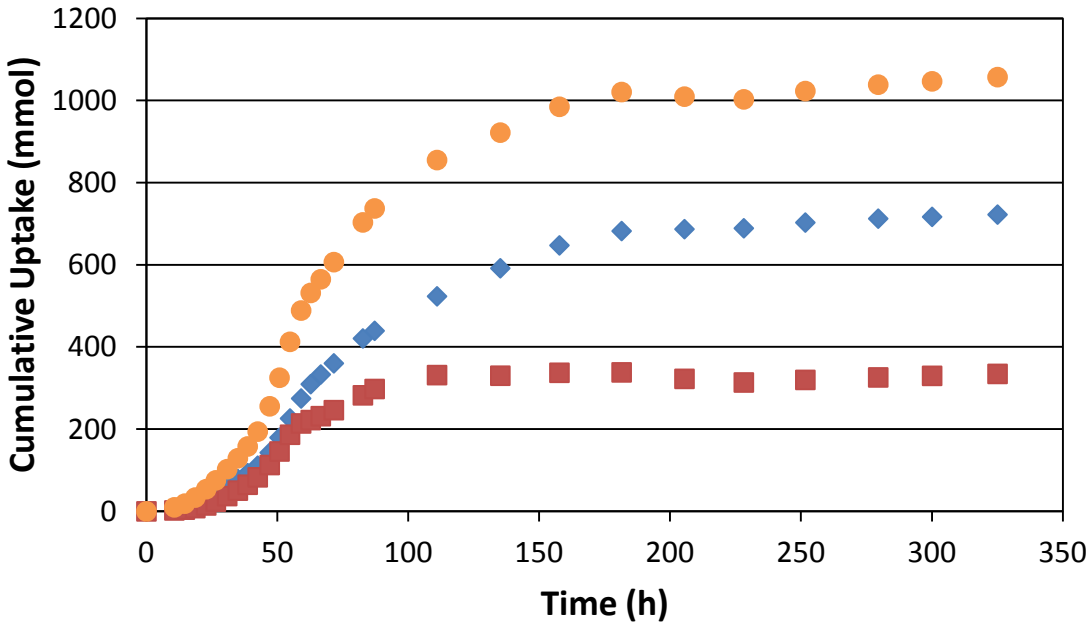

Figure 7.2 Cumulative uptake in CSTR fermentation of syngas SGIE7. CO (◆), H_2 (■), CO+H_2 (●).

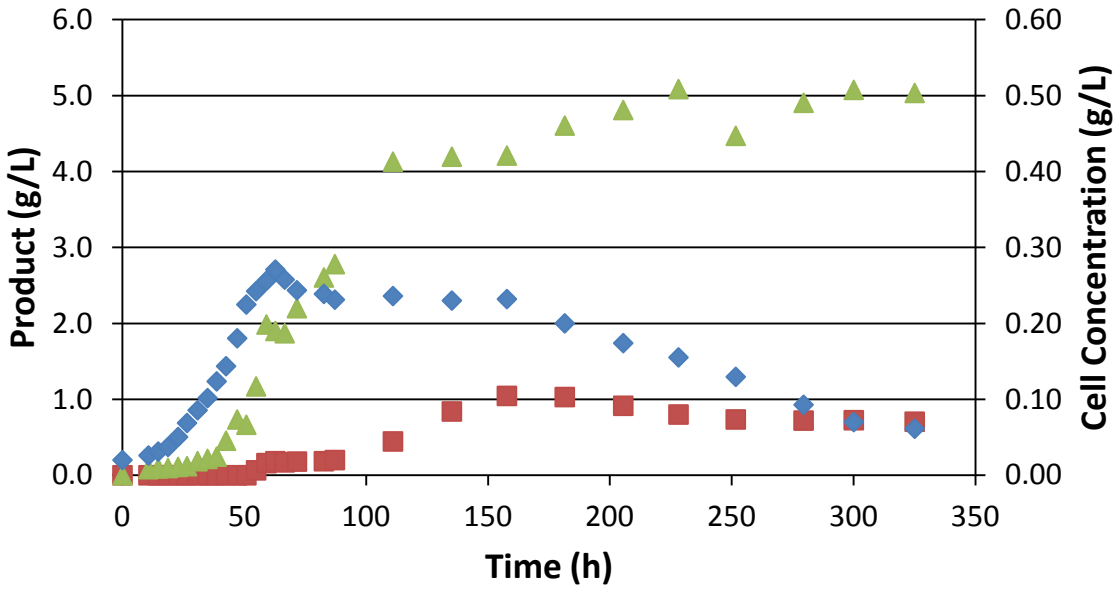

Figure 7.3 Cells and products concentrations in CSTR fermentation of syngas SGIE7. Ethanol (■), acetic acid (▲), cells (◆)

CO conversion of 71% and H_2 conversion of 77% seen in Figure 7.4 were achieved at 300 rpm, CO conversion fell when agitation was aggressively increased to 400 rpm at 55 h and CO inhibited H_2 uptake. Total uptake of CO plus H_2 was highest when both CO and H_2 were consumed at 55 h in Figure 7.5. Both CO and H_2 conversion dropped to 0 after 150 h and the data is not shown to better show the course of active fermentation in the first 100 h.

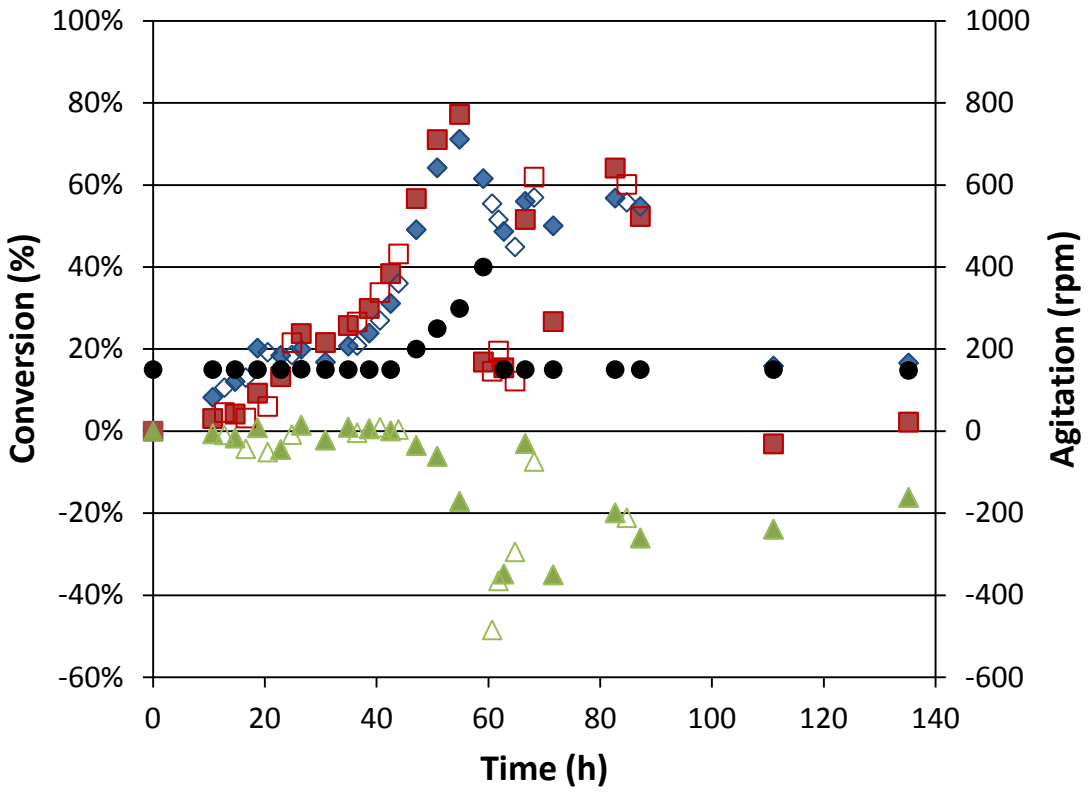

Figure 7.4 Gas conversions and agitation in CSTR fermentation of syngas SGIE7. CO (◆), H_2 (■), CO_2 (▲) and agitation (●). The open symbols indicate only a gas sample was taken.

The sharp inhibition of H_2 uptake after 55 h indicates a step change in CO concentration inside the cell. The increased CO concentration follows a kinetic reduction of cell function, as the CO is present in sufficient concentration to inhibit the hydrogenase, reported to be 7×10^{-9} mol/L at 35°C (equivalent to 8.5×10^{-4} kPa through Henry's Law (Ragsdale and Ljungdahl, 1984)). Although CO concentration increased in the cells after 55 h the pathway reactions, including CO oxidation, slowed (Figure 7.5).

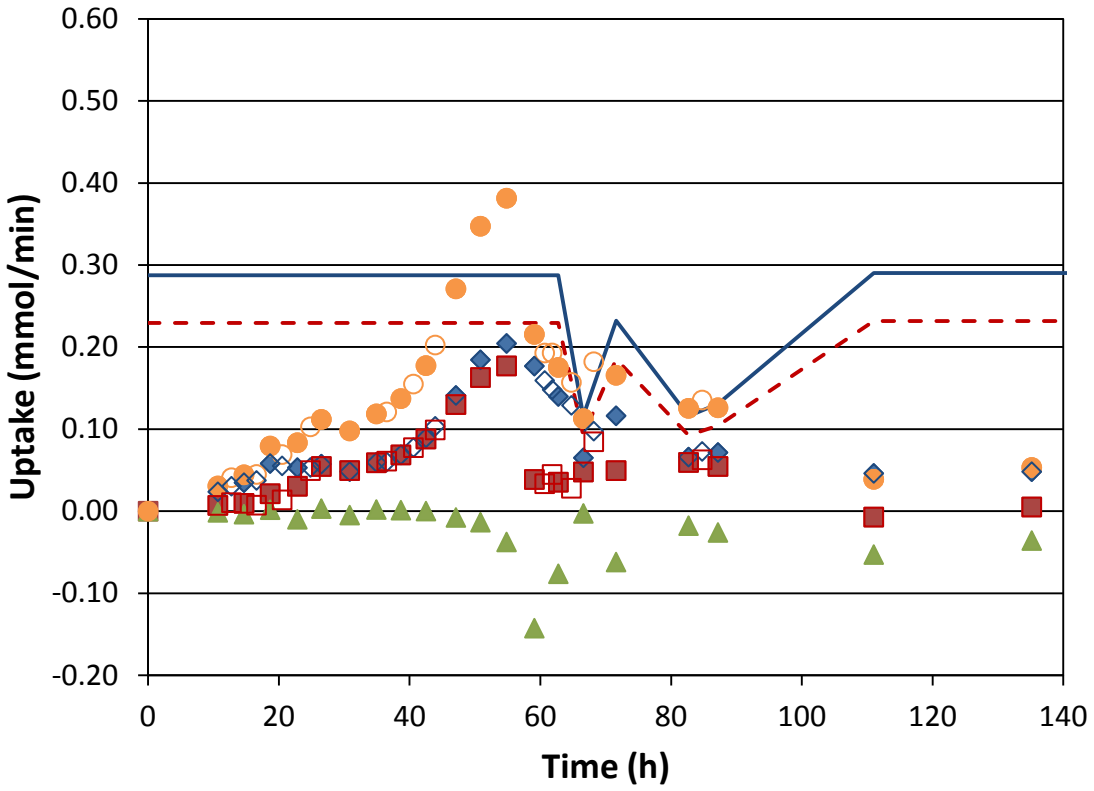

Figure 7.5 Gas uptake in CSTR fermentation of syngas SGIE7. CO (◆), H_2 (■), CO_2 (▲), CO+H_2 (●), CO feed rate (—) and H_2 feed rate (– –). The open symbols indicate only a gas sample was taken.

Kinetic parameters can be derived from the data, as presented in Figure 7.6. The maximum specific uptake of CO is 0.038 mol per gram of cells per hour (mol/g_xh) at 19 h, but drops to 0.020 mol/g_xh as cell concentration increases. CO concentration falls and mass transfer limitation is established. H_2 uptake increases concurrently and specific uptake of H_2 also approaches 0.020 mol/g_xh. The combined specific uptake of reductant is 0.040 mol CO+H_2/g_xh at 55 h (Figure 7.6).

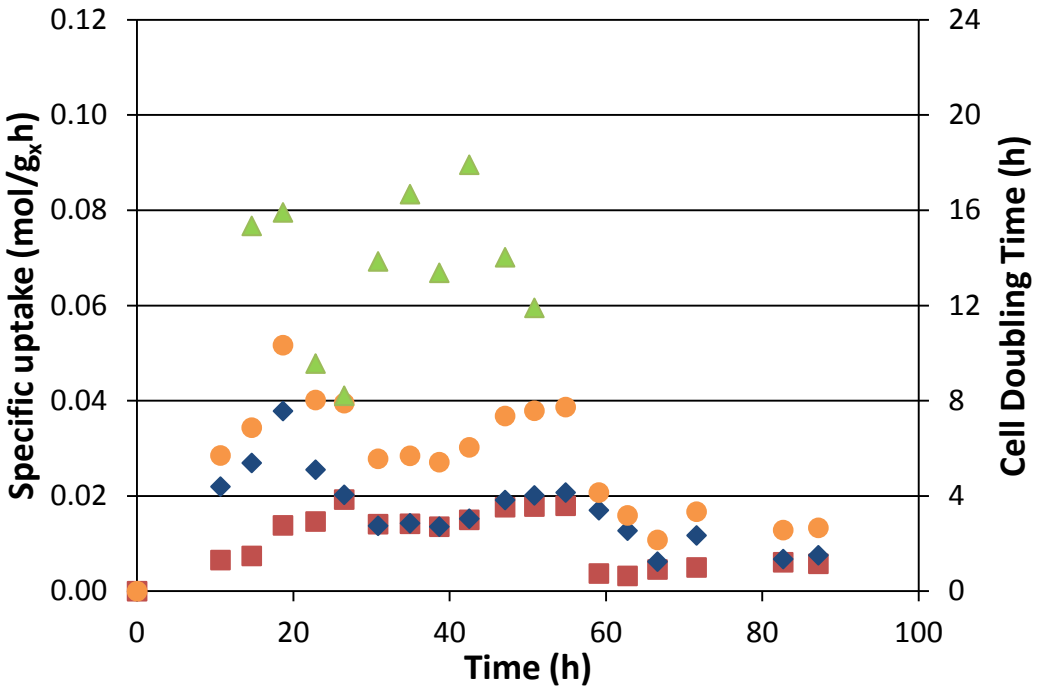

Figure 7.6 Gas specific uptake and cell doubling time in CSTR fermentation of syngas SGIE7. CO (◆), H_2 (■), CO + H_2 (●) and doubling time (▲)

The doubling time of the cells is shown in Figure 7.6 and ranges from 8 to 16 h during the first 50 h of fermentation. The specific growth rate of *C. ragsdalei* in the medium used during this period ranges from 0.087 h^{-1} (t_d = 8 h) to 0.043 h^{-1} (t_d = 16 h). The cell concentration doubled in as little as 3 h (specific growth of 0.231 h^{-1}) in fermentations SGIE1 through SGIE6. This is very fast growth for anaerobic bacteria, and unlikely to result from the syngas uptake alone, as the Wood-Ljungdahl pathway yields no net ATP. *C. ljungdahlii* grows on amino acids from peptone with doubling time as low as 4 h (Doyle, 1991), then exhibits a slower subsequent growth phase on syngas or some sugars. *C. ragsdalei* inoculated into the yeast extract medium without syngas (either CO_2 or N_2 in the bottle headspace) did not grow (data not shown). It is likely that

C. ragsdalei grows very quickly on the combination of syngas and amino acids in the yeast extract, and then maintains cell mass and production at a lower specific uptake after the amino acids are exhausted.

The apparent volumetric mass transfer coefficient for CO uptake, $k_{L,CO}a/V_L$, is calculated assuming mass transfer limitation in Equation 7.7, and is assumed to represent the immediate capacity of the fermentation to transfer CO (Figure 7.7). The apparent $k_{L,H2}a/V_L$ for H_2 and apparent $k_{L,CO2}a/V_L$ for CO_2 can be calculated as in Equation 7.7 from the experimental data at any point in time, and represent the measured mass transfer of these species. However, the apparent $k_{L,CO}a/V_L$ can be used in Equation 7.8 to predict the actual capacity of the fermenter to transfer H_2 and CO_2. The apparent $k_{L,H2}a/V_L$ can be compared to the predicted capacity to assess the degree of mass transfer limitation for H_2. When the apparent value equals the predicted value as seen from 25 h to 55 h in Figure 7.7, the fermentation is nearly mass transfer limited for H_2. However, separation of the apparent $k_{L,H2}a/V_L$ from the predicted value as seen after 55 h indicates a kinetic limit, in this case inhibition of the hydrogenase by accumulated CO. Agitation and gas flow were reduced gradually to maintain $k_{L,H2}a/V_L$ near the expected value and thus support H_2 consumption in the syngas fermentations. Although the expected value of $k_{L,CO2}a/V_L$ is nearly the same as $k_{L,CO}a/V_L$ as the diffusivities are nearly identical (see Table 7.1), the apparent $k_{L,CO2}a/V_L$ in Figure 7.7 is always near 0, since the transfer of CO_2 is low, and typically directed from the saturated liquid back to the gas.

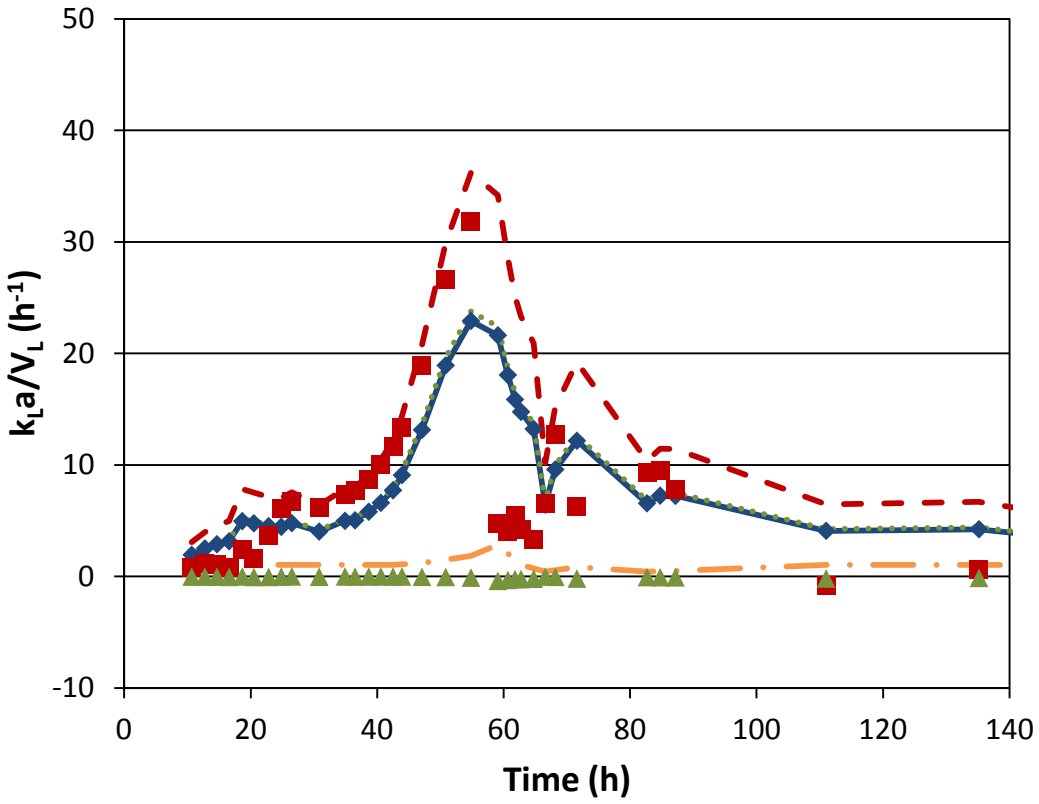

Figure 7.7 Volumetric mass transfer coefficients for CO, H_2 and CO_2 in CSTR fermentation of syngas SGIE7. Apparent k_La/V_L for CO (◆), H_2 (■), CO_2 (▲), and expected capacity for CO (—), H_2 (– –), CO_2 (····), and predicted $k_{L,CO}a/V_L$ from DI water correlation (– · –)

Figure 7.7 also shows the prediction of $k_{L,CO}a/V_L$ derived from previous experiments in the CSTR that used aeration of deionized water to determine $k_{L,O2}a/V_L$ (See Equation 6.33), and includes adjustment from O_2 for use with CO in Equation 7.13.

$$\frac{k_{L,CO}a}{V_L} = 2.94 \times 10^{-7} G^{0.6} N^{2.34} + (0.046G - 6.22 \times 10^{-5} G^2) \qquad 7.13$$

The values should be directly comparable, however the observed $k_{L,CO}a/V_L$ is twelvefold higher than the prediction from O_2 transfer into deionized water. The mass transfer into fermentation medium doubled the observed $k_{L,O2}a/V_L$ in the aeration experiment (see section 6.7.2), but the observed mass transfer during syngas fermentation indicates an enhancement by cell concentration and associated reaction, perhaps by the presence of

the cells in the film at the gas/liquid interface. The presence of cells that catalyze reaction in the liquid film would change not only the hydrodynamic properties of the liquid, but the length of the mass transfer path, which is the effective film thickness. The effect of reaction of gas solutes in mass transfer has been addressed by an enhancement factor (E) for chemical reaction (Charpentier, 1981) and for biological reactions (Garcia-Ochoa and Gomez, 2009). The reactions are described as slow, moderate, fast and very fast, and E can increase apparent $k_L a/V_L$ more than 1,000 fold (Charpentier, 1981), though the biological enhancement for aeration was reported to be up to 30% (Garcia-Ochoa and Gomez, 2009).

Consumption of CO and H_2 in the liquid film during syngas fermentation made the mass transfer in the CSTR a function of the cell concentration, agitation speed and gas feed rate. The dependence of $k_{L,CO}a/V_L$ on cell concentration is seen in Figure 7.8, in which $k_{L,CO}a/V_L$ is higher in later fermentation although agitation and gas flow rate are not changed. The prediction of $k_{L,CO}a/V_L$ from Equation 7.13 seen as the yellow line near the x-axis in Figure 7.8, depends only on the agitation and gas flow and follows the same path from 150 rpm to 400 rpm and back to 150 rpm. The observed value of $k_{L,CO}a/V_L$ depends further on the activity of the cell mass in the fermenter, falling from 15 h^{-1} to 0 at 150 rpm as culture activity slowed late in fermentation. $k_{L,CO}a/V_L$ up to 23 h^{-1} was observed at 300 rpm in the fermentation (Figures 7.7 and 7.8).

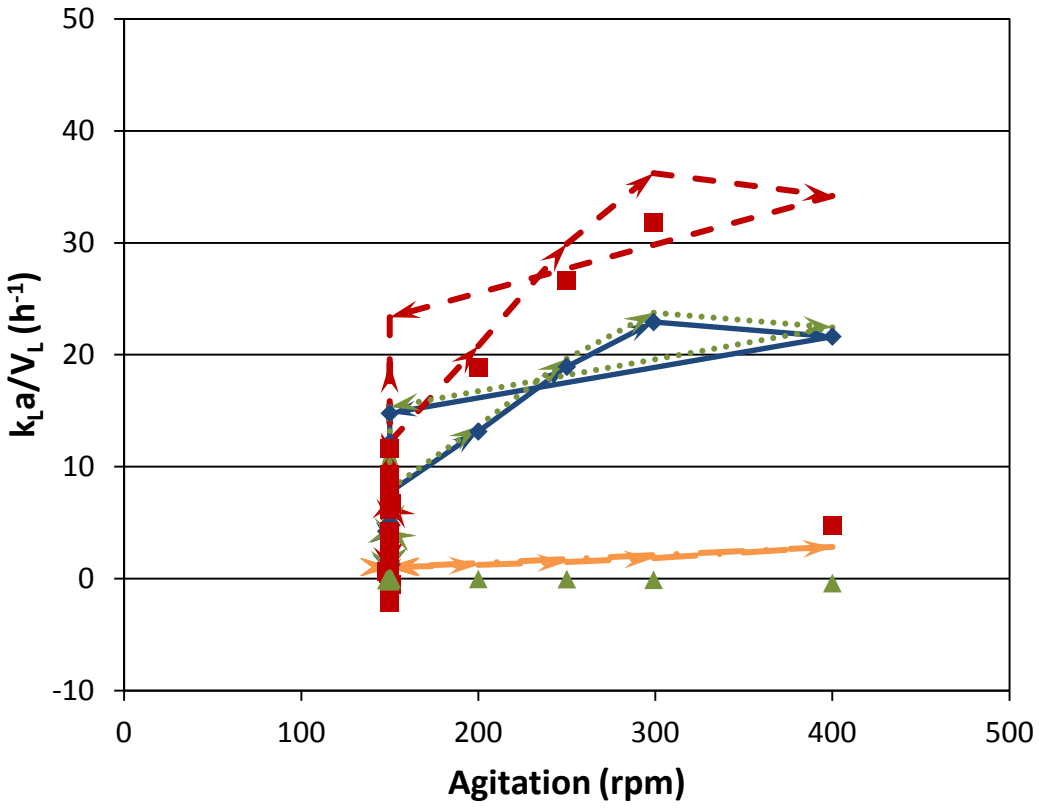

Figure 7.8 Volumetric mass transfer coefficients versus agitation for CO, H_2 and CO_2 in CSTR fermentation of syngas SGIE7. Apparent k_La/V_L for CO (◆), H_2 (■), CO_2 (▲), and expected capacity for CO (—), H_2 (– –), CO_2 (····), and predicted $k_{L,CO}a/V_L$ from DI water correlation (– ·)

The oxidation-reduction potential (ORP) and pH during the early course of fermentation is shown in Figure 7.9. The pH falls as the cell and acetic acid concentrations (Figure 7.3) increase between 15 h and 60 h. The ORP falls after inoculation to -170 mV (SHE) at 15 h and rises to -140 mV as both CO and H_2 conversion rise with increased agitation (to 300 rpm at 54 h, see Figure 7.4). The ORP falls sharply as low as -220 mV when agitation is increased to 400 rpm after 54 h and H_2 conversion is sharply diminished to 17% (Figure 7.4); the ORP rises to -165 mV after gas feed is reduced by 1/3 at 63 h (Figure 7.5), and H_2 conversion recovers slightly. ORP trends lower with H_2 conversion after 82 h. ORP appears to follow the concentration of

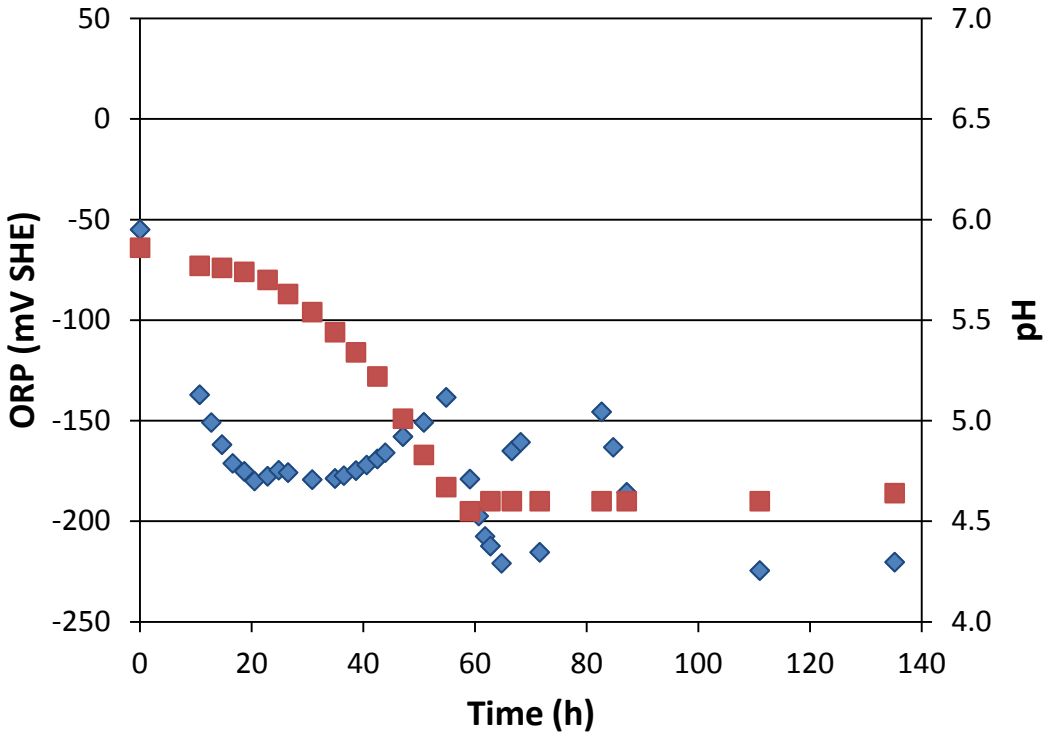

Figure 7.9 Oxidation-reduction potential and pH measured in CSTR fermentation of syngas SGIE7. ORP (◆), pH (■).

accumulated H_2 in the fermentation broth. But, the ORP rises slowly to over 0 mV after 150 h as the activity of *C. ragsdalei* nearly stops (data not shown).

SGIE7 produced 1.05 g/L of ethanol even though the maximum mass transfer is low at $k_{L,CO}a/V_L$ of 23 h^{-1} relative to the $k_{L,CO}a/V_L$ of 23 to 87 h^{-1} shown in Table 7.3 for SGIE1 through SGIE6 that produced 0.1 to 0.24 g/L ethanol. The difference is in the strain of *C. ragsdalei* used in the fermentations. The strain used in SGIE7 yields lower cell concentration (270 mg/L in Table 7.3) and displays a continued uptake of CO and H_2 after growth stops at 60 h. Ethanol production begins as growth slows and continues through the uptake in the stationary phase. This suggests the hypothesis that initial

growth is fast on yeast extract in the medium, followed by much slower growth on syngas that is accompanied by product formation, particularly ethanol, in depleted medium. Growth and cell activity stop when another required component, perhaps Fe^{2+} as suggested by the medium analysis of Table 4.5, is depleted from the fermentation broth. The strain of *C. ragsdalei* used in SGIE1 through SGIE6 yields slightly more cell concentration in the initial growth on yeast extract, and may deplete the Fe^{2+} in the initial growth period, shortening the stationary phase and ethanol production.

7.7.3 Comparison of $k_{L,CO}a/V_L$ from literature

The present study found $k_{L,CO}a/V_L$ for plug flow gas in the CSTR of 23.0 h^{-1} at 300 rpm and 0.008 vvm gas flow, 87 h^{-1} at 600 rpm and 0.015 vvm, and 74 h^{-1} at 700 rpm and 0.009 vvm. This was measured CO transfer into fermentation with *C. ragsdalei* with conversion of CO and H_2 of 70 to 95%. Klasson et al. (1992b) reported $k_{L,CO}a/V_L$ in a CSTR for appreciable CO consumption by a mixed culture of methanogens of 28 h^{-1} at 300 rpm and 101 h^{-1} at 400 rpm; however, $k_{L,CO}a/V_L$ was calculated assuming a "well mixed gas phase" and using the effluent CO concentration. These reported values may be an order of magnitude higher than if calculated using the plug flow assumption for gas in the CSTR.

Munasinghe and Khanal (2010) reported $k_{L,CO}a/V_L$ for a sparger in a 3.0 L water column of 47 h^{-1} with gas of 5 slpm (1.67 vvm), and that $k_{L,CO}a/V_L$ from the sparger increased to 50 h^{-1} with 150 rpm agitation and 54 h^{-1} at 300 rpm. The study used pure CO and transferred into water, and the use of pure CO gas phase makes the distinction between mixed flow and plug flow moot. But, the very high gas loading (1.67 vs 0.008

vvm used in the present study) makes comparison difficult. For CO transfer into water in the 3.0 L CSTR, $k_{L,CO}a/V_L$ of 27.4 h^{-1} is calculated using Equation 7.13 and neglecting the sparger contribution (term in braket) for 1.67 vvm at 300 rpm.

Ungerman and Heindel (2007) reported $k_{L,CO}a/V_L$ for transfer of CO into water in well defined CSTR geometry with dual Rushton impellers, using pure CO and measuring the accumulation of CO in the water. The reported $k_{L,CO}a/V_L$ for 400 rpm agitation was 101 h^{-1} at 0.71 vvm gas, and 151 h^{-1} at 2.14 vvm gas. Again the gas flow is very high, and Equation 7.13 predicts 32 h^{-1} and 62 h^{-1} in the CSTR used in the present study.

The results of the present study are in general agreement with the literature reports, but use actual fermentation conditions that deliver conversion and biological activity. The results from Equation 7.13, correlation for CO transfer into DI water, are similar to the literature reports, which do not reflect the enhancement from active syngas fermentation. Further, the present results are based in the plug flow gas regime that describes gas conversion in a CSTR.

7.8 Conclusions

Mass transfer into active syngas fermentation using *C. ragsdalei* in the CSTR was enhanced 12 fold versus the prediction derived from transfer of O_2 into water. Carefully controlled application of agitation and gas supply to the fermentation achieved appropriate mass transfer capacity in the CSTR to convert up to 95% of both CO and H_2. This result was achieved by limiting transfer of CO to maintain a concentration in the cell that does not inhibit the hydrogenase enzyme. The combined uptake of CO and H_2 yields

higher rates than fermentation based in CO alone, and increases the energy conservation and product yield from syngas.

References

Bakker, A., Smith, J.M., Myers, K.J. 1994. How to Disperse Gases in Liquids. Chemical Engineering, 101 (12), 98-104.

Bird, R.B., Stewart, W.E., Lightfoot, E.N. 2002. Transport Phenomena. 2nd ed, J. Wiley. New York, pp. xii, 895 p.

Charpentier, J.-C. 1981. Mass-Transfer Rates in Gas-Liquid Absorbers and Reactors. in: *Advances in Chemical Engineering*, (Eds.) G.R.C.J.W.H. Thomas B. Drew, V. Theodore, Vol. Volume 11, Academic Press, pp. 1-133.

Doyle, M.L. 1991. Preferred Conditions for Growth and Product Formation by *Clostridium Ljungdahlii* Petc in Complex Media. University of Arkansas,

Garcia-Ochoa, F., Gomez, E. 2009. Bioreactor Scale-up and Oxygen Transfer Rate in Microbial Processes: An Overview. Biotechnology Advances, 27 (2), 153-176.

Hougen, O.A., Watson, K.M., Ragatz, R.A. 1954. *Chemical Process Principles*. *2d ed*. Wiley, New York,, pp.v.

Hu, P., Jacobsen, L.T., Horton, J.G., Lewis, R.S. 2010. Sulfide Assessment in Bioreactors with Gas Replacement. Biochemical Engineering Journal, 49 (3), 429-434.

Hu, S.I., Pezacka, E., Wood, H.G. 1984. Acetate Synthesis from Carbon Monoxide by Clostridium Thermoaceticum. Purification of the Corrinoid Protein. Journal of Biological Chemistry, 259 (14), 8892-8897.

Hurst, K.M. 2005. Effects of Carbon Monoxide and Yeast Extract on Growth, Hydrogenase Activity, and Product Formation of *Clostridium Carboxidivorans* P7. Oklahoma State University,

Klasson, K.T., Ackerson, C.M.D., Clausen, E.C., Gaddy, J.L. 1992a. Biological Conversion of Synthesis Gas into Fuels. International Journal of Hydrogen Energy, 17 (4), 281-288.

Klasson, K.T., Ackerson, M.D., Clausen, E.C., Gaddy, J.L. 1992b. Bioconversion of Synthesis Gas into Liquid or Gaseous Fuels. Enzyme and Microbial Technology, 14 (8), 602-608.

Klasson, K.T., Ackerson, M.D., Clausen, E.C., Gaddy, J.L. 1992c. Mass-Transport in Bioreactors for Coal Synthesis Gas Fermentation. Abstracts of Papers of the American Chemical Society, 204, 125-FUEL.

Kundiyana, D.K., Huhnke, R.L., Wilkins, M.R. 2010. Syngas Fermentation in a 100-L Pilot Scale Fermentor: Design and Process Considerations. Journal of Bioscience and Bioengineering, 109 (5), 492-498.

Lazarus, O., Woolerton, T.W., Parkin, A., Lukey, M.J., Reisner, E., Seravalli, J., Pierce, E., Ragsdale, S.W., Sargent, F., Armstrong, F.A. 2009. Water-Gas Shift Reaction Catalyzed by Redox Enzymes on Conducting Graphite Platelets. Journal of the American Chemical Society, 131 (40), 14154-+.

McCabe, W.L., Smith, J.C. 1976. *Unit Operations of Chemical Engineering*. *3rd ed*. McGraw-Hill, New York, NY,

Menon, S., Ragsdale, S.W. 1996. Unleashing Hydrogenase Activity in Carbon Monoxide Dehydrogenase/Acetyl-Coa Synthase and Pyruvate:Ferredoxin Oxidoreductase. Biochemistry, 35 (49), 15814-15821.

Munasinghe, P.C., Khanal, S.K. 2010. Syngas Fermentation to Biofuel: Evaluation of Carbon Monoxide Mass Transfer Coefficient (K(L)a) in Different Reactor Configurations. Biotechnology Progress, 26 (6), 1616-1621.

Nicholls, D.G., Ferguson, S.J. 2002. *Bioenergetics*. *3rd ed*. Academic Press, pp.297.

Phillips, J.R., Clausen, E.C., Gaddy, J.L. 1994. Synthesis Gas as Substrate for the Biological Production of Fuels and Chemicals. Applied Biochemistry and Biotechnology, 45-6, 145-157.

Phillips, J.R., Klasson, K.T., Clausen, E.C., Gaddy, J.L. 1993. Biological Production of Ethanol from Coal Synthesis Gas - Medium Development Studies. Applied Biochemistry and Biotechnology, 39, 559-571.

Ragsdale, S.W. 2004. Life with Carbon Monoxide. Critical Reviews in Biochemistry and Molecular Biology, 39 (3), 165-195.

Ragsdale, S.W., Ljungdahl, L.G. 1984. Hydrogenase from Acetobacterium-Woodii. Archives of Microbiology, 139 (4), 361-365.

Saxena, J. 2008. Development of an Optimized and Cost-Effective Medium for Ethanol Production by *Clostridium* Strain P11. Dissertation. University of Oklahoma, 131.

Terrill, J.B., Wilkins, M.R., DeLorme, M.J.M., Atiyeh, H.K., Lewis, R.S. 2012. Effect of Energetic Gas Composition on Hydrogenase Activity and Ethanol Production in Syngas Fermentation by Clostridium Ragsdalei. Biological Engineering Transactions, 5 (2), 87-98.

Ungerman, A.J., Heindel, T.J. 2007. Carbon Monoxide Mass Transfer for Syngas Fermentation in a Stirred Tank Reactor with Dual Impeller Configurations. Biotechnology Progress, 23 (3), 613-620.

Wilkins, M.R., Atiyeh, H.K. 2011. Microbial Production of Ethanol from Carbon Monoxide. Current Opinion in Biotechnology, 22 (3), 326-330.

CHAPTER VIII

INTEGRATED COMPUTER MODEL OF SYNTHESIS GAS FERMENTATION

8.1 Abstract

Clostridium ragsdalei uses mechanisms typical of *Clostridia* and many other bacteria, but the syngas fermentation uses the well defined stoichiometry of the Wood-Ljungdahl pathway and relies on mass transfer of CO and H_2 into the cell for production of acetic acid and ethanol. The fermentation mass balance, observed mass transfer and kinetics, and derived thermodynamic parameters are combined in a mathematical model that defines the fermentation. The *in silico* model is used in analysis and planning, and provides an effective new tool for process design and control of fermentation. Mass transfer coefficients were calculated assuming mass transfer limitation for CO to find $k_{L,CO}a/V_L$. The mass transfer coefficient for H_2, $k_{L,H2}a/V_L$, calculated from $k_{L,CO}a/V_L$ using surface renewal theory matched experimental values. Partial pressure of CO inside the cell (p_{CO}^*) was found to be about 10^{-3} kPa about 10,000 times lower than the partial pressure of CO in the gas phase. For H_2, p_{H2}^* was as low as 10^{-2} kPa, but CO_2 was near saturation from CO_2 in the gas phase.

8.2 Keywords

Syngas fermentation, mass transfer, thermodynamics, kinetics, equilibrium, dissolved gas concentration, intracellular pH, intracellular potential, modeling

8.3 Nomenclature

$C_{i,L}$ – molar concentration of *i* in liquid (mol/L)

CSTR – continuously stirred tank reactor

D – impeller diameter in CSTR (mm)

$D_{i,W}$ – diffusivity of gas *i* in water

dn_i/dt – molar rate of transfer of gas species *i* (CO, H_2, CO_2)

E – electrochemical potential of redox couple at actual conditions (mV)

E^0 – standard midpoint potential of redox couple, pH = 0 (mV)

$E^{0'}$ – standard midpoint potential of redox couple, pH = 7 (mV)

E_{Cell} – intracellular electrochemical potential or ORP (mV)

F – Faraday constant (96.485 J/mV mol e^-)

G – gas flow (sccm)

H_i – Henry's Law constant for gas *i* (kPa L/mol)

* – quantity derived from the Henry's law equilibrium

$k_{L,i}a/V_L$ – volumetric mass transfer coefficient for gas *i* (*i* can represent O_2, CO, H_2 or CO_2)

k_L – liquid film mass transfer coefficient

a – area of the gas liquid interface

V_L – liquid volume into which gas is transferred

L – liquid flow (L/h)

N – agitation speed (rpm)

n_e – number of electrons transfer in half cell reaction

ORP – oxidation reduction potential versus the standard hydrogen electrode (mV SHE)

pH_{ic} – intracellular pH

p_i – partial pressure of gas i (kPa),

p_i^* – partial pressure of dissolved gas by Henry's Law

P_T – pressure, total (kPa)

q_i – specific uptake rate of gas i (mol/g_x h)

t – time (s, min, h)

t_d – doubling time for cell growth (h)

R – gas constant (8.314 J/mol K)

T – temperature (K)

vvm – volume of gas per volume of liquid per minute

X – cell concentration (g_x/L)

y_i – molar fraction of gas i in gas phase

ΔG_r – Gibbs free energy change of reaction (kJ/mol)

ΔG^0 – Gibbs free energy change at standard conditions including pH = 0 (kJ/mol)

$\Delta G^{0'}$ – Gibbs free energy change at standard conditions including pH = 7 (kJ/mol)

μ – specific growth rate (g_x/g_x h or h^{-1})

α – exponent of gas flow in correlation

β – exponent of power input in correlation

Δm_H – number of protons released in oxidation reduction reaction

Δp – protonmotive force (mV)

ΔpH – pH differential across the membrane

$\Delta\varphi$ – potential difference (mV) across the membrane

Π – product of products and reactants in reaction mass action ratio

8.4 Introduction

Autotrophic acetogenic bacteria, typically of the genus *Clostridium*, can convert CO and H_2 to acetic acid, ethanol and other useful industrial chemicals. CO and H_2 are the major components in gas produced by combustion of biomass and waste materials with less than stoichiometric O_2, often called synthesis gas, syngas or producer gas. Other sources of CO and H_2 are waste gases from steel production and similar processes. Acetogens derive energy and fix carbon from CO and CO_2 via a series of elementary reactions called the Wood-Ljungdahl or Acetyl-CoA pathway (Drake et al., 2008). The Wood-Ljungdahl pathway is depicted in Figure 8.1, and includes an extension showing the reduction of acetic acid to ethanol (Phillips et al., 1994).

Syngas fermentation to ethanol produces a liquid that has few hazards and is easily stored, transported and used in engines and chemical processes. Achieving high conservation of energy in the CO and H_2 requires high conversion of both CO and H_2 to recovered product. High specificity of product formed, in the present case ethanol, maximizes yield, and high concentration of the desired product enhances recovery. High rates of gas consumption and proportional product formation increase productivity of the fermenter. The optimized combination of these fermentation goals will minimize operating expense and maximize profitability of the process.

The fermentation process is the *in vivo* solution of the mass transfer, stoichiometric, kinetic and thermodynamic parameters extant in the fermenter. CO and H_2 are sparingly

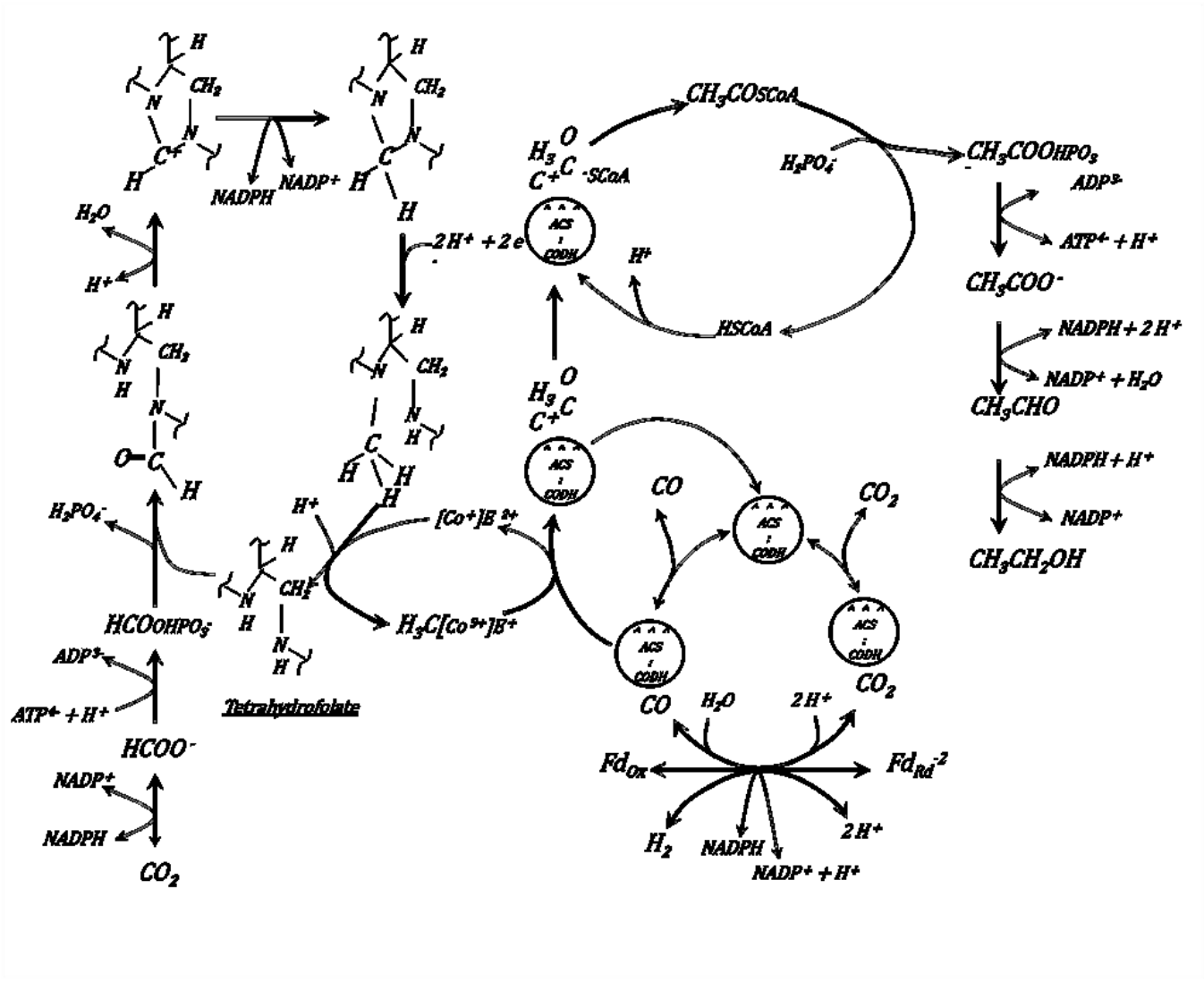

Figure 8.1 The Wood-Ljungdahl or Acetyl-CoA pathway, after Phillips et al. (1994).

soluble in the aqueous fermentation broth and must be continuously transferred, defined by the mass transfer parameters, into the broth to supply the cells for reaction. The cells have a limited capability to process the gas; this capability is defined by the kinetic parameters exhibited by the culture in the chosen medium. Concentrations of the reactant gas species, CO, H_2 and CO_2 are thermodynamic quantities that determine the electrochemical potential (ORP) inside the cells. The ORP can affect proteins and metals in enzymes (Ragsdale, 2004), reduce the activity of the cells and lower the rate of conversion of CO and H_2 to ethanol product. The gas concentrations inside the cell are set by the enzymatic reactions of the production pathway.

The pathway is a series of enzymatic reactions that sums to the overall stoichiometry of production of acetic acid and ethanol from CO and H_2. The stoichiometry defines the relationship of product formation to substrate uptake in syngas fermentation. Individual rates of uptake for CO and H_2 define the mass transfer capacity required to supply the related reactions. The transfer rate of each species will match its reaction rate set by the platform of enzymes specified by the culture genetics and derived from the nutrient medium. CO and H_2 transferred into the cell in excess of the kinetic capacity of the enzyme platform will accumulate up to saturation of the aqueous environment inside the cell. This accumulation of CO and H_2 at the enzymes in the cell determines the rate of the series of reactions, the accumulation of intermediate metabolites, the thermodynamic position of each distinct reaction and the slate of products formed.

Design and control decisions for operation of syngas fermentation are determined considering a conceptual model of the fermentation process. Mass transfer,

stoichiometric, kinetic and thermodynamic correlations for the fermentation processes can be represented mathematically in a set of equations. These equations represent the conceptual model of fermentation derived from the known biochemical pathway and the structure of the cells, and can be used to build a computational model of the fermentation. This computer model is expected to deliver an accurate assessment of fermentation conditions, suitable for design of equipment, and for incorporation in feedback control of gas supply and mass transfer (such as agitation speed in a stirred reactor) to maintain fermenter productivity at high conversions with high selectivity for the desired product.

8.4.1 Pathway

Autotrophic acetogens produce acetic acid from CO, H_2 and CO_2 via the Wood-Ljungdahl pathway (Phillips et al., 1994; Ragsdale, 2008) shown in Figure 8.1. CO and CO_2 provide carbon, while CO and H_2 provide energy in the form of electrons (e^-) and protons (H^+). A two carbon compound, acetyl-CoA, is formed from CO_2 reduced to methyl, combined with CO and Coenzyme A. Acetyl-CoA is the source for all cell materials formed in the chemoautotrophic growth of the acetogens. Most of the acetyl-CoA is converted to acetic acid, recovering an ATP used to induce CO_2 into the reaction sequence. The primary purpose of the Wood-Ljungdahl pathway in acetogens is energy conservation for growth (Drake et al., 2008). Excess electrons can be used to reduce acetic acid through acetaldehyde to ethanol as a store of energy (Strobl et al., 1992; White et al., 1989). The reduction of acetic acid to ethanol is reversible, so that the acetogens can obtain energy for growth or maintenance from oxidation of ethanol to acetic acid (Adams, 2010). The reduction of acetic acid to ethanol represents a redox couple that can be exploited for energy storage and acts as a redox buffer.

8.4.2 Thermodynamics

The Wood-Ljungdahl pathway is an ordered set of chemical reactions occurring in sequence to produce acetyl-CoA, acetic acid and ethanol from CO_2, CO and H_2. Each reaction is mediated by an enzyme that catalyzes the reaction. The reaction proceeds in the direction of favored thermodynamics, for which $\Delta G < 0$. Thermodynamics of biological reactions are addressed in biochemistry texts (Lehninger, 1982; Nicholls and Ferguson, 2002); these treatments discuss the criteria for a reaction to proceed, $\Delta G < 0$, and for thermodynamic equilibrium, $\Delta G = 0$, and the dependence of ΔG on concentration of reactants and products through the mass action ratio (Nicholls and Ferguson, 2002). The effect of pH on ΔG is not discussed extensively, although Lehninger (1982) notes, "Biochemical reactions take place near pH 7.0 and often involve H^+," to introduce the standard free energy at pH 7.0, $\Delta G^{0'}$. The dependence of ΔG on pH and the application in redox reactions in the cell are discussed in Cramer and Knaff (1991). Cramer and Knaff (1991) emphasize the division of the intracellular space where the enzymes reside from the bulk liquid in fermentation. Measurements like pH and oxidation reduction potential (ORP) are taken in the bulk liquid rather than inside the cell. Thermodynamic data for reactions and compounds of interest in biological systems are available in the appendix of Thauer et al. (1977) and this data can be used to define the thermodynamic position of the reactions of the Wood-Ljungdahl pathway.

Boghigian et al. (2010) used a computer algorithm to identify feasible pathways directed to chosen fermentation products as a guide for genetic design of *Escherichia coli*. The algorithm uses a group contribution method to compute the Gibbs free energy of formation (ΔG_f^o) for intermediate metabolites, assess thermodynamic feasibility of the

pathway from the overall free energy change and identify strongly unfavorable individual reactions. The method can direct design to pathways weighted for growth or product formation.

A review of modeling techniques typically directed to identification of feasible pathways for genetic design is given by Medema et al. (2012). Many of these models use thermodynamic analysis and assembly of individual reactions into a pathway to suggest plausible sequences from substrate to product.

Group contribution methods are also used to assess thermodynamics from free energy of formation in Henry et al.(2007) and the thermodynamic potential from reactions at pH 7.0 are used to define the range of concentrations of intermediate metabolites that support mass flux through identified pathways. Generally these models are designed to loosely define potentially feasible paths from substrate converted to products and identify particular reactions that can be down regulated by genetic modification. Thermodynamics have been examined for syngas fermentation (Hu et al., 2011) using transformed thermodynamics and it was concluded that CO was always preferred over H_2 as a substrate for fermentation. CO inhibition of hydrogenase or thermodynamic disfavor was suggested as reason for low and delayed uptake of H_2 in syngas fermentation. These thermodynamic calculations assumed bulk liquid concentration saturated from the gas phase partial pressures of H_2, CO and CO_2. Acetogenic fermentation of gas containing both CO and H_2 can exhibit periods of exclusive CO uptake, but typically, CO and H_2 are consumed together (Phillips et al., 1993).

8.4.3 Mass Transfer

CO and H_2 are absorbed into liquid fermentation medium and into the cells by gas to liquid mass transfer. Mass transfer has been studied for syngas in various fermenters (Klasson et al., 1992; Munasinghe and Khanal, 2010; Vega et al., 1989) with the purpose of providing more mass transfer to achieve higher productivity. However, a transition from a kinetic limit, to a mass transfer limit, and return to kinetic limitation was shown for fermentation in batch bottles for which mass transfer capacity is expected to be constant (Phillips et al., 2011), suggesting that controlled mass transfer is required for successful syngas fermentation.

Vega et al. (1989) modeled mass transfer of CO into fermentation using *Peptostreptococcus productus* to produce acetate and estimated CO conversion and uptake as a function of feed gas flow and $k_{L,CO}a/V_L$. In the model mixed flow of the gas phase using the effluent composition to define $k_{L,CO}a/V_L$ was assumed. This makes $k_{L,CO}a/V_L$ independent of pressure and gas flow, so $k_{L,CO}a/V_L$ changes only with agitation. This model was linked to the kinetic capability of a generic culture to consume a single substrate through a Monod model for CO as substrate (Klasson et al., 1992). It was asserted that the mass transfer will match the kinetic rate in either mass transfer limitation or under kinetic limitation. Klasson et al. (1992a) stated that optimum design and operation will balance the rate of substrate supply and the capacity of the culture to convert the delivered gas.

Mass transfer in the CSTR is addressed by Bakker et al.(1994) and prediction of $k_{L,O2}a/V_L$ into water is based on the geometry of the fermenter, the power input and the gas flow through the liquid. The general method is useful in that mass transfer can be

scaled approximately for similar geometry in the CSTR, and the form matches correlations reviewed in Garcia-Ochoa and Gomez (2009), as in Equation 8.1.

$$\left(\frac{k_{L,CO}a}{V_L}\right)_2 = \left(\frac{k_{L,CO}a}{V_L}\right)_1 \left(\frac{\mathrm{N}_2}{\mathrm{N}_1}\right)^{\alpha} \left(\frac{\mathrm{G}_2}{\mathrm{G}_1}\right)^{\beta} \qquad 8.1$$

Where N is the agitation speed (rpm), and G is the gas flow (ml/min, actual), and states 1 and 2 represent different conditions of agitation and gas flow. The exponents are reported (Garcia-Ochoa and Gomez, 2009) to range from 0.5 to 3 for α with typical value of 1.8, and from 0.3 to 0.8 for β with a typical value of 0.6.

The correlation of Bakker et al.(1994) implies that the appropriate model for gas flow in the CSTR is plug flow, wherein fresh gas enters the liquid volume and the concentration of substrate gas is depleted before the bubble of spent gas leaves the liquid. The mass transfer is defined by the agitation and the volumetric gas flow rate through the liquid. The mass transfer model must appropriately represent the contact of gas and liquid in the fermenter under consideration.

8.4.4 Fermentation Control.

The production of reduced products in the acetone-butanol-ethanol fermentation is effected by nutrient limitation of *Clostridium acetobutylicum* or *C. bejierinckii*, particularly limitation of nitrogen or phosphate (Rogers, 2006). This is described as an acidogenic growth phase that produces acetic and butyric acids, followed by a solventogenic stationary phase in which solvents are produced and the acids are consumed.

The expectation of acidogenesis followed by stationary phase solventogenesis has been popular in describing production of ethanol from synthesis gas by *C. ljungdahlii* and

other related species (Kundiyana et al., 2011; Liu et al., 2012; Maddipati et al., 2011; Ramachandriya et al., 2010; Tracy et al., 2012). The shift to ethanol production was induced by omission of yeast extract and accompanied slower growth in the defined medium to achieve concentrations of more than 20 g/L in continuous culture (Phillips et al., 1993). The manipulation of medium composition to establish metabolic control is the basis of development to commercial production of ethanol via synthesis gas fermentation (Gaddy, 2007). This control is grounded in the reactions of the Wood-Ljungdahl pathway (Phillips et al., 1994) and distributes electrons derived from CO and H_2 toward formation of the reduced product ethanol. The basis of this distribution and control of fermentation is, as yet, poorly defined.

Integration of the conceptual model of syngas fermentation, thermodynamic and mass transfer analyses, and metabolic control derived from the biological pathway in an overall description of the fermentation process will enhance the analysis and process performance, allow more effective planning of experiments and provide a vehicle for feedback of the knowledge derived to provide a more perfect model of the syngas fermentation. The enhanced understanding will reveal additional avenues of research beyond the fermentation of syngas, and can be transformative in the approach to fermentation.

The objective of this chapter is to develop the mathematical equations for mass balance, mass transfer and thermodynamics that form a foundation of a computer model of syngas fermentation. The calculations will be applied in syngas fermentations and comparsion of model predictions with experimental results. The calculations will be extended to identify future opportunities for research and model development.

8.5 Mathematical Model Development

A mathematical model can be used to analyze fermentation data or to predict the performance of planned fermentation. Analysis uses input data from measurements of performance and derived parameter values to develop correlations of culture performance. Predictions are made with assumed input data to specify fermentation performance. The typical input data to the model includes the rate and composition of feed gas, and required or observed conversion of CO and H_2, production of CO_2, ethanol and acetic acid. The model is, as yet, preliminary with no prediction of growth tied to substrate uptake, as the production pathway has no net production of ATP.

The conceptual fermentation model is based on conversion of CO and H_2 to acetic acid and ethanol that is effected at a molecular scale inside the cells. However, measurements are taken and control functions are exercised at the macroscopic scale of the fermenter. Macroscopic, intermediate and microscopic conceptual views of the fermentation are depicted in Figure 8.2, showing the parameters that are effective within each view. Equipment and methods, such as agitation speed in a CSTR, packing design in column reactors, and control of pH, flows and pressures must be used at the macroscopic level to direct the reactions that occur in the microscopic scale. Our conceptual and mathematical models of the fermentation must relate the control actions to the biochemical reactions inside the cell where the results are determined.

8.5.1 Macroscopic scale

Measurements and control parameters are generally available at the macroscopic level of the fermentation. The flows and compositions of the inlet and effluent streams are known and determined to achieve targeted rates of product formation and conversion

of CO and H_2. The medium provides the components for assembly of the platform of enzymes. Minerals and metals that set the active sites of enzymes and cofactors, and essential vitamins that are not synthesized by the culture are provided in this nutrient stream. The design of the nutrient medium affords control of the operating concentration of cells, denoted as X in Figure 8.2. Cell retention can increase the concentration of cells in the fermenter, but to be productive the cells must retain activity in conversion of CO and H_2 to ethanol. Carbon and hydrogen in the carbohydrate and protein structure of the cells that contain the enzymes are taken from CO and H_2 in the feed gas. The CO and H_2 contain the energy that is to be captured in the ethanol product. The effluent gas is the residue of the feed gas. The difference in CO and H_2 content of the inlet and effluent gas streams reflects the conservation of energy to products. The liquid product stream contains the output of the fermentation, the preferred product is ethanol that may be separated and recovered.

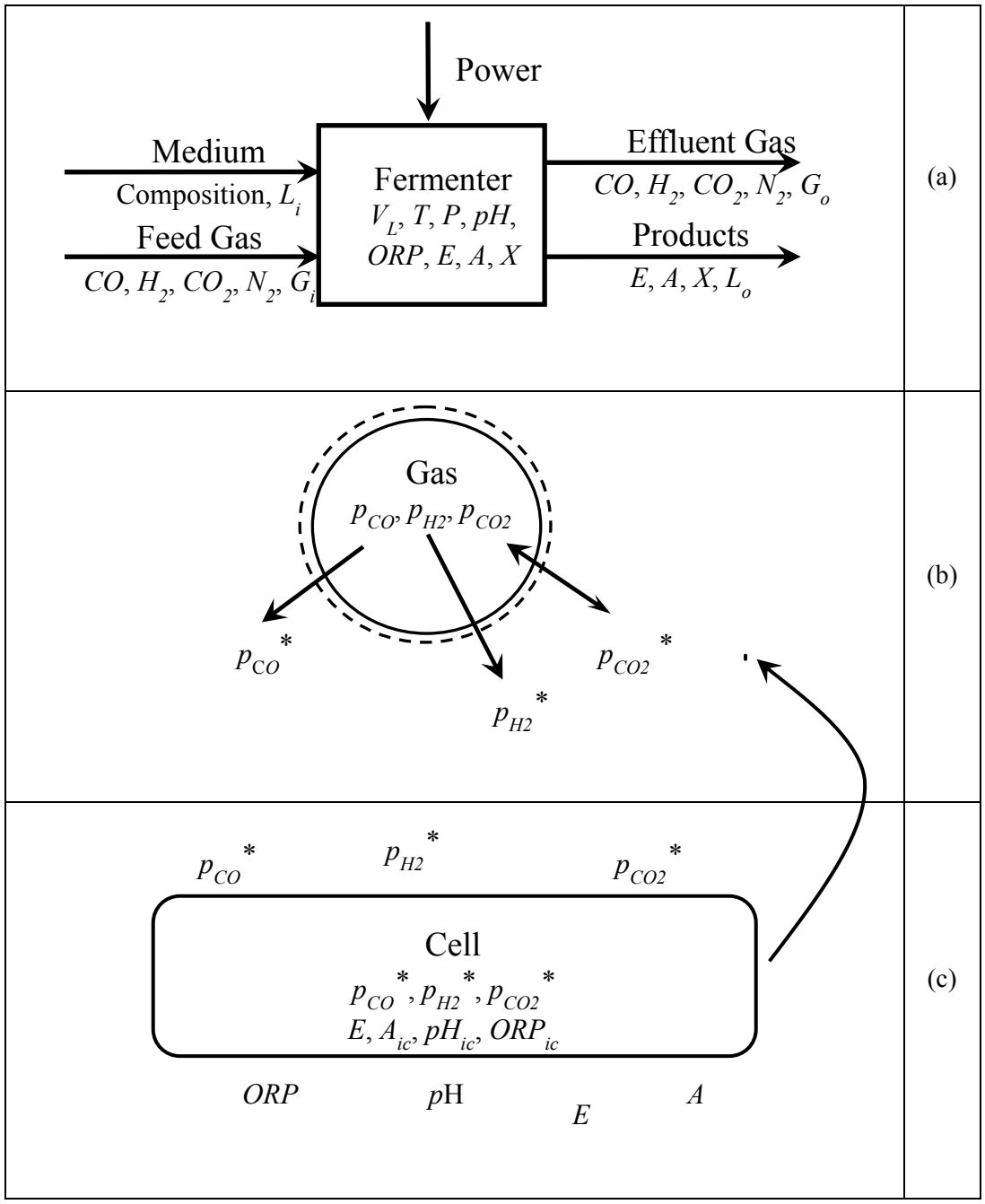

Figure 8.2 Scale of fermentation. (a) Macroscopic level, measureable parameters and controlled inputs. (b) Intermediate level, mass transfer. (c) Microscopic level, in the bulk liquid and inside the cell, separated by the cell membrane. Liquid flow (L) in (L_i) and out (L_o), gas flow (G), gas composition (mole fraction CO, H_2, CO_2, N_2), fermenter liquid volume (V_L), temperature (T), pressure (P), pH, oxidation reduction potential (ORP), liquid concentrations (g/L ethanol (E), acetic acid (A), cells (X)), gas phase partial pressure p_{CO}, p_{H2}, p_{CO2} (kPa), bulk liquid phase gas concentration as partial pressure p_{CO}^*, p_{H2}^*, p_{CO2}^* (kPa), intracellular (pH_{ic})

Wastes that must be processed include a purge of cells, acetate buffer and unrecovered ethanol that are discarded in wastewater. The fermenter system contains the liquid volume, retains the inventory of active cells, receives CO and H_2 absorbed from the gas, and accumulates liquid products, ethanol and acetic acid. Physical parameters that define the fermentation like pH, temperature, pressure and ORP are measured and controlled in the macroscopic environment (Figure 8.2a).

Mass transfer moves CO and H_2 into the liquid volume to supply reactions, and is effected by macroscopic design and control. Mass transfer is promoted by applied power in the form of agitation for gas dispersion in the CSTR or pumping of the liquid in packed column contactors, and gas compression for sparging or membrane transfer. Assessment of performance from rates of change of gas and product compositions, and control of parameters affecting the fermenter performance are conducted at the macroscopic scale of the fermentation.

8.5.2 Intermediate scale

Mass transfer of CO, H_2 and CO_2 in the intermediate view of fermentation provides a bridge between the macroscopic environment of observation and control, and the molecular environment of reaction in Figure 8.2b. CO and H_2 are absorbed and CO_2 is removed through a stagnant liquid film between the gas and the well mixed bulk liquid. Transfer of CO or H_2 is driven by concentration difference across this film at a rate that matches the consumption in the cells. CO and H_2 accumulate in the bulk liquid to a concentration that supports the rate of reaction inside the cells, and the rate of transfer slows to match the reaction rate. Accumulated CO and H_2 can slow reaction through

inhibition of crucial enzymes. The balanced rates of mass transfer and reaction set the dissolved concentrations of the gases and determine the products that are formed.

8.5.3 Microscopic scale

Conversion of CO and H_2 to acetic acid, ethanol and cell mass is conducted on a platform of enzymes contained in the cells (Figure 8.2c). The cell membrane separates the cytoplasm from the bulk liquid fermentation broth, and the enzymes are either suspended in the cytoplasm or associated with or embedded in the membrane. Intracellular conditions of pH, ORP, and chemical composition are related to the bulk liquid by diffusion and membrane transport, and can differ in significant ways that are essential to cell function (Cramer and Knaff, 1990; Nicholls and Ferguson, 2002). The concentrations of dissolved CO, H_2 and CO_2 inside the cells are nearly the same (within 5% difference) as the bulk liquid, since transfer of gas into the cells occurs along a short mass transfer path through a very thin membrane (6-9 nm) with a large total surface area. The observed rates of consumption of gas and formation of products in the defined stoichiometry of the production pathway reveal the mass flux of carbon, protons and electrons through the pathway reactions. The dissolved gas concentrations set the thermodynamics of reactions, determine the kinetic rates, and also set the concentrations of intermediate metabolites. The fermentation happens in this intracellular environment, and the mass flux through the biological pathways can be quantified and controlled to achieve targeted results on the macroscopic scale.

8.5.4 Dissolved gas concentrations.

Since the fermentation reactions occur inside the cell, and rates and thermodynamics are dependent on the concentrations of reactants, starting with CO and

H_2, the intracellular conditions must be defined. The first step in the model development is to define the capacity for mass transfer of CO, H_2 and CO_2, and estimate the concentrations of these gas species in bulk liquid and in the cell.

CO and H_2 are sparingly soluble in water and their solubility depends on the partial pressure of the individual species according to Henry's Law. For CO, as an example

$$C_{CO} = y_{CO}\, P_T / H_{CO} \qquad 8.2$$

Where C_{CO} is the liquid phase concentration of CO, y_{CO} is the gas phase mol fraction of CO, P_T is the total pressure and H_{CO} is the Henry's Law constant for CO. The Henry's Law constants for CO, H_2 and CO_2 at 37°C are given in Table 8.1. Saturated concentration of either CO or H_2 in water under 100 kPa of pure gas will be less than 10^{-3} mol/L. CO and H_2 must be continuously replenished in the liquid medium to support active fermentation. The lowest concentrations of CO and H_2 are inside the cell where the enzymes that catalyze oxidation reside. CO_2, in contrast, is produced in fermentation that consumes CO. CO_2 is transferred from inside the cell through the liquid phase to the gas phase. The concentration of CO_2 will be highest inside the cell.

Table 8.1 Henry's Law constants and diffusivities for gases in water at 37°C [a]

	H (kPa L/mol)	$D_{i,W}$ (m^2/s)
CO	121561	2.50×10^{-9}
H_2	140262	6.24×10^{-9}
CO_2	4240	2.69×10^{-9}
O_2	101300	3.25×10^{-9}

[a] After (Hougen et al., 1954)

The rate of mass transfer of substrate gas from the bulk gas through the gas-liquid interface and the bulk liquid into the cell can be described by film theory (Bird et al., 2002). Diffusion of gas components within the bulk gas is very fast relative to the consumption rate and the concentration of each species is uniform throughout the gas phase. The concentration of each species in the liquid at the interface is at equilibrium with the bulk gas partial pressure as predicted by Henry's Law (Equation 8.2). The liquid at the interface is part of a stagnant film of fluid through which dissolved gas must transfer by diffusion to the bulk liquid. Diffusion is driven by concentration difference and is dependent on the gas diffusivity through water and the thickness of the stagnant film. Outside the liquid film the liquid is assumed to be mobile and turbulent (Charpentier, 1981), and gas transfer within the bulk liquid is by bulk flow at rates far exceeding diffusion, the bulk liquid is assumed to be well mixed and homogeneous. Gas is transferred into the cell by a diffusion process through the cell membrane, which is 6 to 9 nm thick. *C. ragsdalei* cells are typically 0.5 μm diameter by 3 μm, and even at low cell density (0.02 g cells/L) there are more than 10^{10} cells/L of bulk liquid. The surface area of these cells will exceed the area of the gas-liquid interface by 2 to 3 orders of

magnitude in a typical fermentation. Gas to liquid mass transfer rate is controlled by diffusion through the film of stagnant liquid at the gas-liquid interface. The rate of molar gas transfer is proportional to the difference in concentration from the surface of the liquid to the bulk liquid.

As discussed in Chapter 7 and repeated here for clarity, the partial pressure of each component in the gas phase is the product of its mole fraction and the total pressure, for CO

$$p_{CO} = y_{CO} P_T \tag{8.3}$$

And the liquid film mass transfer is represented by Equation 8.4.

$$-\frac{1}{V_L}\frac{dn_{CO}}{dt} = \frac{k_{L,\mathrm{CO}}a}{V_L}\left(c^*_{CO} - c_{CO,L}\right) = \frac{\left(\frac{k_{L,\mathrm{CO}}a}{V_L}\right)}{H_{CO}}\left(p_{CO} - p^*_{CO}\right) \tag{8.4}$$

Where c_{CO}^* is concentration of CO at the interface surface in equilibrium by Henry's Law and $c_{CO,L}$ is concentration in the bulk liquid, p_{CO}^* is the CO partial pressure (kPa) in equilibrium by Henry's Law with the concentration of CO dissolved in the bulk liquid and p_{CO} is partial pressure in the gas bubble, H_{CO} is the Henry's Law constant for CO (kPa L/mol) and V_L is the volume (L) of liquid into which gas is transferred. The molar rate of transfer is $-dn_{CO}/dt$ (mol CO/h) where the negative sign denotes consumption from n_{CO} moles of CO in the bulk gas. The constant of proportionality is ($k_{L,CO}a/V_L$) and is the overall liquid film mass transfer coefficient for CO with units of reciprocal time (h^{-1}). a is the area (m^2) of the gas/liquid interface. The term $k_{L,CO}$ is the liquid film mass transfer coefficient for CO (L/m^2 h). $k_{L,CO}$ includes effects of turbulence in the liquid, hydrodynamic conditions like viscosity that affect film thickness, and the effect of diffusivity in the aqueous phase.

In a CSTR, fresh gas enters as a bubble and is suspended in the liquid while CO and H_2 are removed by mass transfer to the cells. The bubble depleted of CO and H_2 leaves the liquid into the headspace of the fermenter. The difference of CO concentration between the bubble surface and the bulk liquid falls as CO is consumed from the gas bubble. Overall in the CSTR, the effective concentration difference is best represented with a plug flow model and calculated as the logarithmic mean of the concentration difference between the inlet and the bulk liquid, and the concentration difference between the effluent and the bulk liquid.

$$-\frac{1}{V_L}\frac{dn_{CO}}{dt} = \frac{\left(\frac{k_{L,\mathrm{CO}}a}{V_L}\right)}{H_{CO}} \frac{\left(p_{CO,i} - p^*_{CO}\right) - \left(p_{CO,o} - p^*_{CO}\right)}{ln\frac{\left(p_{CO,i} - p^*_{CO}\right)}{\left(p_{CO,o} - p^*_{CO}\right)}} \qquad 8.5$$

Similar equations can be written to describe mass transfer for H_2 and CO_2.

When the diffusion of CO through the liquid film is slow the concentration of gas (particularly CO) in the bulk liquid is depleted by reaction. The concentration difference across the liquid film is at a maximum, and the overall process of gas consumption is mass transfer limited. The concentration of CO in the bulk liquid approaches 0 and

$$p^*_{CO} = 0 \qquad 8.6$$

CO inhibits the enzyme hydrogenase severely at dissolved pressures more than about 2×10^{-3} kPa, and 50% inhibition is reported at 8.5×10^{-4} kPa (Ragsdale and Ljungdahl, 1984). Since 2×10^{-3} kPa is negligible when subtracted from the 1 kPa of CO seen in residual syngas at high conversion, the uptake of H_2 is a sensitive indicator that CO is mass transfer limited. In the case where H_2 and CO are converted simultaneously, CO mass transfer can be calculated, with confidence, assuming zero concentration in the bulk

liquid. The mass transfer capability for CO can be quantified as $k_{L,CO}\,a/V_L$. The mass transfer in the CSTR is calculated according to Equation 8.5, which is solved for $k_{L,CO}\,a/V_L$ with $p_{CO}^{*} = 0$ to obtain Equation 8.7.

$$\left(\frac{k_{L,\mathrm{CO}}a}{V_L}\right) = -\frac{H_{CO}}{V_L}\frac{dn_{CO}}{dt}\,\frac{\ln\left(\frac{p_{CO,i}}{p_{CO,o}}\right)}{p_{CO,i} - p_{CO,o}} \qquad 8.7$$

Where $p_{CO,i}$ is the partial pressure of CO in the inlet gas and $p_{CO,o}$ is the CO partial pressure in the effluent gas. The interfacial area per liquid volume, a/V_L, is the same for the different gas species, and $k_{L,H2}$, $k_{L,CO}$ and $k_{L,CO2}$ differ only by the ratio of the square root of their diffusivities in water. Values of $k_{L,H2}\,a/V_L$ and $k_{L,CO2}a/V_L$ can be predicted from $k_{L,CO}\,a/V_L$ with confidence using Equation 8.8.

$$\frac{k_{L,CO}a}{V_L} = \sqrt{\frac{D_{CO,W}}{D_{H2,W}}}\left(\frac{k_{L,H2}a}{V_L}\right) = \sqrt{\frac{D_{CO,W}}{D_{CO2,W}}}\left(\frac{k_{L,CO2}a}{V_L}\right) \qquad 8.8$$

Where $D_{CO,W}$, $D_{H2,W}$, and $D_{CO2,W}$ are the diffusivities of CO, H_2 and CO_2 in water at fermentation temperature, typically 37°C as given in Table 8.1.

The partial pressures of dissolved H_2 and CO_2, p_{H2}^{*} and p_{CO2}^{*}, can be determined from the gas phase partial pressure, the uptake of H_2 and CO_2 and $k_{L,CO}\,a/V_L$ obtained for mass transfer limited CO. The value of $k_{L,CO}\,a/V_L$ is found from Equation 8.7, which assumes $p_{CO}^{*} = 0$. Using $D_{CO,W}$, $D_{H2,W}$ and $D_{CO2,W}$ to find $k_{L,H2}a/V_L$ and $k_{L,CO2}\,a/V_L$, Equation 8.5 can be written for H_2 and solved explicitly for p_{H2}^{*} as in Equation 8.9, and again writing Equation 8.5 for CO_2 the explicit solution for p_{CO2}^{*} is Equation 8.10. No assumption of mass transfer limitation is made for H_2 or CO_2 in Equations 8.9 and 8.10; however, CO is assumed limited to define the mass transfer coefficients from the experimental data.

$$p_{H2}^{*} = \frac{\left(p_{H2,i} - p_{H2,o} \exp\left[\frac{\left(\frac{k_{L,\mathrm{H2}} a}{V_L}\right)}{H_{H2}} \frac{(p_{H2,i} - p_{H2,o})}{\left(-\frac{1}{V_L}\frac{dn_{H2}}{dt}\right)} \right] \right)}{\left(1 - \exp\left[\frac{\left(\frac{k_{L,\mathrm{H2}} a}{V_L}\right)}{H_{H2}} \frac{(p_{H2,i} - p_{H2,o})}{\left(-\frac{1}{V_L}\frac{dn_{H2}}{dt}\right)} \right] \right)} \quad 8.9$$

$$p_{CO2}^{*} = \frac{\left(p_{CO2,i} - p_{CO2,o} \exp\left[\frac{\left(\frac{k_{L,\mathrm{CO2}} a}{V_L}\right)}{H_{CO2}} \frac{(p_{CO2,i} - p_{CO2,o})}{\left(-\frac{1}{V_L}\frac{dn_{CO2}}{dt}\right)} \right] \right)}{\left(1 - \exp\left[\frac{\left(\frac{k_{L,\mathrm{CO2}} a}{V_L}\right)}{H_{CO2}} \frac{(p_{CO2,i} - p_{CO2,o})}{\left(-\frac{1}{V_L}\frac{dn_{CO2}}{dt}\right)} \right] \right)} \quad 8.10$$

The parameters in Equations 8.9 and 8.10 are as defined above for CO, with dn_{H2}/dt and dn_{CO2}/dt being the uptake rates of H_2 and CO_2 from the experimental data.

8.5.5 The water gas shift reaction and p_{CO}^{*}

CO and H_2 are typically consumed simultaneously and electrons pass from both hydrogenase and CO dehydrogenase to ferredoxin and are distributed to other carriers inside the cell. Electron flow is toward ferredoxin from CO and H_2, and the water gas shift reaction (Equation 8.11) that relates concentrations of CO, H_2 and CO_2 is in thermodynamic equilibrium inside the cell.

$$CO + H_2O \leftrightarrow CO_2 + H_2 \quad 8.11$$

The Gibbs free energy change for the water gas shift reaction can be calculated as in Equation 8.12 with $\Delta G_r = 0$, and for the reaction in Equation 8.11, ΔG_r^o = -19.93 kJ/mol, which was calculated using ΔG_f^o from Thauer et al. (1977).

$$\Delta G_{\mathrm{r}} = \Delta G_{\mathrm{r}}^{\mathrm{o}} + \mathrm{RT}\ln\left(\frac{p_{CO2}^{*} p_{H2}^{*}}{p_{CO}^{*}}\right) = 0 \qquad 8.12$$

The equilibrium mass action ratio (Nicholls and Ferguson, 2002) for the water gas shift reaction can be calculated from Equation 8.12, and p_{CO}* can be calculated with p_{H2}* and p_{CO2}* from Equations 8.9 and 8.10. The units in Equation 8.13 are converted from the standard state of 1 atm H_2 to kPa (101.3 kPa/atm) and for 37°C.

$$\frac{p_{CO2}^{*} p_{H2}^{*}}{p_{CO}^{*}} = e^{\left(\frac{-\Delta G_{\mathrm{r}}^{\mathrm{o}}}{RT}\right)} = 101.3e^{\left(\frac{-(-19.93)}{(0.008314)(310.2)}\right)} = 230{,}100\ kPa \qquad 8.13$$

The calculated value of p_{CO}^{*}, less than 10^{-2} kPa, can be used to check the validity of the assumption of CO mass transfer limitation (i.e., $p_{CO}^{*} = 0$).

This estimation of dissolved gas pressures is only valid when both CO and H_2 are consumed. Hydrogenase is 50% inhibited by 7×10^{-9} mol/L CO (p_{CO}* =8.5×10^{-4} kPa) (Ragsdale and Ljungdahl, 1984), and there are large potential errors (orders of magnitude) in the calculation of p_{CO}* since activity of hydrogenase will be diminished until CO concentration in the cell is less than 7×10^{-9} mol/L. Since accumulated CO will inhibit hydrogenase and slow the oxidation of H_2, the effective pressure of H_2 seen by ferredoxin will be lower (10% or less) than the estimated partial pressure of H_2 delivered to the hydrogenase. Since the calculated p_{CO}^{*} is proportional to p_{H2}^{*}, the dissolved pressures calculated from Equations 8.9 through 8.13 can be higher than p_{CO}^{*} and p_{H2}^{*} operating in the cell reactions. However, p_{CO}^{*} and p_{H2}^{*} calculated from Equations 8.9 through 8.13 are useful as the best available approximation of the thermodynamic condition inside the cell, and are reasonable parameters to characterize reaction kinetics.

8.5.6 Electrochemistry

Many reactions in the Wood-Ljungdahl pathway are oxidation-reduction reactions, in which electrons are transferred from one molecule to another; the electron donor is oxidized, and the electron acceptor is reduced. The water gas shift reaction in Equation 8.11 provides an example; CO is oxidized to CO_2 and H^+ is reduced to H_2. This can be understood as oxidation of CO coupled with reduction of H^+ by writing the half-reactions for CO oxidation, Equation 8.14,

$$CO + H_2O \leftrightarrow CO_2 + 2\,H^+ + 2\,e^- \qquad 8.14$$

and for H^+ reduction, Equation 8.15.

$$2\,H^+ + 2\,e^- \leftrightarrow H_2 \qquad 8.15$$

These half-reactions sum to the overall water gas shift reaction (Equation 8.11), and CO is shown to donate 2 e^- to produce H_2. This reaction is reversible, and H_2 can be oxidized to produce CO from CO_2. Reaction will proceed in the direction for which $\Delta G_r < 0$. The reaction will be in equilibrium when $\Delta G_r = 0$.

The oxidized and reduced forms of a chemical comprise a redox couple, for example H_2/H^+ and CO/CO_2. The oxidized form will accept electrons (and sometimes H^+) to become the reduced form. When the half-reaction is set at the standard conditions of 1.0 mol/L reactants and products, the redox couple will exhibit a characteristic tendency or potential to donate electrons. This potential, measured in volts, with equal concentrations of the oxidized and reduced forms, is the midpoint potential. This is E^o at pH 0. E^o for a half-cell reaction can be calculated from ΔG_r^o as in Equation 8.16 (Nicholls and Ferguson, 2002; Thauer et al., 1977).

$$E° = -\Delta G_r^o / n_e F \qquad 8.16$$

Where n_e is the number of electrons transferred and F is the Faraday constant (0.0965 kJ/mV mol e^-). Note that this potential is a characteristic of the half-cell reaction, not a differential. The Gibbs free energy change for a half-cell reaction, ΔG_r, changes with concentrations of products and reactants. The electrochemical potential of the half-cell changes too. The potential (E) is given by the Nernst Equation (Bailey and Ollis, 1986; Nicholls and Ferguson, 2002).

$$E = -\frac{\Delta G_r}{n_e F} = E^o - \frac{RT}{n_e F} ln\left(\prod C_{(Products)} / \prod C_{(Reactants)}\right) + 2.302\frac{RT}{n_e F}\Delta m_H pH \qquad 8.17$$

The notation ($\Pi C_{Products}/\Pi C_{Reactants}$) represents the mass action ratio for the reaction (Nicholls and Ferguson, 2002), and Δm_H is the number of protons produced in the reaction. E is the potential of the redox couple to donate electrons under the actual conditions, and each redox couple will exhibit its characteristic potential under those conditions. A redox couple with lower (more negative) potential will donate electrons (be oxidized) to couples of higher potential. Two half-cell reactions are combined, an oxidation with a reduction, in a balanced reaction, as shown above for the water gas shift reaction where Equations 8.14 and 8.15 are combined in Equation 8.11. When the reaction reaches equilibrium, $\Delta G_r = 0$ and both redox couples are at the same potential E ($\Delta E_r = 0$).

When mass transfer is rate limiting, the transfer of gas to the cell is the slowest process in the reaction, and all reaction steps in the production pathway are fast relative to the rate of gas supply. Under mass transfer limitation, the reactions of the production pathway approach thermodynamic equilibrium, and all electrochemical half-cell reactions inside the cell are set at the same potential, E_{Cell}. The assumption of thermodynamic equilibrium at one intracellular potential sets a boundary condition that defines the

thermodynamic state of the pathway reactions. The approach of the reactions to this ideal thermodynamic state provides a reasonable and convenient method to describe the reaction set for study and modeling of syngas fermentation.

The potential of the oxidation reduction reactions of the pathway can be estimated by Equation 8.17 with E^o calculated from Equation 8.16. Then Equation 8.17 can be rearranged to calculate the mass action ratio as in Equation 8.18.

$$\left(\prod C_{(Products)} / \prod C_{(Reactants)}\right) = \exp\left[-\frac{\Delta G_r^o}{RT} - \frac{n_e F E}{RT} + 2.302 \Delta m_H pH\right] \qquad 8.18$$

Ratios of products for selected half cell reactions from the Wood-Ljungdahl pathway are presented in Table 8.2. Note that the ratios of products to reactants are ratios of concentrations or partial pressures, except for the partial pressure of H_2. The half cells are typically 2 electron reductions, $n_e = 2$, and that most reductions consume 2 protons, $\Delta m_H = -2$, except NADH/NAD^+ and Fd_r/Fd_o consume one proton and no protons respectively. The values of $\Delta G^{o\prime}$ and $E^{o\prime}$ are calculated at pH 7.0 and match values given by Thauer et al. (1977).

Table 8.2 Selected Half Cell Reactions of the Wood-Ljungdahl Pathway.

Half Cell Reduction	ΔG_r^o (kJ/mol)	E^o (mV)	n_e	Δm_H	$\Delta G_r^{o\prime}$ (kJ/mol)	$E^{o\prime}$ (mV)	Π_{prod}/Π_{react}
$2H^+ + 2e^- \leftrightarrow H_{2(g)}$	0	0	2	-2	79.90	-414	p_{H2}
$CO_2 + 2H^+ + 2e^- \leftrightarrow CO_{(g)} + H_2O$	20.03	-104	2	-2	99.93	-518	p_{CO}/p_{CO2}
$CH_3CHO + 2H^+ + 2e^- \leftrightarrow CH_3CH_2OH$	-41.85	217	2	-2	38.05	-197	C_{Et}/C_{Ald}
$CH_3COOH + 2H^+ + 2e^- \leftrightarrow CH_3CHO + H_2O$	-7.67	40	2	-2	72.23	-374	C_{Ald}/C_{HA}
$NAD^+ + H^+ + 2e^- \leftrightarrow NADH$	21.80	-113	2	-1	61.75	-320	C_{NADH}/C_{NAD+}
$Fd_{Ox} + 2e^- \leftrightarrow Fd_{Rd}$	81.05	-420	2	0	81.05	-420	C_{Fdr}/C_{Fdo}

The electrochemical couples are defined by the mass action ratio of products to reactants in the half cells at given pH; the CO/CO_2 half cell is defined by p_{CO}^{*}/p_{CO2}^{*}, but the H_2 half cell is defined by p_{H2}^{*} alone. The calculated p_{H2}* defines potential at given pH and is the best measure of the internal electrochemical potential, E_{Cell}, that sets the ratio of ethanol to acetic acid attained. Equation 8.18 corelates the concentrations of chemicals inside the cell to the intracellular pH (pH_{ic}) and E_{Cell}.

The partial pressure of dissolved H_2, p_{H2}* referred to the standard state pressure of 1 atm or 101.3 kPa, particularly defines E_{Cell} at given pH_{ic}. The ratio of CO to CO_2, $p_{CO}*/p_{CO2}*$, similarly defines E_{Cell}, but this relationship is used in the calculation of the dissolved pressure of CO, p_{CO}*. For this ratio, p_{CO}* and p_{CO2}* can be in any pressure unit. But the pressure of H_2, p_{H2}*, must be in atm (or as kPa/101.3) for use in these calculations to reference the standard state for H_2 (1 atm). The model uses the assumption of a single cell potential (E_{Cell}) and intracellular pH (pH_{ic}) to calculate the mass action ratios for use in thermodynamic and kinetic calculations. If pH_{ic} is known, E_{Cell} can be calculated.

Equation 8.19 written for acetic acid reduction to acetaldehyde, and again for acetaldehyde reduction to ethanol (see Table 8.2), can predict the ratio of the concentration of ethanol to the concentration of free acetic acid [CH_3COOH].

$$\frac{[CH_3CHO]}{[CH_3COOH]}\frac{[CH_3CH_2OH]}{[CH_3CHO]}=\frac{[CH_3CH_2OH]}{[CH_3COOH]} \qquad 8.19$$

This ratio is set by E_{Cell} and pH_{ic}. The ratio of ethanol to free acetic acid inside the cell $(C_{Et}/C_{HA})_{ic}$ is shown versus E_{Cell} in Figure 8.3 at various pH_{ic}. The required potential is lower as pH_{ic} rises, but very high ratios, greater than 100 mol/mol, are predicted at achievable potentials near the pH range used in fermentation with *C. ragsdalei*.

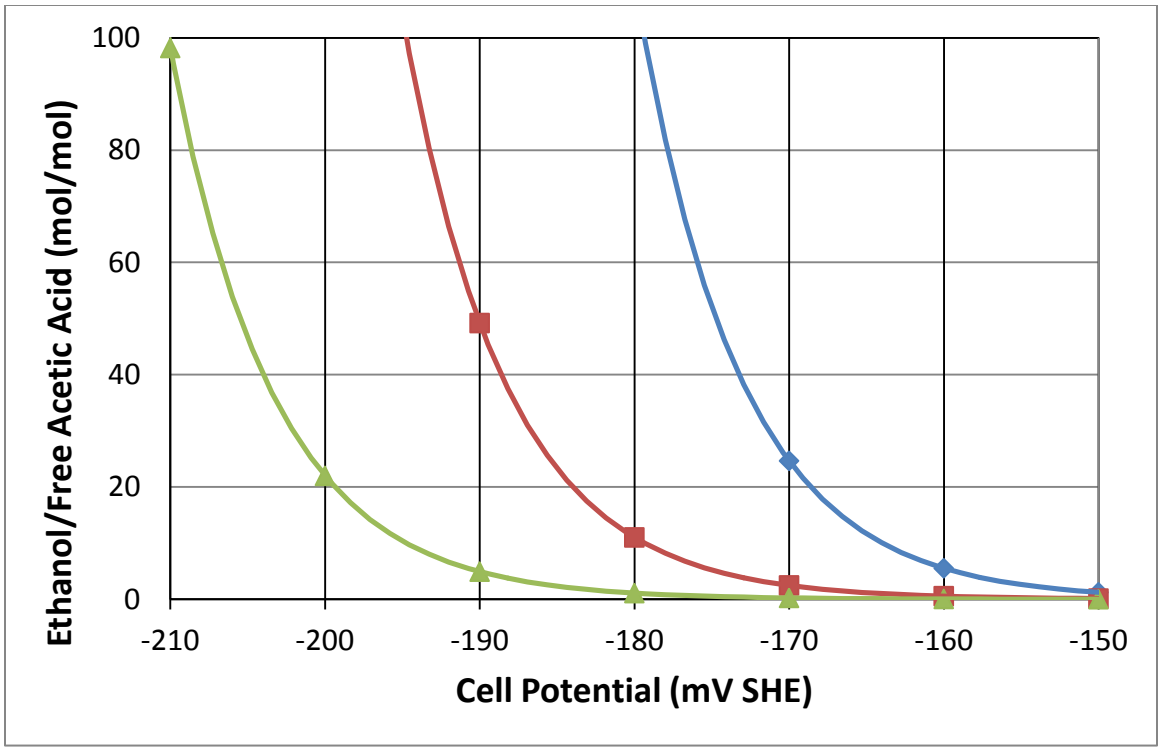

Figure 8.3 Concentration ratio of ethanol to free acetic acid predicted in fermentation of syngas. $(C_{Et}/C_{HA})_{ic}$ ratio at intracellular redox potential for pH_{ic} of 4.5 (◆), 4.75 (■), and 5.0 (▲).

8.5.7 Estimation of pH_{ic} *and* E_{Cell}

Equation 8.18 can be used for the redox couple written as reduction (Table 8.2) with p_{H2}^* (in atm) and again with C_{Et}/C_{HA} to derive an equation for the intracellular potential (E_{Cell}), as in Equations 8.20, 8.21 and 8.22. The unit atm is used in this calculation because the standard state for gas is 1 atm. Alternatively, p_{H2}^* can be expressed in kPa as $(p_{H2}^*/101.3)$ for the calculation.

$$p_{H2}^* = exp\left[-\frac{\Delta G_{r,H2}^o}{RT} - \frac{n_e F E_{Cell}}{RT} + 2.302\Delta m_H pH_{ic}\right] \quad 8.20$$

$$\frac{C_{Et}}{C_{HA}} = exp\left[-\frac{\Delta G_{r,EA}^o}{RT} - \frac{n_e F E_{Cell}}{RT} + 2.302\Delta m_H pH_{ic}\right] \quad 8.21$$

$$E_{Cell} = \frac{-(\ln p^*_{H2} + 4.604 pH_{ic})}{0.07484} = \frac{-\left(\ln\left(\frac{C_{Et}}{C_{HA}}\right)_{ic} - 19.20 + 9.208 pH_{ic}\right)}{0.14967} \quad 8.22$$

This can be simplified eliminating pH_{ic} to relate p_{H2}*(in atm) and $(C_E/C_{HA})_{ic}$

$$\ln\left(\frac{(p^*_{H2})^2}{\left(\frac{C_{Et}}{C_{HA}}\right)_{ic}}\right) = -19.20 \quad 8.23$$

For acetic acid, as a weak acid, the ratio of acetate to free acetic acid is

$$\frac{C_{Ac}}{C_{HA}} = 10^{(pH - pK_a)} \quad 8.24$$

And across the membrane

$$\left(\frac{C_{Ac}}{C_{HA}}\right)_{ic}\left(\frac{C_{HA}}{C_{Ac}}\right) = 10^{(pH_{ic} - pH)} \quad 8.25$$

Where *ic* represents the intracellular value of concentration of acetate (CH_3COO^-) and free acetic acid (CH_3COOH), and pH, and no subscript indicates the values measured outside the cell. Then, assuming that the ethanol concentration is the same inside the cell and outside, and assuming that acetate concentration is the same across the membrane, as for facilitated diffusion, pH_{ic} can be obtained from Equation 8.25

$$pH_{ic} = pH + \log\left(\frac{C_{Et}}{C_{HA,ic}}\frac{C_{HA}}{C_{Et}}\right) \quad 8.26$$

And combining Equations 8.23 and 8.26 to eliminate $(C_{Et}/C_{HA})_{ic}$

$$pH_{ic} = pH + \log\left(\frac{(p^*_{H2})^2 e^{19.20}}{\left(\frac{C_{Et}}{C_{HA}}\right)}\right) \quad 8.27$$

The internal pH (pH_{ic}) can be calculated from the dissolved H_2 (in atm), the external pH and the measured concentrations of ethanol and acetic acid in the fermentation broth. The accuracy of these results is subject to the error of the assumptions that allow the calculation. The ethanol concentration will change slightly across the membrane, but the

assumption of facilitated transport of acetate to equalize the concentration across the membrane is advanced to address the chemical potential created by the pH difference near the pK_a of acetic acid. The calculated pH_{ic} can be entered in Equation 8.22 to obtain the intracellular potential, E_{Cell}.

8.6 Results and Discussion

8.6.1 Fermentation control

Calculation of $k_{L,CO}\,a/V_L$, $k_{L,H2}\,a/V_L$, $k_{L,CO2}\,a/V_L$, p_{CO}^*, p_{H2}^* and p_{CO2}^* has been coded in an Excel spreadsheet, and used to guide fermentation in the CSTR using a model syngas mix. The controlled fermentation has achieved up to 95% conversion of both CO and H_2 simultaneously, and has been used to define the kinetic parameters for the acetogenic culture, *Clostridium ragsdalei*, used in experiments SGIE1 through SGIE7 (Table 8.3).

Table 8.3 Summary of syngas fermentations in the CSTR

Experiment	SGIE1	SGIE2	SGIE3	SGIE4	SGIE5	SGIE6	SGIE7
Gas flow (sccm)	75	38.2	17.5	17.7	17.7	17.7	17.7
vvm	0.030	0.015	0.008	0.008	0.008	0.008	0.008
Max. Agitation (rpm)	400	600	280	650	900	700	400
Cumulative Uptake (mmol)	1042	1573	1600	1900	1680	1700	1000
Cell Conc (mg/L)	270	320	328	304	350	310	270
Ethanol (g/L)	0.1	0.13	0.09	0.13	0.19	0.24	1.05
Acetic acid (g/L)	6.0	6.6	7.0	7.0	6.6	6.7	5.0
Max CO conversion	36%	86%	68%	92%	95%	95%	71%
Max H_2 Conversion	0%	82%	75%	94%	96%	95%	77%
Max $k_{L,CO}a/V_L$ (h^{-1})	52	87	22.5	46.3	63.8	73.6	23.0
at G (sccm)[a]	75	38.2	17.5	17.7	19.4	20.3	17.7
at N (rpm)[a]	400	600	280	650	900	700	300

[a] Gas flow and agitation speed for maximum $k_{L,CO}a/V_L$

C. ragsdalei was grown in the CSTR in seven experimental runs and the results are summarized in Table 8.3. Calculation of $k_{L,CO}\,a/V_L$, $k_{L,H2}\,a/V_L$, $k_{L,CO2}\,a/V_L$, p_{CO}^{*}, p_{H2}^{*} and p_{CO2}^{*} was used in each run to maintain consumption of H_2 as a significant portion of the total gas used. Fermentation started with low cell concentration and limited kinetic capacity to convert CO and H_2. The gas flow was set at a rate that was expected to be mostly converted in later fermentation, and with low agitation of 150 rpm to reduce mass transfer until uptake of both CO and H_2 was established. This procedure reduces inhibition of the culture by oversupply of gas and reduces the lag phase before cell growth starts.

Once growth begins, the dissolved gas concentrations are low and the culture aggressively consumes both CO and H_2 to derive energy for production of cell materials. The fermentation quickly becomes mass transfer limited and the agitation must be increased to supply more gas to feed the increasing cell mass. This energy is required in the form of ATP and as reduced intracellular electron carriers, such as nicotinamide adenine dinucleotide (NADH), flavin adenine dinecleotide ($FADH_2$) and ferredoxin (Fd). The mass transfer in the CSTR is characterized by the overall volumetric mass transfer coefficient (k_La/V_L) for each gas species, CO, H_2 and CO_2. The apparent k_La/V_L were calculated for CO, H_2 and CO_2 from the observed gas uptake and compositions of the inlet and effluent gas over the course of fermentation using Equation 8.5 for each gas assuming that p_{CO}^{*}, p_{H2}^{*} and p_{CO2}^{*} are 0 as in Equation 8.7. The apparent k_La/V_L is the mass transfer coefficient calculated when mass transfer limitation is assumed. CO is assumed to be mass transfer limited and the apparent $k_{L,CO}\,a/V_L$ is assumed to equal the actual $k_{L,CO}\,a/V_L$ whenever fermentation is active, particularly when H_2 is consumed. The

value of $k_{L,CO}\,a/V_L$ observed in Figure 8.4 sets the expectation of mass transfer capacity for all gases through Equation 8.8. The predicted $k_{L,CO2}\,a/V_L$ by Equation 8.8 and shown in Figure 8.4 is 4% higher than $k_{L,CO}a/V_L$. However, the observed or apparent $k_{L,CO2}\,a/V_L$ is near 0. Little transfer of CO_2 is observed as there is small molar production of CO_2 and the liquid is saturated at the concentration in equilibrium with CO_2 in the effluent gas. The apparent $k_{L,H2}\,a/V_L$ is within 10% of that predicted from $k_{L,CO}\,a/V_L$ using Equation 8.8 between 23 and 55 h of fermentation (Figure 8.4). After 55 h the apparent $k_{L,H2}\,a/V_L$ is lower than the predicted value, except when the agitation or gas feed rate is adjusted after 64 and 72 h . This indicates that scaling $k_{L,CO}\,a/V_L$ using the square root of the ratio of the diffusivities for CO and H_2 is valid, and that after 55 h the available

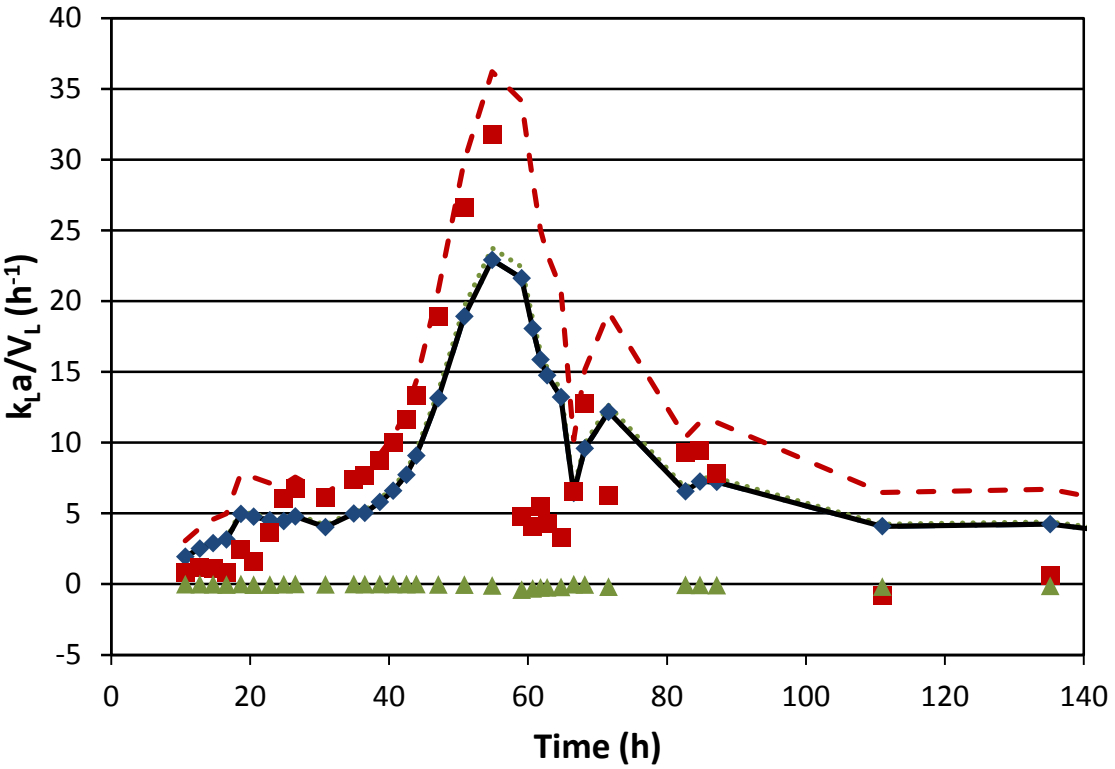

Figure 8.4 Volumetric mass transfer coefficients for CO, H_2 and CO_2 in CSTR fermentation of syngas SGIE7. Apparent k_La/V_L for CO (◆), H_2 (■), CO_2 (▲), and predicted capacity for CO (—), H_2 (– –), and CO_2 (····).

capacity for transfer of H_2 is not used efficiently. The loss of H_2 efficiency is likely the result of accumulation of CO greater than 7×10^{-9} mol/L in the fermentation broth that inhibits the hydrogenase enzyme.

Figure 8.5 shows the conversions of CO and H_2 achieved in the course of the fermentation, the production of CO_2 denoted as negative conversion and the agitation speed. Initial conversion is low and is limited to CO through about 18 h. However, H_2 conversion begins at about 20 h and quickly increases to exceed percent conversion of CO by 30 h with agitation speed of 150 rpm. The agitation speed was increased from 150 rpm at 40 h to 400 rpm at 55 h. Each increase in agitation speed increased the gas

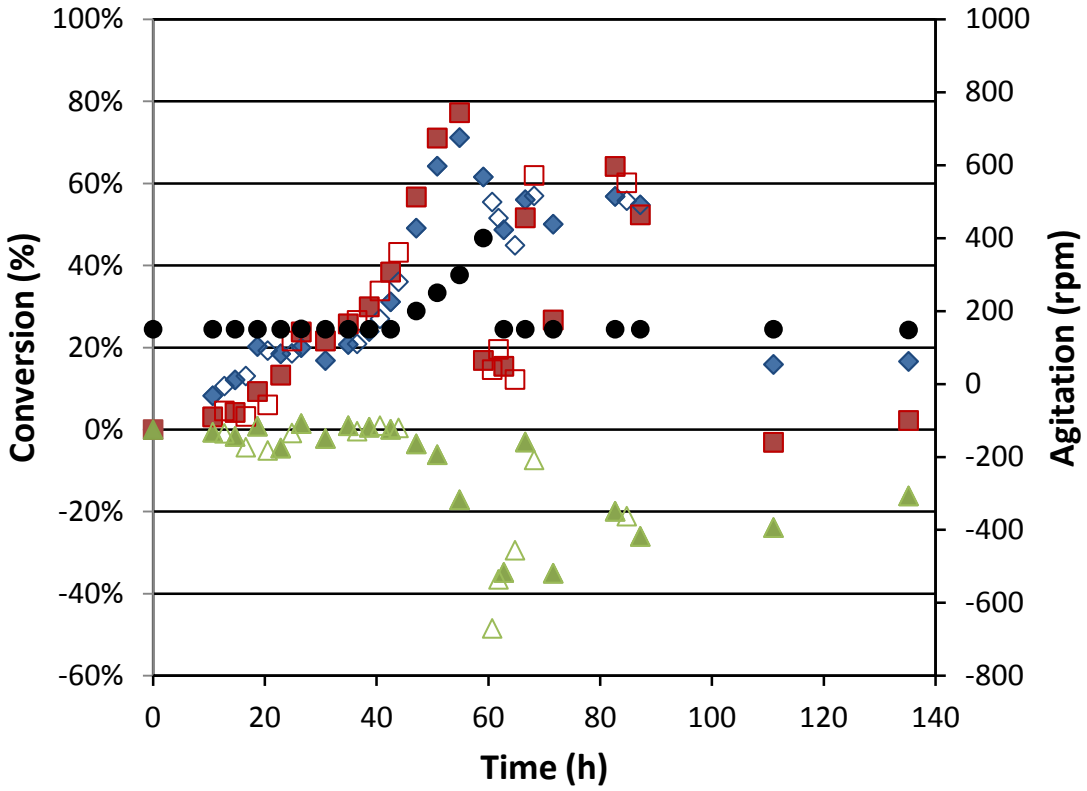

Figure 8.5 Gas conversions and agitation in CSTR fermentation of syngas SGIE7. CO (◆), H_2 (■), CO_2 (▲) and agitation (●). Open symbols are data when only a gas sample was taken.

conversion, up to 72% for CO and 77% for H_2, until the last increase from 300 to 400 rpm precedes a drop of CO conversion to 62% and H_2 converson to only 18%. After 60 h of fermentation the agitation speed was maintained at 150 rpm. Conversion of H_2 and CO was recovered by reducing gas flow (Figure 8.6) from 17.5 to 7.1 sccm at 64 h, and again from 14.1 to 7.1 sccm at 72 h.

The molar uptake of CO, H_2 and their sum ($CO+H_2$), and the inlet molar flow rates of CO and H_2 are shown in Figure 8.6. The gas uptake follows the course seen in conversion, and the highest total uptake occurs at 55 h before the agitation is increased to 400 rpm and the H_2 conversion is diminished. H_2 uptake recovered slightly after the feed

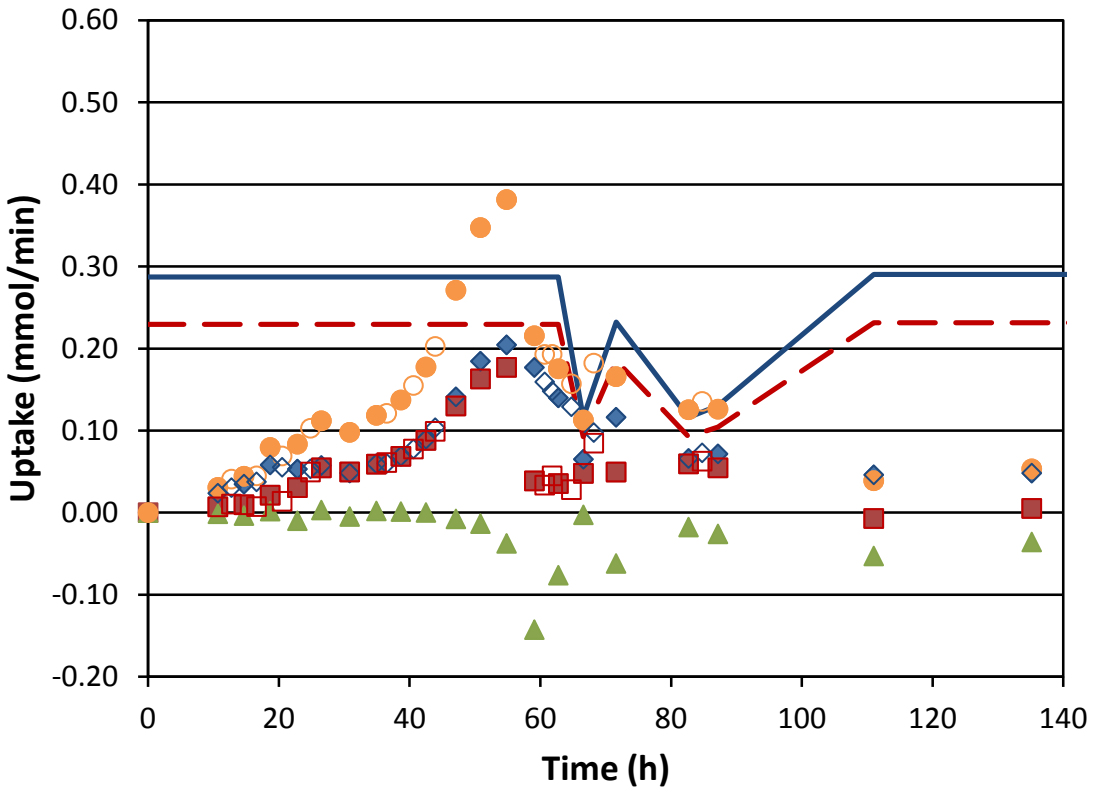

Figure 8.6 Gas uptake in CSTR fermentation of syngas SGIE7. CO (◆), H_2 (■), CO_2 (▲), $CO+H_2$ (●), CO feed rate (—) and H_2 feed rate (– –). Open symbols are data when only a gas sample was taken.

gas rate was cut at 64 h, but remained low through the rest of the fermentation. CO uptake also diminished after 55 h.

The bulk liquid concentrations of dissolved gases, shown as the equilibrium partial pressure using Henry's Law (Equation 8.2), are plotted in Figure 8.7. The calculation has large potential error (orders of magnitude) when H_2 is not converted, as p_{CO}^* is calculated from the pressure of H_2 in the bulk liquid (p_{H2}^*), but is in equilibrium with the effective H_2 pressure that is generally less than p_{H2}^* when the hydrogenase enzyme is inhibited by CO. H_2 is not converted before 20 h and after 90 h of this fermentation. The dissolved CO pressure can be higher or lower than that calculated, as the equilibrium of the water gas shift reaction (Equation 8.11) has not been established.

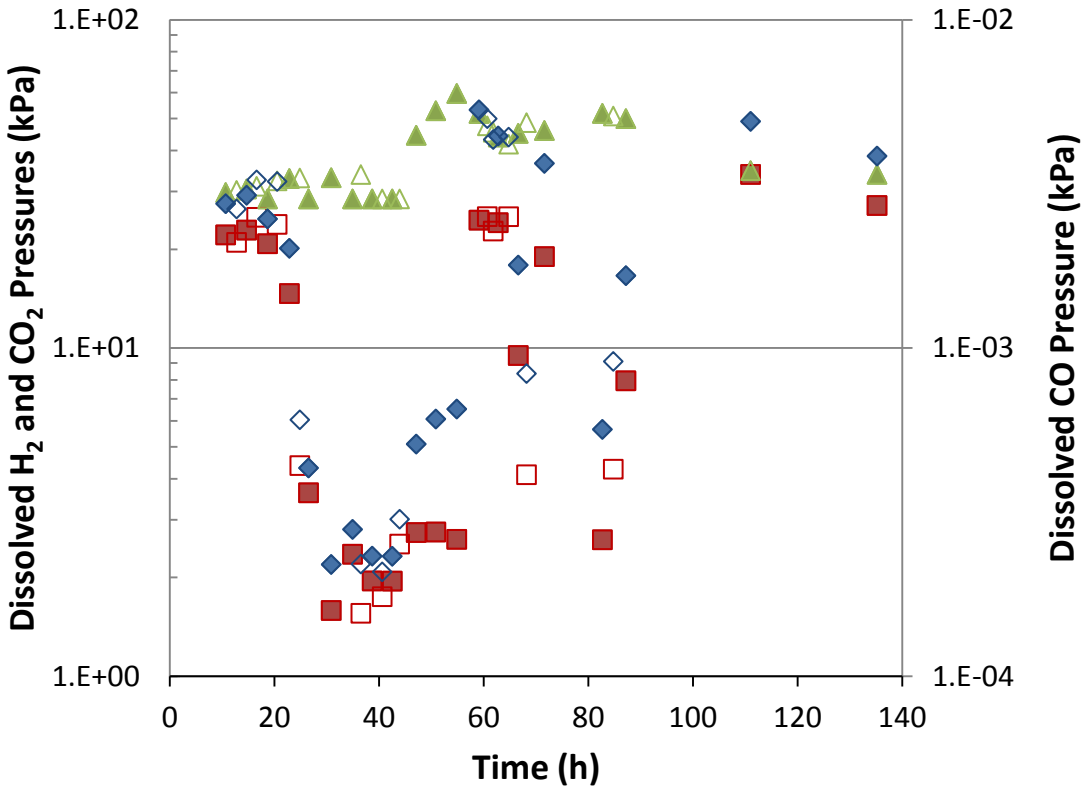

Figure 8.7 Partial pressures of dissolved CO, H_2 and CO_2 in CSTR fermentation of syngas SGIE7. CO (◆), H_2 (■) and CO_2 (▲). Open symbols are data when only a gas sample was taken.

However, as H_2 conversion is established after 20 h of fermentation, the equilibrium of the water gas shift reaction is established inside the cells, $k_{L,CO}\,a/V_L$ is more certain, and dissolved pressures can be calculated with good confidence. Here, "good confidence" denotes values of acceptable accuracy to be useful in scientific and engineering calculations, in some cases ±100% or more. Note that p_{CO}^* is less than p_{H2}^* and p_{CO2}^* by about 4 orders of magnitude (a factor of 10^{-4}). This supports the assumption of CO mass transfer to an arithmetic zero. The value of p_{CO}^* that inhibits the hydrogenase enzyme can be estimated from Figure 8.7 to be about 10^{-3} kPa and H_2 uptake is decreased.

The inhibition of H_2 uptake rate is further illustrated in Figure 8.8, which depicts the ratio of H_2 to CO uptake as a function of dissolved CO. H_2 partial pressure in the gas phase is high when the rate of uptake is low, so the actual concentration in the liquid will be high and near saturation. At the same time, the uptake of CO is relatively high, suggesting that sufficient cell mass and hydrogenase enzyme is present to effect the conversion of H_2 proportional to the CO conversion. The dissolved H_2 pressure, p_{H2}^*, is high when H_2 is not consumed and high p_{H2}^* should increase the reaction consuming H_2. Increased H_2 uptake is not observed until p_{CO}^* falls below 2×10^{-3} kPa, and p_{H2}^* also falls as a consequence of consumption. These observations clearly imply CO inhibition of hydrogenase above 10^{-3} kPa dissolved CO pressure. Inhibition of the hydrogenase enzyme lessens gradually as p_{CO}^* decreases.

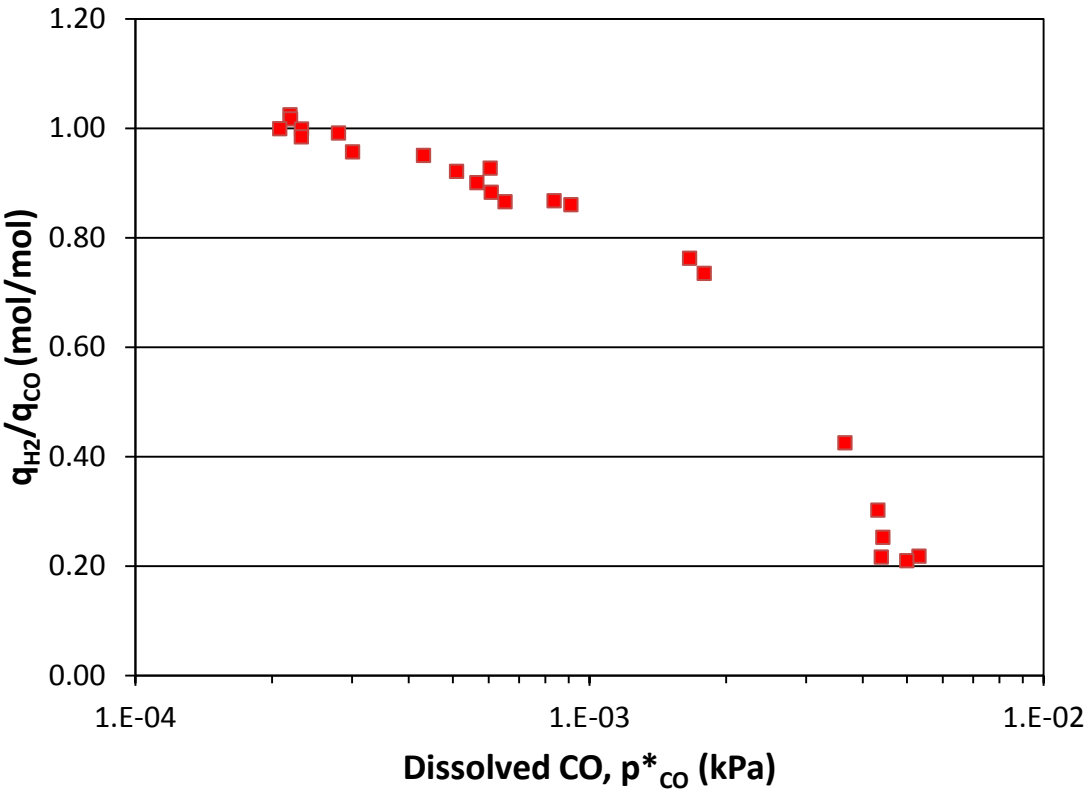

Figure 8.8 Ratio of H_2 uptake to CO uptake versus dissolved CO in CSTR fermentation of syngas SGIE7.

The cumulative uptake of the energy substrates CO and H_2 over the course of this fermentation (SGIE7) in the CSTR is shown in Figure 8.9. CO and H_2 are consumed for the first 110 h of the fermentation, with slow consumption of CO after that up to 180 h. The fermentation was followed through 350 h, with little additional uptake of CO or H_2. A total of 1000 mmol of CO plus H_2 was consumed by the culture over 182 h.

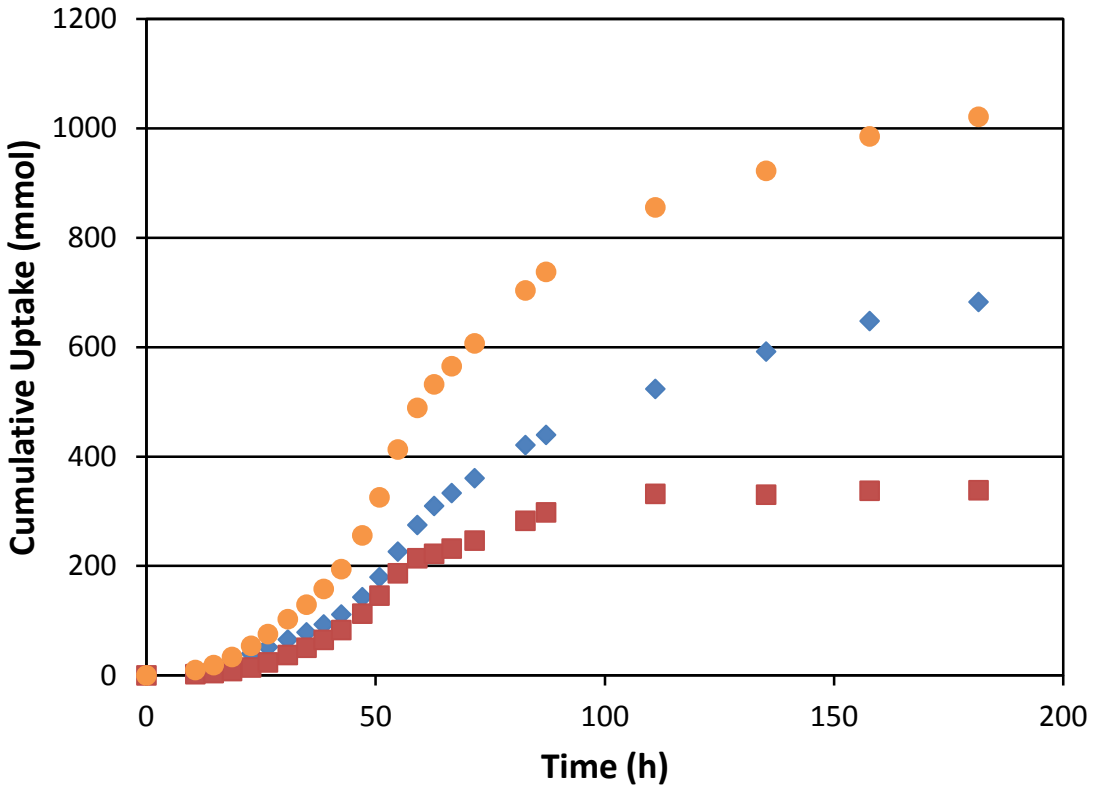

Figure 8.9 Cumulative uptake in CSTR fermentation of syngas SGIE7. CO (◆), H2 (■), CO + H2 (●).

The products of the fermentation are shown in Figure 8.10, with the primary product being acetic acid. About 1 g/l of ethanol was produced between 50 h and 150 h of the fermentation. Cell concentration of 0.27 grams of cells per liter (g_x/L) was achieved. Cell concentration peaked at 55 h of the fermentation, coincident with the loss of H_2 conversion. This indicates that a nutrient limitation was reached that slowed growth and energy demand to support growth. The slower uptake indicates onset of a kinetic limitation that limits the rate of gas conversion. Mass transfer, which should have increased with the increased agitation speed to 400 rpm at 54 h, exceeded capability of the culture to consume the CO and H_2, CO accumulated in the fermentation broth and H_2 uptake was reduced from CO inhibition.

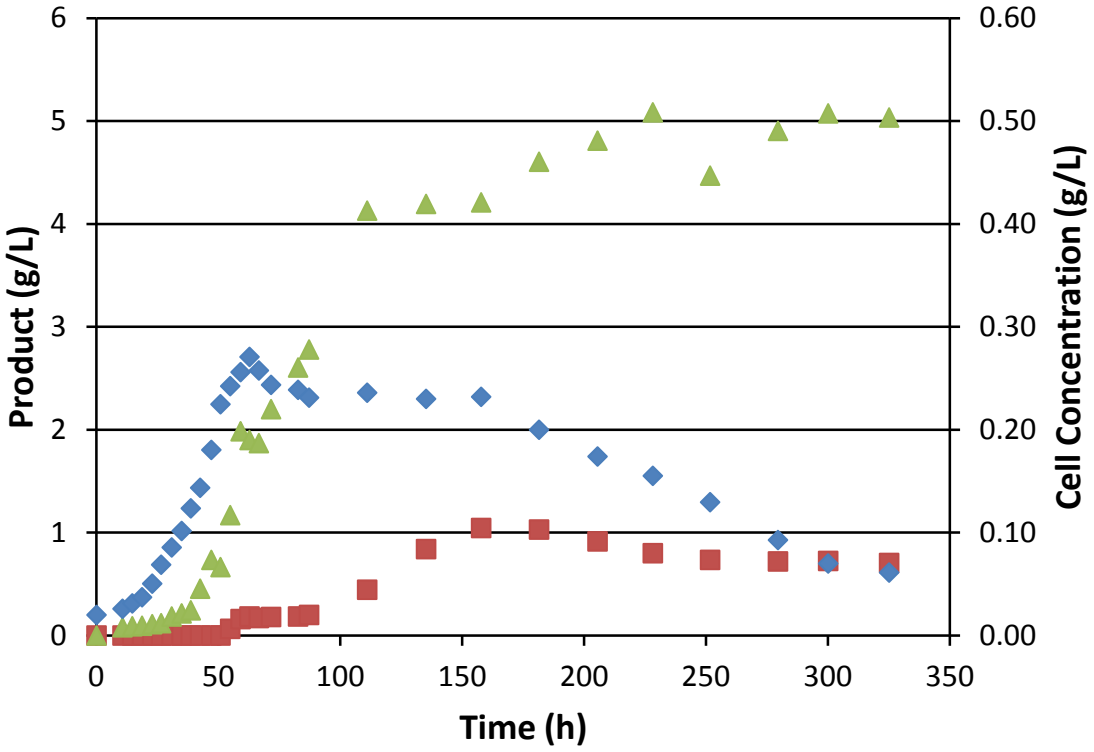

Figure 8.10 Cells and products concentrations in CSTR fermentation of syngas SGIE7. Ethanol (■), acetic acid (▲), cells (◆).

The data shown in Figures 8.4 through 8.10 represent SGIE7, which was one of seven fermentations run in the 3 L CSTR to assess the batch fermentation, gain skill in operation and develop the control strategy. Analysis of syngas fermentation in the CSTR used a mathematical model to guide control decisions regarding agitation intensity and feed gas flow. Greater than 90% conversion of both CO and H_2 was achieved in three of these fermentations with agitation speeds of 650, 700 and 900 rpm; $k_{L,CO}a/V_L$ up to 74 h^{-1} was demonstrated (at 700 rpm). The inhibition of H_2 uptake by CO followed a similar pattern for all fermentations, with inhibition above 10^{-3} kPa dissolved CO pressure.

8.6.2 Estimation of intracellular pH_{ic} and potential E_{Cell}

The intracellular pH_{ic} and potential (E_{Cell}) calculated for external pH values of 5.0 and 4.5 are shown in Table 8.4 for varied dissolved H_2 (inside and outside the cell) and C_{Et}/C_{HA} outside the cell. In Table 8.4, p_{H2}^* and C_{Et}/C_{HA} are specified, then pH_{ic} is calculated using Equation 8.27, and E_{Cell} is finally calculated from pH_{ic} using Equation 8.22. The indicated pH_{ic} is the pH that provides equilibrium with the specified C_{Et}/C_{HA} at that specified p_{H2}^*. E_{Cell} is already determined when pH_{ic} and p_{H2}^* are known.

As an example, choosing p_{H2}^* of 0.01 atm and C_{Et}/C_{HA} of 1.0 with external pH of 5.0, pH_{ic} is 9.34 shown as bold and underlined in Table 8.4. If pH_{ic} was lower than 9.34 the thermodynamic expectation would be that p_{H2}^* would decrease and C_{Et}/C_{HA} would increase to achieve equilibrium.

In a second example, C_{Et}/C_{HA} rises from 1 to 100 when p_{H2}^* changes from 0.0001 to 0.001 (kPa/101.3) and the pH_{ic} is 5.34 for external pH of 5.0; the value of E_{Cell} changes from -205 to -236 mV (see the plain underlined data with external pH at 5.0). With an external pH of 4.5, C_{Et}/C_{HA} again rises from 1 to 100 when p_{H2}^* changes from 0.0001 to 0.001 (kPa/101.3), but the pH_{ic} is 4.84 and the value of E_{Cell} changes from -175 to -205 mV (see the plain underlined data with external pH of 4.5).

In a third contrasting example, C_E/C_{HA} rises from 0.01 to 1000 when p_{H2}^* changes from 0.0001 to 0.01 (kPa/101.3) and the pH_{ic} changes from 6.84 to 5.84 even though the value of E_{Cell} remains at -298 mV (see the bold italic data with external pH of 4.5).

Table 8.4 Intracellular pH and potential from p_{H2}*. The ratio of ethanol to free acetic acid outside the cell C_E/C_{HA} is varied at pH 5.0 or 4.5 outside the cell.

pH = 5				
p_{H2}* (kpa/101.3)	0.1	0.01	0.001	0.0001
C_E/C_{HA} (mol/mol)	**pH$_{ic}$** (from Equation 8.27)			
0.01	13.34	11.34	9.34	7.34
0.1	12.34	10.34	8.34	6.34
1	11.34	**9.34**	7.34	5.34
10	10.34	8.34	6.34	4.34
100	9.34	7.34	5.34	3.34
1000	8.34	6.34	4.34	2.34
C_E/C_{HA} (mol/mol)	E_{cell} (mV SHE) (from Equation 8.22)			
0.01	-790	-636	-482	-328
0.1	-728	-574	-421	-267
1	-667	-513	-359	-205
10	-605	-451	-298	-144
100	-544	-390	-236	-82
1000	-482	-328	-175	-21
pH = 4.5				
p_{H2}* (kPa/101.3)	0.1	0.01	0.001	0.0001
C_E/C_{HA} (mol/mol)	**pH$_{ic}$** (from Equation 8.27)			
0.01	12.84	10.84	8.84	***6.84***
0.1	11.84	9.84	7.84	5.84
1	10.84	8.84	6.84	4.84
10	9.84	7.84	5.84	3.84
100	8.84	6.84	4.84	2.84
1000	7.84	***5.84***	3.84	1.84
C_E/C_{HA} (mol/mol)	E_{cell} (mV SHE) (from Equation 8.22)			
0.01	-759	-605	-451	***-298***
0.1	-698	-544	-390	-236
1	-636	-482	-328	-175
10	-574	-421	-267	-113
100	-513	-359	-205	-52
1000	-451	***-298***	-144	10

The data in these examples show the dependence of C_{Et}/C_{HA} on the combination of pH_{ic} and E_{Cell}. Internal pH of 5.6 with a potential difference across the membrane of 80 mV (low *E* inside) was reported at external pH of 5.0 for *Clostridium thermoaceticum* grown on glucose (Baronofsky et al., 1984). This is similar to the differences in Table 8.4. The value of p_{H2}^* from experiment are 1 kPa (10^{-2} atm) and up, higher than the pressures predicted by Table 8.4 for pH_{ic} of 5 to 6. This suggests that effective p_{H2}^* is lower than the p_{H2}^* estimated in analysis of the current experiments, and that inhibition of hydrogenase decreases the efficiency of H_2 in current fermentation practice. This presents an opportunity for process improvement.

In fermentation of pure substrates CO/CO_2 and H_2/CO_2 in batch bottles with *C. ljungdahlii*, uptake of H_2 was slightly faster (mol/h) with lower cell concentration than for fermentation with CO/CO_2 (Phillips et al., 1994). The CSTR fermentation presented here is as yet CO inhibited with p_{CO}^* above 2×10^{-4} kPa, and the untapped H_2 could provide more ethanol with greater conservation of energy if the fermentation control is refined. The processing of H_2 on the hydrogenase enzyme is slowed by CO inhibition, and the water gas shift analysis is in error as the full potential of dissolved H_2 is not available. The inhibition produces a lower effective H_2 pressure that is consistent with the product ratio seen.

8.6.3 Model summary

Our conceptual model of the syngas fermentation is developed from the physical processes like mass transfer of CO and H_2, structure of the cell and configuration of the equipment, and the mechanisms used in the transformation of gas to product. This conceptual model is under development guided by our ongoing research.

The reactions of the Wood-Ljungdahl pathway define the stoichiometry and the expected mass balance is generally confirmed in the observed results. Mass transfer of CO and H_2 is driven by concentration differences that are sustained by reaction. Fermentation kinetic parameters are set by one or two limiting reaction rates. The overall currents of carbon, protons and electrons through the reaction circuits are set by these limited rates and determine the products of fermentation.

Mass transfer is described mathematically by assuming limitation of transfer for CO, with transfer to essentially 0 concentration in the bulk liquid and cells. The mass transfer is characterized as $k_{L,CO}a/V_L$ and scaled to find the capacity to transfer H_2 and CO_2. The concentrations of dissolved CO, CO_2 and H_2 inside the cell at the sites of reaction in the enzymes are calculated using the defined mass transfer capacities and assuming the water gas shift is in equilibrium. The calculated concentrations of CO, H_2 and CO_2 can be used in kinetic and thermodynamic calculations to define the fermentation.

The supply of CO via the applied mass transfer can inhibit the uptake of H_2. H_2 is an effective driver of production if not inhibited. When CO inhibition is low, indicated by consumption of H_2, the concentration of dissolved H_2 and the intracellular pH define the electrochemical potential inside the cell. Important reactions involved in the pathway of production are oxidation reduction reactions that are driven by the cell potential. This potential poises these significant reactions near thermodynamic equilibrium with $\Delta G_r = 0$, and this boundary condition allows calculation of conditions in the cell. The ratio of ethanol to free acetic acid is a key and measurable parameter defined by these

calculations. The predictions of the model are supported by the ratio of ethanol to acetic acid measured in the fermentation.

No net ATP to support cell growth is produced by the reactions of the Wood-Ljungdahl pathway; unlike growth on glucose that produces 2 ATP in production of 2 acetyl CoA (Tracy et al., 2012). Autotrophic growth of acetogens is dependent on ATP formed by an ATPase via a chemiosmotic mechanism (Cramer and Knaff, 1991). The ATPase is driven by the protonmotive force that results from the combination of the potential difference and the pH difference across the cell membrane as in Equation 8.28 (Cramer and Knaff, 1991).

$$\Delta p = \Delta\varphi - \frac{2.3RT}{F}\Delta pH \qquad 8.28$$

The protonmotive force, Δp, forces conformation change in the ATPase that frees ATP to the cell. The potential difference, $\Delta\boldsymbol{\varphi}$, is the difference of the intracellular potential, E_{Cell} and the ORP measured in the bulk liquid, and the pH difference (ΔpH) is between the calculated intracellular pH_{ic} and the measured bulk liquid pH. The calculation of pH and potential inside the cell make possible the study of growth supported by ATPase embedded in the membrane (Das and Ljungdahl, 1997; Ivey and Ljungdahl, 1986; von Ballmoos et al., 2008). Further, ethanol production is seen to begin as growth slows and when ATP would be expected to accumulate. The accumulation of ATP will affect both pH and potential inside the cell, and affect the production of ethanol relative to acetic acid. Our model is a tool to better understand this transition that is critical to biofuel production.

8.7 Conclusions

The mass balance from syngas fermentation agreed well with that expected from the stoichiometry of the production pathway, and the measured rates of CO and H_2 uptake feed the mass transfer calculations. Assumption of equilibrium thermodynamics, in particular equilibrium of the water gas shift reaction, inside the cells gave explicit equations for the concentrations of CO, H_2 and CO_2 at the enzyme active sites inside the cells. The calculated concentrations of reactants are appropriate for thermodynamic and kinetic calculations.

Application of the model in analysis of syngas fermentation gave estimates of the CO, H_2 and CO_2 dissolved pressures consistent with the assumptions of the model development, and particularly showed dissolved CO at 2×10^{-3} kPa partial pressure inhibits hydrogenase in *C. ragsdalei*. Calculation of dissolved CO was used to successfully control agitator speed and gas feed rate to maintain high energy conservation and culture activity in syngas fermentation.

The model was extended to calculate the intracellular pH and electrochemical potential in syngas fermentation. These values can be combined with pH and ORP measured in the bulk fermentation broth to define membrane potentials useful in future growth and kinetics studies.

References

Adams, S.S., S. Scott and C-W Ko. 2010. Method for Sustaining Microorganism Culture in Syngas Fermentation Process in Decreased Concentration or Absence of Various Substrates.

Bailey, J.E., Ollis, D.F. 1986. *Biochemical Engineering Fundamentals*. *2nd ed*. McGraw-Hill, New York,

Bakker, A., Smith, J.M., Myers, K.J. 1994. How to Disperse Gases in Liquids. Chemical Engineering, 101 (12), 98-104.

Baronofsky, J.J., Schreurs, W.J.A., Kashket, E.R. 1984. Uncoupling by Acetic Acid Limits Growth of and Acetogenesis by *Clostridium Thermoaceticum*. Applied and Environmental Microbiology, 48 (6), 1134-1139.

Bird, R.B., Stewart, W.E., Lightfoot, E.N. 2002. Transport Phenomena. 2nd ed, J. Wiley. New York, pp. xii, 895 p.

Boghigian, B.A., Shi, H., Lee, K., Pfeifer, B.A. 2010. Utilizing Elementary Mode Analysis, Pathway Thermodynamics, and a Genetic Algorithm for Metabolic Flux Determination and Optimal Metabolic Network Design. Bmc Systems Biology, 4.

Charpentier, J.-C. 1981. Mass-Transfer Rates in Gas-Liquid Absorbers and Reactors. in: *Advances in Chemical Engineering*, (Eds.) G.R.C.J.W.H. Thomas B. Drew, V. Theodore, Vol. Volume 11, Academic Press, pp. 1-133.

Cramer, W.A., Knaff, D.B. 1991. Energy Transduction in Biological Membranes : A Textbook of Bioenergetics. Springer study ed. in: *Springer advanced texts in chemistry*, Springer-Verlag. New York, pp. xiv, 579 p.

Das, A., Ljungdahl, L.G. 1997. Composition and Primary Structure of the F1f0 Atp Synthase from the Obligately Anaerobic Bacterium Clostridium Thermoaceticum. Journal of Bacteriology, 179 (11), 3746-3755.

Drake, H.L., Gossner, A.S., Daniel, S.L. 2008. Old Acetogens, New Light. in: *Incredible Anaerobes: From Physiology to Genomics to Fuels*, (Eds.) J. Wiegel, R.J. Maier, M.W.W. Adams, Vol. 1125, pp. 100-128.

Gaddy, J.L., D. K. Arora, C-W Ko, J. R. Phillips, R. Basu, C. V. Wikstrom and E. C. Clausen. 2007. Methods for Increasing the Production of Ethanol from Microbial Fermentation. 7285402.

Garcia-Ochoa, F., Gomez, E. 2009. Bioreactor Scale-up and Oxygen Transfer Rate in Microbial Processes: An Overview. Biotechnology Advances, 27 (2), 153-176.

Henry, C.S., Broadbelt, L.J., Hatzimanikatis, V. 2007. Thermodynamics-Based Metabolic Flux Analysis. Biophysical Journal, 92 (5), 1792-1805.

Hougen, O.A., Watson, K.M., Ragatz, R.A. 1954. *Chemical Process Principles*. *2d ed*. Wiley, New York,, pp.v.

Hu, P., Bowen, S.H., Lewis, R.S. 2011. A Thermodynamic Analysis of Electron Production During Syngas Fermentation. Bioresource Technology, 102 (17), 8071-8076.

Ivey, D.M., Ljungdahl, L.G. 1986. Purification and Characterization of the F1-Atpase from Clostridium Thermoaceticum. J. Bacteriol., 165 (1), 252-257.

Klasson, K.T., Ackerson, C.M.D., Clausen, E.C., Gaddy, J.L. 1992. Biological Conversion of Synthesis Gas into Fuels. International Journal of Hydrogen Energy, 17 (4), 281-288.

Kundiyana, D.K., Wilkins, M.R., Maddipati, P., Huhnke, R.L. 2011. Effect of Temperature, Ph and Buffer Presence on Ethanol Production from Synthesis Gas by "Clostridium Ragsdalei". Bioresource Technology, 102 (10), 5794-5799.

Lehninger, A.L. 1982. *Principles of Biochemistry*. Worth Publishers, New York, N.Y,

Liu, K., Atiyeh, H.K., Tanner, R.S., Wilkins, M.R., Huhnke, R.L. 2012. Fermentative Production of Ethanol from Syngas Using Novel Moderately Alkaliphilic Strains of Alkalibaculum Bacchi. Bioresource Technology, 104, 336-341.

Maddipati, P., Atiyeh, H.K., Bellmer, D.D., Huhnke, R.L. 2011. Ethanol Production from Syngas by Clostridium Strain P11 Using Corn Steep Liquor as a Nutrient Replacement to Yeast Extract. Bioresource Technology, 102 (11), 6494-6501.

Medema, M.H., van Raaphorst, R., Takano, E., Breitling, R. 2012. Computational Tools for the Synthetic Design of Biochemical Pathways. Nature Reviews Microbiology, 10 (3), 191-202.

Munasinghe, P.C., Khanal, S.K. 2010. Syngas Fermentation to Biofuel: Evaluation of Carbon Monoxide Mass Transfer Coefficient (K(L)a) in Different Reactor Configurations. Biotechnology Progress, 26 (6), 1616-1621.

Nicholls, D.G., Ferguson, S.J. 2002. *Bioenergetics*. *3rd ed*. Academic Press, pp.297.

Phillips, J.R., Atiyeh, H.K., Lewis, R.S., Huhnke, R.L. 2011. Mass Transfer and Kinetic Limitations During Synthesis Gas Fermentation by Acetogenic Bacteria. *American Society of Agricultural and Biological Engineers Annual International Meeting 2011, August 7, 2011 - August 10, 2011*, Louisville, KY, United states. American Society of Agricultural and Biological Engineers. pp. 4567-4578.

Phillips, J.R., Clausen, E.C., Gaddy, J.L. 1994. Synthesis Gas as Substrate for the Biological Production of Fuels and Chemicals. Applied Biochemistry and Biotechnology, 45-6, 145-157.

Phillips, J.R., Klasson, K.T., Clausen, E.C., Gaddy, J.L. 1993. Biological Production of Ethanol from Coal Synthesis Gas - Medium Development Studies. Applied Biochemistry and Biotechnology, 39, 559-571.

Ragsdale, S. 2004. Life with Carbon Monoxide. Critical Reviews in Biochemistry & Molecular Biology, 39 (3), 165-195.

Ragsdale, S.W. 2008. Enzymology of the Wood-Ljungdahl Pathway of Acetogenesis. in: *Incredible Anaerobes: From Physiology to Genomics to Fuels*, (Eds.) J. Wiegel, R.J. Maier, M.W.W. Adams, Vol. 1125, pp. 129-136.

Ragsdale, S.W., Ljungdahl, L.G. 1984. Hydrogenase from Acetobacterium-Woodii. Archives of Microbiology, 139 (4), 361-365.

Ramachandriya, K.D., DeLorme, M.J., Wilkins, M.R. 2010. Heat Shocking of Clostridium Strain P11 to Promote Sporulation and Ethanol Production. Biological Engineering, 2 (2), 115-131.

Rogers, P., J-S Chen and M. J. Zidwick. 2006. Organic Acid and Solvent Production. in: *The Prokaryotes*, (Eds.) M. Dworkin, S. Falkow, E. Rosenberg, K.-H. Schleifer, E. Stackebrandt, Springer New York, pp. 511-755.

Strobl, G., Feicht, R., White, H., Lottspeich, F., Simon, H. 1992. The Tungsten-Containing Aldehyde Oxidoreductase from Clostridium-Thermoaceticum and Its Complex with a Viologen-Accepting Nadph Oxidoreductase. Biological Chemistry Hoppe-Seyler, 373 (3), 123-132.

Thauer, R.K., Jungermann, K., Decker, K. 1977. Energy Conservation in Chemotrophic Anaerobic Bacteria. Microbiol. Mol. Biol. Rev., 41 (1), 100-180.

Tracy, B.P., Jones, S.W., Fast, A.G., Indurthi, D.C., Papoutsakis, E.T. 2012. Clostridia: The Importance of Their Exceptional Substrate and Metabolite Diversity for Biofuel and Biorefinery Applications. Current Opinion in Biotechnology, 23 (3), 364-381.

Vega, J.L., Antorrena, G.M., Clausen, E.C., Gaddy, J.L. 1989. Study of Gaseous Substrate Fermentations: Carbon Monoxide Conversion to Acetate. 2. Continuous Culture. Biotechnology and Bioengineering, 34 (6), 785-793.

von Ballmoos, C., Cook, G.M., Dimroth, P. 2008. Unique Rotary Atp Synthase and Its Biological Diversity. Annual Review of Biophysics, 37, 43-64.

White, H., Strobl, G., Feicht, R., Simon, H. 1989. Carboxylic-Acid Reductase - a New Tungsten Enzyme Catalyzes the Reduction of Non-Activated Carboxylic-Acids to Aldehydes. European Journal of Biochemistry, 184 (1), 89-96.

CHAPTER IX

SUMMARY AND FUTURE WORK

9.1 Summary of the present study

- Methods for culture of acetogens, particularly *Clostridium ragsdalei* were developed.
- Production medium, defining the function, cost and requirements for major components of the nutrient medium that supports growth and function of *C. ragsdalei* were developed.
- Effects of mass transfer of CO and H_2 were examined, including:
    - Characterization of $k_{L,CO}a/V_L$ and $k_{L,H2}a/V_L$ for batch fermentation in serum bottles
    - Characterization of $k_{L,O2}a/V_L$ in the CSTR into water and into fermentation medium without fermentation, and development of a correlation for $k_{L,CO}a/V_L$ into water
    - Characterization of $k_{L,CO}a/V_L$ and $k_{L,H2}a/V_L$ into fermentation with *C. ragsdalei* in the CSTR, which showed an order of magnitude increase of mass transfer for CO and H_2 with fermentation
    - The values of $k_{L,CO}a/V_L$, $k_{L,H2}a/V_L$, $k_{L,CO2}a/V_L$ and $k_{L,O2}a/V_L$ are proportional by the square root of the ratio of their diffusivities, as predicted by the surface renewal theory of liquid film mass transfer
    - $k_{L,CO}a/V_L$ and $k_{L,H2}a/V_L$ for fermentation of syngas in the CSTR are dependent on agitation speed, gas flow, and cell concentration
- A conceptual model of syngas fermentation based in the reaction stoichiometry of the Wood-Ljungdahl pathway, and mass transfer of CO and H_2 that supply energy and carbon for the process was developed.
- Engineering analysis of mass transfer, and thermodynamic analysis of the reactions were combined to develop a mathematical model of syngas fermentation

- The mathematical model developed was used to
    - Guide fermenter operation, resulting in increased energy conservation for up to 95% conversion of both CO and H_2
    - Derive thermodynamic parameters required for thermodynamic and kinetic characterization of *C. ragsdalei* in the syngas fermentation, including
        - The dissolved concentrations of CO, H_2 and CO_2 inside the cells
        - Estimate of pH and electrochemical potential (ORP) inside the cells
    - Demonstrate the thermodynamic feasibility of high selectivity for ethanol in production from syngas fermentation

9.2 Future work

- Design minimal defined medium for higher cell growth and sustained function
- Use continuous fermentation to attain higher cell concentration, sustained culture activity and steady state analysis
- Control fermentation gas and agitation using the model analysis to maintain high conversions of H_2 and CO
- Incorporate calculation of the intracellular conditions of p_{CO}^*, p_{H2}^*, p_{CO2}^*, pH and ORP in the standard fermentation analysis
- Study the protonmotive force (Δp) defined by the differential of pH (ΔpH) and potential difference ($\Delta\boldsymbol{\varphi}$) across the cell membrane, which can be calculated from the intracellular values and the measured values from the fermenter probes, and correlate with growth

$$\Delta p = \Delta\varphi - \frac{2.3RT}{F}\Delta pH \qquad 9.1$$

- Develop predictions of gas consumption, growth and product formation, and further refine the mathematical model
- Use the model for process design and control.

APPENDICES

A. Stoichiometry

The production of ethanol and acetic acid from synthesis gas is represented in the literature by the pure component stoichiometry, production from either CO or H_2/CO_2 (Barik et al., 1988; Drake et al., 2008; Hurst and Lewis, 2010; Phillips et al., 1994; Ukpong et al., 2012; Vega et al., 1989). The pure component stoichiometries are given as follows

For production of acetic acid

$$4\,CO + 2\,H_2O \rightarrow CH_3COOH + 2\,CO_2 \qquad \text{A.1}$$

$$4\,H_2 + 2\,CO_2 \rightarrow CH_3COOH + 2\,H_2O \qquad \text{A.2}$$

And for production of ethanol

$$6\,CO + 3\,H_2O \rightarrow CH_3CH_2OH + 4\,CO_2 \qquad \text{A.3}$$

$$6\,H_2 + 2\,CO_2 \rightarrow CH_3CH_2OH + 3\,H_2O \qquad \text{A.4}$$

Production can proceed from the pure components (Phillips et al., 1994), but fermentation with syngas, containing CO, CO_2 and H_2 typically shows simultaneous uptake of H_2 and CO (Maddipati et al., 2011; Phillips et al., 1993). The similar stoichiometry from H_2 and CO to form products, 4 moles per mole of acetic acid and 6 moles per mole of ethanol, reinforce that CO and H_2 both act as reductant, providing indistinguishable electrons for the subsequent production reactions.

Intermediate stoichiometries can be written beginning with production from pure CO and substituting one H_2 for one CO and reducing consumption of H_2O and production of CO_2 by one for each step.

$$4\,CO + 2\,H_2O \rightarrow CH_3COOH + 2\,CO_2 \quad \text{A.5}$$

$$3\,CO + H_2 + H_2O \rightarrow CH_3COOH + CO_2 \quad \text{A.6}$$

$$2\,CO + 2\,H_2 \rightarrow CH_3COOH \quad \text{A.7}$$

$$CO + 3\,H_2 + CO_2 \rightarrow CH_3COOH + H_2O \quad \text{A.8}$$

$$4\,H_2 + 2\,CO_2 \rightarrow CH_3COOH + 2\,H_2O \quad \text{A.9}$$

In this way 5 balanced equations are obtained showing the "quantum", or molecular production of acetic acid from any combination of four, H_2 and CO, with two net carbons fixed in acetic acid. Similarly, 7 balanced equations are obtained showing the "quantum" production of ethanol from a combination of six, H_2 and CO, with two net carbons fixed in ethanol.

$$6\,CO + 3\,H_2O \rightarrow CH_3CH_2OH + 4\,CO_2 \quad \text{A.10}$$

$$5\,CO + H_2 + 2\,H_2O \rightarrow CH_3CH_2OH + 3\,CO_2 \quad \text{A.11}$$

$$4\,CO + 2\,H_2 + H_2O \rightarrow CH_3CH_2OH + 2\,CO_2 \quad \text{A.12}$$

$$3\,CO + 3\,H_2 \rightarrow CH_3CH_2OH + CO_2 \quad \text{A.13}$$

$$2\,CO + 4\,H_2 \rightarrow CH_3CH_2OH + H_2O \quad \text{A.14}$$

$$CO + 5\,H_2 + CO_2 \rightarrow CH_3CH_2OH + 2\,H_2O \quad \text{A.15}$$

$$6\,H_2 + 2\,CO_2 \rightarrow CH_3CH_2OH + 3\,H_2O \quad \text{A.16}$$

The overall stoichiometry observed in fermentation will be the average of the "quantum" stoichiometries; for example, 4.3 moles CO plus 1.7 moles H_2 can produce 1 mole of ethanol.

The substitution of H_2 for CO as reductant in fixing 2 carbons in product, either acetic acid or ethanol, suggests a general stoichiometry independent of the origin of electrons, whether from CO or H_2. Reductant ($2\ H^+ + 2\ e^-$) is provided by either CO or H_2, while carbon comes from CO and CO_2. The methyl group of acetic acid is formed from CO_2 and the carbonyl is formed from CO.

The general stoichiometry of acetic acid formation is

$$CO + CO_2 + 6H^+ + 6e^- \rightarrow CH_3COOH + H_2O \qquad \text{A.17}$$

And the general stoichiometry of ethanol formation is

$$CO + CO_2 + 10H^+ + 10\ e^- \rightarrow CH_3CH_2OH + 2H_2O \qquad \text{A.18}$$

Consumption of 4 reductant (including CO and H_2) and 2 carbon (CO or CO_2 including the CO used as reductant) will produce acetic acid. Consuming 6 reductant per 2 carbon will produce ethanol. The energy available in the reaction is associated with the reductant. Since H^+ and e^- are supplied by oxidation of CO or H_2 the general equation can be written for acetic acid production as

$$\mathrm{CO} + CO_2 + (n\ \mathrm{CO} + (3-n)H_2) \rightarrow CH_3COOH + n\ CO_2 + (1-n)\ H_2O \qquad \text{A.19}$$

$$3 \geq n \geq -1$$

and for ethanol production as

$$\mathrm{CO} + CO_2 + (n\ \mathrm{CO} + (5-n)H_2) \rightarrow CH_3CH_2OH + n\ CO_2 + (2-n)\ H_2O \qquad \text{A.20}$$

$$5 \geq n \geq -1$$

For reaction on a molecular level, *n* is an integer and Equations A.19 and A.20 represent the quantum stoichiometry. But on a molar level of reaction, *n* is not restricted to integer values and Equations A.19 and A.20 represent the average stoichiometry.

B. Derivatives for Kinetic and Thermodynamic Parameters

Description of fermentation kinetics incorporates time differentials of measured parameters that describe the cell culture. The specific growth rate is the production of cell mass per unit of cell mass per time, g_x/g_x h or h^{-1}, and calculated as

$$\mu = \frac{1}{X}\frac{dX}{dt} \qquad \text{B.1}$$

The specific uptake for CO or H_2 is the consumption of the gas per unit cell mass per time, mol/g_x h.

$$q_{CO} = \frac{1}{XV_L}\frac{dn_{CO}}{dt} \qquad \text{B.2}$$

$$q_{H2} = \frac{1}{XV_L}\frac{dn_{H2}}{dt} \qquad \text{B.3}$$

$$q_{CO+H2} = \frac{1}{XV_L}\frac{dn_{CO+H2}}{dt} \qquad \text{B.4}$$

The differential quantities can be estimated at specific time using a curve fit of the cell concentration as in Figure B.1, and curve fit of the gas inventory as in Figure B.2. The cell concentration and inventory of CO and H_2 are defined by polynomial curve fit of the measured data. The analysis is shown for bottle Pr2B6 to illustrate the procedure. The analysis was applied for each of the eight bottles in the study with comparable results, but the derived data have not yet been correlated. The differential quantities derived from the curve fit analysis of carefully timed and taken fermentation data allow calculation of the specific growth, and specific uptake, and the contemporary dissolved concentrations of CO, H_2 and CO_2. This data can be correlated to study kinetics on the cellular level.

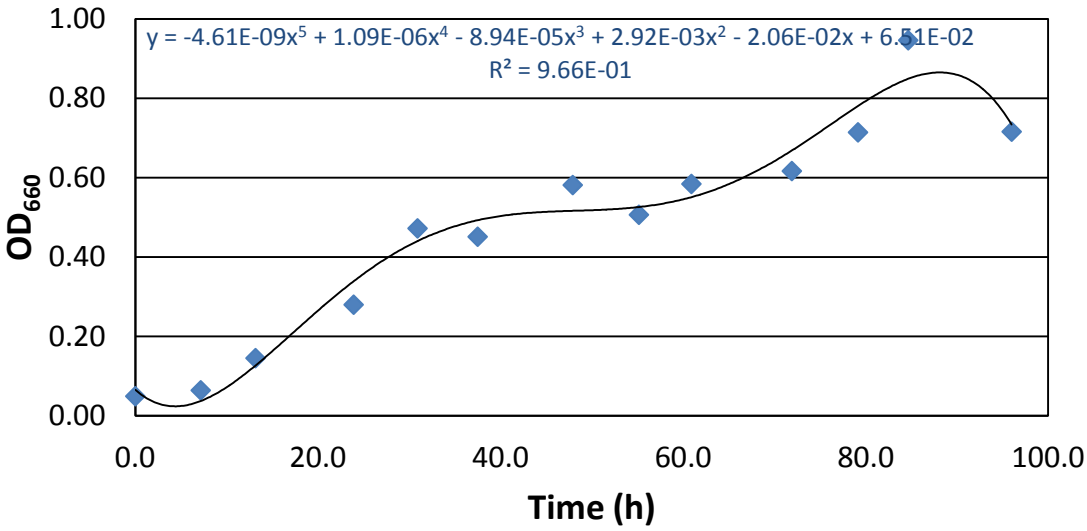

Figure B.1 Curve fit polynomial for cell growth in bottle Pr2B6 syngas fermentation with100 ml liquid.

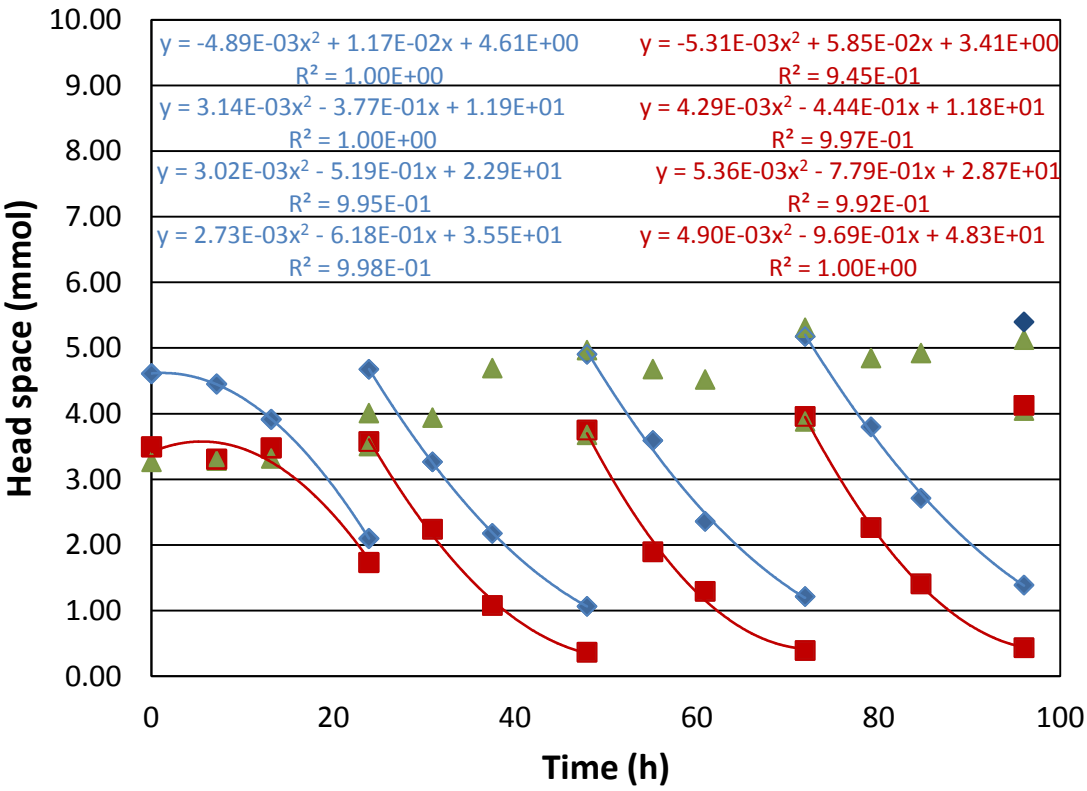

Figure B.2 Curve fit polynomial segments for CO and H_2 inventory in bottle Pr2B6 syngas fermentation with100 ml liquid. CO (◆), H_2 (■) and CO_2 (▲).

The gas inventory is discontinuous when gas is replaced, and the curve fit is obtained from segments of the data. The polynomial has no theoretical significance, but generally describes the observed data with R^2 greater than 0.98. Consumption of CO or H_2 (*dn/dt* in equation 5.1) should fall as gas is depleted with exponential decay shaping the curve as seen for both CO and H_2 in Figure B.2 between 24 and 96 h. The shape of the curve up to 24 h of fermentation is not an exponential decay and the fermentation is kinetically limited, not mass transfer limited, during this period of initial cell growth. The polynomial is a good description of the fitted parameter (*n*) and is easily differentiated to obtain an equation in time (*t*) for the slope that represents the rate of change (*dn/dt*).

The curve fit equation should be examined for goodness of fit, and used where the equation reasonably matches the original data. The initial and final points used for the cell concentration in Figure B.1 are not well represented by the equation, and the slopes are wrong by inspection; only the interior points from 8 to 88 h were used for kinetic and mass transfer analysis. The segments of data in Figure B.2 used for the CO and H_2 inventory are generally descriptive of the observed data, with a few exceptions. The initial H_2 consumption is typically near zero from CO inhibition of hydrogenase, and the curve fit is at times difficult. The curve fit compensates for error in the data, but is subject to error with as few as 4 data points per segment. Generally the curve fit polynomial represents the data well enough, has the shape expected for mass transfer limitation, and gives the differential quantities that can be used with good confidence.

A variation of the curve fit for gas uptake was used for Experiment Pr3 with 50 mL of liquid medium where the gas was maintained near the initial pressure and

composition by replacing the headspace gas after every sample. The gas uptake for CO and H_2 (dn_{CO}/dt and dn_{H2}/dt) were taken from a curve fit of the cumulative uptake, since the gas inventory was continually discontinuous. The technique is demonstrated in Figure B.3 for bottle Pr3B6, and the data is fitted to a polynomial for CO and for H_2 over the course of the fermentation. The curve fit does not pick up differences in dn_{CO}/dt or dn_{H2}/dt as the pressure drops, but gives a useful approximation of constant rate at the pressure and composition maintained in the experiment. This technique gives an average uptake rate over the sampling period, and is less accurate than the method used in the Pr2 experiment where additional sampling shows rate change as the CO, H_2 and pressure is depleted in those bottles between gas replenishment.

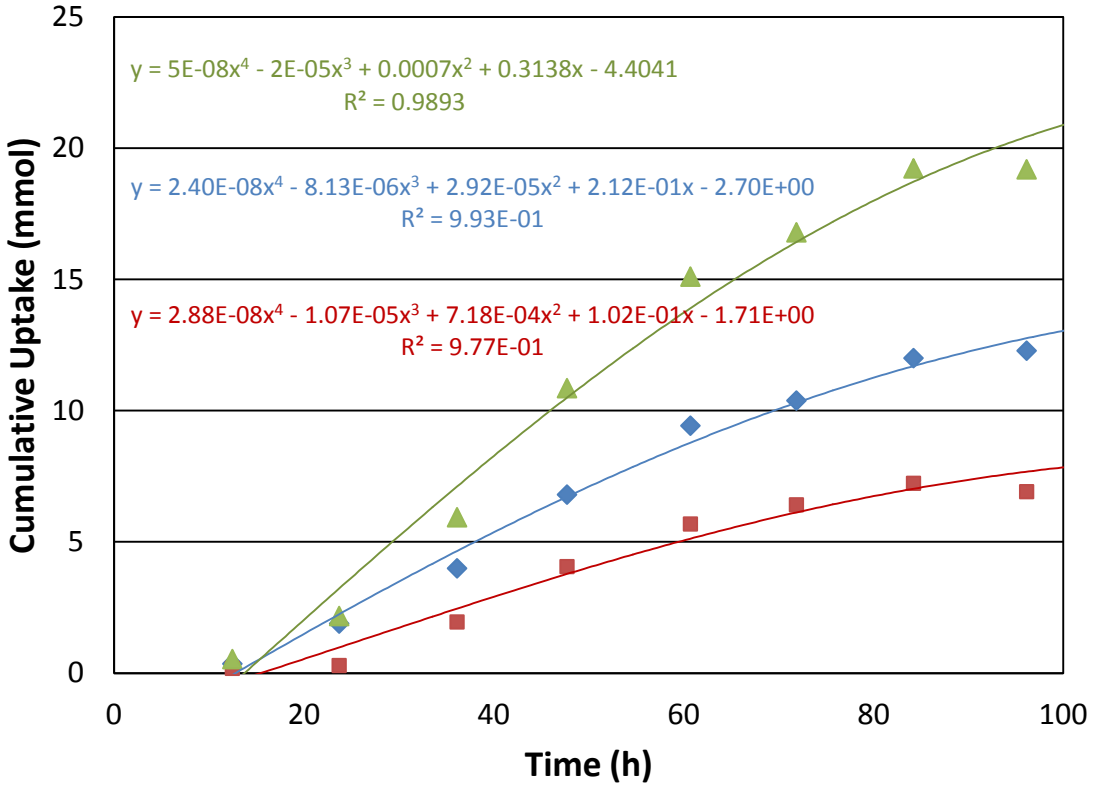

Figure B.3 Curve fit polynomial segments for CO, H_2 and CO+H_2 cumulative uptake in bottle Pr3B6 syngas fermentation with100 ml liquid. CO (◆), H_2 (■) and CO + H_2 (▲).

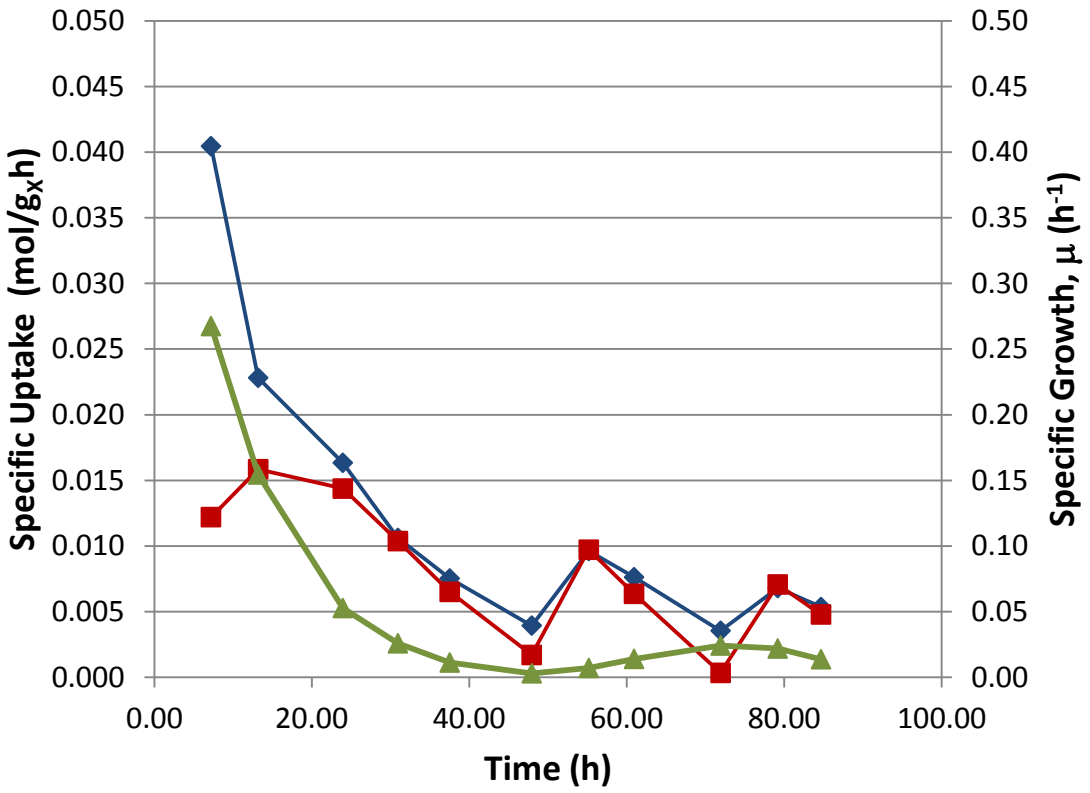

Figure B.4 Kinetic parameters derived from a curve fit of experimental data for syngas fermentation in bottle Pr2B6 with100 ml liquid. Specific uptake of CO (◆), Specific uptake of H_2 (■), Specific growth rate of *C. ragsdalei* (▲).

The CO and H_2 uptake rates and the rate of cell growth derived from the curve fit analysis were combined with the measured quantities to calculate specific uptake of CO and H_2, and specific growth rate at the time of sampling. These kinetic parameters are plotted over the course of fermentation in Figure B.4. Initially the specific uptake of CO is high at 0.04 mol CO/g_x h while specific uptake of H_2 is low. After 24 h of fermentation the specific uptake of H_2 is nearly equal to that of CO, despite higher partial pressure of CO during this period, see Figure B.5. The concentration of CO in the bulk liquid and inside the cell has fallen below the level that severely inhibits H_2 uptake, and this lower concentration should slow CO uptake as seen in Figure B.4. The specific

growth rate of *C. ragsdalei* in Figure B.4 starts high near 0.25 h^{-1} (doubling time of 2.8 h) while the medium is rich in proteins and amino acids from yeast extract, but drops below 0.015 h^{-1} by 40 h as these medium components are consumed.

References

Barik, S., Prieto, S., Harrison, S.B., Clausen, E.C., Gaddy, J.L. 1988. Biological Production of Alcohols from Coal through Indirect Liquefaction. Applied Biochemistry and Biotechnology, 18, 363-378.

Drake, H.L., Gossner, A.S., Daniel, S.L. 2008. Old Acetogens, New Light. in: *Incredible Anaerobes: From Physiology to Genomics to Fuels*, (Eds.) J. Wiegel, R.J. Maier, M.W.W. Adams, Vol. 1125, pp. 100-128.

Hurst, K.M., Lewis, R.S. 2010. Carbon Monoxide Partial Pressure Effects on the Metabolic Process of Syngas Fermentation. Biochemical Engineering Journal, 48 (2), 159-165.

Maddipati, P., Atiyeh, H.K., Bellmer, D.D., Huhnke, R.L. 2011. Ethanol Production from Syngas by Clostridium Strain P11 Using Corn Steep Liquor as a Nutrient Replacement to Yeast Extract. Bioresource Technology, 102 (11), 6494-6501.

Phillips, J.R., Clausen, E.C., Gaddy, J.L. 1994. Synthesis Gas as Substrate for the Biological Production of Fuels and Chemicals. Applied Biochemistry and Biotechnology, 45-6, 145-157.

Phillips, J.R., Klasson, K.T., Clausen, E.C., Gaddy, J.L. 1993. Biological Production of Ethanol from Coal Synthesis Gas - Medium Development Studies. Applied Biochemistry and Biotechnology, 39, 559-571.

Ukpong, M.N., Atiyeh, H.K., De Lorme, M.J.M., Liu, K., Zhu, X., Tanner, R.S., Wilkins, M.R., Stevenson, B.S. 2012. Physiological Response of Clostridium Carboxidivorans During Conversion of Synthesis Gas to Solvents in a Gas-Fed Bioreactor. Biotechnology and Bioengineering, 109 (11), 2720-2728.

Vega, J.L., Prieto, S., Elmore, B.B., Clausen, E.C., Gaddy, J.L. 1989. The Biological Production of Ethanol from Synthesis Gas. Applied Biochemistry and Biotechnology, 20-1, 781-797.

VITA

John Randall Phillips

Candidate for the Degree of

Doctor of Philosophy

Thesis: FERMENTATION OF SYNTHESIS GAS TO ETHANOL

MEDIUM DESIGN, MASS TRANSFER AND INTEGRATED MODEL

Major Field: Biosystems Engineering

Biographical:

Education:

Completed the requirements for the Doctor of Philosophy in Biosystems Engineering at Oklahoma State University, Stillwater, Oklahoma in May, 2013.

Completed the requirements for the Master of Science in Chemical Engineering at University of Arkansas, Fayetteville, Arkansas, in 1989.

Completed the requirements for the Bachelor of Science in Chemical Engineering at University of Arkansas, Fayetteville, Arkansas in 1981.

Experience:

Research Engineer, Biosystems and Agricultural Engineering, Oklahoma State University, Stillwater, Oklahoma, 2010 to 2013

Engineering Manager, INEOS Bio, Fayetteville, Arkansas, 2008 to 2009

Manager of Engineering, Bioengineering Resources, Inc., Fayetteville. Arkansas, 1994 to 2008

Graduate Studies, University of Arkansas, Fayetteville, Arkansas, 1986 to 1994

Process Engineer, S & B Engineers and Constructors, Houston, Texas, 1981 to 1986

Professional Memberships: Professional Engineer, Arkansas Certificate 11642